Collaborative Optical Wireless Communication Systems

Mohammed Alhartomi

Submitted in accordance with the requirements for the degree of Doctor of Philosophy

University of Leeds

School of Electronic and Electrical Engineering

December 2015

The candidate confirms that the work submitted is his own, except where work forming part of jointly authored publications has been included. The contribution of the candidate and the other authors to this work has been explicitly indicated below. The candidate confirms that appropriate credit has been given within the thesis, where reference has been made to the work of others.

The work in Chapter 4 of the thesis has appeared in publications as follows:

1. Alhartomi, M.A.; Alsaadi, F.E.; Elmirghani, J.M.H., "Collaborative multibeam transmitter and imaging receiver in realistic environment," in *Transparent Optical Networks (ICTON), 2015 17th International Conference on* , pp.1-6, 5-9 July 2015.

My contribution: Literature review; developing the new idea of collaborative adaptive beam clustering method (CABCM) for the design of multiuser OW systems; modelling the proposed system where the total transmit power is collaboratively distributed among beams based on MRC technique. I designed the imaging receiver and simulated the system at low data rate (30 Mb/s) and higher data rates (2.5 Gbit/s and 5 Gbit/s). I studied and analysed the system in different multiuser scenarios, producing results of the proposed systems in Matlab, and comparing them with baseline configurations, LSMS and CDS systems.

Dr Alsaadi: Help with developing the idea of CABCM; and with the preparation of article.

Professor Elmirghani: Developed the idea of collaborative adaptive beam clustering method (CABCM); developed the receiver structure design; and helped with the preparation of the article.

2. Alhartomi, M. A.; Alsaadi, F. E.; Elmirghani, J. M., "Collaborative adaptive optical wireless system in realistic indoor environment," in *Networks and Optical Communications - (NOC), 2015 20th European Conference on* , pp.1-6, June 30 2015-July 2 2015.

My contribution: Literature review; extending and improving the idea of collaborative adaptive beam clustering method (CABCM) and developing collaborative adaptive line strip system (CALSMS) for the design of multiuser OW systems. I designed the imaging receiver and simulated the system at higher data rates (2.5 Gbit/s and 5 Gbit/s) in a realistic environment. I produced results of the proposed systems in Matlab and compared them to find the most suitable geometry for indoor multiuser OW systems.

Dr Alsaadi: Helped with developing the ideas and with the preparation of article.

Professor Elmirghani: Developed the ideas of collaborative adaptive beam clustering method (CABCM) and collaborative adaptive line strip system (CALSMS); developed the receiver structure design and helped with the preparation of the article.

The work in Chapter 5 of the thesis has appeared in publications, as follows:

3. Alhartomi, M. A.; Elmirghani, J. M. H., "Max-Min Fair Power Adaptation for Indoor Collaborative Multibeam Systems," to be submitted to *IEEE/OSA Journal of Lightwave Technology*.

My contribution: Literature review, developing and designing ideas (new Max-Min fair power adaptation algorithm) for use in indoor collaborative multibeam systems; designing imaging receiver and simulating system at higher data rates (2.5 Gbit/s and 5 Gbit/s); producing results of the proposed systems employing the new algorithm in Matlab; and comparing them with the original CABCM to find the most suitable geometry for indoor multiuser OW systems.

Professor Elmirghani: Originating the idea of Max-Min fair power adaptation algorithm in conjunction with an imaging receiver.

The work in Chapter 6 of the thesis has appeared in publications, as follows:

4. Alhartomi, M. A.; Alsaadi, F. E.; Elmirghani, J. M. H., "Mobile optical wireless system using fast beam angle, delay and power adaptation with angle diversity

receivers," in *Transparent Optical Networks (ICTON), 2012 14th International Conference on* , pp.1-5, 2-5 July 2012.

My contribution: Literature review; developing the new idea of fast beam angle; delay and power adaptation to speed up the adaptation process through efficient use of a divide and conquer algorithm; designing an angle diversity receiver with seven detectors; simulating system at low data rate (30 Mb/s) and comparing the results with original MBAAS system, where a reduction in the system adaptation time by factor of 10 was achieved.

Dr Alsaadi: Helped with developing the idea and with the preparation of article.

Professor Elmirghani: Originating the new idea of fast beam angle, delay and power adaptation algorithm with angle diversity receiver; and helped with the preparation of article.

5. F. E. Alsaadi, M. A. Alhartomi, and J. M. H. Elmirghani, "Fast and Efficient Adaptation Algorithms for Multi-Gigabit Wireless Infrared Systems," *Lightwave Technology, IEEE/OSA Journal of*, vol. 31, no. 23, pp. 3735-3751, 2013.

My contribution: Literature review; investigating the complexity of the fast adaptation algorithm in comparison with the original MBAAS algorithm; evaluating the system at higher data rates (15 Gbit/s) in a realistic office environment.

Dr Alsaadi: Literature review; extending the idea of fast adaptation algorithms; developing new clustering patterns; and help with the preparation of article.

Professor Elmirghani: Enhancing the idea of fast adaptation algorithms with angle diversity receivers; and help with the preparation of the article.

The work in Chapter 7 of the thesis has appeared in publications, as follows:

6. Alhartomi, M. A.; Alsaadi, F. E.; Elmirghani, J. M. H., "Collaborative Multi-Gigabit OW Systems Employing Fast and Efficient Algorithms with Imaging Reception," to be submitted to *IEEE/OSA Journal of Optical Communications and Networking*.

My contribution: Literature review; developing and extending the idea of fast adaptation algorithms in indoor collaborative multibeam OW systems; modelling the new collaborative multibeam systems with imaging receiver; simulating the systems at low data rate (30 Mb/s) and at higher data rates (2.5 Gbit/s and 5 Gbit/s); studying the system in the presence of stationary users as well as a coexisting mobile user; and producing results of the proposed systems in Matlab and comparing them with the original CABCM system.

Dr Alsaadi: Help with developing the idea and with the preparation of the article.

Professor Elmirghani: Developing the extended idea of fast adaptation algorithms for indoor collaborative multibeam OW systems, coupled with an imaging receiver; and help with the preparation of the article.

To:

My parents, brothers, sisters, my wife, my son and my daughter

Acknowledgements

First and foremost, I thank and praise Allah (Subhana Wa Taala) for endowing me with health, patience, and knowledge to complete this work. This research project presented here could not have been accomplished without the help and encouragement of my supervisor, Professor Jaafar Elmirghani. I am grateful for his invaluable expertise, teaching, guidance and friendship. His emphasis on securing a good balance between theory and practice has been a guideline through my research. I feel very honoured to have had the chance to work with Professor Elmirghani. I must express my deepest gratitude to my parents, my brothers, my sisters, my wife, my son, and my daughter for their continued prayers, love, patience, and encouragement. I am also indebted to University of Tabuk for funding my studies.

Abstract

Current and future wireless data transmission applications, such as high quality audio/video streaming or high-speed Internet access demand wireless communications links that provide large throughputs. Although, wireless communication links are mostly based on signal transmission in radio frequency spectrum (RF), optical wireless (OW) communication has the potential to become a viable complement to RF signal transmission. OW systems offer a number of advantages over their RF counterparts, including freedom from fading, abundance of unregulated bandwidth, and immunity against interference from electrical devices. However, they are affected by background noise attributed to natural and artificial light sources and multipath propagation. The former degrades the signal-to-noise ratio, while the latter constrains both bandwidth and the maximum achievable data rate.

The aim of this thesis is to investigate the use of collaborative transmit power adaptation in the design of indoor OW spot-diffusing systems, hence increasing the received power of each coexisting receiver to enable higher data rates. The investigations in this work include the use of imaging diversity receivers to eliminate unwanted background noise signals. Imaging collaborative adaptive multibeam transmitters are proposed to increase the received optical signals power, reduce the delay spread and enable the system to operate at higher data rates. The work also introduces Max-Min fair power adaptation to distribute power fairly among users. Furthermore, the work investigates a new fast adaptation algorithm based on a divide-and-conquer methodology to reduce the system computational cost. This method can effectively optimise the spots' locations and spatially optimises the spots distribution for multibeam angle, power and delay adaptation systems.

Contents

List of Figures

List of Tables

List of Abbreviations

AEL	**A**ccessible **E**mission **L**imit
ALSMS	**A**daptive **LSMS**
ATM	**A**synchronous **T**ransfer **M**ode
APDs	**A**valanche **P**hoto-**D**iode**s**
BMDO	**B**allistic **M**issile **D**efence **O**rganisation
BCM	**B**eam **C**lustering **M**ethod
BPSK	**B**inary **P**hase **S**hift **K**eying
BJT	**B**ipolar-**J**unction **T**ransistor
BER	**B**it-**E**rror-**R**ate
BN	**B**ackground **N**oise
CABCM	**C**ollaborative **A**daptive **B**eam **C**lustering **M**ethod
CALSMS	**C**ollaborative **A**daptive **L**ine **S**trip **M**ulti-spot diffusing **S**ystem
CDMA	**C**ode **D**ivision **M**ultiple **A**ccess
CFAAS	**C**ollaborative **F**ast Beam **A**ngle **A**daptation **S**ystem
CFAPAS	**C**ollaborative **F**ast Beam **A**ngle and **P**ower **A**daptation **S**ystem
CP	**C**ommunication **F**loor
CPC	**C**ompound **P**arabolic **C**oncentrator
CGH	**C**omputer-**G**enerated **H**ologram
CDS	**C**onventional **D**iffuse **S**ystem
CHS	**C**onventional **H**ybrid **S**ystem
DARPA	**D**efence **A**dvanced **R**esearch **P**rojected **A**gency

DPIM	**D**igital **P**ulse **I**nterval **M**odulation
DBS	**D**irect **B**inary **S**earch
EGC	**E**qual **G**ain **C**ombining
FEAAS	**F**ast and **E**fficient **A**ngle **A**daptive **S**ystem
FEADAS	**F**ast and **E**fficient **A**ngle and **D**elay **A**daptive **S**ystem
FEADPAS	**F**ast and **E**fficient **A**ngle, **D**elay and **P**ower **A**daptive **S**ystem
FET	**F**ield-**E**ffect-**T**ransistor
FOV	**F**ield-**O**f-**V**iew
FLCB	**F**luorescent **L**amps with **C**onversion **B**allast
FLEB	**F**luorescent **L**amps with **E**lectronic **B**allast
FEC	**F**orward **E**rror **C**orrection
hps	**H**alf **P**ower **S**emi-angle
Ir	**I**nfra**r**ed
IrDA	**I**nfrared **D**ata **A**ssociation
IM/DD	**I**ntensity **M**odulation and **D**irect **D**etection
IEC	**I**nternational **E**lectro-technical **C**ommission
ISI	**I**nter **S**ymbol **I**nterference
LDs	**L**aser **D**iode**s**
LEDs	**L**ight **E**mitting **D**iode**s**
LOS	**L**ine-**O**f-**S**ight
LSMS	**L**ine **S**trip **M**ulti-spot diffusing **S**ystem
LC	**L**iquid **C**rystal

LANs	**L**ocal **A**rea **N**etwork**s**
LPF	**L**ow **P**ass **F**ilter
MRC	**M**aximum **R**atio **C**ombining
MAC	**M**edium **A**ccess **C**ontrol
Max-Min CABCM	**Max-Min C**ollaborative **A**daptive **B**eam **C**lustering **M**ethod
MBAAS	**M**ulti-**B**eam **A**ngle **A**daptive **S**ystems
MBAPAS	**M**ulti-**B**eam **A**ngle and **P**ower **A**daptive **S**ystems
MSM	**M**ultiple **S**ub-carrier **M**odulation
MPE	**M**aximum **P**ermissible **E**xposure
NASA	**N**ational **A**eronautics and **S**pace **A**dministration
NRZ-OOK	**N**on-**R**eturn to **Z**ero **OOK**
OOK	**O**n-**O**ff **K**eying
OW	**O**ptical **W**ireless
PCs	**P**ersonal **C**omputers
PAR 38	Philips PAR 38 Economic
PIN	**P**ositive-**I**ntrinsic **N**egative
PM	**P**ulse **M**odulation
PPM	**P**ulse **P**osition **M**odulation
PFDR	**P**yramidal **F**ly-eye **D**iversity Receiver
QoS	**Q**uality **o**f **S**ervice
RF	**R**adio **F**requency
RZ-OOK	**R**eturn to **Z**ero **OOK**

rms	**R**oot-**M**ean-**S**quare
SB	**S**election-**B**est
SNR	**S**ignal-to-**N**oise **R**atio
SM	**S**ub-carrier **M**odulation
SSM	**S**ingle **S**ubcarrier **M**odulation
VFIr	**V**ery **F**ast **I**nfra**r**ed

List of Symbols

ϑ	Incident angle with respect to the transmitter's normal
ϑ_d	Incident angle of the direct ray with respect to the transmitter's normal
ϕ	Angle of the incident ray with respect to the normal of the reflective element 1
φ_1	Angle of the first reflected ray with respect to the normal of the reflective element 1
φ_2	Angle of the first reflected ray with respect to the normal of the reflective element 2
γ_1	Angle of the reflected ray from the reflective element 1 to the reflective element 2 with respect to the normal of the reflective element 1
γ_2	Angle of the reflected ray from the reflective element 1 to the reflective element 2 with respect to the normal of the reflective element 2
δ	Angle of incidence with respect to the receiver's normal
α_s	Transmission beam angles with respect to the transmitter normal
Δt	Bin width
η	Quantum efficiency of the device
Γ	FET noise factor
λ	Wavelength
μ	Mean delay
ψ_c	Concentrator's acceptance semi-angle
ρ	Reflection coefficient
ρ_1	Reflection coefficient of the first reflective elements
ρ_2	Reflection coefficient of the second reflective elements
σ_0	Standard deviation of the shot noise component associated with logic 0
σ_1	Standard deviation of the shot noise component associated with logic 1
σ_{bn}	Standard deviation of the background shot noise component

σ_{pr}	Standard deviation of the preamplifier shot noise component
${\sigma_t}^2$	Total noise variance
θ_x	Transmission angle in the *x*-axis
θ_y	Transmission angle in the *y*-axis
θ_{steps}	Angle adaptation step size
θ_x^{start}	Start scanning angle in the *x*-axis scan range
θ_x^{end}	End scanning angle in the *x*-axis scan range
θ_y^{start}	Start scanning angle in the *y*-axis scan range
θ_y^{end}	End scanning angle in the *y*-axis scan range
θ_x^{opt}	The optimum transmission angle in the *x*-axis
θ_y^{opt}	The optimum transmission angle in the *y*-axis
A	Entrance area of the concentrator
A'	Exit area of the concentrator
$A_{eff}(\delta)$	Effective signal-collection area
A_R	Collection area
Az	Azimuth angle
B	Bit rate
BW	Receiver Bandwidth
c	Speed of light
C_d	Detector capacitance
C_g	FET gate capacitance
D	Root mean square delay spread
dA	Reflection surface element area
dP	Power radiated into a solid-angle element
d_x	The horizontal distance separating the receiver's normal and the reception area centre alongside the *x*-axis

d_y	The horizontal distance separating the receiver's normal and the reception area centre alongside the *y*-axis
El	Elevation angle
G	Open-loop voltage gain
g_m	FET transconductance
h	Reception area height
$h(t)$	Impulse response of the channel
$h^{(k)}(t)$	Impulse response due to the k^{th} reflection
h_p	Planck's constant
h_s	Height of the spots
$I(t, Az, El\ )$	Received photocurrent at the output of the detector at a certain location
J	Total number of photodetectors
k	Boltzmann's constant
L	Total number of lamps
M_t	The total number of reflecting elements
N	Internal refractive index
N_s	Total number of spots
N_{user}	Total number of users
n	Mode number that determines the shape of the radiated beam
$n_{element}$	Mode number that determines the shape of the reflected beam from reflection elements
$\hat{n}_1$	Normal of the reflective element 1
$\hat{n}_2$	Normal of the reflective element 2
$\hat{n}_R$	Normal of the receiver
$\hat{n}_S$	Normal of the source
$O(n)$	Complexity order of an algorithm
P_{bn}	Total received background power at the receiver
P_{dA}	Power radiated by a surface element

$P_{i,s}$	Power requested by a receiver i from a spot s
P_{LOS}	Direct received power
P_e	Probability of error
P_{n_d}	Direct received noise power
$P_{n_{reflection}}$	Total noise power received through the reflecting elements
$P_{reflection}^{(1)}$	Power received by the first-order reflection
$P_{reflection}^{(2)}$	Power received by the second-order reflection
P_s	Average transmitted optical power
P_{s0}	The power associated with logic 0
P_{s1}	The power associated with logic 1
$P_{s,MRC_{Coll}}$	The adapted power for a spot *j* requested by *n* receivers based on MRC scheme
P_{Total}	The total received power at the receiver
q	Electronic charge
$Q(.)$	Gaussian function
R	Photodetector responsivity
R_f	Feedback resistance
R_1	Distance between the reflective element 1 and the transmitter
R_2	Distance between the receiver and the reflective element 1
R_3	Distance between the reflective element 1 and the reflective element 1
R_4	Distance between the receiver and the reflective element 2
$R(\vartheta)$	Radiation intensity pattern
R_d	Direct link distance between the receiver and the transmitter (source)
r_{hc}	Radius of the hemispheric concentrator
r_{det}	Radius of the photodetector
r_R	Position vector of the receiver
r_S	Position vector of the source

t	Absolute time
T	Absolute temperature
$T(n)$	Time complexity
$T_c(\delta)$	Transmission factor of concentrator
$T_F(\delta)$	Transmission factor of filter
x	Distance between the receiver and the y-z wall
$x(t)$	Transmitted instantaneous optical power
x_r	Distance between the imaging receiver and the *y*-*z* wall
y_r	Distance between the imaging receiver and the *x*-*z* wall
z_x	The height of the centre of a reception area on the *y*-*z* wall
z_y	The height of the centre of a reception area on the *x*-*z* wall

1 Introduction

1.1 Why Optical Wireless?

The use of light as a means of communication is a well-established concept. In early times, many forms of optical wireless (OW) phenomena were used to communicate over distance, such as smoke, fires, flags and semaphore. Smoke signals were used to send messages over long distances and deciphered at the other end, and beacon fires on mountain tops were used to announce the commencement of holy days. OW communication has played an important role in warfare, where it served to convey information from reconnaissance teams to units in contact with the enemy. Another form of OW communication is using mirrors to reflect sunlight to a distant observer, as the movement of a mirror produces flashes of light that can be used to send Morse code [1]. This simple and effective method was in use beyond 1935 [1] for military, forestry and survey work.

The dawn of modern-day OW communication dates to 1880, when Alexander Graham Bell and Sumner Trainer developed and patented the photophone (radiophone), a device that allowed for the transmission of sound on a beam of light [2]. The photophone functioned in similar way to the telephone, only it used modulated light as a means of projecting the information while the telephone depends on electricity. Bell's photophone was based on electronic detection in which optical signals were converted to electrical signals through the use of a selenium crystal.

The principle of the photophone was the basis of the modern fibre optics. These days, this technology has prompted a giant leap forward and it currently transports over 80 per cent of the world's telecommunication traffic [1]. Unsurprisingly, modern fibre optic communications offer much higher data rates with a better quality of service (QoS) than their progenitor [3].

The modern era of OW communications coincided with the invention of the first laser in 1960 [4], when an intense, coherent light operating at a single wavelength first became available. This achievement was the start of a growing body of research on optical communication. At that time, research was funded by government agencies: Defence Advanced Research Projected Agency (DARPA); the Ballistic Missile Defence Organisation (BMDO); and the National Aeronautics and Space Administration (NASA). The aim was to develop a communication link between submarines beneath the surface of the oceans and satellites orbiting Earth.

Over the past four decades, OW communication has greatly expanded with applications in many areas of telecommunications. Their diversity is wide ranging, from very short distance optical interconnects of a few centimetres, short point-to-point optical links (within 1m), local area networks (LANs), to outdoor free space optical links (in km). The use of OW links can establish communication channels even millions of kilometres apart, as evidenced by the use OW communication in NASA's exploratory space missions. For shorter terrestrial distances, free space networks connected to nodes with a separation distance of couple of kilometres are shown to be feasible [3]. On a much smaller scale,

indoor OW links have successfully penetrated our homes, yet little attention has been paid to this invisible, vital technology.

Infrared (Ir) wireless communication is a form of OW in which light waves are used in free-space propagation in the near infrared band as a transmission medium for communication. The Ir signal is electromagnetic radiation whose wavelengths are banded between 780 nm and 1550 nm [5]. The band of 780 to 950 nm is the preferred option for inexpensive Ir systems. Therefore, the wavelength of 850 nm is considered in this thesis. Moreover, the deployment of the Ir standard enabled the use of Ir technology in many products ranging from television remote control devices to Infrared Data Associated (IrDA) ports. IrDA ports currently have a worldwide installed base of over 200 million units with 40 per cent annual growth [6]. OW is also widely available in personal computers, personal digital assistants and devices of all types.

Apart from the various applications of OW that are currently in daily life use, Ir wireless communication has the potential to mitigate the increasing issue of spectrum shortage. The basis of most current wireless systems is radio frequency (RF), which increases demand on the RF spectrum and limits its ability to accommodate new high bit rate services [7], [8]. This adds complexity to the design of radio subsystems such as transmitters and receivers, translated into additional cost to the radio system. The demand for high speed communication and wider bandwidth is the main motivating factor behind the focus on the optical medium as a means for indoor wireless communications [9]-[60]. Carrier waves within the radio frequency range provide limited bandwidth up to tens of MHz, whereas OW signals are capable of extending this bandwidth by several orders of

magnitude. Additionally, the RF spectrum is regulated by international or regional organisations, while the Ir spectrum is free and has no such restrictions. Optical signals are confined to the environment (i.e., room) in which they originate; optical signals do not penetrate walls and hence there is no interference to users in other parts of the indoor environment. This offers immunity to interference caused by other RF devices, as well as making it possible to use the same wavelength in other rooms.

The confinement of Ir signals adds a degree of security at the physical layer, reducing the need for data encryption. Ir communication links provide freedom from fading [36], and this reduces the design complexity. Typical dimensions of a photodetector in OW system with an area of $1cm^2$ are a million wavelengths squared [61], hence the OW detector averages over the Rayleigh fading and the mobile user experiences no fading [36], [61]. These favourable features, combined with inexpensive transceiver components such as light emitting diodes (LEDs) and positive-intrinsic negative (PIN) detectors, may signify that OW communication links could rival radio counterparts.

OW communication links are not without their drawbacks. In indoor infrared-based applications, optical signals are subject to attenuation and dispersion due to multipath propagation caused by light bouncing off reflective surfaces (walls and ceiling). Since reflective surfaces in indoor environments have a diffuse nature, the transmitted signal reaches the receiver through various paths of differing lengths. This triggers transmitted pulse spread, which leads to intersymbol interference (ISI) [9]. A further drawback of OW links is that they are affected by intense ambient light sources. Ambient light arising from artificial lamps (incandescent and fluorescent) emits a substantial amount of power

within the wavelength range of silicon photodetectors, giving rise to signals corrupted by background noise (BN) [26], [27]. Moreover, OW channels are subject to eye and skin safety regulations restricting the maximum permitted optical power radiating from commercial transmitters [62]-[64]. In order to collect sufficient signal power and to achieve an acceptable performance (i.e., a bit error rate (BER) of 10^{-9}), the photodetectors of OW receivers must have a large photosensitive area. However, the photodetector capacitance is directly proportional to its area; in other words, the large photosensitive area produces a high capacitance that limits the achievable receiver bandwidth [28].

Table 1.1: Comparison of optical wireless and radio frequency systems for indoor wireless communication environments

	Optical wireless system	**Radio system**
Advantages	▪ Abundance of unregulated large bandwidth. ▪ No interference between links operating in different rooms. ▪ Possibility of frequency reuse in different parts of the same building. ▪ Security and freedom from spectrum regulation and licensing. ▪ Freedom from fading. ▪ Low cost components.	▪ Transmission through walls is possible. ▪ High mobility. ▪ The omni directional portable antenna is relatively insensitive to rotation.
Disadvantages	▪ Intersymbol interference due to multipath dispersion. ▪ Background shot noise induced by ambient light ▪ The need for a wired backbone to interconnect OW access points in different rooms. ▪ Transmit optical power is restricted by eye safety regulations.	▪ Regulated bandwidth. ▪ Multipath fading. ▪ Low security. ▪ Interference between users in different rooms. ▪ Expensive for the moment without guarantee of high bit rates.

Although significant research has been undertaken and various techniques have been proposed to alleviate these limitations associated with OW systems, much more work is still needed before even a fraction of the potential bandwidth is exploited in practical systems. The research presented in this thesis aims to address the above-mentioned limitations of OW systems and provide practical solutions, increasing the system data rate or enabling high data rates in multi-user communications. OW can be considered as a complement to wireless radio rather than direct competitor. Infrared is the ideal choice in environments in which radio systems are not desirable; for example, inside a hospital or an aircraft. A comparison of optical wireless and radio frequency systems is given in Table 1.1.

1.2 Research Objectives

The primary objectives of this work are to:

1- Investigate the viability of designing indoor optical wireless systems that address OW environment impairments with the aim of modelling proper transmitter and receiver configurations for high-speed OW applications.

2- Investigate the use of transmission power adaptations in order to increase the receivers' SNRs so the system can achieve higher data rates, particularly in the presence of multiple receivers in a realistic indoor office.

3- Investigate the use of fairness methods to distribute the transmission power between beams when multiple users are present.

4- Investigate a fast and efficient method to reduce system complexity when transmitter beam angle adaptation is employed, and study additional adaptation methods that can improve the optical wireless system performance.

5- Extend the capabilities of the fast and efficient methods introduced to the multiple-receiver scenarios and examine their efficiency in conjunction with imaging receivers.

1.3 Research Contributions

The author in this thesis has:

1- Further developed an existing ray-tracing algorithm to model and analyse the characteristics of the indoor optical wireless channel catering for the direct line-of-sight (LOS), first and second order reflections. The mathematical channel model includes channel impulse response, multipath dispersion, and the optical power induced by ambient light in various transmission and detection configurations. This model was transformed into a comprehensive software package to carry out the simulation in Matlab, to evaluate the performance of OW diffuse/spot-diffusing systems.

2- Proposed collaborative adaptive optical wireless systems in conjunction with imaging receivers. Two collaborative adaptive multibeam systems were introduced, including the collaborative adaptive line strip multibeam system (CALSMS) and the collaborative adaptive beam clustering method (CABCM). The author has evaluated the performance of the proposed systems in realistic indoor environments under two multiple receiver scenarios:

a. Stationary receivers, where all receivers are fixed in chosen locations.

b. One mobile receiver (moves along the y-axis line at constant x-axis) while the other receivers are stationary.

In each scenario, a number of multiple receiver cases were considered, including the presence of two, three and five users in the room.

3- Introduced a novel Max-Min collaborative adaptive beam clustering method (Max-Min CABCM) to the design of OW systems to distribute the transmit power fairly between the beams, and hence improve the system performance in the presence of multiple receivers with transmitter or/and receiver mobility. The proposed methods were examined and compared to the original CABCM based on a collaborative maximum ratio combining technique.

4- Introduced a novel method (fast and efficient angle adaptation algorithm) to speed up the adaptation process through efficient use of a 'divide and conquer' algorithm by recursively breaking down the scanning process and focusing it onto a smaller region at each iteration. The proposed method compared to the original multibeam angle adaptive systems (MBAAS) is shown to reduce the computation cost by a factor of 20. Three adaptive multibeam transmitter configurations were presented, analysed and compared:

a. Fast and efficient angle adaptive system (FEAAS).

b. Fast and efficient angle and delay adaptive system (FEADAS).

c. Fast and efficient angle, delay and power adaptive system (FEADPAS).

These configurations were evaluated in conjunction with an angle diversity receiver of seven branches. In a useful result for wireless communications, mobile

multibeam 15 Gbit/s OW systems were shown to be feasible through the introduction of: fast and efficient beam angle and beam power adaptation; optimised spot-diffusing pattern; and angle diversity receivers. Still higher data rates are possible using these systems.

5- Designed, investigated and evaluated the performance of a collaborative mobile OW system that employs fast and efficient algorithms combined with an imaging receiver. The proposed method, a collaborative fast and efficient angle and power adaptation (CFAPAS) algorithm, was introduced to the collaborative multibeam system design to optimise the spots' locations and distribution (the number and pattern of spots), with the aim of effectively reducing the impact of mobility, maximising the receivers' SNRs, reducing the computation time required and improving link performance.

These contributions are supported by the following publications:

Journals

1. F. E. Alsaadi, M. A. Alhartomi, and J. M. H. Elmirghani, "Fast and Efficient Adaptation Algorithms for Multi-Gigabit Wireless Infrared Systems," *Lightwave Technology, IEEE/OSA Journal of*, vol. 31, no. 23, pp. 3735-3751, 2013.
2. Alhartomi, M. A.; Elmirghani, J. M. H., "Max-Min Fair Power Adaptation for Indoor Collaborative Multibeam Systems," to be submitted to *IEEE/OSA Journal of Lightwave Technology.*
3. Alhartomi, M. A.; Alsaadi, F. E.; Elmirghani, J. M. H., "Collaborative Multi-Gigabit OW Systems Employing Fast and Efficient Algorithms with Imaging

Reception," to be submitted to *IEEE/OSA Journal of Optical Communications and Networking.*

Conferences

4. Alhartomi, M.A.; Alsaadi, F.E.; Elmirghani, J.M.H., "Collaborative multibeam transmitter and imaging receiver in realistic environment," in *Transparent Optical Networks (ICTON), 2015 17th International Conference on* , pp.1-6, 5-9 July 2015.
5. Alhartomi, M.A.; Alsaadi, F.E.; Elmirghani, J.M.H., "Collaborative adaptive optical wireless system in realistic indoor environment," in *Networks and Optical Communications - (NOC), 2015 20th European Conference on* , pp.1-6, June 30 2015-July 2 2015.
6. Alhartomi, M.A.; Alsaadi, F.E.; Elmirghani, J.M.H., "Mobile optical wireless system using fast beam Angle, delay and power adaptation with angle diversity receivers," in *Transparent Optical Networks (ICTON), 2012 14th International Conference on* , pp.1-5, 2-5 July 2012.

1.4 Overview of the Thesis

Chapter 2 provides a general review of OW communication systems presenting the merits and limitations of such types of communication, and indoor OW link classifications. Previous advances in this type of communication are outlined.

Chapter 3 presents the model of the OW channel in the indoor environment which is referred to in all communication scenarios investigated in this work. The simulation method adopted to model the communication channel is described in detail. Major OW transmitter configurations, including the basic diffuse system (CDS) and two spot-diffusing geometries (LSMS and BCM), are studied and used as the baseline to evaluate the novel configurations proposed in this study.

Chapter 4 presents a performance evaluation of collaborative adaptive multibeam systems in a realistic indoor environment. The spot-diffusing configurations (LSMS and BCM) analysed in Chapter 3 are developed where collaborative beam adaptation, in the presence of multiple receivers, is considered. High data rates are shown to be feasible when such configurations are combined with imaging receivers.

A novel Max-Min fair power adaptation method combined with an imaging receiver is introduced in Chapter 5. The chapter focuses on the fairness of power distribution when adapting beams' power in the presence of multiple users. The results indicate significant performance improvements in terms of SNR distribution fairness compared to the original imaging CABCM system, especially for receivers in less successful locations.

Chapter 6 introduces a novel fast and efficient angle adaptation method for the OW diversity spot-diffusing system design to optimise the spot distribution (number and pattern of spots) spatially with the aim of maximising receiver SNR, as well as significantly reducing the computation time. A fast adaptation approach based on a 'divide and conquer' methodology is proposed, resulting in a number of adaptation

algorithms: a fast and efficient angle adaptive system (FEAAS); a fast and efficient angle and delay adaptive system (FEADAS); and a fast and efficient angle, delay and power adaptive system (FEADPAS). These three new multibeam transmitter configurations, in conjunction with an angle diversity receiver of seven branches, are analysed and compared to quantify the proposed systems' performance. Significant improvements in the SNR with OW channel bandwidths of more than 15 GHz can be achieved, enabling some of the proposed systems to maintain higher data rates (15 Gbit/s and beyond).

Collaborative high-speed OW systems employing fast and efficient algorithms in conjunction with imaging receiver are presented in Chapter 7. The chapter gives a link design that is less sensitive to room geometry than CABCM and CALSMS, as the diffusing spots can be targeted in clusters at optimum locations to maximise the coexisting receivers' SNRs. The power can also be redistributed among beam clusters (hence, among spots) to improve the SNRs of the receivers further. In this approach, the link design collaboratively adapts the beam angle and beam power, enabling the system to adapt to room geometry and to transmitter and receiver mobility, effectively to maximise the SNRs of all coexisting receivers.

A summary of the contributions of the present study and some ideas towards further research are provided in Chapter 8.

2 Literature Review

2.1 Introduction

Infrared (Ir) wireless local area network (LAN) systems have attracted attention due to their high-speed capabilities. With their distinct features such as their unregulated spectrum, inexpensive subsystems and electromagnetic interference immunity, optical wireless communication has been regarded as a promising technique for indoor wireless networks [36]. Since the pioneering work of Gfeller and Bapst [9], the use of infrared radiation for indoor applications has been evaluated and widely investigated [9]-[49], [53]-[59]. The most promising feature of Ir transmission is the high bandwidth availability for high-speed optical communications. The infrared spectrum is well characterised, at terahertz (THz) frequencies, and can support, in theory, a bandwidth of the order of a few hundred gigahertz (GHz). Although the promise of such a large potential bandwidth is an attractive proposition, it is not the only feature that made OW technology an attractive candidate for indoor wireless communication systems. Both the advantages and disadvantages of indoor OW systems are considered to enable wider understanding.

Besides unregulated bandwidth abundance, OW links offer several other advantages over their radio counterparts because of the nature of light. Ir signals cannot penetrate walls or other opaque obstacles, which eliminates interference between neighbouring rooms in a building. Due to the fact that OW signals are contained in the room, OW systems have a degree of security at the physical layer between links operating in different rooms.

Additionally, optical transceiver components, including LEDs, laser diodes (LDs), PIN photodiodes and avalanche photodiodes typically cost less than similar components used in radio.

In addition, optical transceivers make use of simple intensity modulation and direct detection (IM/DD) techniques. Intensity modulation, in which the desired waveform is modulated onto the instantaneous power of the carrier, is performed by varying the drive current of LEDs or laser diodes (the intensity of radiated light is controlled). Direct detection is performed by producing an electric current that proportional to the incident optical power, through the use of PIN photodiodes or avalanche photodiodes. When an OW link employs IM/DD, the short optical wavelength and relatively large photodetector area result in efficient spatial diversity, which prevents multipath fading [61]. Freedom from multipath fading significantly simplifies the OW links' design. In addition to the above-mentioned features, Ir links have some of the properties of RF, such as the relative freedom of the user from fixed networks. In OW systems, the network backbone can feed OW transceivers that act as access points, and then communicate with end users, as shown in Figure 2.1.

Moreover, notwithstanding the above advantages, wireless Ir links suffer from two major impairments. The first is multipath dispersion, associated with the non-directed indoor OW channel which leads to significant ISI that can cause system degradation [9], [16]. The second is sensitivity to additive shot noise due to sunlight and artificial light.

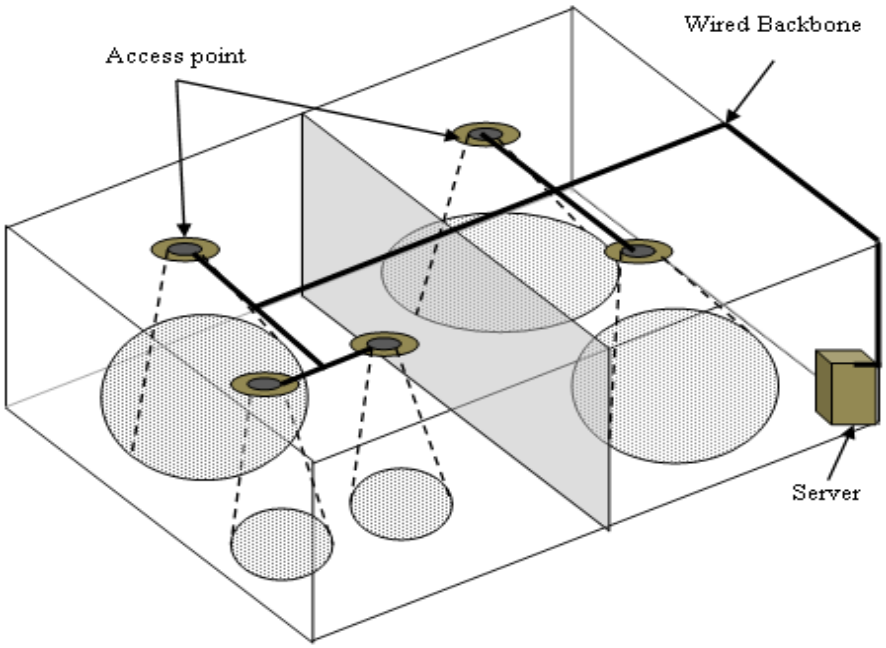

Figure 2.1: Access points in a local area network for connecting OW devices with a wired network.

The impairments imposed by the wireless infrared channel are not the only factors that limit the performance of OW systems; OW networks rely on a fibre distribution network that feeds access points, as optical signals cannot penetrate through walls and opaque objects. Furthermore, the maximum transmission power is constrained by eye and skin safety regulations [62]-[64]. Therefore, a large photodetector area is required to collect sufficient optical power to achieve an acceptable performance (BER < 10^{-9}). However, a large photosensitive area produces a high capacitance that limits the achievable bandwidth.

Over the past two decades, a variety of system solutions have been proposed to mitigate the impairments imposed by OW channels, and to cope with the resultant high capacitance from the increase of the photodetector area. Novel technologies for OW systems such as computer generated holograms and optical leaky feeders were analysed

[17], [18]. Improvements in the system performance were achieved through the use of different lens and filter structures [45]. Several novel cellular OW systems were demonstrated in [20]-[23], [30], [35], [47] in which the OW systems investigated operated at bit rates of up to 155Mbit/s. An OW system in an asynchronous transfer mode (ATM) network was reported to achieve a data rate of up to 1Gbit/s [31]. Infrared transmission systems have been used in various indoor applications such as remote control devices, headphones, conferencing systems and video transmission systems [10], [24], and in short-range low data rate OW links for computer accessories such as mice, printers, calculator, and palm top PCs [25].

This chapter gives an overview of previous research in the field of OW systems with the aim of illustrating the fundamentals of OW communications and provides a brief overview of OW links. The design challenges of indoor OW systems are presented in Section 2.3. An overview of data transmission and reception is also given. Modulation schemes used in OW systems are discussed. The chapter concludes by describing standards currently used in indoor OW systems.

2.2 Classification of OW Links

Optical wireless transmission links are often classified into categories based on the existence of a direct path between the transmitter and receiver, and the degree of transmitter and receiver directionality [36]. Using these facts, two most common classes of indoor OW links can be defined: LOS and non-LOS transmission systems. LOS links rely upon a direct path between the transmitter and receiver (transmitter must see the

receiver), regardless of their beam angles, while non-LOS links generally rely upon light reflection from diffuse reflecting surfaces (walls and ceilings). LOS links provide high power efficiency and minimise multipath dispersion, but can suffer from shadowing. Non-LOS systems provide robustness against signal blockage and shadowing, enabling mobile users to connect and collaborate instantly in a wireless environment. However, they are more prone to multipath dispersion, which causes pulse spread and ISI, in addition to poor power efficiency and much-reduced data rates compared to LOS links.

Furthermore, both LOS and non-LOS systems can be divided into directed, hybrid and diffuse systems depending on the transmission radiation pattern and the receiver field-of-view (FOV). A directed link can be formed when both transmitter and receiver are directed; that is, have a narrow beam transmitter and a small FOV receiver. The transmitter and the receiver inherently require alignment in order to establish a communication link, which makes systems using directed configuration less convenient to use in certain applications [12], [13], [65]-[68]. A hybrid link can be established by using a transmitter and a receiver with different degrees of directionality; that is, a transmitter with narrow beam radiation and a wide FOV or vice versa. A diffuse link can be established when transmitters and receivers employ a single wide beam radiation and a wide FOV detector, respectively. A conventional diffuse system (CDS) employing a wide beam transmitter and a wide FOV receiver, both pointing up towards the ceiling, is an example of a typical diffuse system. In a CDS system, the transmitted signal reaches the receiver through multiple diffuse reflective surfaces. Link classifications are illustrated in Figure 2.2.

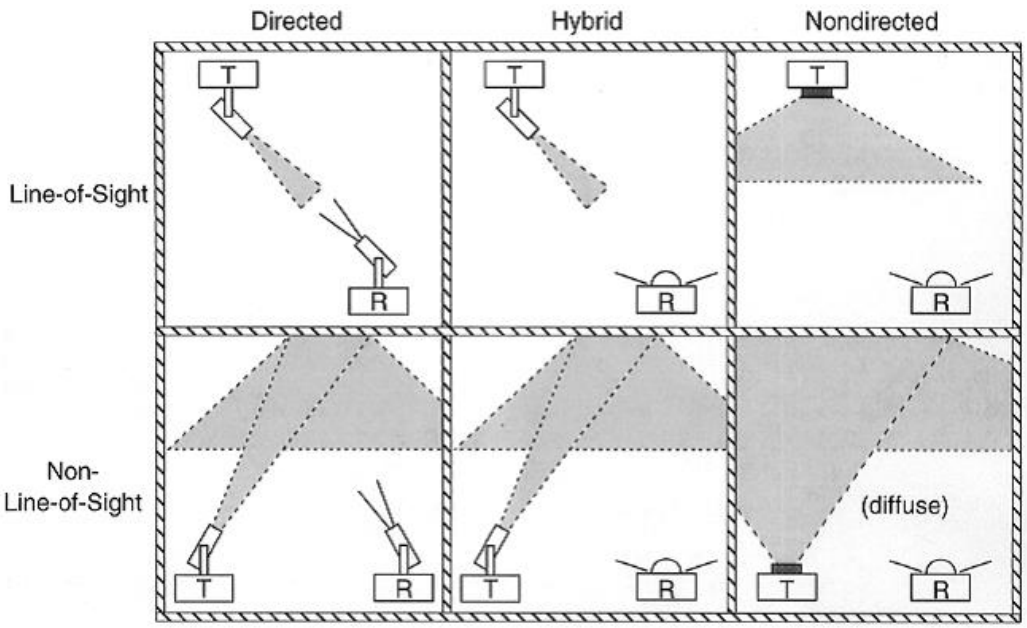

Figure 2.2: Classification of OW links [36].

2.3 Limitation of Indoor Optical Wireless

Unlike outdoor OW systems, indoor OW systems are free from atmospheric impact. However, there are essentially four impairments that limit data transmission in indoor OW systems, namely: background noise; multipath dispersion; photodetector high capacitance; and optical safety requirements. These limitations are briefly discussed in this section.

2.3.1 Background Noise

In contrast to pure fibre optic systems where the relevant light signal is kept separate from background noise sources, OW systems are distorted by ambient light noise. OW receivers detect both ambient light noise and the desired signal. In the indoor OW environment, background noise (BN) can originate from direct sunlight and artificial

light, which corrupts the optical signal. Fluorescent and incandescent lamps are the most common artificial light sources. The BN sources produce a substantial amount of power within the wavelength range of silicon photodetectors, as well as introducing shot noise, and can saturate the photodetector when the intensity is high [26], [69]. The use of optical filters may reduce the influence of ambient light which can be much stronger than the transmitted data signal [70]. The spectral power densities of three common ambient noise sources are shown in Figure 2.3 (a). A combined silicon photodiode-daylight filter is illustrated in Figure 2.3 (b).

The impact of ambient light sources on OW transmission has been widely studied [67]-[75]. It was reported that sunlight and incandescent light (for example, halogen and tungsten filament lamps) introduce a higher level of BN compared to fluorescent lighting, tungsten filaments being the worst BN spectral source. Despite using inexpensive daylight filters to alleviate the influence of BN sources in OW systems, tungsten filament and halogen lamps emit light within the pass-band of a daylight filter [73], resulting in light-induced noise that reaches the receiver and creates significant shot noise. Sunlight is not expected to change abruptly, so its background irradiance can be modelled as a stream of photons with slow intensity variation. Light from both artificial and natural sources is then converted by the photodetector into a photocurrent that consists of two different noises: a DC current component and a shot noise component. The shot noise at the photodetector can be modelled as an additive white Gaussian noise (AWGN) [76]. AC-coupling can be employed to easily remove the DC current noise component.

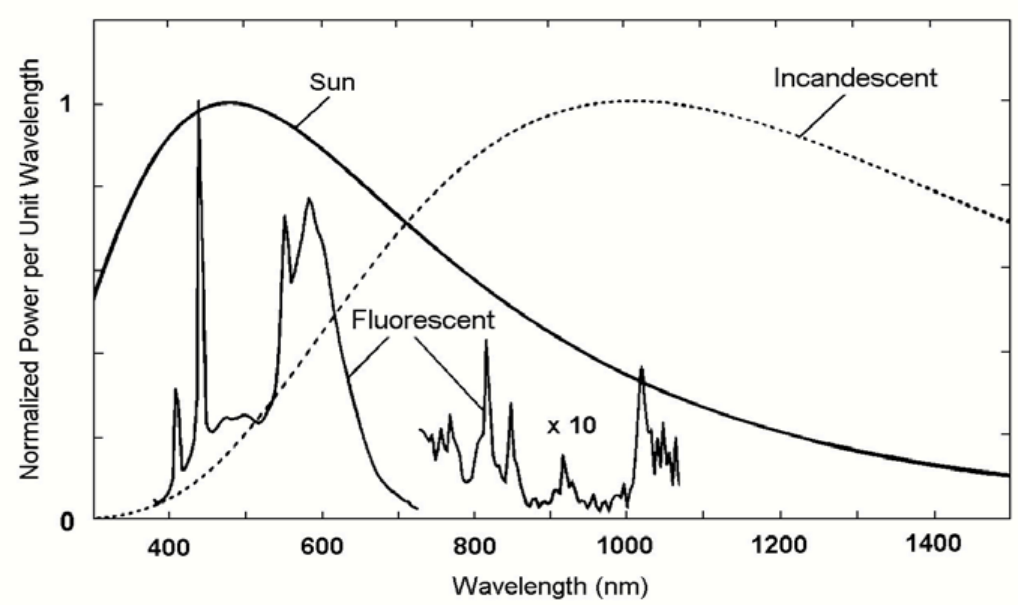

(a) Spectral power densities of three common ambient noise sources.

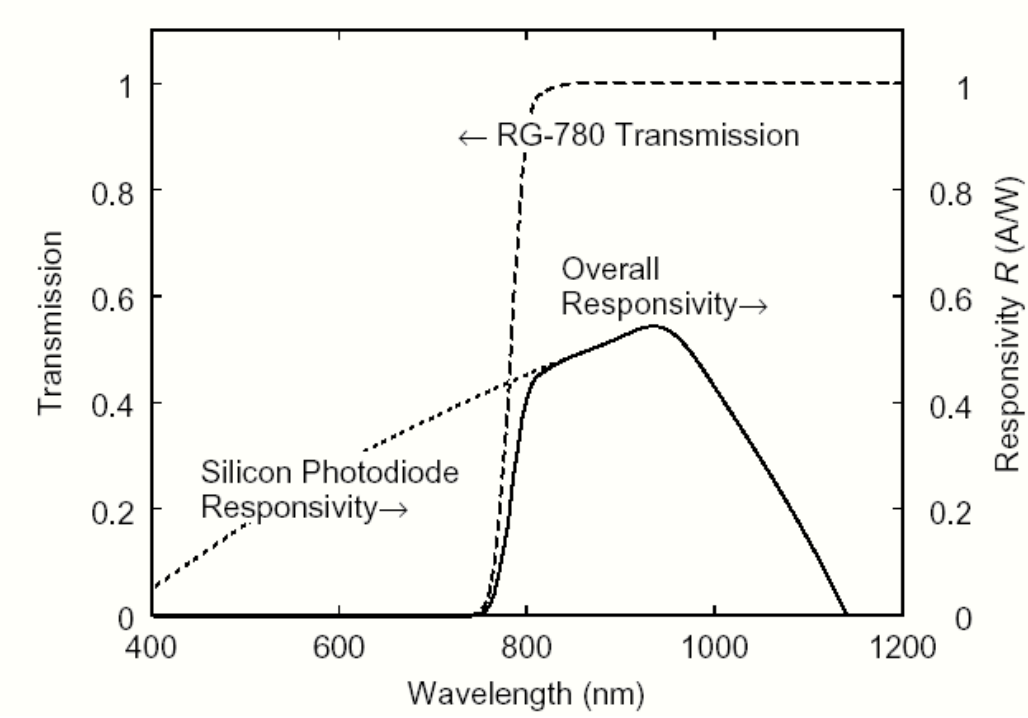

(b) Transmission of a silicon photodiode employing a daylight filter.

Figure 2.3: Optical power spectra of different light sources [36].

Due to cyclic variation of artificial light intensity, light sources produce periodic interference. The interfering signal produced by incandescent lamps is a near-perfect sinusoid with a frequency double the frequency of the mains power supply [69]. The DC

current component and the interfering signal of the BN can be effectively eliminated by using an electrical high-pass filter. However, even with the use of such a filter the level of background shot noise current produced by incandescent lamps is much higher than with fluorescent lights with low- or high-frequency filters [26]. This is a result of the fact that the spectrum of incandescent light, such as halogen and tungsten filament lamps, falls within the passband of the daylight filter [73]. Moreover, incandescent light sources are highly directive and can lead to a burn-out effect of the received signal, predominantly underneath the light source. Narrow optical band-pass filters may only be employed in conjunction with laser transmission, and not with LEDs [77].

Fluorescent lights are classified into two categories: fluorescent lights with conventional ballast (FLCB) and fluorescent lights with electronic ballast (FLEB). Most of the fluorescent lights' optical power is emitted outside the pass-band of a daylight filter [67-75], which means that the amount of received optical power from the daylight filtered fluorescent lamp is very small compared with the corresponding power of the other light sources. However, the electrical interference produced by a fluorescent lamp, is a distorted sinusoid with a much broader spectrum than that of an incandescent lamp. Fluorescent light flickers at a constant rate, determined by the lamp drive frequency, and can induce spectral lines in the resulting photodetector current [70], [72]-[75], [78]. The electrical spectrum of the photocurrent, generated by FLEB, has higher frequencies up to few MHz [68]. The effect of the electrical spectrum components can be mitigated through the use of electrical high-pass filter and a careful choice of modulation scheme, but this can induce a very large power penalty and can lead to further ISI problems in particular

at a data rate of 10 Mb/s and beyond [75]. An effective technique using differential detection was introduced to combat these difficulties [79]. The same technique was analysed by Moreira *et al*. who found that it can reduce all types of artificial light interference [72]. Furthermore, it has been demonstrated that interference induced by fluorescent lights can be further reduced by using spread spectrum techniques [80].

Several techniques have been considered to reduce the effect of the ambient light noise [54], [55], [62]-[64], [81]-[93]. A narrow beam optical source coupled with a small FOV receiver can be employed to eliminate background noise. Angle diversity receivers can also be used to mitigate the influence of ambient light noise [32], [54]-[56], [82], [83], where multiple non-imaging receiving elements point in different directions. The receiving elements can help reduce the effect of ambient light noise by collecting the strongest possible optical signal and restricting the ambient light. Although an improvement in performance can be achieved by using an angle diversity receiver, it can be bulky and relatively expensive since a separate optical concentrator is required for each receiving element. Angle diversity receivers have been studied and are reported in this study. An alternative choice that can substantially reduce the influence of background noise, significantly mitigating ISI and improving the OW system's performance, is an imaging receiver [44], [47], [94]-[97]. This was first proposed by Yun and Kavehrad, and consists of a collection of photodetectors that share a single imaging optical concentrator (e.g., a lens) [44]. The imaging concentrator with an acceptance semi-angle (ψ) forms an image of the received rays on a large number of photodetectors.

It has been reported that an imaging receiver coupled with a multibeam transmitter can reduce the required transmitter power by more than 20 dB, in comparison with a wide FOV non-imaging receiver [96]. Imaging receivers offer two main advantages over non-imaging angle diversity receivers. First, the receiver can be fabricated in a smaller size and costs less, since all detectors share the same optical concentrator. Second, all the photodetectors can be laid out in a single planar array, enabling the use of a large number of photodetector pixels. In this study, a custom design imaging receivers is analysed in order to determine suitable system designs for use in collaborative OW systems (Chapters 4, 5 and 7).

2.3.2 Multipath Dispersion

Channel dispersion associated with multipath propagation is a major impairment in optical wireless transmission. In an indoor OW diffuse channel, multipath propagation occurs when the transmitted signal reaches the optical receiver via multiple paths due to reflections off ceiling, walls and other objects. Multipath dispersion causes the received pulse to spread, which in turn results in ISI. The impact of ISI induced by multipath propagation can be normally measured by calculating the channel root-mean square delay spread. Diffuse systems are more prone to the effects of multipath propagation due to their larger beam width and larger FOV receiver that lead to more potential reflectors and relatively more reflected light being received. In contrast, directed LOS links provide almost negligible multipath dispersion since the transmitted signal reaches the receiver directly where a narrow beam transmitter and a narrow FOV receiver are used. In a typical

indoor OW environment (i.e., a typical room size), the ISI induced by multipath dispersion is a major degrading factor when the data rate exceeds 10 Mb/s [36].

Multipath propagation characteristics for indoor OW links have attracted great attention in order to come up with solutions that can reduce the effect of multipath dispersion. Several techniques have been proposed to mitigate multipath propagation and hence reduce the impact of ISI. Angle diversity receivers using a number of narrow FOV detectors, which are aimed in different directions, can be used instead of a single wide FOV receiver [32], [51], [98]. Careful design using these detecting elements can result in a significant reduction in multipath dispersion. A number of diversity receiver structures have been proposed in attempts to determine the optimum structure that can help combat multipath dispersion, such as the pyramidal fly-eye diversity receiver (PFDR) [54], [55], [58], [59], [99], [100]. The PFDR has been further optimised with the goal of improving the link performance [50], [54]. Angle diversity receivers have two main drawbacks: their large size and high cost of fabrication. An alternative approach is an imaging receiver that can alleviate these limitations and effectively combat the influence of multipath dispersion and ambient light noise. Imaging receivers are discussed and analysed in Chapters 4, 5 and 7.

Apart from techniques to mitigate the impact of multipath dispersion that focus on the receiver design, various techniques have been proposed to optimise optical transmitters. Transmitter beam diversity has been proposed in order to improve the performance of OW systems [43], [46], [53], [60], [99-[101]. The concept of multibeam transmitters was first proposed by Yun and Kavehrad [44], where the transmitter generates multiple

diffusing spots pointed in different directions towards the reflecting surfaces (ceiling and walls). The multibeam transmitter, coupled with a narrow FOV diversity detector, has the advantage of both: directed LOS and diffuse links, as well as combating the effect of ambient light noise sources and multipath dispersion. Significant performance improvements can be achieved when OW systems adopt a line strip multibeam system (LSMS) in conjunction with an angle diversity receiver [98]-[100], [102]. Furthermore, LSMS with diversity reception was evaluated in complicated room designs and proven to be successful in improving the system performance [101], [103]. In [98], [101], [103], the authors analysed and compared the performance of LSMS to different OW system configurations, including a conventional hybrid system (CHS) (where the transmitter is angled downward) and CDS. Furthermore, a beam clustering method (BCM) was developed and shown to be a promising alternative spot-diffusing geometry [104], [105].

2.3.3 Photodetector High Capacitance

Major sources of noise in the electrical signal that follows the photodetector of an indoor OW system include significant components, such as shot noise induced by the BN, thermal noise induced by the bias resistance of the photodetector preamplifier, and amplifier or f^2 noise component due to channel thermal noise of the front-end FET [49]. There are other sources of noise such as the photodiode dark current noise and shot noise from the received signal, however these have a small impact compared to other noise sources. In addition to the impact of the noise, the optical infrared transmitted power is restricted by eye and skin safety regulation [106], which imply that a photodetector with a large photosensitive area should be employed in order to maximise the optical power

collected. Unfortunately, photodetector capacitance is directly proportional to the photosensitive area, which means a large photodetector area equates to large capacitance. The large capacitance at the input of an amplifier operates as a low pass filter (LPF) that attenuates the high frequency components of the received signal, hence restricting the attainable bandwidth. However, the dominant white thermal noise that is observed after the input stage will not be attenuated. This thermal noise degrades the SNR at higher signal frequencies. When a white noise process following a LPF is referred back to the input of the filter, its power spectral density becomes quadratic in frequency, so-called f^2 noise. Due to the fact that the f^2 noise variance in an amplifier is proportional to the square of the capacitance (hence the square of the photodetector area), its effect can be reduced by using a photodetector array as a replacement for a single photodetector [107]. If the receiver is well-designed, this type of noise can be negligible [107], therefore it is ignored in this study.

In order to maximise the signal power collected while avoiding the photodetector high capacitance, the effective range of reception angles of each photodetector should be increased. This can be done by using a custom-built lens as in [96], or by using a hemispherical lens when non-imaging diversity receivers are used, as in [36]. Moreover, circuit design techniques, such as bootstrapping [28], can be used to reduce the effect of the high photodetector capacitance.

2.3.4 Optical Safety Regulations

The maximum optical power allowed to be radiated by an optical transmitter must meet eye and skin safety regulations [62]-[64], which add more limitations to indoor OW systems. Optical radiation can present a hazard to eyes and skin if the exposure is high enough. The degree of the hazard varies markedly according to several factors, including exposure level, exposure time, beam characteristics and the operating wavelength. The most suitable wavelength band for the majority of infrared applications is typically 780–950 nm, due to the availability of optical transceivers at low cost [63]. However, electromagnetic radiation in this band can pass through the human cornea and may cause thermal damage to the human eye, and is therefore subject to regulations.

The common sources of light in OW transmission are LDs and LEDs, as explained in Section 2.4. In general, both sources emit an optical power within the 700–1550 nm wavelength band, which may cause eye damage if absorbed by the retina. When a beam of light enters the eye, the energy density of an incident light can be magnified and focused by the human eye onto the retina by factors of 100 thousand or more [108], and the Maximum Permissible Exposure (MPE) levels are therefore very small. The far-infrared band with optical wavelengths above 1400 nm have less effect due to the fact that light is absorbed by the cornea and lens, making operation attractive at these wavelengths. Therefore, it is suggested that the 1550 nm band may be better suited to infrared transmission links, but devices in this band are relatively costly [36].

The eye and skin safety standards of infrared transmitters are regulated by the International Electro-technical Commission (IEC) [109], which provides guidelines on the safety of optical beams. LD/LED products are classified into Class 1, 2, 3A and 3B, as shown in Table 2.1. Each is defined based on the accessible emission limit (AEL) metric, which depends on the wavelength, diameter and emission semi-angle of the optical source. Class 1 is the least powerful, therefore IEC requires that transmitters in indoor environment must be Class 1 eye safe under all circumstances of use. Class 3B is the most powerful band and generally used for outdoor point-to-point communication links. Observing Table 2.1, it is indicated that the indoor systems employing point laser sources must not launch power exceeding 0.5mW at the wavelength regions within which low cost devices operate.

Various techniques were proposed in order to reduce the potential dangers of higher power emissions. For example, wide beam sources can significantly reduce the risk of eye damage. Since indoor infrared transmission links employ LDs under very tight link budget restrictions, LDs operating in the Class 3B band can be considered Class 1 eye safe if optical diffusers are used to spread their radiation over a wide emission angle. Such a diffuser can attain almost 70 per cent efficiency. Another type of diffuser that employs a computer-generated hologram (CGH) was proposed as a beam-splitting element [44], [110]-[112]. This breaks up the optical beam, thereby diffusing the image of the laser-spot on the retina with a diffraction efficiency of near 100 per cent. This approach yields a Lambertian radiation pattern that gives the freedom to tailor the source radiation pattern to the system's individual requirements.

However, holograms are not without downsides, a so-called hot spot is produced in the middle of the diffuser pattern. Although careful manufacture can reduce the hot spot intensity, a hot spot may result in a reduction in the maximum permitted transmit power [110]. This issue can be resolved by using an integrating-sphere diffuser, which offers an eye-safe emission power in the range of 100mW–1W [113].

Table 2.1: Safety classification for a point source emitter [106].

	Wavelength			
	1550nm Infrared	1310nm Infrared	880nm Infrared	650nm Visible
Class 1	< 10mW	< 8.8mW	< 0.5mW	< 0.2mW
Class 2	N/A	N/A	N/A	0.2 – 1mW
Class 3A	10 – 50mW	8.8 – 45mW	0.5 – 2.5mW	1 – 5mW
Class 3B	50 – 500mW	45 – 500mW	2.5 – 500mW	5 – 500mW

2.4 Transmission of Optical Wireless Data

The main function of optical transmitters is to convert an electrical signal into optical form and then launch the resulting optical signal into the optical link. Inexpensive infrared sources and the high sensitivity of low-capacitance and low cost silicon detectors in the short wavelength, make the band 780–950 nm the preferred choice for a large number of OW systems. Unfortunately, the Ir radiation in this band is extremely dangerous, as explained in Section 2.3.4, so careful selection of the optical transceiver is essential. The two most common optical emitters for infrared transmission are LDs and LEDs. Choosing one over the other depends on their advantages and limitations, as well as their suitability for a particular system.

In term of safety, LEDs are generally considered eye-safe because they emit light from an extended surface area and can emit over a relatively wide spectral range, whereas LDs may pose a safety hazard since they are a point source so need to comply with eye safety constraints. However, the spectral linewidth of LEDs is broad compared to the spectral linewidth of LDs (typically 25–100 nm for LEDs compared to a linewidth as narrow as 5 nm for LDs). Therefore, systems based on LD emitters can benefit from the use of narrow-band capability to reject ambient light noise [114], [115].

Typically LEDs are used for directed-LOS or hybrid systems where they emit light into semi-angles (at half power) in a range of almost 10^{o}–30^{o}, which is enough to satisfy the angular requirements of such applications. In contrast, divergence in LDs is very narrow, which makes them suitable for use in directed point-to-point links. Alternatively, LD sources can be pointed toward the reflective surface where reflected energy offers a diffuse pattern. While the modulation bandwidth of LEDs is limited to tens of megahertz, the modulation bandwidth of LDs extends from hundreds of megahertz to tens of gigahertz. This makes LDs preferred over LEDs at high communication data rates. Furthermore, LDs present higher electro-optic power conversion efficiencies than LEDs (efficiencies of 30–70% for LDs and 10–20% for LEDs). Another important factor is the cost of components. LEDs generally are low cost while the cost of LDs ranges from moderate to high. Since LDs are the best choice for high speed transmission, they require a diffuser to destroy their spatial coherence and spread radiation over a sufficiently extended emission aperture and emission angle when used in diffuse OW links; a computer-generated hologram may be used [53].

2.5 Reception of Optical Wireless Data

An OW receiver converts the received optical signal into an electrical signal suitable for further processing. The essential part of such a process is the photodetector that collects the signal, which is in the form of optical pulses representing '1' and '0' bits, and converts it directly into electrical current. The photodetector is often positioned behind a front end that consists of a concentrator and an optical filter. The concentrator is used to enhance the collection efficiency of the receptors, while the optical filter can attenuate ambient light noise. The front end is followed by a preamplifier and a detection circuit driven by a clock extracted by a clock recovery module. The main components of the OW receiver are discussed next.

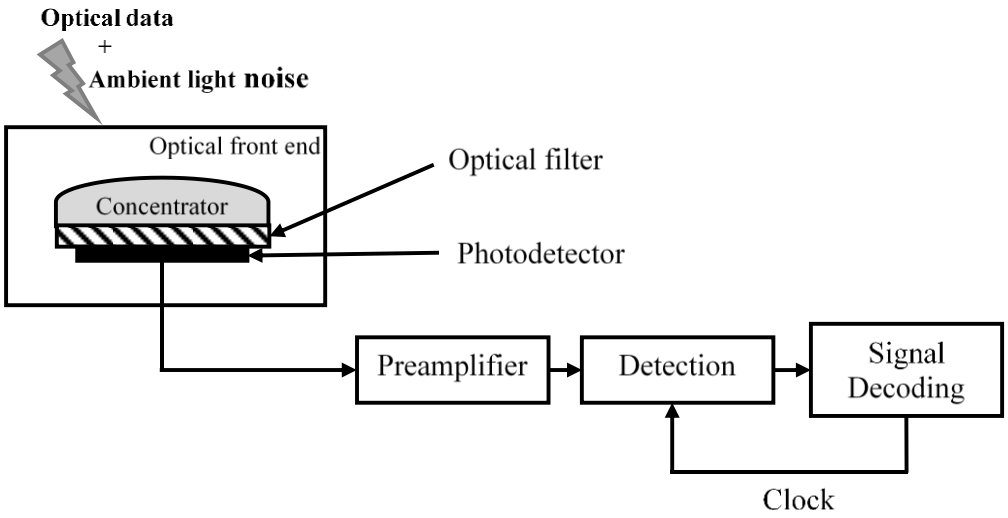

Figure 2.4: Block diagram of a typical OW receiver.

2.5.1 Concentrator

The objective of using an optical concentrator is to improve the collection efficiency of the receiver by transforming a set of rays incident on a large area into a set of rays

emerging from a smaller area that matches a photodetector area. This implies that the optical receiver can use photodetectors with a smaller photosensitive area and hence a lower capacitance. However, a higher level of the collection efficiency leads to collecting more signal power as well as more ambient light power in the form of BN. The influence of BN can be reduced by using optical filters.

In OW systems, optical concentrators may be of an imaging or non-imaging variety. Non-imaging concentrators are commonly used in short-range infrared systems. An idealized non-imaging concentrator [116] with an internal refractive index N_c can achieve a transmission gain:

$$T_C(\delta) = \begin{cases} \frac{N_C^2}{sin^2(\psi_C)}, & where \quad 0 \leq \delta \leq \psi_C \\ 0 & \delta > \psi_C \end{cases}, \tag{2.1}$$

where the concentrator transmission gain $T_C(\delta)$ rapidly approaches zero when the reception angle δ exceeds the concentrator's acceptance semi-angle ψ_C, usually $\psi_C \leq 90^o$. It should be noted that there is a trade-off between the concentrator transmission gain and its acceptance semi-angle where the gain increases when the acceptance semi-angle decreases. The non-directional hemispheric concentrator is a common non-imaging concentrator that can achieve an acceptance semi-angle of 90° and an optical gain of N_C^2 [79]. This optical gain (N_C^2) can be achieved when that the radius r_{hc} of the hemispheric concentrator meets the following condition [117]:

$$r_{hc} \geq N_C \times r_{det}, \tag{2.2}$$

where r_{det} is the photodetector radius. The compound parabolic concentrator (CPC) is another common type of non-imaging concentrators that is widely used in infrared links [17], [116]-[118]. The CPC is an angle-transforming device that concentrates and collects light from a large input area A_{in} down into small detector area A_{det}, yielding an optical gain $G = A_{in}/A_{det}$. It can achieve a much higher optical gain than that of a hemispheric concentrator at the expense of a narrower ψ_c, making it an appropriate choice for directed links. In order to mitigate the influence of ambient light noise and hence improve the SNR, narrow CPC elements can be used along with an angle diversity receiver [118]. An optical filter may be placed on the CPC's front surface, as shown in Figure 2.5.

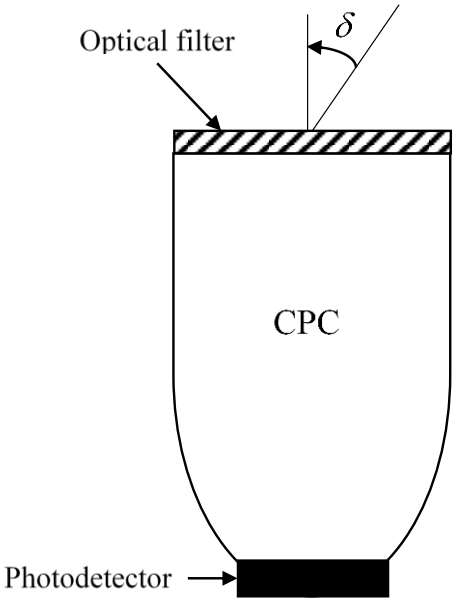

Figure 2.5: Compound parabolic concentrator (CPC) with planar optical filter.

2.5.2 Optical Filter

The dominant noise source in an indoor OW system is ambient background light. To reduce its influence, optical filters can be used before detection by photodiode to limit

the optical bandwidth of the receiver. Optical wireless receivers can use either high pass filters or band pass filters to eliminate ambient radiation. High pass filters allow the passage of light at the wavelength beyond the cut-off wavelength (set near 700 nm in order to stop visible light). The transmission characteristics of high pass filters are substantially independent of the incident angle due to their construction (coloured glass or plastic). Due to this they are the most commonly used optical filters in commercial infrared systems. The transmission of a common high pass filter, superimposed upon the responsivity curve of a typical silicon photodiode, is shown in Figure 2.3 (b).

Bandpass filters, on the other hand, are usually constructed of multiple thin dielectric layers, and rely upon optical interference in the Fabry-Perot cavities formed [36], [84]. Such filters can achieve narrow bandwidth, resulting in superior ambient light rejection (bandwidths below 1 nm are available commercially). However, their transmission characteristics depend heavily on the angle of incidence. In order to enhance the SNR, the optical spectrum of the transmitter must lie within the filter bandwidth. This implies that LD transmitters with narrow optical bandwidth should be used when the filter bandwidth is made smaller.

2.5.3 Photodetector

A photodetector is a square law opto-electronic device that performs the inverse operation of light emitting devices; that is, it converts the incident radiant light into an electrical signal. On account of the fact that the received light in OW links is usually of a very low intensity, the detector should possess these desirable characteristics:

- High efficiency of conversion (responsivity) at the operating wavelength.
- Efficient signal collection process to ensure that it does not introduce additional noise.
- Low-bias voltage requirements are usual in portable devices together with tolerance to temperature fluctuations.

There are a number of additional attractive qualities that most practical applications must possess. The photodetector should be small, lightweight, rugged, reliable, and cost-effective. It also should be insensitive to age (long-lasting) and environment. Two types of photodiodes that are commonly used in OW systems design are silicon PIN photodiodes and Avalanche photodiodes (APDs). Both are available with a large detection area which can increases the collected optical power [21], [119]-[121].

Ordinary PIN photodiodes are currently used in almost all commercial infrared links as a result of being simpler to design, cheaper and require less complex biasing than APDs. The downside is that they are less sensitive. A greater transmitter power and a receiver with a larger lens diameter can be used to compensate for the disparity in sensitivity, however APDs provide an improvement in the link budget due to their power margin. An APD provides an inherent electrical gain through repeated electron ionisation, where photo-generated carriers generate secondary carriers via impact ionisation [121]. The internal gain mechanism helps overcome the thermal noise from preamplifiers and thus increases the receiver SNR. This makes the APD an appropriate choice in direct detection optical receivers when a small amount of BN introduces shot noise. APD-based receivers provide perfect infrared link performance when ambient light is weak [21], [36], [61],

[79]. However, severe degradation in the SNR occurs when ambient-induced noise is dominant [79]. This is a result of an increase in the variance of the shot noise due to the random nature of the internal APD gain.

The basic steady-state operation of a photodiode can be characterised by the instantaneous photocurrent (I_p) it produces in response to an instantaneous optical power (P). The instantaneous photocurrent can be expressed as:

$$I_p = R \cdot P \tag{2.3}$$

where R is the photodiode responsivity (A/W). The responsivity represents the opto-electronic conversion factor from the optical domain to the electrical domain and is a key parameter in link modelling. The responsivity can be modelled as:

$$R = \frac{q\zeta\lambda}{h_p c} \tag{2.4}$$

where q is the electron charge, λ is the wavelength, h_p is the Planck's constant, and c is the speed of light. The internal quantum efficiency of the device is ζ, which represents the probability that an incident photon creates an electron-hole pair. Responsivities of characteristic silicon photodiodes are typically in the range of 0.5–0.75 A/W.

2.5.4 Preamplifier

Optical receiver preamplifiers can be classified into three types, based on their configuration. These types are low impedance, high impedance and trans-impedance preamplifiers. The low impedance configuration is the simplest preamplifier structure.

Although this type is the most straightforward and has a wide bandwidth, it is at the cost of high noise and poor receiver sensitivity in direct detection systems. The high impedance preamplifier, on the other hand, provides high receiver sensitivity, but an equalisation amplifier must be used to compensate the limitation imposed on its frequency response by the front-end RC time constant. In contrast, a trans-impedance amplifier offers a good compromise between the wide bandwidth of the low impedance design and the low noise of the high impedance design. It also provides a large dynamic range and a wide bandwidth due to negative feedback, as well as avoiding the need for equalisation (usually). Therefore it is suitable in most infrared link applications [120]. However, the noise level of the trans-impedance amplifier is higher and its sensitivity is lower than that of the high impedance amplifiers. The level of the noise can be reduced using a field-effect transistor (FET) as a front-end device instead of a bipolar-junction transistor (BJT) [120], [122]. However, a BJT may achieve superior results in terms of power consumption [122]. In this thesis, both trans-impedance amplifiers (FET and BJT) are considered.

2.6 Modulation Techniques

In OW systems, modulation takes place in two steps. First, the transmitted information is coded as waveforms, and these are modulated onto the instantaneous power of the carrier. Since optical wireless links suffer from extensive amplitude fluctuations, direct amplitude modulation is not the preferred choice. The most popular form of optical transmitter is intensity modulation that conveys data on an optical carrier. This section, first defines an

IM/DD channels, and then discuss the most suitable modulation schemes used over an indoor OW channel: On-Off Keying (OOK); and Pulse Modulation (PM).

2.6.1 IM/DD Channel

Modulation techniques for most radio wireless communication systems include frequency, phase or amplitude modulation. In OW communications links, coherent optical transmitters modulate the frequency or phase of an optical carrier directly [75], [108]. However, more expensive narrow-linewidth sources are required in order to detect optical signals, particularly those following diffuse propagation paths [36]. Intensity modulation (IM) is the simplest modulation technique to convey data in an optical carrier, where the waveform of the information is modulated onto the instantaneous power of the transmitted energy at the desired wavelength. IM is the preferred choice due its simplicity, where it can be achieved through the variation of the bias current of a LD or LED. Unlike RF channels, where a data stream is contained in the amplitude, phase or frequency of the carrier, here it is contained in the intensity of the optical carrier in an OW channel. It is worth noting that the transmitted signal must be positive, since the intensity can never be negative. Direct detection (DD) is the most practical down-conversion technique used at the receiver end to recover information, in which a photodetector generates a photocurrent proportional to the received instantaneous optical power as depicted in Figure 2.6. Since the desired waveforms are modulated onto the instantaneous power and typical detector areas are millions of square wavelengths, the output current is proportional to the total received power.

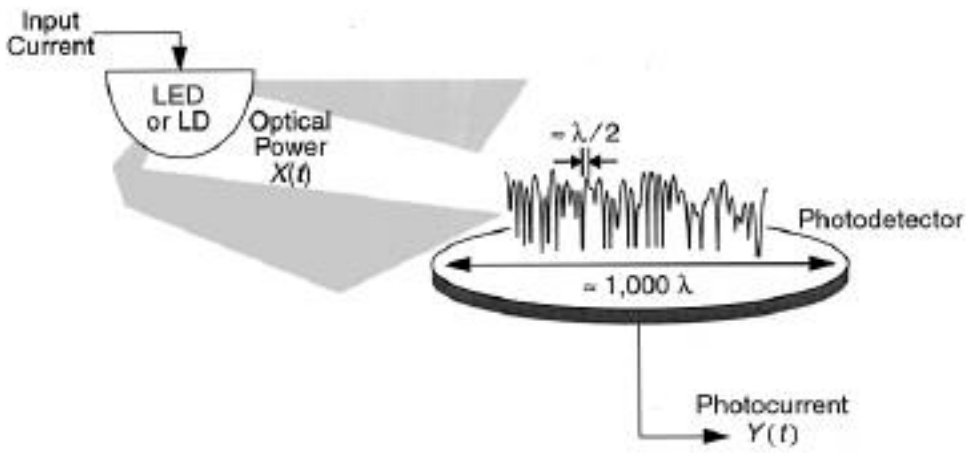

Figure 2.6: Transmission and reception in an infrared link with IM/DD [79].

The modelling of a basic OW channel employing IM/DD is depicted in Figure 2.7. It comprises an infrared source as a transmitter and a photodetector as a receiver. At the transmitter side, the input data stream is converted into a photocurrent varying over time that drives the transmitter to produce optical radiation. The optical signal then reaches the receiver through multipath propagation. A square law detector is used at the receiver side. It squares and then integrates the amplitude of the received electric signal to find the intensity. It then produces a photocurrent proportional to the received instantaneous power; that is, proportional to the square of the received electric signal. The detector in an OW system is illuminated by ambient light sources inducing shot noise. Since the transmitted optical signal arrives at the receiver through various reflective surfaces within a room, the IM/DD channel can be modelled as a baseband linear system, with instantaneous optical power $x(t)$ and received instantaneous photocurrent $y(t)$ that is the integral of the received instantaneous power at the detector surface, and an impulse response $h(t)$, which is fixed for a given transmitter and receiver set-up.

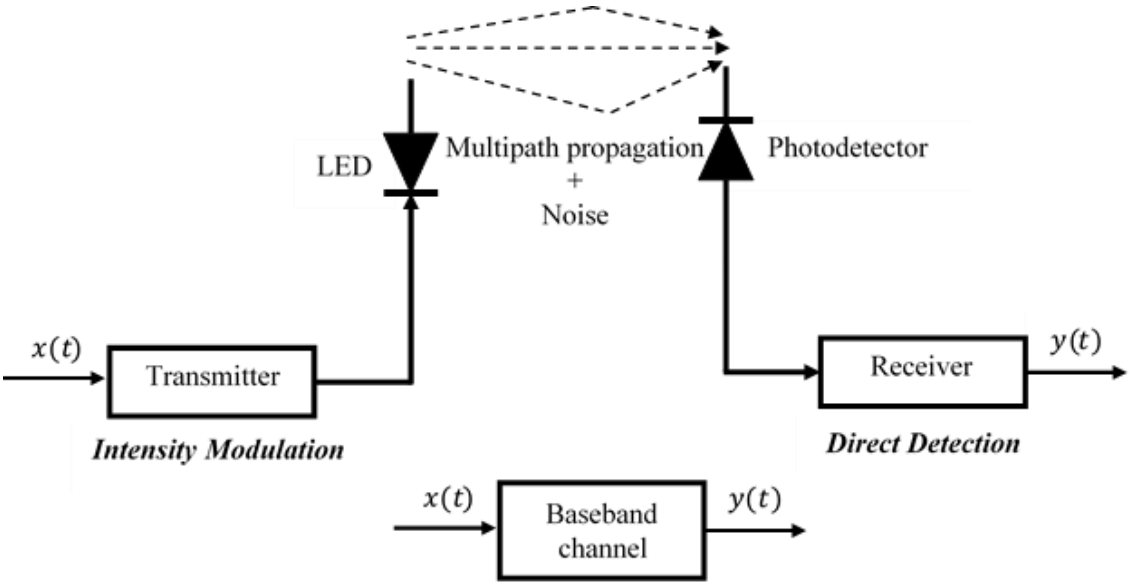

Figure 2.7: Channel model of an OW link.

The indoor IM/DD channel can be characterised by [36]:

$$I(t) = R\, x(t) \otimes h(t) + R\, n(t) \tag{2.5}$$

where t is the absolute time, R is the photodetector responsivity, $\otimes$ denotes convolution, and $n(t)$ is the background noise (BN), which is modelled as white and Gaussian, and independent of the received signal. The possible modulation techniques for indoor OW systems are reviewed next.

2.6.2 On-Off Keying (OOK)

OOK is the most reported modulation scheme for IM/DD in OW communication [36], [61]. In OOK modulation, each bit is simply sent by pulsing the light source (LDs or LEDs) on or off during each bit period. A '1' bit is encoded when the light source is ON and an optical signal is transmitted, and a '0' bit is encoded when no signal is transmitted (no pulse).

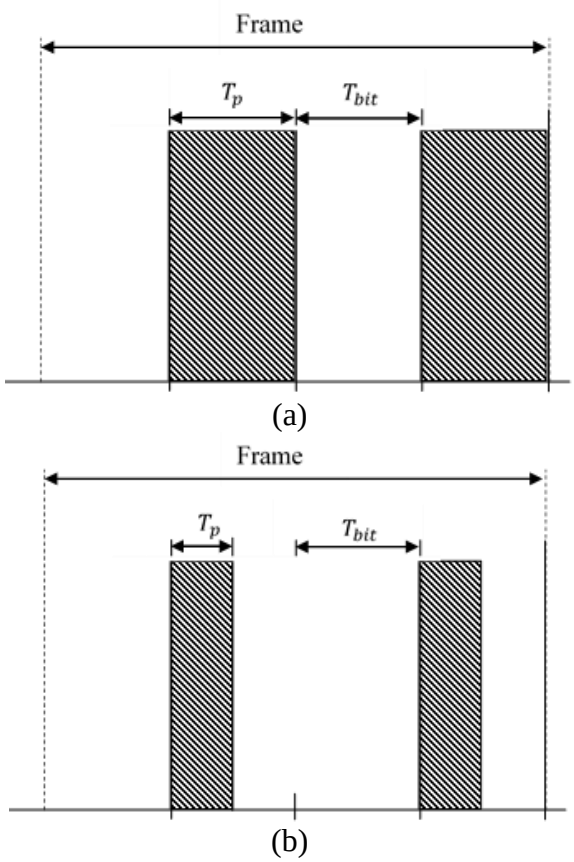

Figure 2.8: Basic OOK signal.

Two modulation schemes can be driven from OOK modulation, namely non-return-to-zero OOK (NRZ-OOK) and return-to-zero OOK (RZ-OOK), with for example a 50% duty cycle for RZ, as shown in Figure 2.8. In the NRZ-OOK scheme, a pulse with duration (T_p) equal to the bit duration (T_{bit}) is transmitted to represent one, while the pulse occupies only the partial duration of bit in the RZ-OOK scheme. NRZ-OOK provides high bandwidth efficiency at the cost of high average power, whereas the bandwidth efficiency of RZ-OOK depends on the duty cycle. Due to the simplicity of the OOK modulation technique and the ability of LD/LED to switch on and off at rates into Gbit/s, OOK is an appropriate modulation scheme for high bit rate OW systems [20], [22], [23], [30]. However, the effect of multipath dispersion is significant at these rates. Several

techniques can be used to mitigate the impact of multipath dispersion such as the use of equalisation techniques [20], [30], [123], [124].

2.6.3 Pulse Position Modulation (PPM)

Infrared communication links require high average-power efficiency to minimise ocular hazards and power consumption. Pulse position modulation is a modulation format that can achieve high average power efficiency at the cost of relatively poor bandwidth efficiency [67], [125], [126]. Therefore, PPM is more susceptible to multipath-induced ISI than OOK. PPM is an orthogonal modulation technique in which a block of $log_2 L$ input bits is mapped to one of L distinct waveforms. PPM uses frames (a single symbol time) consisting of L time slots. In each frame, a constant power is transmitted during one of these time slots, while $L - 1$ slots remain empty. Each frame can be concluded by a guard interval to avoid interframe interference and help for timing extraction purposes. However, a larger bandwidth may be required as a result of inclusion of guard intervals. A 16-PPM scheme with a guard interval is illustrated in Figure 2.9, in which the frame with T_{frame} is divided into L slots with T_{slot} duration.

The PPM modulation scheme has been widely used in optical communication systems [63], [64], [127]-[134]. Pérez-Jiménez et al. proposed an improved PPM where pulses have a raised-cosine shape [135] providing 30 per cent more bandwidth efficiency than basic PPM. It has been reported that PPM performance can be improved by adopting a trellis-coded modulation (TCM) [136] designed to maximise the minimum Euclidean distance between allowed signal sequences. Furthermore, in conjunction with code

division multiple access (CDMA), PPM has been shown to support a number of concurrent users [129], [137]. Kaluarachi et al. in [138] proposed a digital pulse interval modulation (DPIM) scheme where pulses can be transmitted in a variable length frame rather than the fixed frame used in PPM. Data in DPIM can be encoded as a number of slots between adjacent pulses which provides higher transmission capacity than PPM.

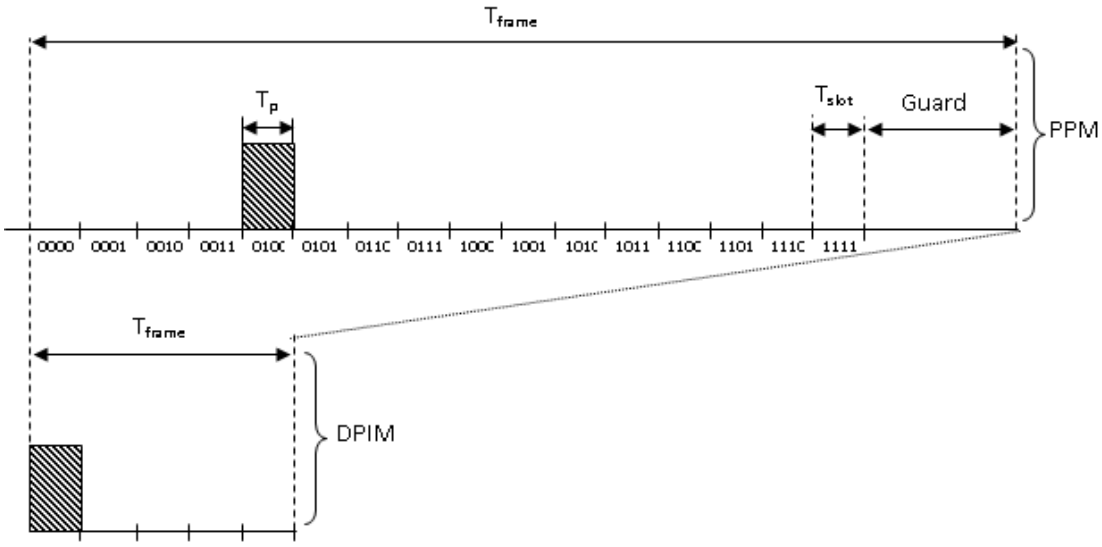

Figure 2.9: Transmission signal for 4 bits in 16 time slots 16-PPM and DPIM.

2.7 OW Applications and Standards

The importance of the infrared technology has been demonstrated by the range of available applications that incorporate Infrared Data Association (IrDA) ports. The non-profit organization, IrDA, was established in 1993 by a group of industry organisations such as IBM, Hewlett-Packard and Intel with other large computer players such Microsoft and Apple. It was formed in order to develop and publish the hardware and software standards used in infrared communication links. The standards published since then by

IrDA cover a broad range of applications, including appliances, telecommunication and computing devices. IrDA is used in excess of 300 million electronic devices such as desktop PCs, notebooks, tablet PCs, printers, digital cameras, mobile phones, personal digital assistants (PDAs), toys, and so forth [63], [64]. Over the last decade, the IrDA has developed and endorsed standards for the following signal rates: 2.4 kbit/s; 9.6 kbit/s; 19.2 kbit/s; 38.4 kbit/s; 57.6 kbit/s; 115.2 kbit/s; 0.576 Mbit/s; 1.152 Mbit/s; 4 Mbit/s; and 16 Mbit/s [63], [64], [86], [93]. Bit rates of up to 115.2 kbit/s employ RZ-OOK modulation with a duty cycle of 0.1875, while links that operate at 0.576 Mbit/s and 1.152 Mbit/s employ RZ-OOK with a duty cycle of 0.25. Links operating at 4 Mbit/s utilise a 4-PPM modulation scheme with pulse duration of 125 ns [63]. The IrDA developed a standard called Very Fast Infrared (VFIr) for data rates of 16 Mbit/s [93]. Using this standardisation, infrared can be extended to applications and settings that require connectivity beyond 4 Mbit/s [86].

The IrDA is currently developing standards for faster data rates beyond 100 Mb/s, and has issued standards for 1 Gb/s OW communications [139]. Following these developments, several companies have introduced products that make use of optical wireless technology, and many other such products are entering the market [131]-[133].

2.8 Summary

This chapter has provided a literature review of the main issues associated with the physical layer of an OW communication system. It gave an overview of OW links classifications (LOS and diffuse). Special attention was given to the design challenges of

indoor OW systems, including ambient light noise, multipath dispersion, high photodetector capacitance, and eye safety. An overview of the methods proposed to reduce the effects of these impairments, was also presented. This chapter has also addressed various communication scenarios, system transmission-receiving components and the most common modulation techniques in OW communication links. The chapter concluded by giving an overview of the current commercial infrared wireless systems and described the associated standards.

3 Indoor Optical Wireless Channel Modelling

3.1 Introduction

To understand the performance limits and design challenges of indoor OW links, thorough characterisation of the OW channel is essential. This is performed by evaluating its impulse response, which can be used to analyse channel distortion. This chapter investigates models for indoor optical wireless channels, formed by a transmitter and receiver through the use of simulation tools. Simulation packages are based on geometrical modelling of indoor environments using a recursive method, which includes multiple reflection orders. Background noise and multipath propagation are the major challenges with indoor optical wireless channels, and can reduce the received optical power and hence significantly degrade system performance. The former degrades the signal-to-noise ratio (SNR), while the latter limits the maximum achievable data rate.

Optical wireless links are often categorised into two basic schemes: direct line-of-sight (LOS) and diffuse systems. Direct LOS links rely upon a direct path between the transmitter and receiver, while diffuse systems generally rely upon light reflected by walls, ceilings and other diffuse reflecting surfaces. Direct LOS links provide high power efficiency and minimise multipath dispersion, but can suffer from shadowing. Diffuse systems are robust against signal blockage and shadowing, enabling mobile users to connect and collaborate instantly in a wireless environment. However, they are more prone to multipath dispersion, which causes pulses to spread and create inter-symbol

interference (ISI), in addition to poor power efficiency and a much-reduced data rate compared to direct LOS links. A diffuse transmitter can be replaced by multibeam transmitters, leading to a considerable SNR improvement that reduces multipath dispersion and mitigates shadowing. A multibeam transmitter benefits from the advantages of both direct LOS and non-LOS components. One way to achieve a multibeam transmitter involves using a computer-generated hologram as a beam splitting element, as in [43], [53], or using multiple narrow-beam transmitters, as in [32], [140]. Significant performance improvement can be achieved through the use of a line strip multi-spot diffusing system (LSMS) [98], [100], [102]. Another multibeam geometry that can improve system performance is the beam clustering method [104], [105]. The performance of OW communication links can be further enhanced by reducing the multipath dispersion and ambient noise through the use of diversity receiver [54]-[60], [140]-[152].

In this work, the performance of the pure diffuse system (CDS) and two multibeam configurations (LSMS and BCM), in conjunction with a single wide FOV receiver and an angle diversity receiver, is evaluated under the constraints of ambient light noise, multipath dispersion and mobility. Simulation carried out using MATLAB and its results are presented in Section 3.8. These attractive multibeam geometries (LSMS and BCM) will be considered as baselines, in addition to the CDS, to facilitate comparisons with new systems presented later in the thesis.

3.2 Channel Characteristics

Intensity modulation (IM) is the most viable modulation technique for indoor OW communication links in which the desired waveform is modulated onto the instantaneously transmitted power. The most practical down-conversation technique is direct detection (DD), whereby a photodetector generates a current that is proportional to the instantaneous received optical power [36]. The indoor OW channel using IM/DD may be modelled as a baseband linear system and characterised by its impulse response $h(t)$ [99],

$$I(t, Az, El) = \sum_{m=1}^{M_t} R\, x(t) \otimes h_m(t, Az, El) + \sum_{m=1}^{M_t} R\, n_m(t, Az, El), \qquad (3.1)$$

where t is the absolute time, Az and El are the directions of arrival in azimuth and elevation angles, M is the total number of reflecting elements, $x(t)$ is the transmitted instantaneous optical power, $\otimes$ denotes convolution, and $n_m(t, Az, El)$ represents the received background noise at a receiver, which is modelled as white and Gaussian, and independent of the received signal. $R = 0.5\ A/W$ is the photodetector responsivity and $I(t, Az, El)$ is the received instantaneous current at the output of the photodetector at a certain position, due to M reflecting elements. The size of the photodetector is in the order of thousands of wavelengths, leading to an efficient spatial diversity that prevents multipath fading. It should be noted that the $x(t)$ in (3.1) represents power rather than amplitude, which implies that the signal must be non-negative: that is, $x(t) \geq 0 \quad \forall\, t$. Also, average transmitted power should not exceed the value specified by eye safety standards.

3.3 Simulation Environment

In order to assess the effect of diffuse transmission on the performance of indoor OW systems under the impact of multipath propagation, user mobility and background noise, simulations were developed in a rectangular room. For comparison purposes, three baseline systems, namely CDS, LSMS and BCM, were simulated, based on a mathematical formulation using a ray-tracing algorithm built in MATLAB. The simulation was performed in an empty rectangular room of 8m × 4m × 3m (length × width × height). Experimental measurements have shown that most building materials, including plaster walls but with the exception of glass, are approximately Lambertain reflectors [9]. In this study, it was assumed that all the reflecting surfaces in the set-up room were Lambertain reflectors of high reflectivity (reflection coefficient of 0.8 for walls and ceiling, 0.3 for floor). Reflections from doors and windows were considered to be the same as reflections from walls.

A realistic indoor environment is considered in Chapter 4. To model the reflections, the room's reflecting surfaces were divided into a number of equally sized square-shaped reflection elements of area dA and reflection coefficient ρ. These elements acted as secondary emitters and were modelled as Lambertian reflectors. Reflections up to second order were considered, since third-order reflections and higher produce a weak contribution to the received optical power, as shown in previous investigations [9], [16], [23], [33], [108]. The size of the surface element dA controls the accuracy of the received impulse response shape, and therefore a surface element size of 5cm × 5cm for first-order reflections, and 20cm × 20cm for second-order reflections were used for all the

configurations considered. The chosen values kept computation time within reasonable time limits and measures. These element sizes, particularly for first-order reflections, captured the important feature sizes in the room and smaller element sizes did not result in any significant improvement in the accuracy of the received impulse response shape [56].

In order to simulate the proposed systems (CDS with a wide FOV receiver; LSMS and BCM both with an angle diversity receiver) under mobility, all configurations used an upright transmitter with 1 W optical power, and the transmitter was placed at three different locations on the CF: (2m, 4m, 1m), (1m, 1m, 1m) and (2m, 7m, 1m). In multibeam configurations, computer-generated holograms (CGH) are assumed to be mounted on the emitter to shape its output to multiple narrow beams that, in turn, form a lattice of diffusing spots on the ceiling (LSMS configuration), and on the ceiling and two end walls (BCM configuration). CGHs can be used to generate static beam intensities [43], [53]. To facilitate the characterisation of the received data, the receiver was located at different positions along the x-axis of the communication floor (CF) with a photosensitive area of 1cm^2. The room illumination was assumed to be provided by eight spotlights placed at equidistant distances on the ceiling. These lamps represent ambient background noise, for which the model is given in Section 3.5.

3.4 Multipath Propagation Model

An optical signal emitted by a transmitter reaches a receiver through paths of various lengths. These depend on the relative positions of the transmitter, reflectors and receiver,

in addition to the movement of surrounding objects and people. However, changes on paths are slow in comparison with the transmission data rate, thus the channel is stationary for a given fixed configuration. In multipath propagation, different components arrive at the receiver at different times. This causes the transmitted signal to spread resulting in ISI that limits the transmission rates. Note that the increase in the difference in paths length that separate the shortest and longest paths leads to an increase in multipath dispersion. Multipath propagation can be fully characterised by the channel impulse response $h(t)$, which can be represented approximately as a scaled and delayed Dirac delta functions [16].

In order to assess the impact of multipath dispersion, the impulse response has to be evaluated. Simulation packages based on a ray-tracing algorithm were developed for arbitrary configurations of transmitter and receiver in a rectangular room, as described in Section 3.3. The room was divided up into a number of discrete reflection elements (diffuse reflectors), which were assumed to be ideal Lambertian reflectors. For instance, when a transmitter placed at the ceiling pointed down and a receiver on communication floor, transmitted signal reaches the receiver through different paths at different times. Since third-order reflections and higher do not produce a significant change in the received optical power, reflections up to second-order are considered. Thus, three paths are traced in our channel model including LOS path, first- and second-order paths. The received instantaneous optical power for LOS, first- and second reflections can be computed using (3.10), (3.14) and (3.17), respectively. Temporal discretisation is occurred due to dividing the room to a number of reflecting elements, resulting in a finite

sum of scaled delta function. The effect of discretisation can be reduced by subdividing time into bins of widths Δt and grouping the powers received within each bin into a single received power. This accounts for the smoothness seen in the resulting impulse responses presented in this thesis.

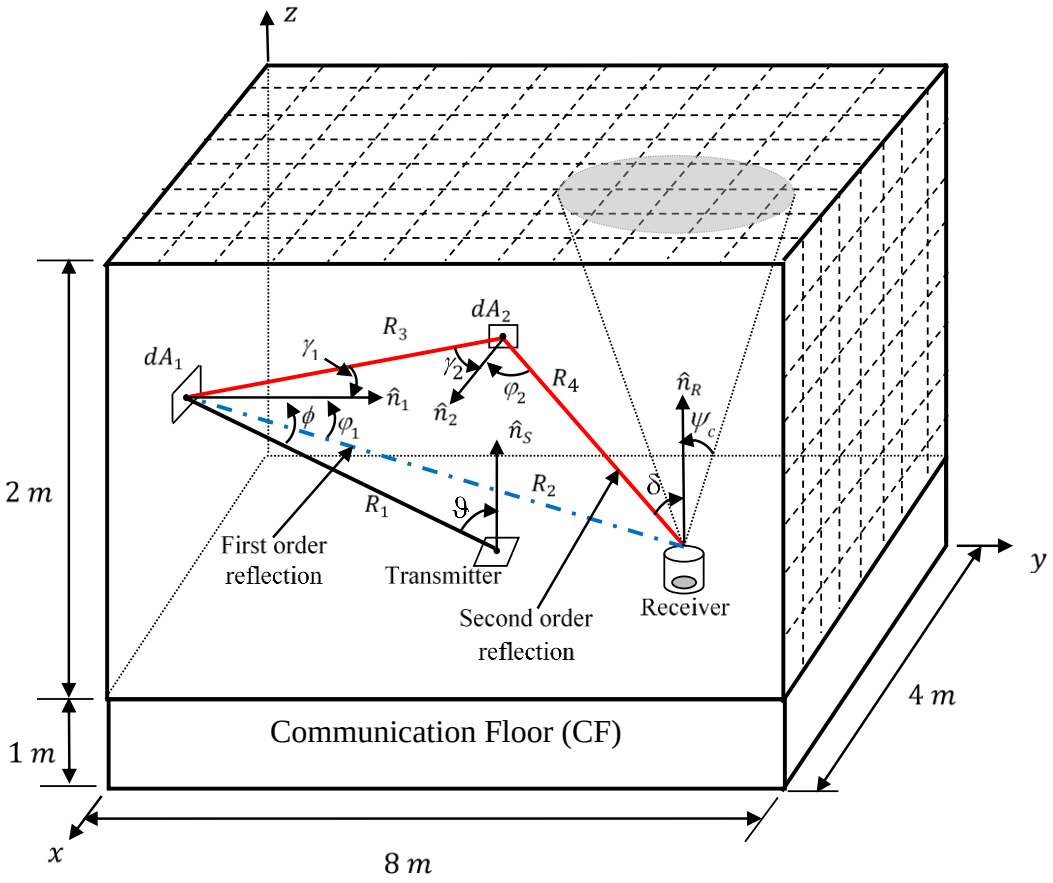

Figure 3.1: Ray tracing set-up for OW channel.

In this work, the received optical powers and delays for all reflection surfaces were calculated and combined at the receiver to produce the channel impulse response. Theoretically, an OW signal undergoes an infinite number of reflections, and therefore the channel impulse response can be given as:

$$h(t) = \sum_{k=0}^{\infty} h^{(k)}(t)\,, \tag{3.2}$$

where $h^{(k)}(t)$ is the impulse response due to the k^{th} reflection. Since up to second-order reflections are considered, k takes values of 0, 1, and 2. Figure 3.1 shows the ray-tracing set-up for OW channel when full diffuse transmission is employed. The transmitter and receiver models and the reflections analysis are defined in Section 3.4.1.

3.4.1 Source and Receiver Models

A wide-beam optical source can be represented by a position vector r_s, a source power P_s, a source unit vector (the normal perpendicular to the plane on which the source is placed) $\hat{n}_s$, and a radiation intensity pattern $R(\vartheta)$.[1]. The radiation intensity pattern $R(\vartheta)$ may be defined as the optical power emitted from the transmitter at angle ϑ with respect to $\hat{n}_s$ per unit solid angle. A diffuse source with a generalised Lambertain radiation pattern can be described as in [9]:

$$R(\vartheta) = \frac{n+1}{2\pi} P_s cos^n(\vartheta), \quad -\frac{\pi}{2} \leq \vartheta \leq \frac{\pi}{2}, \tag{3.3}$$

where n is the mode number that determines the shape of the radiation beam, where the higher the n, the narrower the light beam. A transmitter source emits radiation in ideal Lambertian distribution $(n = 1)$, with a half-power semi-angle equal to 60°. The coefficient $((n+1)/2\pi)$ ensures that integrating $R(\vartheta)$ over the surface of a hemisphere

[1] To simplify notation, a point source S can be denoted by $S = \{r_S, \hat{n}_s, n\}$.

results in the total average source power P_s. The n mode number of the transmitted beam is related to the half-power semi-angle (hps), thus can be given as:

$$n = \frac{-ln(2)}{ln\big(cos(hps)\big)}, \tag{3.4}$$

A single receiving element may be represented in a similar way to an optical source. It can be characterised by its position r_R, its orientation $\hat{n}_R$, detector area A_R, and FOV. The scalar angle FOV is defined so that a receiver only detects light rays whose angles of incidence with respect to the receiver normal $\hat{n}_R$ are less than FOV. Accordingly, changing the receiver's FOV can eliminate unwanted reflections or noise. The optical receiver detects an optical power directly proportional to its effective light-collection area $A_{eff}(\delta)$, which can be given as [36]:

$$A_{eff}(\delta) = A_R\, cos(\delta)\, rect(\delta/FOV)\,, \tag{3.5}$$

where δ is the angle of reception with respect to the receiver normal $\hat{n}_R$, and the rectangular function $\big(rect(\delta/FOV)\big)$ is defined by:

$$rect(\delta/FOV) = \begin{cases} 1 & for \quad (\delta/FOV) \leq 1 \\ 0 & for \quad (\delta/FOV) > 1 \end{cases}, \tag{3.6}$$

Increasing the photodetector area leads to an increment in the received optical power, however it is expensive and tends to decrease receiver bandwidth and increase receiver noise. Therefore, adding a concentrator and filter in front of the detector can help to increase the effective area and attenuate the ambient light, and can be presented as:

$$A_{eff}(\delta) = T_F(\delta)\ T_C(\delta)\ A_R\ cos(\delta)\ rect\left(\delta/\psi_C\right), \tag{3.7}$$

where $T_F(\delta)$ is the filter transmission factor, $T_C(\delta)$ is the concentrator transmission factor, and ψ_C is the concentrator FOV (semi-angle). In our calculation, the angle of the incident ray with respect to the source normal; the angle of the reflected ray with respect to the normal of the reflecting surfaces; and the angle of the received ray with respect to the normal of receiver take values between $-90°$ and $90°$.

3.4.2 Line-of-Sight and Multiple-Order Reflections Models

Experimental measurements in an indoor communication environment have shown that a wide variety of common building materials are efficient diffuse infrared reflectors [9]. In this study, it is assumed that all reflection elements in indoor settings approximate ideal Lambertain reflectors with $n_{element} = 1$. It was found through previous investigations that third-order reflections and higher make a small contribution to the received optical power [9], [16], [36], [53], so reflections up to second order are considered in this study.

The channel impulse response can be obtained by tracing all possible rays from the emitting source (transmitter and reflection elements) to the receiver, then calculating the power and the time associated with each ray. The time taken for a light ray to travel from a source to the receiver may be computed by dividing the ray path by the light velocity in free space. Based on the incidence angle of a light ray, the optical power received (dP) on a square surface element with area (dA) due to a Lambertian source can be expressed as:

$$dP = R(\vartheta)\frac{dA}{R^2}\,cos(\phi)\,, \tag{3.8}$$

where R is the distance between the source and the surface element and ϕ is the angle of the incident ray with respect to the surface element normal. The reflecting surface element then becomes a secondary emitter with total radiated power (P_{dA}), dependent on its reflection coefficient (ρ), and can be given as:

$$P_{dA} = \rho\, dP\,, \tag{3.9}$$

In order to calculate the received power at an optical receiver, a ray-tracing algorithm can be used. The ray-tracing set-up for first- and second-order reflections, in the case of a fully diffuse configuration (where both transmitter and receiver are placed on the CF pointing straight upward), is shown in Figure 3.1. The analyses of LOS, first-order reflections and second-order reflections are defined next.

3.4.2.1 Line-of-Sight (LOS) Analysis

A LOS link occurs when a source and receiver have a clear, direct line of sight between them; that is, the receiver on the CF faces upwards and the source on ceiling faces downwards (see Figure 3.2). The LOS link depends on the distance between the source and the receiver (R_d) and on their orientation with respect to LOS. It should be noted that the transmission from LOS source can be modelled reasonably using a generalised Lambertian radiant intensity. Using the source and receiver models described in Section 3.4.1, the LOS component can be calculated as:

$$P_{LOS}^{(0)} = \frac{n+1}{2\pi R_d^2} P_s \, T_F(\delta) \; T_C(\delta) \, A_R \cos^n(\vartheta_d) \cos(\delta) \, rect\left(\delta / \psi_C\right), \qquad (3.10)$$

where ϑ_d is the angle of incidence of the direct ray with respect to the source normal.

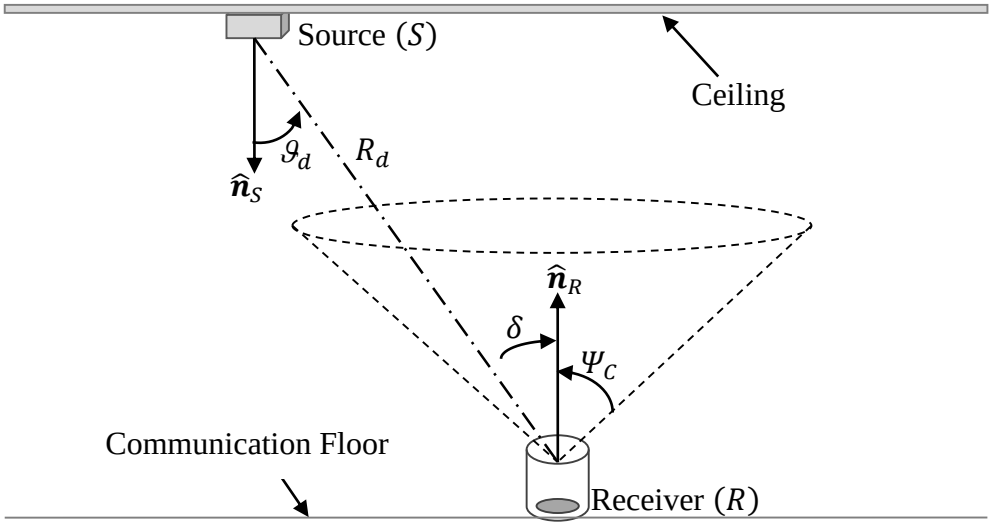

Figure 3.2: Direct Line-of-Sight model.

3.4.2.2 First-Order Reflections Analysis

Given a particular source and receiver in a room with ideal Lambertian reflectors, a light ray can reach the receiver through a reflection element, deriving first-order reflection as shown in Figure 3.3. The power received by a surface element with an area dA_1 and a reflection coefficient ρ_1 in the first-order reflection can be modelled as:

$$P_{reflection}^{(1)} = \frac{n_{element}+1}{2\pi R_2^2} \, P_{dA_1} \; cos^{\,n_{element}}\left(\varphi_1\right) A_{eff}(\delta), \qquad (3.11)$$

where φ_1 is the angle of the reflected ray towards the receiver with respect to the normal of dA_1 and R_2 is the distance between the surface element dA_1 and the receiver. dP_{dA_1} is the optical power received on a reflecting surface with an area dA_1due to a Lambertian source with $n = 1$, can be calculated by subtitling equation (3.3) into (3.8)

$$dP_{dA_1} = \frac{n+1}{2\pi R_1^2} P_s \, dA_1 \, \cos^n(\vartheta) \, cos(\phi), \tag{3.12}$$

where R_1 is the distance between the transmitter and the surface element dA_1. The surface element dA_1 becomes a secondary transmitter, emitting optical power P_{dA_1} in a Lambertain pattern with $n = 1$, and can be calculated as:

$$P_{dA_1} = \rho_1 \, dP_{dA_1} = \frac{n+1}{2\pi R_1^2} P_s \, dA_1 \, \rho_1 \cos^n(\vartheta) \, cos(\phi), \tag{3.13}$$

The total received power due to first-order reflection $P_{reflection}^{(1)}$ can be written by substituting equations (3.7) and (3.13) into (3.11)

$$P_{reflection}^{(1)} = \frac{(n+1)(n_{element}+1)}{4\pi^2 R_1^2 R_2^2} \rho_1 P_S T_F(\delta) T_C(\delta) dA_1 A_R \cos^n(\vartheta) \cos(\phi) \cos^{n_{element}}(\varphi_1) \cos(\delta) rect(\delta/\psi_C), \tag{3.14}$$

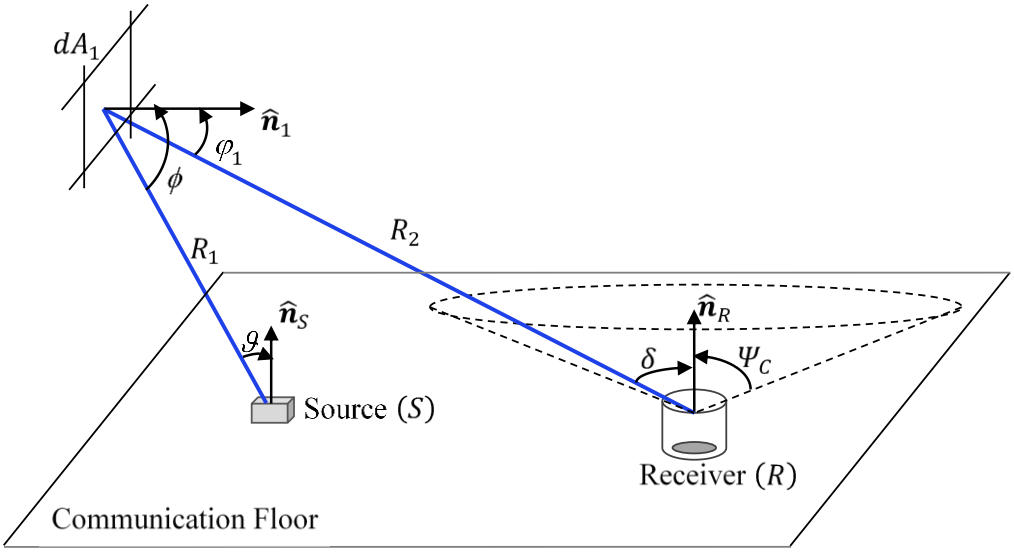

Figure 3.3: Ray tracing for first-order reflection analysis.

3.4.2.3 Second-Order Reflections Analysis

The second-order reflection occurs when the light is reflected again by additional surfaces, using the Lambertian model once more, and can be computed following the analysis shown in the previous section. By observing Figure 3.4, the optical power that is reflected by the surface element dA_1 and is received at a surface element with an area dA_2 can be given as:

$$dP_{dA_2} = \frac{n_{element} + 1}{2\pi R_3^2} P_{dA_1} \, dA_2 \, \cos^{n_{element}}(\gamma_1) \, cos(\gamma_2), \tag{3.15}$$

where $\gamma_1$and $\gamma_2$are the angles of the reflected ray towards the surface element dA_2 with respect to the normal of surface elements $\hat{\boldsymbol{n}}_1$ and $\hat{\boldsymbol{n}}_2$, respectively. R_3 is the distance between the two reflecting surfaces. The reflecting surface element dA_2 with a reflection coefficient ρ_2 can be modelled as a Lambertian source with $n_{element} = 1$, and therefore the radiated power can be written in a way similar to Equation (3.9):

$$P_{dA_2} = \rho_2 \, dP_{dA_2} \, , \tag{3.16}$$

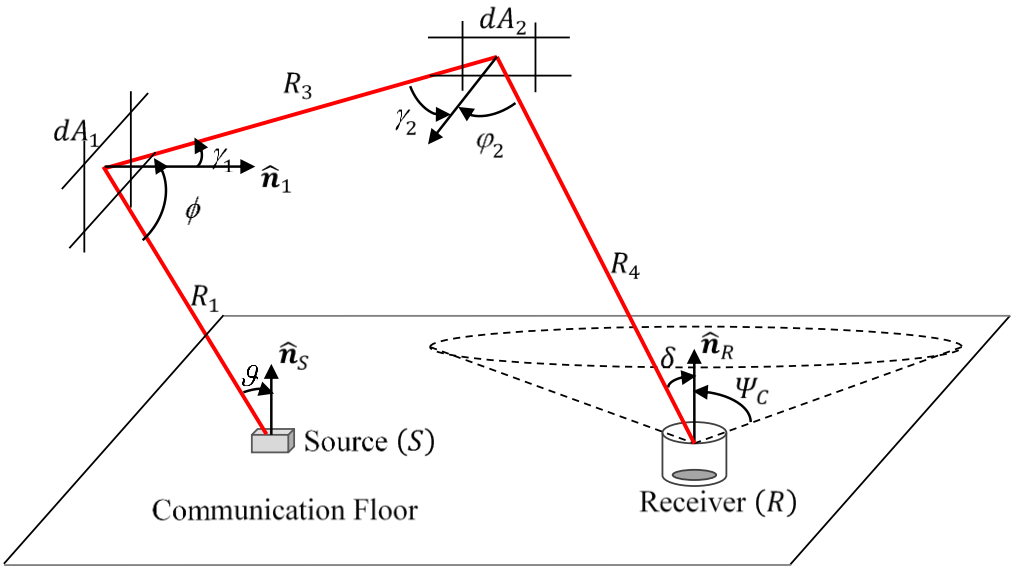

Figure 3.4: Ray-tracing model for second-order reflection.

and the total power at the receiver is given as:

$$P_{reflection}^{(2)} = \frac{(n+1)(n_{element}+1)^2}{8\pi^3 R_1^2 R_3^2 R_4^2} \rho_1 \rho_2 P_S T_F(\delta) T_C(\delta) dA_1 dA_2 A_R \cos^n(\vartheta) \cos^{n_{element}}(\gamma_1) \cos(\gamma_2) \cos^{n_{element}}(\varphi_2) \cos(\delta) rect(\delta/\psi_C), \quad (3.17)$$

where φ_2 is angle of the reflected ray towards the receiver with respect to the normal of dA_2 and R_4 is the distance between the surface element dA_2 and the receiver. Considering the power received via LOS, first- and second-order reflections, the total optical power combined at the receiver can be given as:

$$P_{Total} = P_{LOS}^{(0)} + \sum_{i=1}^{M} P_{reflection_i}^{(1)} + \sum_{i=1}^{N} P_{reflection_i}^{(2)}, \quad (3.18)$$

where M and N are the total number of reflecting elements for the first and second order reflections in the room, respectively.

Observing Figure 3.1, the simulation parameters R_1, R_2, R_3, R_4, R_d, ϑ, ϑ_d, ϕ, φ_1, φ_2, γ_1, γ_2, δ_1, δ_2 and δ_d can be calculated as in Table 3.1, where $\boldsymbol{r}_1$ and $\boldsymbol{r}_2$ are the positons of the surface elements dA_1 and dA_2, respectively. It should be noted that position vectors are in Cartesian coordinates (x, y, z) and are used in the same format throughout this study. The reception angle δ is here classified into three angles δ_1, δ_2 and δ_d, according to the type of the received component, where δ_d is the angle associated with the direct LOS component and δ_1 and δ_2 are with first- and second-order reflections, respectively. Subdividing the room into discrete elements leads, moreover, to temporal discretisation, turning the impulse response from continuous function of time to scaled delta functions.

Table 3.1: Ray-tracing algorithm calculation.

Link distance[2]	**Associated angles**	
	Transmission angle[3]	**Reception angle**[4]
$R_1 = \lvert\mathbf{r}_1 - \mathbf{r}_S\rvert = \sqrt{(x_1 - x_S)^2 + (y_1 - y_S)^2 + (z_1 - z_S)^2}$	$\cos\vartheta = \hat{\mathbf{n}}_S \cdot \frac{(\mathbf{r}_1 - \mathbf{r}_S)}{R_1}$	$\cos\phi = \hat{\mathbf{n}}_1 \cdot \frac{(\mathbf{r}_S - \mathbf{r}_1)}{R_1}$
$R_2 = \lvert\mathbf{r}_R - \mathbf{r}_2\rvert = \sqrt{(x_R - x_2)^2 + (y_R - y_2)^2 + (z_R - z_2)^2}$	$\cos\varphi_1 = \hat{\mathbf{n}}_1 \cdot \frac{(\mathbf{r}_R - \mathbf{r}_1)}{R_2}$	$\cos\delta_1 = \hat{\mathbf{n}}_R \cdot \frac{(\mathbf{r}_2 - \mathbf{r}_R)}{R_2}$
$R_3 = \lvert\mathbf{r}_2 - \mathbf{r}_1\rvert = \sqrt{(x_2 - x_1)^2 + (y_2 - y_1)^2 + (z_2 - z_1)^2}$	$\cos\gamma_1 = \hat{\mathbf{n}}_1 \cdot \frac{(\mathbf{r}_2 - \mathbf{r}_1)}{R_3}$	$\cos\gamma_2 = \hat{\mathbf{n}}_2 \cdot \frac{(\mathbf{r}_1 - \mathbf{r}_2)}{R_3}$
$R_4 = \lvert\mathbf{r}_R - \mathbf{r}_2\rvert = \sqrt{(x_R - x_2)^2 + (y_R - y_2)^2 + (z_R - z_2)^2}$	$\cos\varphi_2 = \hat{\mathbf{n}}_2 \cdot \frac{(\mathbf{r}_R - \mathbf{r}_2)}{R_4}$	$\cos\delta_2 = \hat{\mathbf{n}}_R \cdot \frac{(\mathbf{r}_2 - \mathbf{r}_R)}{R_4}$
$R_d = \lvert\mathbf{r}_R - \mathbf{r}_S\rvert = \sqrt{(x_R - x_S)^2 + (y_R - y_S)^2 + (z_R - z_S)^2}$	$\cos\vartheta_d = \hat{\mathbf{n}}_S \cdot \frac{(\mathbf{r}_R - \mathbf{r}_S)}{R_d}$	$\cos\delta_d = \hat{\mathbf{n}}_R \cdot \frac{(\mathbf{r}_s - \mathbf{r}_R)}{R_d}$

To achieve temporal smoothing comparable to the actual $h^k(t)$, time is broken into bins of width Δt and the total power received in each bin is grouped, while an identical histogram is achieved, as Δt and dA approach zero. A good choice for the time interval is $\Delta t = \sqrt{dA}/c$, which is roughly the time light takes to travel between neighbouring reflective elements [16]. It should be noted that reducing the surface elements size also results in improved resolution in impulse response evaluation, increasing the computation time. Thus the surface element size dA has to be chosen in order to keep the computation time within acceptable limits [9], [16], [32], [33].

[2] The distance between the ray source and reception.
[3] The angle of transmission with respect to the normal of the source.
[4] The angle of reception with respect to the normal of destination.

3.5 Ambient Light Modelling

Unlike fibre optic systems, indoor OW communication systems are subjected to artificial ambient light such as incandescent and fluorescent lamps. At an optical receiver, ambient light can be received at an average power much larger than the desired signal, resulting in electrical currents causing shot noise. Certain measures such as optical filters can be employed to reduce the influence of background noise [78]. Natural and artificial light sources both contribute to the generation of shot noise on the optical receiver photodiode. Interference from daylight through windows and doors is not considered in this study (a usual practice in OW studies due to the more damaging effect of artificial light sources, especially spot lights which cause burnout effects when the receiver is placed directly under such a source [73], a more accurate study should however include the effects of day light through windows and doors). For the characterisation of background noise induced by ambient light, the room was illuminated by eight halogen spotlights (Philips PAR 38 Economic (PAR38)), which caused high levels of optical spectral corruption to the received data stream. The Philips PAR38 emits an optical power of 65 W in a Lambertain beam with $n_{Lamp} = 33.1$, which corresponds to $hps = 11.7^{o}$ based on experimental measurements [27], [73]. The eight spotlights were spaced regularly across the ceiling at 1m distance from all walls and equal separation distances of 2m, as shown in Figure 3.5. The Cartesian coordinates of the eight lamps are (1m, 1m, 3m), (1m, 3m, 3m), (1m, 5m, 3m), (1m, 7m, 3m), (3m, 1m, 3m), (3m, 3m, 3m), (3m, 5m, 3m), and (3m, 7m, 3m). An ambient light source such as incandescent lamp can be modelled as a Lambertian source based on previous studies [73], [153], and independent of the received

signal. Therefore, the total background noise power received at the receiver by such a source (l) can be calculated as a summation of noise power arrived via LOS (P_{n_d}), first-second-order reflection ($P_{n_{reflection}}$), which can generally be given as:

$$P_n = P_{n_d} + P_{n_{reflection}}\,, \tag{3.19}$$

where P_{n_d} is the direct path component of the BN and $P_{n_{reflection}}$ is the total received noise power through the reflecting surfaces over the room, as shown in Figure 3.5. Following the LOS and reflection analysis previously given, P_{n_d}, can be calculated as:

$$P_{n_d} = \frac{n_l + 1}{2\pi R_d^2} P_l\, T_F(\delta)\;\; T_C(\delta)\, A_R\, cos^{n_l}(\vartheta_d) cos(\delta)\, rect\big(\delta/\psi_C\big), \tag{3.20}$$

and $P_{n_{reflection}}$ is given by:

$$P_{n_{reflection}} = \frac{(n_l+1)(n_{element}+1)}{4\pi^2 R_1^2 R_2^2} \rho_1 P_l T_F(\delta) T_C(\delta) dA_1 A_R \cos^{n_l}(\vartheta) \cos(\phi) \cos^{n_{element}}(\varphi_1) \cos(\delta) rect(\delta/\psi_C)\,, \tag{3.21}$$

The total background noise power P_{bn} collected at an optical receiver at a certain location from all light sources can be given as:

$$P_{bn} = \sum_{l=1}^{L} \left(P_{n_d} + \sum_{m=1}^{M} P_{n_{reflection}} \right)_l\,, \tag{3.22}$$

where L is the total number of lamps (in our case, eight).

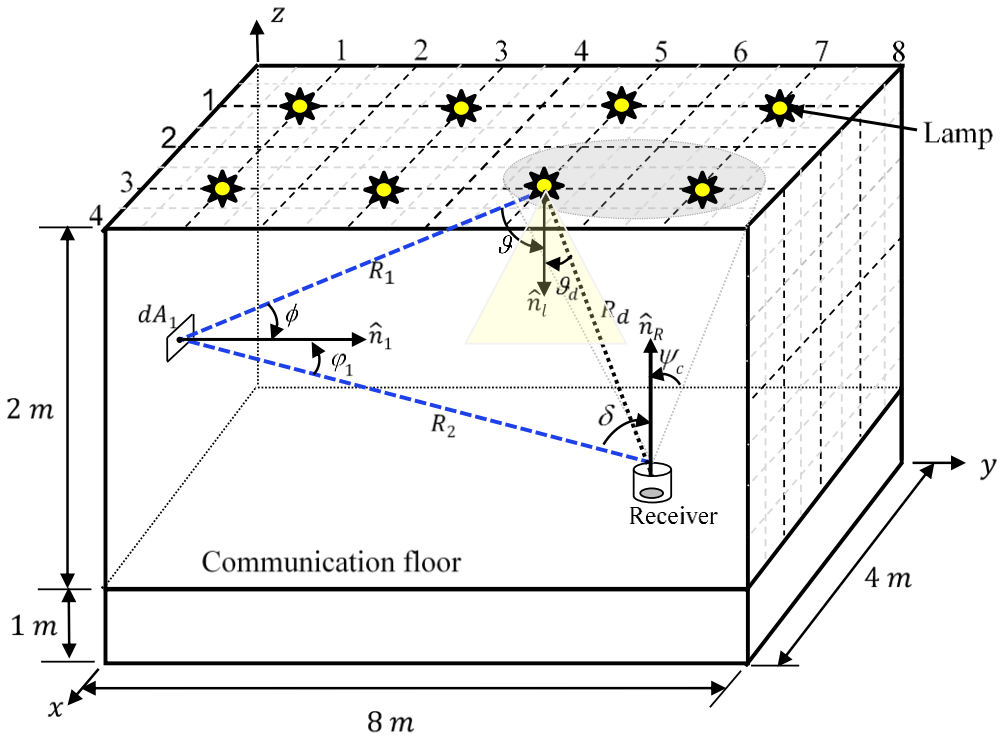

Figure 3.5: Model of the ambient light.

3.6 Angle Diversity Receiver

The most basic receiver configuration widely investigated is a wide field-of-view (FOV) receiver [16], [23], [36], [54]. The receiver employs a single detector with a wide angle of reception (FOV=90°) and an active area of 1cm^2. Moreover, a non-imaging diversity receiver is considered and compared with the wide FOV receiver.

Unlike the single wide FOV receiver, an angle diversity receiver consists of a detector array of narrow-FOV detectors oriented in different directions. Several researchers have studied the diversity reception technique in an indoor OW environment [44], [46], [53]-[59], [98], [99], [102], [105], [112], [141], [142], [154], [155]. It has been shown that the narrow-FOV detectors allow the receiver to reduce the effect of background noise

produced by the ambient light and to eliminate undesired signals, hence reduce the multipath distortion. The flexibility in diversity receiver configuration leads to an additional degree of freedom where the narrower FOVs can be used to reduce the background noise and reject unwanted signals. However, optimum FOVs have to be identified as below a certain FOV, the reduction in noise power is not significant compared to the loss of signal power.

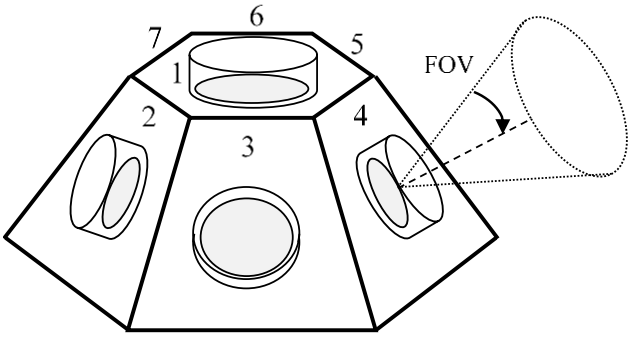

(a)

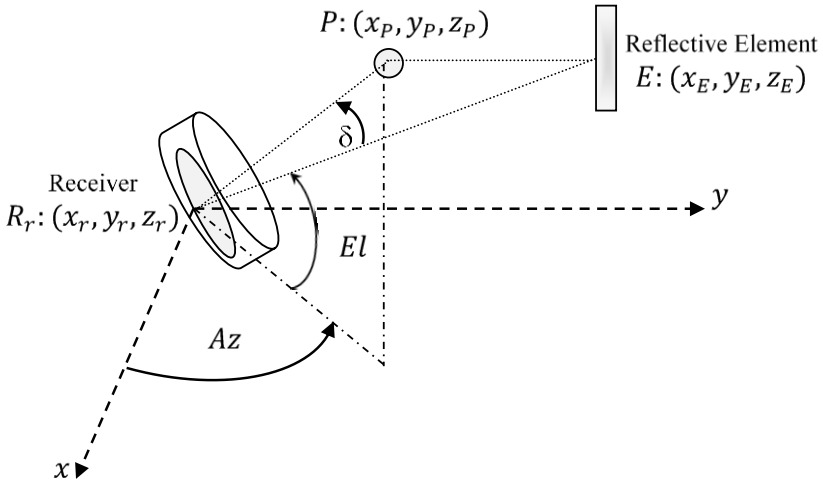

(b)

Figure 3.6: Angle diversity detection scheme: (a) Physical structure of a seven branches angle diversity receiver; and (b) Azimuth and elevation angle analysis for diversity receiver.

The photocurrents received at each detector are amplified separately, and the resulting electrical signals can be processed using different techniques such as select-best (SB), maximum ratio combining (MRC) and equal gain combining (EGC). Previous work [99] has shown that, compared to MRC techniques, the EGC scheme produces substandard SNR, and is more complex than SB, hence MRC and SB are employed in this work. The diversity detection scheme consists of seven photodetectors, as illustrated in Figure 3.6. Each detector points in a certain direction defined by two angles: azimuth (Az) and elevation (El). While the El of the side branches remains at 35°, the seventh faces upwards with El of 90°, and the Az for the seven branches of the receiver are fixed at 0°, 0°, 45°, 135°, 180°, 225° and 315°. The FOV of the top detector is set to 20° while the six side photodetectors are set to 35°. The receiver's angles (Az, El, FOV) were selected through an optimisation similar to that used in [54], [56] to achieve the best SNR. The diversity receiver is always located on the CF with a photosensitive area of each detector of 1cm^2 and a responsivity of $0.5\ \text{A/W}$. Since the side branches of the angle diversity receiver are inclined, modifications to the calculation of the reception angle (δ) are required. Following the analysis given in [54], the reception angles can be calculated considering El and Az angles and the reflective element.

Observing Figure 3.6 (b), a point P at coordinates of (x_P, y_P, z_P) was defined, located on the detector's normal, 1m above the detector. The reception angle of light from a reflecting point E at coordinates of (x_E, y_E, z_E) on a ceiling or wall incident to a detector of a diversity receiver is given by [54]:

$$\cos(\delta) = \frac{\left|\overrightarrow{PR_r}\right|^2 + \left|\overrightarrow{ER_r}\right|^2 - \left|\overrightarrow{EP}\right|^2}{2\left|\overrightarrow{PR_r}\right|^2\left|\overrightarrow{ER_r}\right|^2} \tag{3.23}$$

where the $\left|\overrightarrow{PR_r}\right|$, $\left|\overrightarrow{ER_r}\right|$ and $\left|\overrightarrow{EP}\right|$ represent the distances between the detector (R_r), the defined point (P) and the reflective element (E), as shown in Figure 3.6 (b), and can be given as:

$$\left|\overrightarrow{PR_r}\right|^2 = 1 + \left(\frac{1}{\tan(El)}\right)^2, \tag{3.24}$$

$$\left|\overrightarrow{ER_r}\right|^2 = (x_r - x_E)^2 + (y_r - y_E)^2 + (z_r - z_E)^2, \tag{3.25}$$

$$\left|\overrightarrow{EP}\right|^2 = \left[\left(\left(\frac{\cos(Az)}{\tan(El)}\right) + x_r\right) - x_E\right]^2 + \left[\left(\left(\frac{\sin(Az)}{\tan(El)}\right) + y_r\right) - y_E\right]^2 + \left[(z_r + 1) - z_E\right]^2, \tag{3.26}$$

The angle diversity receiver was implemented in conjunction with multibeam transmitters (LSMS and BCM), so that limited rays are received by the detectors, whose angles of incidence lie within the detectors' FOV.

3.7 Mobile system configuration

Multibeam transmitters have been proposed as a way to minimise multipath dispersion in a configuration that simulates a diffuse link. Unlike diffuse systems, where rays go in all directions, optical transmitters with multiple narrow beams generate different spots on reflective areas (on ceiling or walls). In this chapter, two attractive multi-spot diffusing configurations (LSMS and BCM) are studied and evaluated under the constraint of multipath dispersion, BN and user mobility [98]-[100], [102], [104], [105], [141]-[143], [149], [156]-[162]. In conjunction with a wide FOV receiver (FOV=90°) and an angle

diversity receiver, the multibeam systems are simulated and compared with classic diffuse system (CDS with a wide FOV receiver).

3.7.1 Conventional Diffuse System (CDS)

The CDS is the basic OW configuration and has been extensively investigated [9], [16], [23], [32], [33], [51], [108]. The conventional diffuse link consists of a single beam transmitter with a fully diffuse source ($n_{source} = 1$) and a wide FOV receiver, as shown in Figure 3.7. Both the transmitter and the receiver are placed on the communication floor (1m above the ground) and pointed upwards, in which case there is no LOS link between them. In conventional system, a receiver normally collects signals that have undergone one or more reflections off a ceiling or wall. For comparison purposes, a conventional diffuse transmitter combined with a wide FOV has been simulated to determine its impulse response, delay spread and SNR.

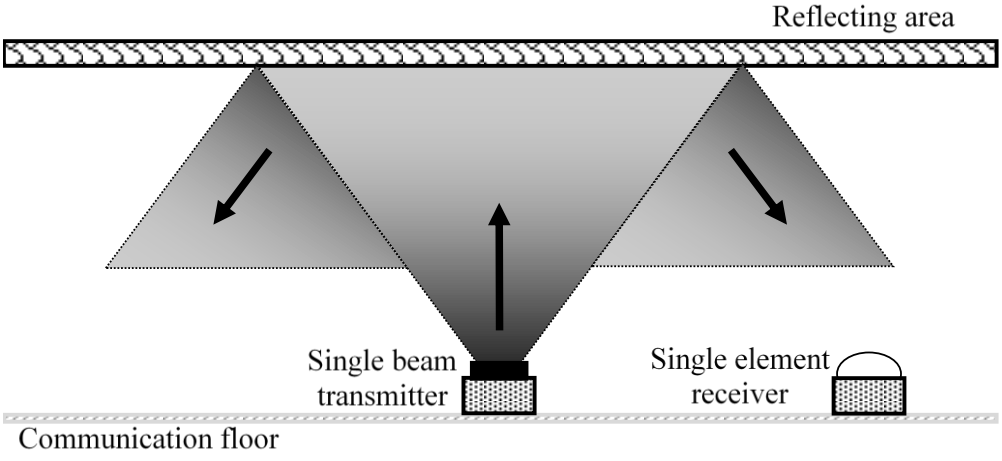

Figure 3.7: Conventional diffuse system with a single beam transmitter and a single element receiver.

3.7.2 Line Strip Multibeam System (LSMS)

The multispot diffusing link first proposed by Yun and Kavehard [44] consisted of narrow beams oriented in different directions and has been widely investigated since [43], [46], [53], [112]. The LSMS is a simple structure of a multispot diffusing system that has been analysed and compared to the CDS and different diffusing techniques, and has been shown to produce SNR improvements [98]-[100], [102], [156]. The LSMS system employs a mutibeam transmitter that produces 80×1 beams aimed at the ceiling with equal intensities to form a line strip of diffusing spots in the middle of the ceiling at $x = 2\text{m}$ when the transmitter is at the centre of the room, as shown in Figure 3.8 (a). The difference in distance between contiguous spots is 10cm. The total optical power emitted by the multibeam transmitter in LSMS system is 1W and remains unchanged for the purpose of comparison with CDS, therefore $12.5m\text{W}$ is allocated to each spot. To achieve a spot-diffusing transmitter, a holographic diffuser can be used mounted at the front of the optical beam source [30], [112]. A computer-generated hologram (CGH) beam splitter is an alternative technique that can produce particular spot intensities [43], [53]. The illuminated spots on the reflective surface (ceiling or wall) become secondary distributed emitters that emit Lambertian radiation [43], [46], [52], [53], [60], [98]-[100], [102], [110], [156]. Since the beams emerging from the transmitter in the multispot channel are nearly collimated, the path loss between the transmitter and the ceiling is ignored, based on the practical findings in [44].

In order to evaluate the performance of the multisport diffusing geometry (LSMS) under mobility, the multibeam transmitter is positioned on the CF in two different locations at

(1m, 1m, 1m) and (2m, 7m, 1m) as shown in Figure 3.8 (b). The positions of the diffusing spots are accordingly affected by the mobility of the LSMS transmitter. When the transmitter moves from the centre of the room, some of the spots appear on one of the walls. The LSMS transmitter has a constant spot distribution, hence the transmission beam angles are unchangeable at all transmitter locations. Therefore, these transmission beam angles have been considered as reference points to compute the new locations of the spots.

To compute the transmission beam angle associated with each diffusing spot at coordinates of (x_s, y_s, z_s), a reference location of the transmitter $(x_T, y_T, z_T) = (2\text{m}, 4\text{m}, 1\text{m})$ is considered. The transmission beam angle α_s with respect to the transmitter normal can be calculated by using the trigonometry of rectangular triangles, whereby spot angles are determined at the reference point and taken into account for each transmitter movement. The beam angles can be computed, by observing Figure 3.9, as:

$$\alpha_s = tan^{-1}\left(\frac{y_T - y_s}{h_s}\right), \qquad 1 \leq s \leq N_s \tag{3.27}$$

where $h_s = z_s - z_{CF}$ is the height of the diffusing spots above the CF, $z_{CF} = 1m$ is the height of the communication floor and the total number of the spots is N_s.

When the transmitter is relocated [i.e. at the room corner at (1m, 1m, 1m) where some spots appear on xz-wall, as illustrated in Figure 3.9], the spot locations and heights change accordingly. Considering the reference points (the transmission beam angles), the new height of spot on the wall (z_s) can be calculated as:

$$z_s = \frac{y_T - y_s}{\tan(\alpha_s)} + z_{CF}, \tag{3.28}$$

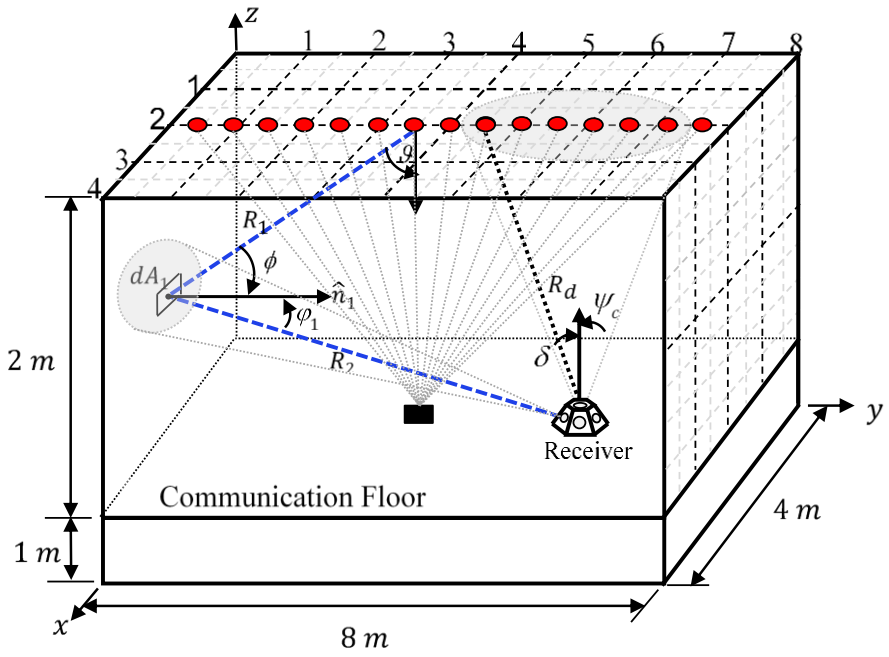

(a)

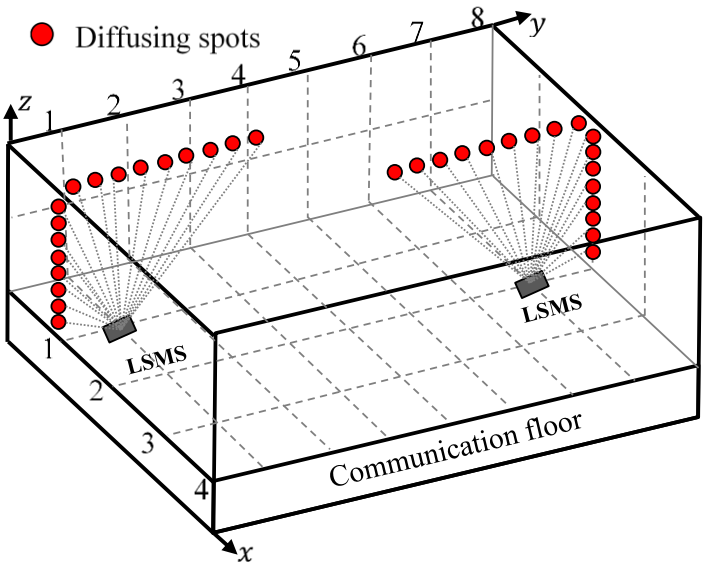

(b)

Figure 3.8 Line strip configuration: (a) Propagation model for LSMS with an angle diversity receiver when the transmitter is at the centre of the room; (b) Mobile LSMS at two transmitter locations (1m, 1m, 1m) and (2m, 7m, 1m)

Based on the reference points and the transmitter location, our computations are performed for all spots to determine the locations of the new spots (on the ceiling and/or walls). The LSMS system offers better SNR than the basic diffuse configuration (CDS), however SNR fluctuation is still accrued when a wide FOV receiver is used. To tackle the SNR fluctuation and eliminate undesired signal, an angle diversity receiver is employed and is evaluated in this chapter. Moreover, the LSMS system performance degrades as a consequence of transmitter mobility, therefore a beam clustering method (BCM) is considered. The BCM consists of the clusters aimed at the ceiling and end walls, and is described next.

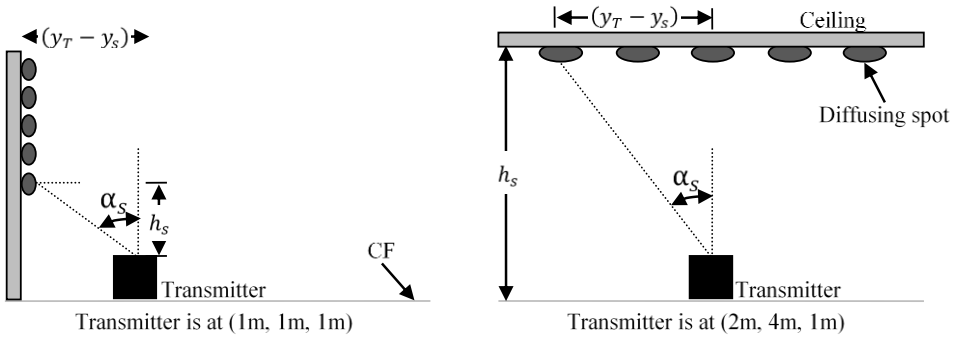

Figure 3.9: Spot distribution on ceiling and wall for mobile LSMS at two transmitter locations

3.7.3 Beam Clustering Method (BCM)

The spot distribution pattern is based on a beam clustering method proposed and examined in [104], [105]. The BCM employs 100 diffusing spots grouped in three clusters, with 80 diffusing spots on the ceiling and 10 spots on each end wall. The separation between adjacent spots on the ceiling is 10 cm, and when the transmitter is at the room centre there 20cm between the spots illuminated on the end walls.

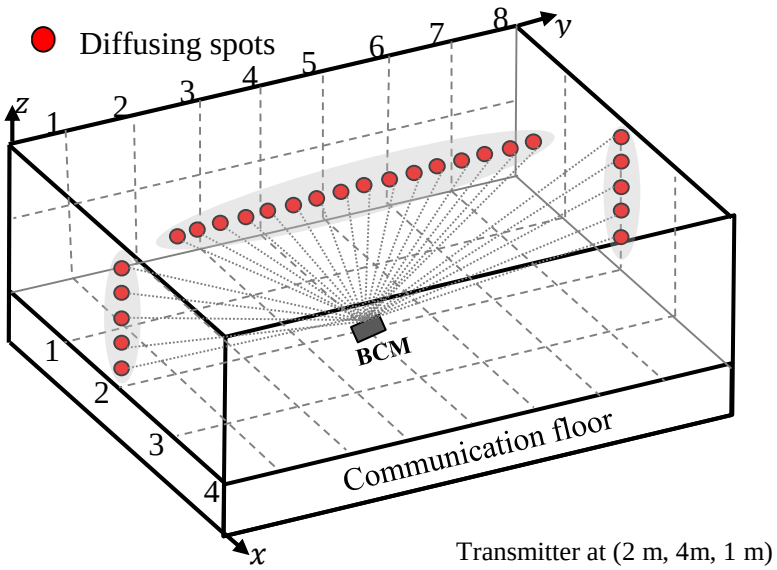

(a)

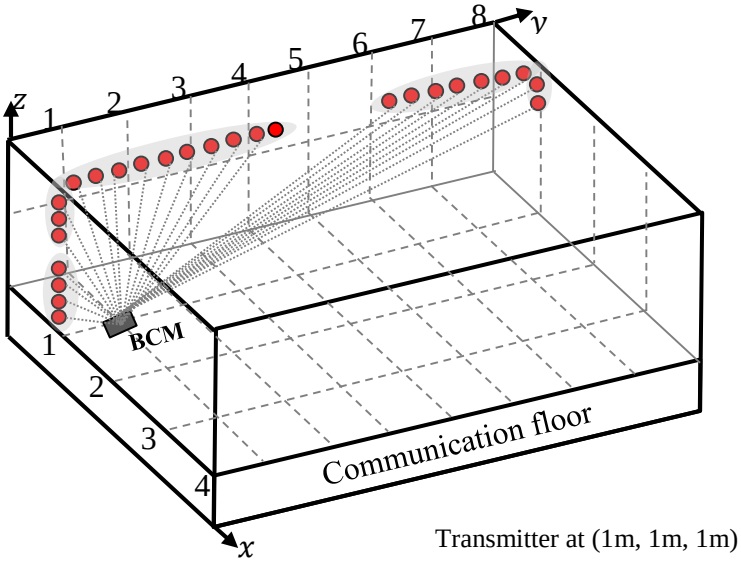

(b)

Figure 3.10: Mobile beam clustering method when transmitter is at (a) the centre of the room (b) the corner of the room.

To enable comparison with previous systems (CDS and LSMS), the total emitted power level (1W) remains constant, therefore each spot contributes 10mW. The total number and the distribution pattern of the diffusing spots were chosen to alleviate the poor performance when transmitter mobility is an issue, based on an optimisation similar to

[104], [105]. Computations similar to those in Section 3.7.2 were used to calculate BCM beam angles and new locations of diffusing spots due to transmitter mobility. To aid visualisation of the mobile BCM configuration, Figure 3.10 shows a limited number of diffused spots in the OWC system at transmitter locations (2m, 4m, 1m) and (1m, 1m, 1m).

3.8 Simulation Results

The simulation was used to assess the performance of the multispot diffusing systems (LSMS and BCM) combined with an angle diversity receiver under the constraints of ambient light noise, multipath dispersion and mobility. To facilitate comparison, these multibeam systems and a fully diffuse system in conjunction with a wide FOV receiver are also considered. A simulation tool similar to the one developed by Barry *et al*. [16] was developed and used to calculate the received power and produce the impulse response at each transmitter-receiver location. The simulation results are reported in terms of impulse response, delay spread and SNR.

3.8.1 Impulse Response

The indoor OW channel is essentially a multipath channel, and therefore the channel impulse response can be used to specify the received optical power that results from multipath propagation. The impulse responses of CDS with a wide FOV receiver and the spot-diffusing configurations (LSMS and BCM) with a wide FOV receiver and an angle diversity receiver are illustrated in Figure 3.11. The depicted results compare the power level (μW) as a function of time (ns) between different configurations (CDS, LSMS and

BCM) when the transmitter is at the room centre (2m, 4m, 1m) and the receiver is at the corner of the room (1m, 1m, 1m). The curves presented are a result of convolving the impulse response with a rectangular transmitted pulse of 1W at a 50Mbit/s bit rate. It should be noted that the resultant power profile at each photodetector is the sum of the received powers due to the total diffusing spots.

It is clearly seen that the multibeam configurations perform better than the diffuse system (CDS). This is attributed to the presence of direct LOS components between the secondary transmitters (diffusing-spots) and the receiver. The optical power associated with the CDS is $0.064\mu\text{W}$, whereas it is $0.617\mu\text{W}$ and $0.516\mu\text{W}$ for LSMS and BCM configurations in conjunction with a wide FOV receiver, respectively. It is observed that an increase in signal delay spread occurs when a single element receiver with a wide FOV is used. The diffusing-spot structures (LSMS and BCM) integrated with the angle diversity receiver have the smallest delay spread while maintaining high power level, in comparison with other arrangements that use a wide FOV receiver. This is manifest in the confined impulse response shown in Figure 3.11, and is a result of restricting the FOV of the diversity receiver. The narrow FOV of the diversity receiver allows it to limit the range of rays accepted as well as the number of diffusing-spots' contributions.

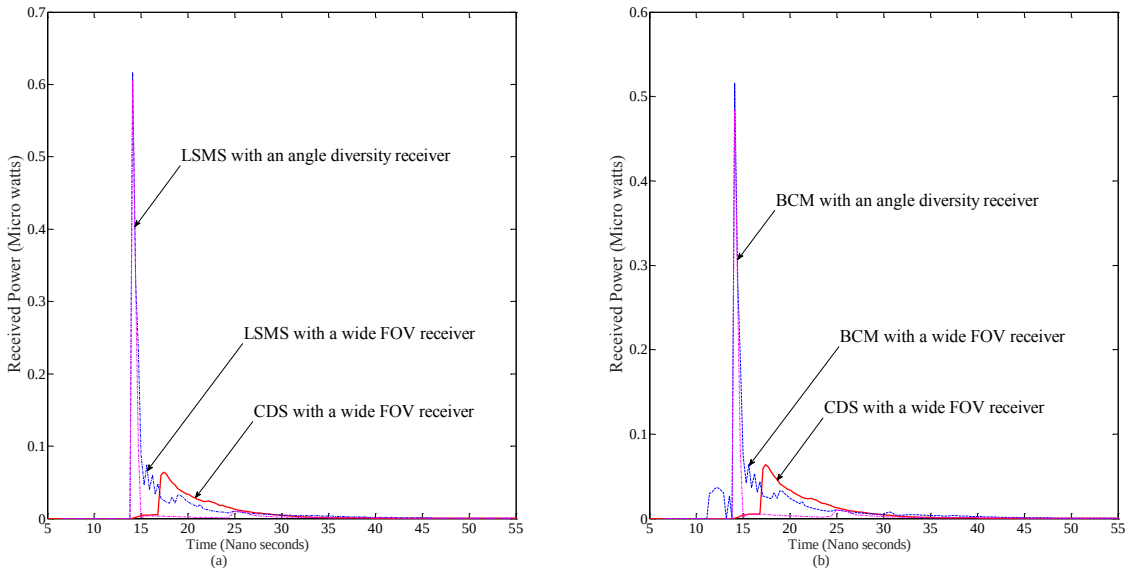

Figure 3.11: Impulse response of CDS with a wide FOV receiver and multibeam configurations: [(a) LSMS; and (b) BCM] with a wide FOV receiver and an angle diversity receiver at transmitter and receiver locations of (2m, 4m, 1m) and (1m, 1m, 1m) respectively

3.8.2 Delay Spread

Indoor OW links are subject to multipath dispersion due to diffuse transmission, which results in ISI. In order to estimate the distortion caused by temporal dispersion, the root-mean-square (rms) delay spread (D) values can be used. Delay spread gives an indication of the ISI experienced in the received optical signal and is given by [53]:

$$D = \sqrt{\frac{\sum_i (t_i - \mu)^2 h^2(t_i)}{\sum_i h^2(t_i)}}\ , \text{ where } \mu = \frac{\sum_i t_i h^2(t_i)}{\sum_i h^2(t_i)}, \tag{3.29}$$

where μ is the mean delay and t is the time delay associated with the received optical power $h(t)$.

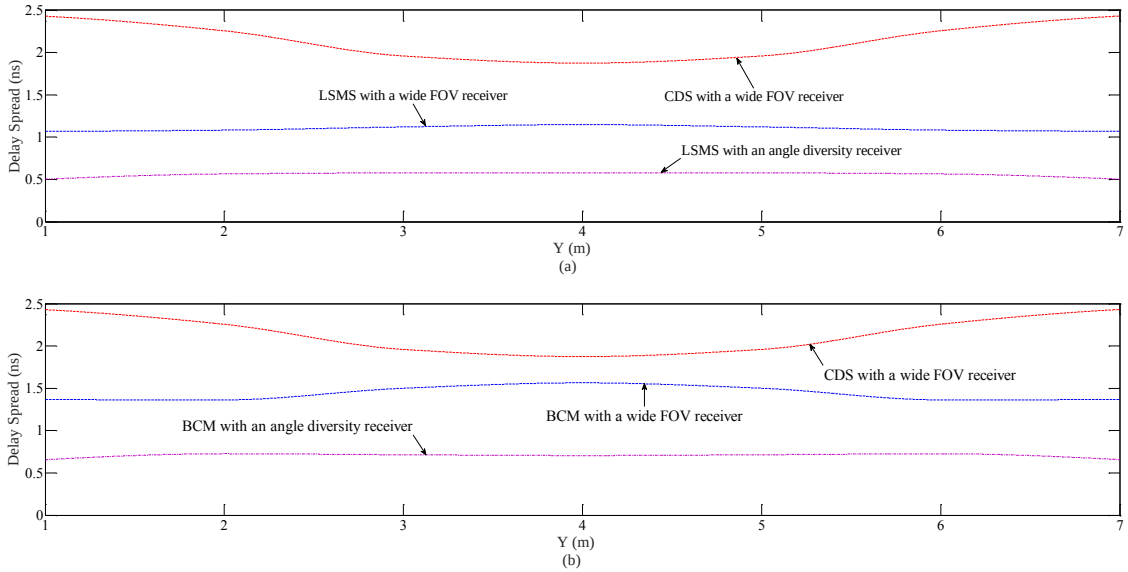

Figure 3.12: Delay spread for CDS with a wide FOV receiver and two spot-diffusing configurations with a wide FOV receiver and an angle diversity receiver at x=1m and along the y-axis (a) LSMS; and (b) BCM.

For comparison purposes, the delay spread distribution for CDS with a wide FOV receiver and the spot-diffusing configurations (LSMS and BCM) with a wide FOV receiver and an angle diversity receiver are calculated, when the transmitter is placed at the centre of the room and the receiver is moved across the x=1m line. The findings indicate that the transmitter–receiver separation distance has an impact on the delay spread in the case of the diffuse system. That is, the delay spread decreases when the transmitter is at the room centre and the receiver moves towards the centre. It can be seen from Figure 3.12 that the delay spread associated with both multibeam configurations (LSMS and BCM) is much lower than that of the CDS system. For example, when the transmitter is located at the centre of the room and the receiver is 3m away, there is a reduction in delay spread from 2.4ns associated with the CDS to 1.1ns and 1.3ns for the LSMS and BCM, respectively. This is due to the fact that the spot-diffusing structure covers the surroundings uniformly, allowing the receiver to collect signals from the

nearest spots. Furthermore, the results in Figure 3.12 show that the multibeam configurations integrated with an angle diversity receiver reduce the delay spread by a factor of more than 4 relative to the CDS. This is due to the multibeam structure, where it can maintain LOS components in all receiver locations as well as the limited FOV of the diversity receiver [54].

3.8.3 SNR Calculation

Indoor OW communication links are strongly impaired by the shot noise induced by ambient light noise, which reduces the SNR of the system. Since the system is based on IM/DD, the SNR is proportional to the square of the received optical power [79]. Therefore, SNR is a good measure to evaluate the impact of data transmission limitations, such as background illumination and eye safety regulations. The bit error rate (BER) in an indoor mobile OW communication system using OOK can be calculated based upon the Gaussian approximation [163]. In the BER analysis, the error probability can be defined as

$$P_e = P(0) \times P_{e0} + P(1) \times P_{e1}, \tag{3.30}$$

where $P(0)$ and $P(1)$ are the probability of receiving a '1' and '0', respectively, P_{e0} is the probability of receiving '1' when '0' is transmitted, and P_{e1} is the probability of receiving '0' when '1' is transmitted. In the case where the number of bits in the message sequence is large, the transmission of '0' and '1' are equiprobable, and then $P_e = P_{e0} + P_{e1}/2$. The conditional probabilities P_{e0} and P_{e1} depends on probability density and can be defined by:

$$P_{e0} = \frac{1}{\sigma_0\sqrt{2\pi}} \int_{D}^{\infty} e^{-\left(\frac{(i_0-x)^2}{2\sigma_0^2}\right)} dx \tag{3.31}$$

$$P_{e1} = \frac{1}{\sigma_1\sqrt{2\pi}} \int_{-\infty}^{D} e^{-\left(\frac{(i_1-x)^2}{2\sigma_1^2}\right)} dx \tag{3.32}$$

where i_0 and i_1 are the mean photocurrents associated with logic '0' and '1'; σ_0 and σ_1 are the noises associated with logics; and D is the decision level. B changing the variables, we can get:

$$P_{e0} = \frac{1}{\sqrt{2\pi}} \int_{Q_0}^{\infty} e^{-\frac{x^2}{2}} dx \tag{3.33}$$

$$P_{e1} = \frac{1}{\sqrt{2\pi}} \int_{-\infty}^{Q_1} e^{-\frac{x^2}{2}} dx \tag{3.34}$$

where $Q_0 = D - i_0/\sigma_0$ and $Q_1 = i_1 - D/\sigma_1$. If '0' and '1' are equally likely, then $Q_0 = Q_1 = Q$. This yields from (3.33) and (3.34) the decision level D:

$$D = \frac{\sigma_1 i_0 + \sigma_0 i_1}{\sigma_0 + \sigma_1}, \tag{3.35}$$

From (3.34) and (3.35), Q can be given as:

$$Q = \frac{i_1 - i_0}{\sqrt{\sigma_0^2} + \sqrt{\sigma_1^2}}, \tag{3.36}$$

The power P_0 and P_1 in '0' and '1' bits are related to i_0 and i_1 as

$$i_0 = R \cdot P_0 = R \cdot (P_{s0} + P_{bn}) \tag{3.37}$$

$$i_1 = R \cdot P_1 = R \cdot (P_{s1} + P_{bn}) \tag{3.38}$$

Subtracting (3.37) from (3.38) yields $i_1 - i_1 = R(P_{s1} - P_{s0})$, therefore (3.36) becomes

$$Q = \frac{R(P_{s1} - P_{s0})}{\sqrt{\sigma_0^2} + \sqrt{\sigma_1^2}}, \tag{3.39}$$

Since the two error probabilities P_{e0} and P_{e1} are set equal for minimal error, the probability of error in (3.30) can be given as

$$P_e = \frac{1}{\sqrt{2\pi}} \int_{Q_0}^{\infty} e^{-\frac{x^2}{2}} dx = \frac{1}{2} erfc\left(\frac{Q}{\sqrt{2}}\right) \tag{3.40}$$

where $erfc(x) = 1 - erf(x)$ is the complementary error function, and erf(x) is the error function. The P_e can be approximated as

$$P_e = \frac{1}{Q\sqrt{2\pi}} e^{\left(-\frac{Q^2}{\sqrt{2}}\right)} \tag{3.41}$$

where $Q(\cdot)$ is is the Gaussian function that assumes a value of 6 at probability of error $P_e = 10^{-9}$, corresponding to an SNR of 15.56 dB for conventional OOK systems.

Infrared transmissions are confined to the room in which they originate due to the fact that light do not penetrate through walls or other opaque barriers. This signal confinement prevents interference between links operating in different rooms. However, indoor OW signals are subjected to distortion due to multipath dispersion, which results in ISI. A good measure of the severity of ISI induced by a multipath channel is the channel rms delay spread, as discussed previously in 3.8.2. Taking the impact of pulse spread caused by the ISI into account, where P_{s1} and P_{s0} accounts for the eye closure at the sampling instant, the SNR can be expressed as in [104]:

$$SNR = \left(\frac{R \times (P_{s1} - P_{s0})}{\sigma_t}\right)^2, \tag{3.42}$$

where P_{s1} and P_{s0} are the powers associated with logic 0 and 1, respectively. R is the photodetector responsivity, and σ_t is $\sigma_0 + \sigma_1$ [163], the noises associated with the signal. The total noise variance σ_t^2 is a summation of three noise variance components:

background light-induced shut noise σ_{bn}^2, the noise associated with the preamplifier components σ_{pr}^2 and the noise induced by the received signal power σ_{si}^2. The σ_{si}^2 consists of two components: shot noise current σ_{s1}^2 associated with P_{s1} and shot noise current σ_{s0}^2 associated with P_{s0}. This signal-dependent noise σ_{si}^2 is very small and can be ignored, based on the experimental findings presented in [56]. The noises σ_0 and σ_1 associated with logic 0 and 1 respectively and can be calculated as:

$$\sigma_0 = \sqrt{\sigma_{pr}^2 + \sigma_{bn}^2 + \sigma_{s0}^2} \;\; and \;\; \sigma_1 = \sqrt{\sigma_{pr}^2 + \sigma_{bn}^2 + \sigma_{s1}^2} \; . \tag{3.43}$$

To enable comparison with previous work [156], [162], the preamplifier used for the 50Mbit/s OOK system (20ns pulse duration) is the 70 MHz PIN-BJT design by Elmirghani *et al.* [28], with a noise spectral density of $2.7\text{pA}/\sqrt{\text{Hz}}$. The preamplifier shot noise can be written as:

$$\sigma_{pr} = 2.7 \times 10^{-12} \times \sqrt{70 \times 10^6} = 0.023 \; \mu\text{A} \; , \tag{3.44}$$

The background shot noise component (σ_{bn}) can be computed from its respective associated power level (P_{bn}) as:

$$\sigma_{bn} = \sqrt{2RqP_{bn}BW} \; , \tag{3.45}$$

where q, P_{bn} and BW are the electron charge, the received background optical power and receiver bandwidth, respectively. Substituting (3.43) into (3.42), the SNR can be expressed as:

$$SNR = \left(\frac{R(P_{s1} - P_{s0})}{\sqrt{\sigma_{pr}^2 + \sigma_{bn}^2 + \sigma_{s0}^2} + \sqrt{\sigma_{pr}^2 + \sigma_{bn}^2 + \sigma_{s1}^2}} \right)^2 . \quad (3.46)$$

For simplicity in the case of angle diversity, SB is considered to process the resulting electrical signal from the different photodetectors (J). Therefore, Equation (3.46) can be re-written as:

$$SNR_{SB} = max_j \left(\frac{R\left(P_{s1_j} - P_{s0_j}\right)}{\sqrt{\sigma_{pr_j}^2 + \sigma_{bn_j}^2 + \sigma_{s0_j}^2} + \sqrt{\sigma_{pr_j}^2 + \sigma_{bn_j}^2 + \sigma_{s1_j}^2}} \right)^2 , \ 1 \leq j \leq J \quad (3.47)$$

where J is the number of photodetectors. In order to compare the SNR results to the work of other researchers in the literature, neither an optical concentrator nor an optical filter was used. In this chapter, the SNR results are reported according to pulse propagation simulations. Figure 3.13 shows the SNR of the three proposed configurations, namely CDS, LSMS and BCM, in conjunction with a wide FOV receiver. The SNR calculations were performed for the previous configurations operating at 50Mbit/s under the constraints of background noise and multipath dispersion, when the receiver moves along the x = 1m and x = 2m lines respectively, at three transmitter positions: (1m, 1m, 1m), (2m, 4m, 1m) and (2m, 7m, 1m). Note that the BN has substantial effect on OW performance when a wide FOV receiver is employed, mainly underneath the light sources at $y = 1, 3, 5, 7m$. The findings, in Figure 3.13 (a), show that the SNR of the CDS is at a maximum (along the *y-axis*) at points far from the noise sources and close to the transmitter. For example, when the transmitter and the receiver are co-located at the room centre, the CDS's SNR is at its highest value.

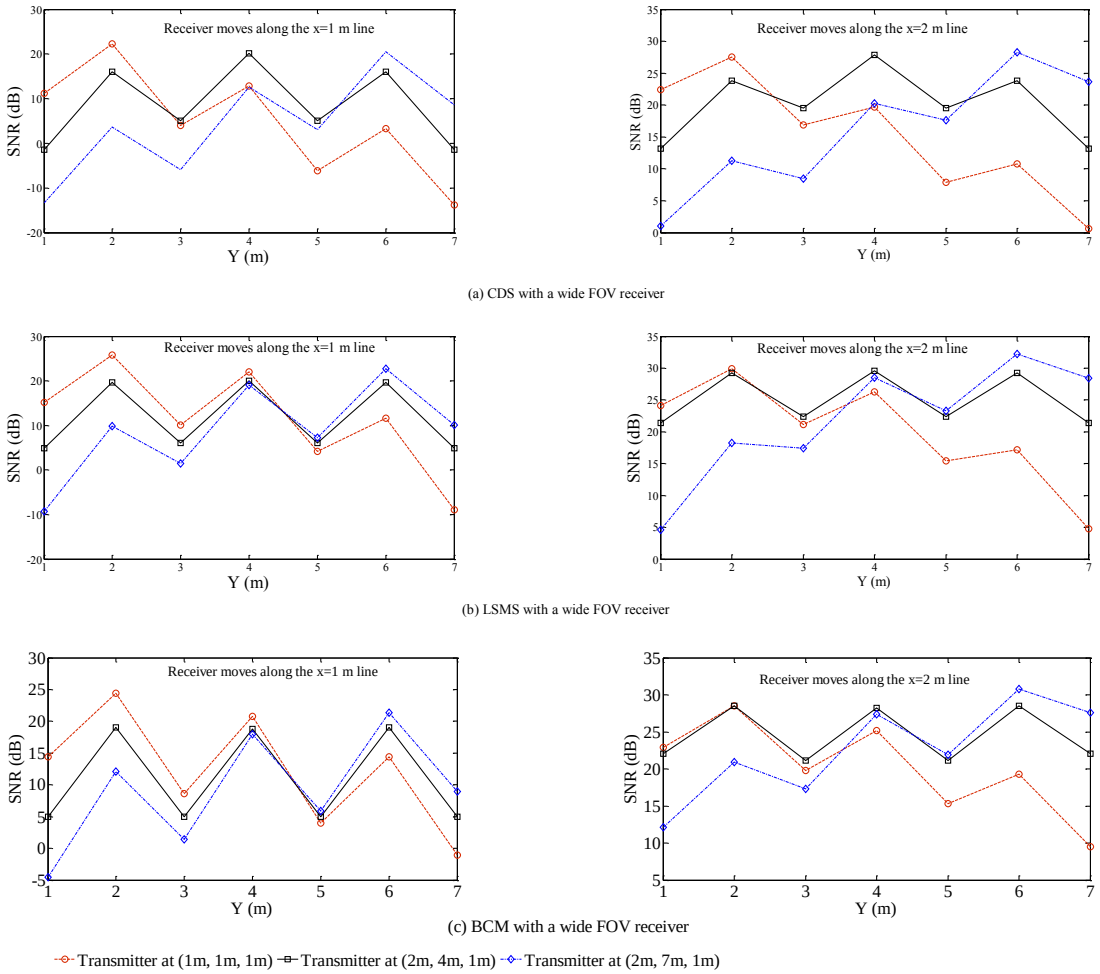

Figure 3.13: SNR of the three proposed configurations with a wide FOV receiver at constant x receiver position, along the y-axis (a) CDS; (b) LSMS; and (c) BCM.

The lowest SNR value occurs at a 6m transmitter–receiver separation distance when the receiver is underneath the spotlight in the room corner. This is attributed to two facts: the separation distance between the transmitter and the receiver, where it is at a minimum at the maximum SNR peak and greatest at the lowest SNR peak). Secondly, the noise distribution has a strong value at locations beneath the spotlights. In comparison, the multispot diffusing systems (LSMS and BCM) improved the optical signal reception in locations with poor connections such as when the transmitter or receiver is in the corner of the room. For example, an SNR improvement of 4 dB can be achieved when the LSMS

replaces the CDS when the transmitter and receiver are at (2m, 7m, 1m) and (1m, 1m, 1m), respectively. This is due to adopting a spot-diffusing structure, where the receiver can collect a strong signal through the use of direct LOS components. Further SNR improvement of 6dB can be achieved when the diffusing spots are clustered on the ceiling and the two end walls.

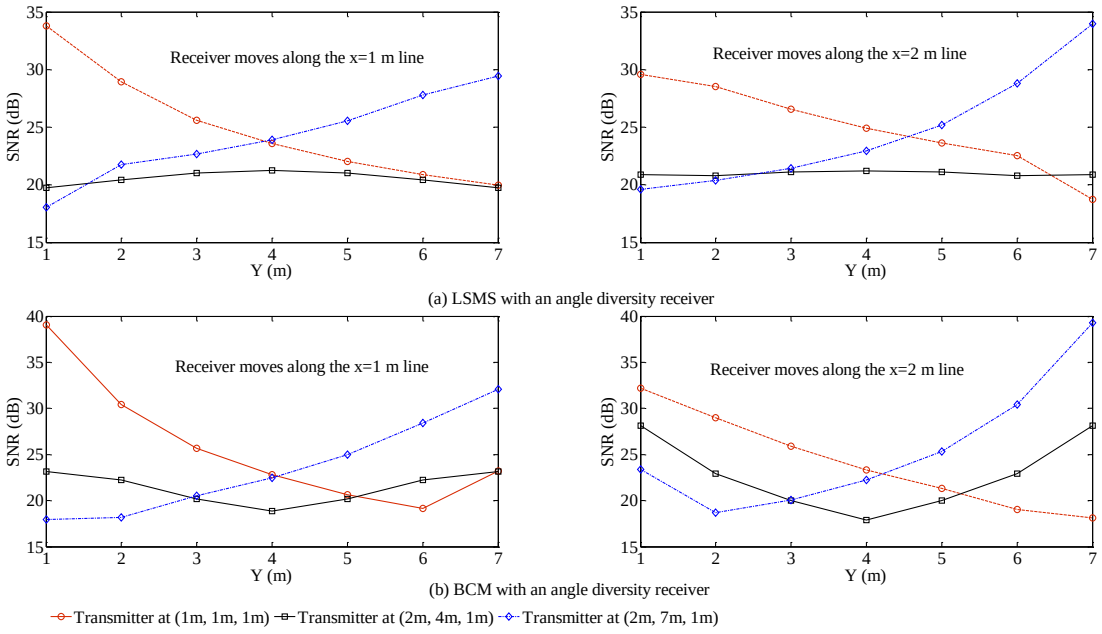

Figure 3.14: SNR comparison of the multibeam configurations: with an angle diversity receiver (a) LSMS; and (b) BCM.

In OW configurations combined with a wide FOV receiver, mobility can induce substantial SNR performance degradation. In comparison, an improvement in signal reception is clearly discernible when multibeam configurations (LSMS and BCM) are integrated with an angle diversity receiver, in spite of moving the transmitter over three different locations. A uniform SNR over the entire CF when the transmitter is placed at the room centre can be achieved through a combination of spot-diffusing systems (i.e. LSMS is employed) and a diversity receiver, as shown in Figure 3.14. Moreover, the

BCM structure (having two beam clusters at the end walls) increases the SNR level when the receiver is located close to the room sides or at the corner. The results reported in this chapter for the CDS, LSMS and BCM were compared with findings presented in [156] and a good match was observed.

3.9 Summary

Characterisation of indoor OW channel is essential for effective link design. In this chapter, the tools used to simulate the OW channel propagation were presented. The simulation was performed using Matlab, based on a ray-tracing algorithm for up to second-order reflections. The impact of background noise, mobility and multipath propagation were discussed and evaluated. For comparison purposes and to form the basis of the subsequent work in this thesis, two multibeam geometries, namely LSMS and BCM, were studied and compared to the CDS. It is shown that the pure diffuse system suffers multipath dispersion, which causes pulse spread and extreme ISI. The spot-diffusing transmitter was shown to be a promising technique that can enhance the performance of OW systems owing to combining LOS and non-LOS features.

The findings show that the proposed configurations with a wide FOV receiver are highly sensitive to ambient light noise and multipath dispersion. Therefore, the spot-diffusing systems were integrated with an angle diversity receiver to reduce the effect of multipath dispersion and background noise. SNR improvement of more than 21dB is observed when the LSMS with diversity reception replaces the CDS with a wide FOV receiver. Moreover, it is observed that the SNR can be further improved when the BCM with an

angle diversity receiver is employed. The configurations evaluated in this chapter will be considered as base line systems to enable comparison with new systems described in the thesis.

4 Optical Wireless Collaborative Multiuser Systems Employing Beam Power Adaptation and Imaging Detection in Realistic Indoor Environment

4.1 Introduction

Multi-spot diffusing optical transmitters have been proven effective to remove the restriction of maintaining direct LOS, and merge both LOS and non-LOS features [104, 156]. However, basic multispot diffusing configurations (such as LSMS and BCM) are vulnerable to user mobility. Due to this fact, a power adaptation technique is employed to enhance the received optical power at a particular receiver location. In a single user scenario, the power adaptive multibeam transmitter assigns higher power to beams nearest to the receiver in the interest of improving the receiver SNR [154], [155], [160]-[162], [164]. The authors in [158] have considered several multi-user scenarios where receivers are positioned in different layouts and a comparison between collaborative combining techniques, such as maximum ratio combining (MRC) and equal gain combining (EGC), was reported. It was found that the MRC scheme offers comparable SNR over multiple receivers (users), and therefore it is adopted in our proposed system. LSMS and a non-imaging angle diversity receiver have been employed in [158], where the collaborative system is evaluated at low data rates. An imaging receiver is an

alternative choice to angle diversity receiver, which can effectively reduce the impact of BN as well as the multipath dispersion. Furthermore, BCM is yet another attractive configuration that can replace the LSMS and allow the system to cover its surroundings through the three clusters of diffusing spots. The combination of these methods (multibeam geometry and the imaging receiver) adds a number of degrees of freedom to link design. In this chapter, multi-user collaborative OW systems based on an adaptive multibeam transmitter and imaging receivers are introduced. The proposed systems are examined in a realistic office environment that consists of windows, a door, mini-cubicles, bookshelves, and other objects. The proposed transmitter and receiver configuration helps to mitigate the shadowing effect, reduces multipath dispersion and improves the system performance under transmitter–receiver mobility at high data rates.

In this chapter we first introduce a collaborative multibeam transmitter to the design of OW systems where high data rates are shown to be feasible. Then, we model our collaborative adaptive beam clustering method (CABCM) in conjunction with an imaging receiver, considering two room scenarios: an empty room and a real office environment [165], [166]. Moreover, consideration is given to the other elements of the real indoor environment, namely ambient light noise and multipath dispersion, and the performance is evaluated. Our goal here is to increase the received optical power and improve the signal-to-noise ratio (SNR) at each coexisting receiver when the system operates in a multiuser scenario. The proposed system (Imaging CABCM) is evaluated at 30Mbit/s to enable comparison with previous work, and is also assessed at higher bit rates: 2.5Gbit/s and 5Gbit/s. Simulation results show that the mobile Imaging CABCM system offers a

significant performance improvement, including a reduction in background noise (BN) effect, a strong received power, reduction in delay spread and improvement in the SNR over multiuser line strip multibeam system (LSMS). However, the performance degrades gradually with an increase in the number of users.

4.2 Simulation Set-up and Room Configurations

In this section, the characteristics of the mobile channel formed by the combination of a collaborative adaptive multibeam transmitter and imaging receivers (users) are investigated. The simulation was developed in a room with dimensions of 4m × 8m × 3m (width×length× height) for two different arrangements denoted as Room A and B. Figure 4.1 shows Room B that has three large glass windows, a door, a number of rectangular-shaped cubicles with surfaces parallel to the room walls, and other furniture such as bookshelves and filing cabinets. The walls (including ceiling) and floor of the room are modelled as ideal Lambertian reflectors with a reflectivity of 0.8 for the ceiling and walls, and 0.3 for the floor. Apart from the door, two of the walls at x=4m (yz-wall) and y=8m (*xz*-wall) are covered with bookshelves and filing cabinets with a 0.4 reflectivity. It is assumed that several desks, tables and chairs within the CF are placed in the room with a 0.3 reflectivity. Additionally, signals reaching the cubic office partitions are assumed to be either blocked or absorbed. In Room A, reflections from doors and windows are considered to be the same as reflections from walls. Each surface element is approximated as an ideal Lambertian reflector and treated as a small transmitter that diffuses the received signal from its centre.

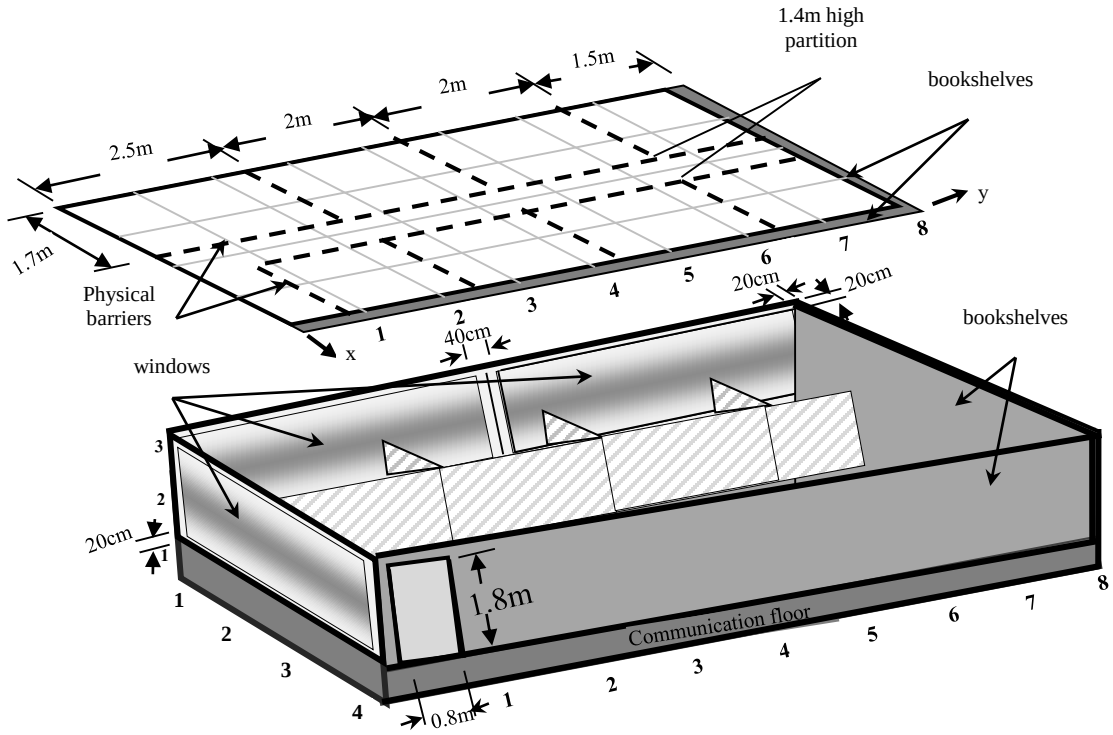

Figure 4.1: Schematic representation of a realistic indoor office environment (Room B)

Surface elements of 5×5cm for first-order reflections and 20×20cm for second-order reflections were used. Reflections up to second order are considered, since third-order reflections and higher produce a weak contribution to the received optical power, as shown through previous investigations [9], [108].In order to investigate the collaborative OW system under mobility, the multibeam transmitter is placed in different locations, pointed upward. It emits 1W optical power. Computer-generated holographic beam-splitters are assumed to be mounted on the emitter to generate multiple narrow beams, forming multiple clusters of line spots (100 diffusing spots are considered, in our case, and each spot is assigned 10mW). A liquid crystal device can be used to adapt the power among the beams at low complexity, having microsecond to millisecond response times

[167]. A low data rate feedback channel is assumed between the transceiver so that the receiver can relay to the transmitter the SNR associated with each spot. A diffuse link or an additional beam (diffusing-spot) can be used to provide the feedback channel. The room illumination is assumed to be provided by eight spotlights ('Philips PAR 38 Economic' (PAR38)). The eight spotlights are placed on the ceiling 1m away from walls at an equal separation distance of 2m, as illustrated in Figure 3.5. Furthermore, an imaging receiver is implemented in order to minimise the BN effect, reduce multipath dispersion and improve the system performance.

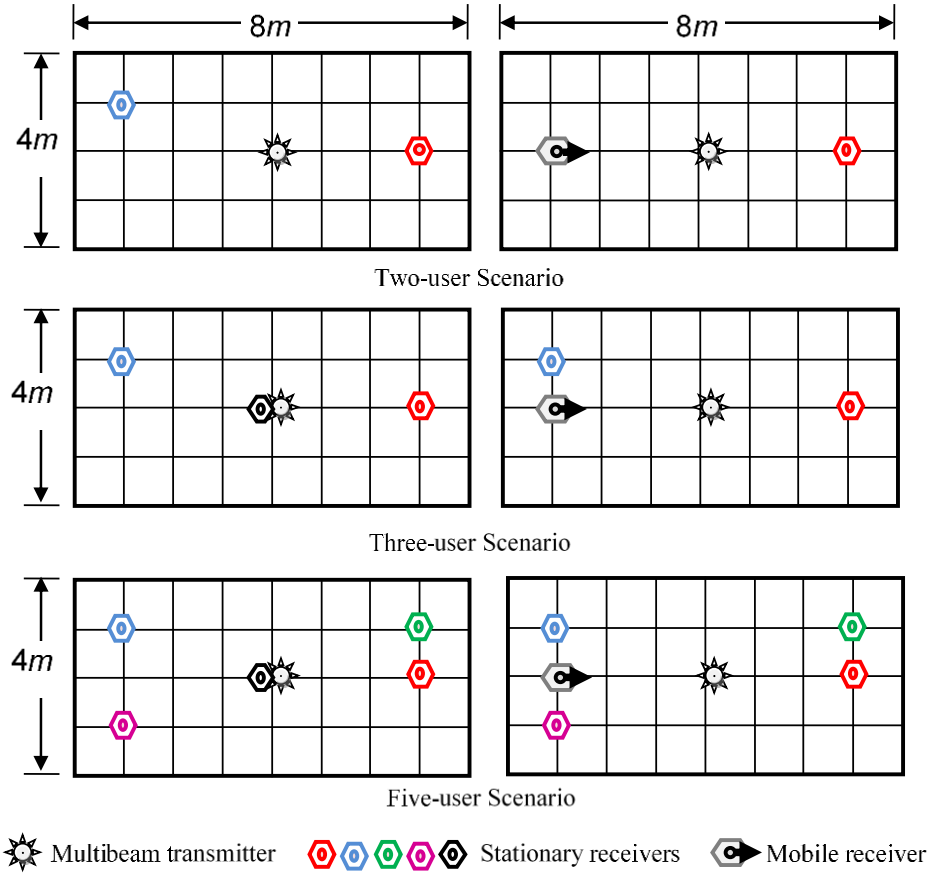

(a) Users are fixed

(b) One user is moving along *x-axis* and the others are fixed

Figure 4.2: Transmitter and receiver positions on the communication floor when the transmitter is located at the room centre (2m, 4m, 1m).

Table 4.1: Simulation parameters

Parameter	**Configuration Uplink Transmission**			
Room				
Length	8m			
Width	4m			
Height	3m			
ρ _x_z Wall	0.8			
ρ _y_z Wall	0.8			
ρ _x_z op. Wall	0.8			
ρ _y_z op. Wall	0.8			
ρ _Floor	0.3			
Transmitter				
Number of Transmitter	1			
Location (x, y, z)	(1,1,1)	(2,1,1)	(2,4,1)	(2,7,1)
Elevation	90°	90°	90°	90°
Azimuth	0°	0°	0°	0°
Imaging Receiver				
Number of Present Receivers	2	3		5
Detector array's area	$2cm^2$			
Number of Pixels	200			
Area of Pixel	$1mm^2$			
Elevation	90°			
Azimuth	0°			
Acceptance semi-angle	65°			
Time bin duration	0.3ns		0.01 s	
Bounces	1		2	
Number of elements	32000		2000	
dA	5cm × 5cm		20cm × 20cm	
Spot lamps				
Number of spot lamps	8			
Locations (x, y, z)	(1,1,3), (1,3,3), (1,5,3), (1,7,3)			

		(3,1,3), (3,3,3), (3,5,3), (3,7,3)	
Wavelength		850 nm	
Bandwidth	30MHz	2.5GHz	5GHz
Bit rate	30Mbit/s	2.5Gbit/s	5Gbit/s

In order to evaluate the proposed method in a collaborative environment, multi-user scenarios are considered, as depicted in Figure 4.2. Three cases were investigated involving two, three and five receivers. In these cases, we consider two scenarios. The first has stationary receivers, as seen in Figure 4.2 (a). In the second, a user is at a constant *x*-axis and moves along the *y*-axis, while the other users are stationary, as shown in Figure 4.2 (b). The receivers' positions are based on several criteria. These include the separation distance between the transmitter and the receiver; that is, 6m horizontal distance between the transmitter and the receiver The weakest points in the communication links, transmitter or/and receiver mobility and the number of coexisting users in the room are also considered in the studied cases. Additional simulation parameters are given in Table 4.1. The proposed imaging systems will be next described.

4.3 Imaging Receiver Design

Unlike the wide FOV receiver, an angle diversity receiver employs multiple receiving elements oriented in different directions [32], [36]. It can significantly reduce background noise and multipath dispersion as well as restrict unwanted signals. However, it requires a separate optical concentrator for each detector, which may be extremely bulky and costly. As an alternative solution, imaging receivers have been proposed to combat the diffuse system's limitations (multipath dispersion and ambient light) [94], [96]. The

imaging receiver has two advantages over nonimaging receivers. First, it reduces the size and cost, since all photodetectors share one concentrator. Secondly, a single planer array is utilised for all the photodetectors, facilitating the use of a large number of pixels. In this section, an imaging receiver is implemented in order to minimise the BN effect, reduce multipath dispersion and improve the system performance. The imaging receiver uses an imaging concentrator that forms an image onto photodetector pixels, each equipped with a separate preamplifier. The photocurrents received in the pixels can be amplified separately, and the resulting electrical signals are processed in an approach that maximises the power efficiency of the system. Several possible diversity schemes such as select-best (SB), and MRC can be considered. The imaging receiver employs a detector array segmented into J equal-sized rectangular-shaped pixels, as shown in Figure 4.3. It is assumed that there are no gaps between the pixels; therefore, the total area of the receiver detector array exactly fits the exit area of the concentrator. Using such a pixel shape ensures that the signal image spot falls on no more than four pixels. In our imaging receiver's analysis, the photodetector array is segmented into 200 pixels and the employed imaging concentrator is similar to that used in [96]. The transmission factor of this imaging concentrator is given by [96]:

$$T_{c,IMG}(\delta) = -0.1982\delta^2 + 0.0425\delta + 0.8778\ , \tag{4.1}$$

where δ is measured in radians and represents the reception angle. Our imaging receiver concentrator has a refractive index N = 1.7 and the entrance area considered is $A =$

$9\pi/4\,\text{cm}^2$ with concentrator's acceptance semi-angle restricted to $\psi_a = 65^o$. The receiver's exit area is $\acute{A} = A\ sin^2(\psi_a)/N^2$.

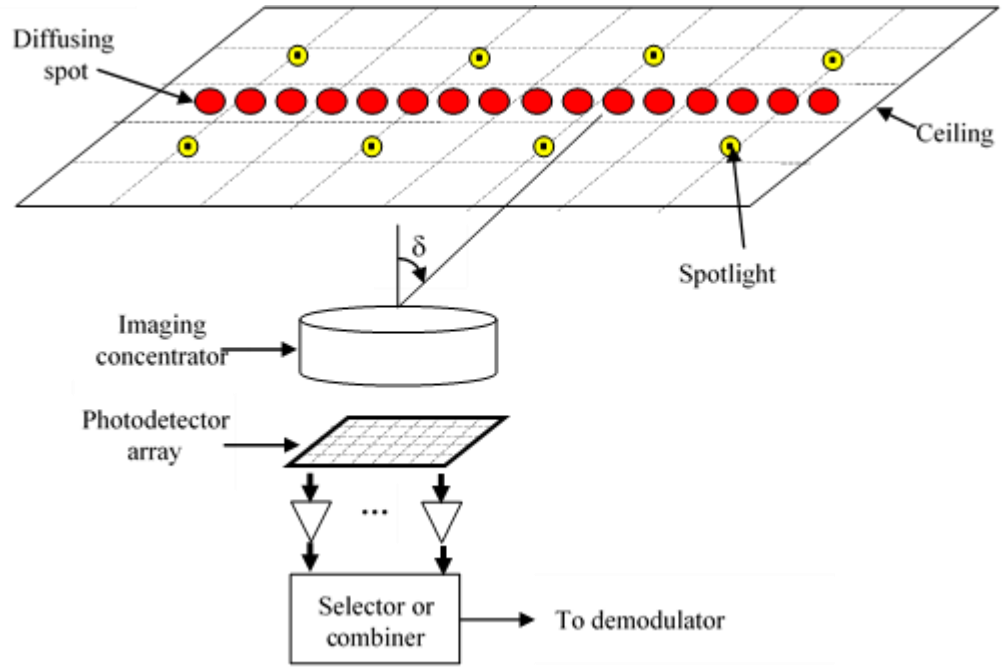

Figure 4.3: Physical structure of the imaging receiver

In our case, the receiver perceives the entire ceiling when it is placed in the middle of the room at (2m, 4m, 1m), subdividing the ceiling into 200 segments (10 × 20). Each segment (reception area) is cast onto a single pixel. Note that the reception area seen by each pixel varies as the imaging receiver moves. The reception area can be defined by computing the reception angles associated with each pixel (see Figure 4.4). The reception angles α_x and α_y with respect to the receiver's normal along the x and y lines can be calculated as:

$$\alpha_x = \tan^{-1}\left(\frac{d_x}{h}\right) \quad and \quad \alpha_y = \tan^{-1}\left(\frac{d_y}{h}\right), \tag{4.2}$$

where d_x and d_y are the *x*-axis and *y*-axis horizontal separations between the receiver's normal and the reception area centre, respectively, and h is the height of the reception area above the CF. These reception angles are considered as reference points at all

receiver locations. For example, when the receiver is relocated from (2m, 4m, 1m) to (1m , 1m, 1m), some of the reception area start to appear on one of the walls (either *x*-*z* wall or *y*-*z* wall). The heights of the reception area z_x and z_y that show on the walls will change accordingly and can be calculated by observing Figure 4.4 (b), as:

$$z_x = \frac{x_r}{\tan(\alpha_x)} \quad and \quad z_y = \frac{y_r}{\tan(\alpha_y)}, \tag{4.3}$$

where x_r and y_r are the horizontal separation distances between the imaging receiver and the *x*-*z* and *y*-*z* walls. In this chapter, the new reception areas are determined based on the reference points (reception angles) following the calculation described above.

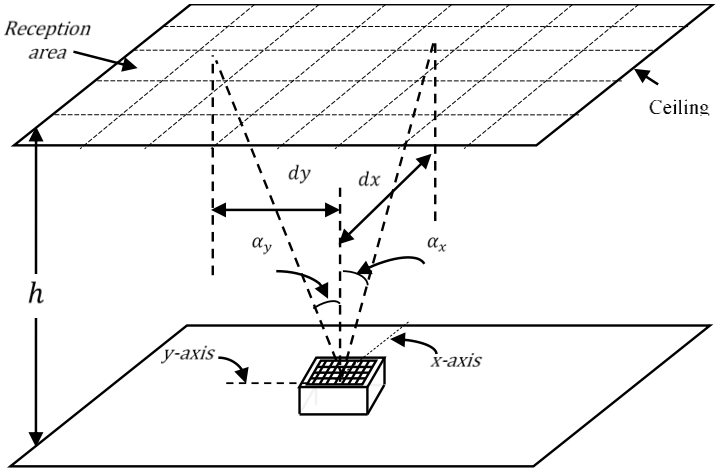

(a)

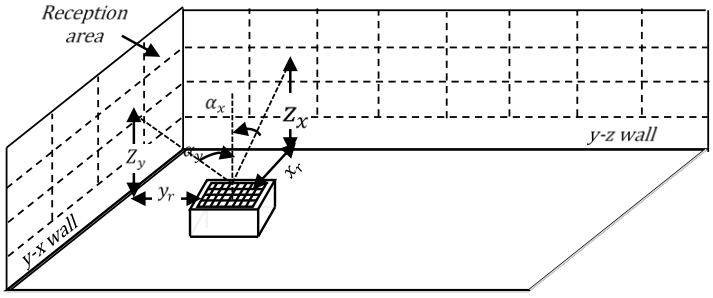

(b)

Figure 4.4: Two cases of reception areas distribution associated with photodetector array when the receiver is placed at: (a) the centre of the room (2m, 4m, 1m); and (b) the room corner (1m, 1m, 1m).

4.4 Collaborative Multi-beam Transmitters Configurations

Adaptive transmit power OW systems (such as adaptive LSMS and adaptive BCM) have been shown to be an effective means of improving the performance of point to point OW communication links [154], [155], [160], [162]. However, one or more receiver locations will suffer in the case of a broadcast situation as the multibeam transmitter adapts the transmit power to a particular location. In this section, a description of collaborative transmit power adaptation algorithm is given, as well as two collaborative multibeam systems.

4.4.1 Collaborative Power Adaptation Algorithm

In mobile OW spot-diffusing systems, the amount of received power varies with the distance between the receiver and the diffusing spots. The power adaptation technique is a possible solution to enhance the received power, and hence improve system performance. Unlike the basic spot-diffusing systems proposed in [104], [156], where the total power is distributed equally among beams, the adaptive multibeam transmitter adjusts the power distribution so that spots near the receiver are allocated the highest power level. The spot distribution pattern based on the LSMS and BCM geometries proposed and examined in [99], [104] (and presented in Section 3.7) are extended in this

chapter, where the total power distribution is collaboratively adapted among the beams. The power allocated to each spot is calculated using collaborative combining technique (in this work, collaborative MRC is considered), based on the number of coexisting receivers. In the collaborative MRC, the power allocated to each spot according to an MRC rule where the optimised power for each spot is proportional to the coexisting receivers' SNRs. This approach aims to maximise the SNRs of the coexisting receivers by allocating higher power levels to the spots that contribute to their SNRs. For a collaborative transmitter and multiple receivers at a given set of coordinates, the collaborative adaptive algorithm adjusts the transmitting powers of the individual beams as follows:

1. Distribute the total power, 1W, on the spots in equal intensities.
2. The transmitter individually turns on each spot *s*, and computes the power ($P_{i,s}$) requested by receiver *i* as well as calculate the SNR (γ_i).
3. Inform the transmitter of the SNR associated with the spot by sending a feedback signal at a low data rate. This feedback channel can be implemented using a diffuse link or by modulating an additional beam.
4. Repeat steps 1 and 2 for all the spots.
5. Re-distribute the transmit power among the spots using collaborative MRC technique. The power of spot *s* can be computed using (4.4).

In the presence of a single user, the transmitted power can be adapted based on the single receiver location and the transmitter location. However, in a multiuser scenario (for example single transmitter and several receivers placed at different locations) a collaborative combining technique is required. Previous work has shown that the power

can be optimally distributed collaboratively among the multiple receivers (users) in an LSMS configuration [158].

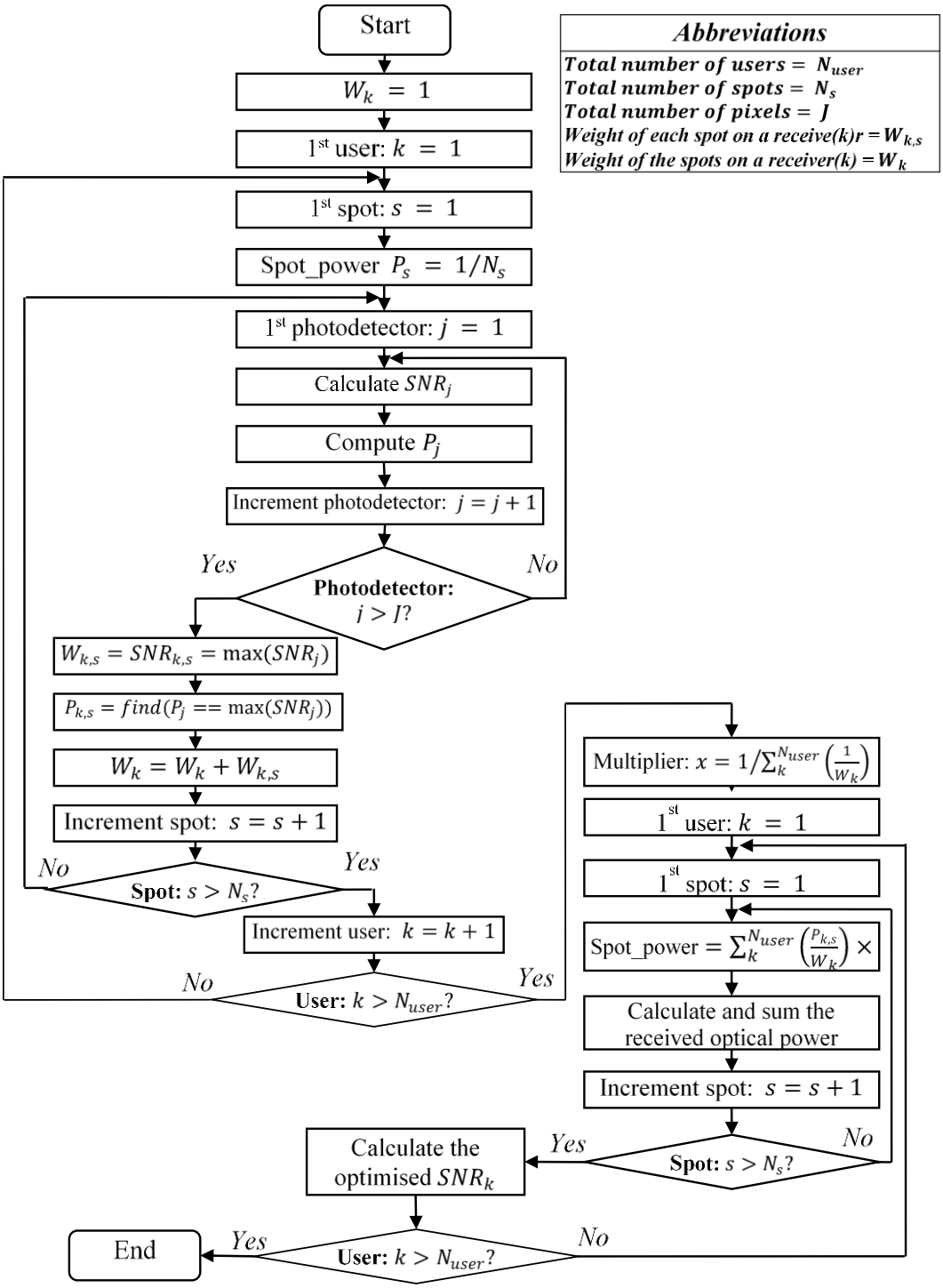

Figure 4.5: Flowchart of collaborative power adaptation algorithm based on collaborative MRC technique

The findings of [158] have shown that collaborative MRC offers uniform SNR improvement over collaborative EGC, therefore it is considered in this chapter. The collaborative EGC approach averages the beams' powers according to power requested by the *n* receivers, in which case the total power requested by each spot is averaged by the number *n* (ratio of $1/n$ is considered). In our collaborative algorithm, the adapted power for a spot *j* requested by *n* receivers can be defined, based on MRC approach, as in [158]:

$$P_{s,MRC_{Coll}} = \sum_i^n \left(\frac{P_{i,s}}{\gamma_i}\right) \times x \,, \tag{4.4}$$

where γ_i is the computed SNR for receiver *i* when the transmitted power is distributed equally and $P_{i,s}$ is the power requested by receiver *i* for the spot *s*. The factor *x* is used as a multiplier in order to maintain that the reallocated power is equal to the transmit power (i.e. 1 W), and can be defined as:

$$x = \frac{1}{\sum_i^n \left(\frac{1}{\gamma_i}\right)}, \tag{4.5}$$

For a simple case of only two coexisting receivers, the multiplier *x* is written as:

$$x = \frac{SNR_1 \times SNR_2}{SNR_1 + SNR_2} \tag{4.6}$$

The flowchart of collaborative power adaptation based on collaborative MRC technique is illustrated in Figure 4.5.

4.4.2 Collaborative Adaptive LSMS (CALSMS)

In this section we extend the treatment of the proposed system examined in [156] (and presented in Section 3.7.2), which has been optimised in [161], [154], by introducing the collaborative transmitted power adaptation implemented on the beam (spot) powers and considering the coexistence of multiple receivers. The collaborative adaptive LSMS (CALSMS) employs a spot distribution pattern similar to the basic LSMS where 80 × 1 beams are aimed at the ceiling at different intensities. When the transmitter is in the centre of the room, a line strip of 80 diffusing spots is formed with a distance of 10cm between adjacent spots and along the x=2m line. The CALSMS transmitter considers the number of existing users within the room and redistributes the transmit power among beams according to the algorithm described earlier in this section. Figure 4.6 (a) shows the CALSMS configuration when two receivers are present and located at (1m, 1m, 1m) and (2m, 4m, 1m).

4.4.3 Collaborative Adaptive BCM (CABCM)

The spot distribution pattern based on a beam clustering method proposed and examined in [105], [142], [168] is extended in this system, where the total transmit power is adaptively distributed among the beams using a collaborative combining technique. The power allocated to each spot is calculated using a collaborative combining technique (in

this work collaborative MRC is considered), based on the number of coexisting receivers. In contrast to previous work [158], where the collaborative transmitter is coupled with a non-imaging angle diversity receiver, in this system an imaging receiver is employed. Our system employs 100 diffusing spots with a total power of 1W and each spot is allocated a different power level. The adaptive multibeam clustering transmitter produces 100 × 1 beams that form three groups of spots aimed at the three main surfaces: ceiling and two end walls. The CABCM geometry employs three clusters of beams, distributed when the transmitter is at the room centre as follows: 10 spots on each wall and 80 spots on the ceiling. The spot distribution structure in the CABCM is similar to that in BCM, shown in Figure 4.6 (b). With a collaborative transmitter and multiple receivers at a given set of coordinates, the collaborative adaptive algorithm previously described in this section is employed to adjust the transmitting power of the individual beams.

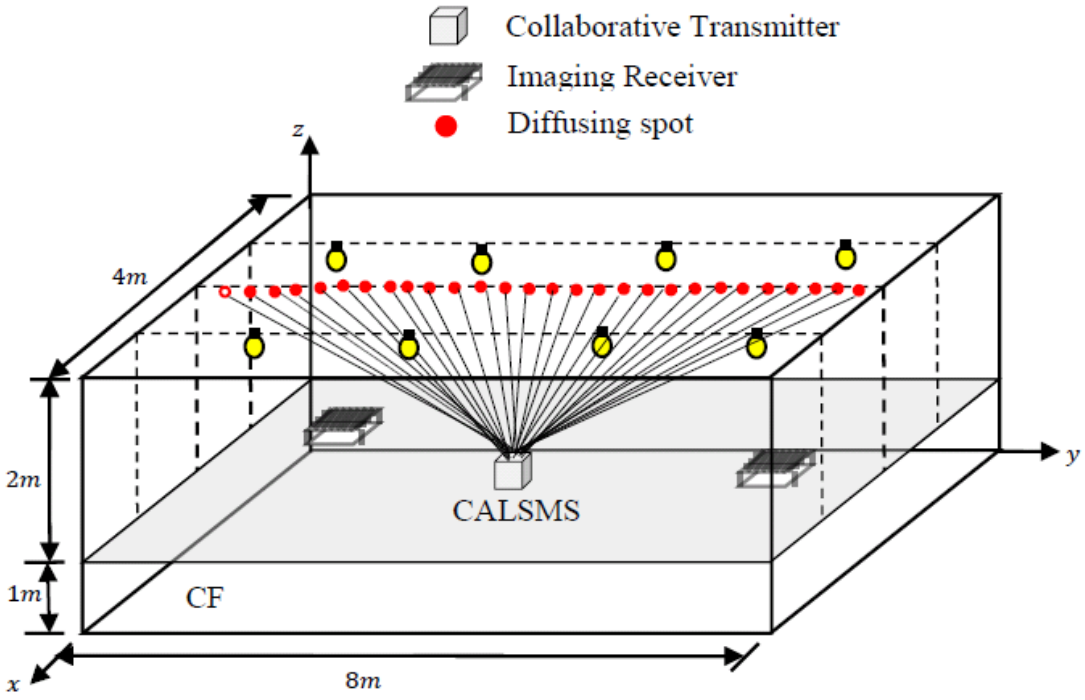

(a) CALSMS

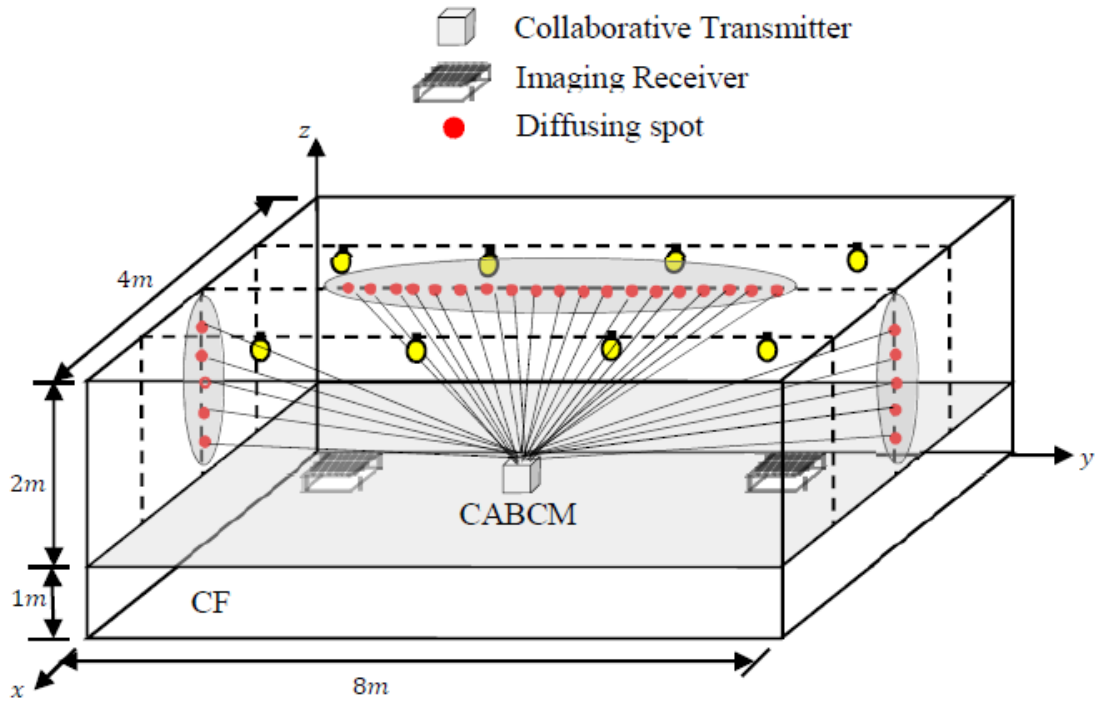

(b) CABCM

Figure 4.6: Collaborative multibeam transmitter configurations when the transmitter is placed at the room centre (2m, 4m, 1m) and two receivers are located at (1m, 1m, 1m) and (2m, 7m, 1m)

4.5 Simulation Results

4.5.1 Delay Spread Evaluation and Channel Bandwidth

For delay spread assessment, we considered two user scenarios where the first user moves along the x = 1m line and the second user is fixed at (2m, 7m, 1m). Figure 4.7 compares the delay spread distribution of the proposed mobile OW configurations for the mobile receiver (receiver moves along the x=1m line) when the transmitter is placed at the centre of the room (2m, 4m, 1m), in Room A. In multiuser systems, it can be seen that the

multibeam transmitter coupled with angle diversity receiver reduces the delay spared from 2.4ns to 0.5ns, due to the limited range of rays captured by the receiver.

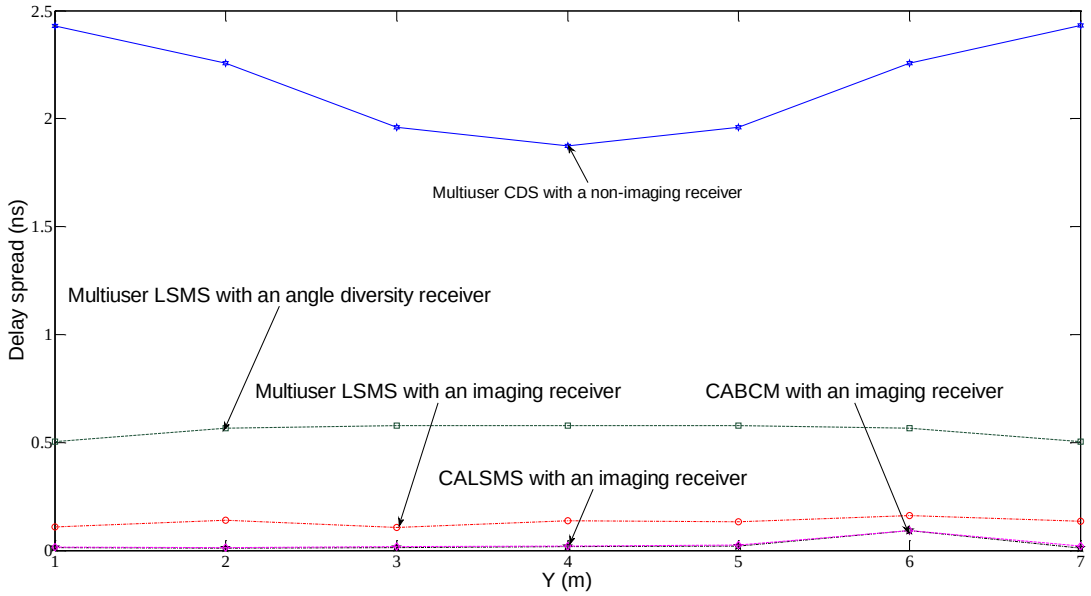

Figure 4.7: Delay spread distribution for the proposed configurations.

Furthermore, the imaging multiuser LSMS offers further reduction from 0.5ns to 0.11ns over the non-imaging multiuser LSMS, as a result of receiving a limited range of rays in a small pixel with narrow FOV. A significant reduction in the delay spread, by a factor of 25 at one of the least successful locations considered (1m, 1m, 1m), compared with multiuser systems, is achieved when one of the proposed collaborative multibeam system is employed. This is attributed to the allocation of higher power levels to the spots nearest to the receivers and the limited range of rays accepted in a small pixel with narrow FOV.

The results can be visualised as a bandwidth efficiency improvement, as seen in Table 4.2. The results indicate that the proposed methods produce significant improvements in the overall system bandwidth (i.e. channel included). At a transmitter–receiver separation of

6m, our imaging CABCM offers an increase in bandwidth from almost 300MHz to 5.27GHz when the CABCM replaces the multiuser LSMS. The channel bandwidths of our proposed systems are comparable, which can be explained on a similar basis to those highlighted in relation to delay spread when transmitted collaborative power adaptation is implemented. It can be seen clearly that the proposed collaborative adaptive multibeam systems are appropriate choices to combat multipath dispersion, and hence enable the system to achieve higher data rates.

Table 4.2: 3dB channel bandwidth of the proposed systems

Configuration	**3 dB channel bandwidth (GHz)**						
	Y (m)						
	1	**2**	**3**	**4**	**5**	**6**	**7**
Multiuser CDS (wFOV)	0.045	0.056	0.071	0.073	0.074	0.083	0.08
Multiuser LSMS (ADR)	0.021	0.024	0.087	0.23	0.14	0.29	0.27
Multiuser LSMS (IMG)	0.29	0.64	1.22	1.19	1.03	1.01	0.93
CALSMS (IMG)	5.2	5.3	5.3	5.69	5.5	5.66	5.7
CABCM (IMG)	5.27	5.35	5.28	5.67	5.47	5.7	5.71

4.5.2 SNR Analysis

In this section we analyse the performance of our proposed imaging collaborative multibeam configurations in terms of SNR, when the OW system operates at different bit rates, 30Mbit/s, 2.5Gbit/s and 5Gbit/s, in the presence of ambient light noise, multipath propagation and mobility. Comparisons with the multiuser CDS and multiuser LSMS operating at 30Mbit/s are also presented. Different multiuser scenarios are considered.

Following the SNR analysis given in Section 3.8.3, which interprets the impact of the pulse spread caused by ISI, the total noise variance refers to how the input of each pixel of the imaging receiver is made up of three components. These include the pre-amplifier noise variance component σ_{pr}^2, the background light-induced shot noise variance σ_{bn}^2 and the shot noise variance components associated with P_{s0} and P_{s1} which are σ_{s0}^2 and σ_{s1}^2, respectively. The latter, the signal-dependent noise (σ_{si}^2), is very low and can be ignored, based on experimental findings [69]. The narrow FOVs associated with the pixels of the imaging receiver reduce the ambient-induced shot noise σ_{bn}^2, which can be calculated using (3.45). The 30Mbit/s OOK preamplifier employed in our imaging systems utilises the PIN FET transimpedance pre-amplifier used in [96]. For simplicity, the FET gate leakage and $1/f$ noise is ignored. Therefore, the pre-amplifier noise variance is given by [96]:

$$\sigma_{pr}^2 = \frac{4kT}{R_f} I_2 B + \frac{16\pi^2 kT\Gamma}{g_m} (C_d + C_g)^2 I_3 B^3 \tag{4.7}$$

Observing (4.7), the pre-amplifier noise variance consists of two noise terms that represent thermal noise from the feedback resistor and from the FET channel resistance. In the first term; k is the Boltzmann's constant, T is absolute temperature, R_f is the feedback resistance, $I_2 = 0.562$, and B is the bit rate. In the second term, Γ is the FET channel noise factor, g_m is the FET transconductance, $I_3 = 0.0868$, C_d and C_g are the detector and FET gate capacitances respectively. It is assumed that $C_g \ll C_d$, in order to simplify the calculations. The capacitance per detector area unit η_c is fixed as the capacitance C_d is proportional to the detector area A', i.e., $C_d = \eta\ A'$. Beside the 30Mbit/s

bit rate, we consider higher bit rates of 2.5Gbit/s and 5Gbit/s. We assume that the receiver bandwidth is equal to the bit rate B, which imposes the condition $R_f = G/2\pi BC_d$ where G is a limited open-loop voltage gain. Therefore, (4.7) can be written as:

$$\sigma_{pr}^2 = \frac{8\pi kT}{G}\eta_c A' I_2 B^2 + \frac{16\pi^2 kT\Gamma}{g_m}\eta_c{}^2 A'^2 I_3 B^3. \tag{4.8}$$

In our calculation, we used parameter values similar to that used in [96]: $\Gamma = 1.5$, $T = 295K$, $R = 0.54\frac{A}{W}$, $G = 10$, $g_m = 30$ms, and $\eta_c = 112\text{pF/cm}^2$. At higher data rates of 2.5Gbit/s and 5Gbit/s, we used the PIN FET receiver in [169]. In this chapter, the resultant electrical signals are processed using SB and MRC approaches. The SB method chooses the pixel with highest SNR, and the obtained SNR is given by:

$$SNR_{IMG,SB} = \max_j \left(\frac{R \times \left(P_{s1j} - P_{s0j}\right)}{\sigma_{0j} + \sigma_{1j}} \right)^2 \quad 1 \le j \le J \tag{4.9}$$

where J is the number of pixels considered ($J = 200$). Note that as the number of pixels increases (with a fixed total detection area), the area of each pixel decreases so that the noise variance per pixel decreases. Adder circuit can be used to combine the output signal of all branches. Each input to the circuit is added with a weight (is proportional to its SNR), thereby maximizing the SNR of the weighted sum. The output signals of pixels are combined using weights equal to:

$$w_j = \frac{R(P_{s1j} - P_{s0j})}{\left(\sigma_{0j} + \sigma_{1j}\right)^2} \qquad 1 \le j \le J \tag{4.10}$$

in which the SNR obtained using MRC is given by:

$$SNR_{IMG,MRC} = \frac{\left(\sum_{j=1}^{J} R\left(P_{s1j} - P_{s0j}\right) w_j\right)^2}{\sum_{j=1}^{J} \left(\sigma_{0j} + \sigma_{1j}\right)^2 w_j^2} \tag{4.11}$$

$$\begin{aligned} SNR_{IMG,MRC} &= \frac{\left(\sum_{j=1}^{J} R\left(P_{s1j} - P_{s0j}\right) \frac{R\left(P_{s1j} - P_{s0j}\right)}{\left(\sigma_{0j} + \sigma_{1j}\right)^2}\right)^2}{\sum_{j=1}^{J} \left(\frac{R\left(P_{s1j} - P_{s0j}\right)}{\left(\sigma_{0j} + \sigma_{1j}\right)^2}\right)^2 \left(\sigma_{0j} + \sigma_{1j}\right)^2} \\ &= \sum_{j=1}^{J} \left(\frac{R\left(P_{s1j} - P_{s0j}\right)}{\left(\sigma_{0j} + \sigma_{1j}\right)}\right)^2 = \sum_{j=1}^{J} SNR_j \end{aligned} \tag{4.12}$$

It easy to show that the SNR achieved with MRC is higher than with SB method, at the cost of increased circuit complexity [96]. This complexity is related to the increased signal processing so as to obtain the appropriate weighting gain factor compared to the SB.

4.5.2.1 Collaborative Stationary Receivers

In this section, we evaluate SNR of the proposed imaging collaborative multibeam systems (CALSMS and CABCM) when receivers are fixed in certain locations in the room. The layout of the receivers is shown in Figure 4.2 (a). The number of receivers was increased gradually when two, three and five users were present. To investigate the impact of the transmitter mobility, we consider two transmitter locations: when the transmitter is at the room centre (2m, 4m, 1m) and at (2m, 1m, 1m). Simulation results are quoted when the system operates under the constraints of BN and multipath dispersion at 30Mbit/s. The results show that the SNR obtained by MRC can achieve better performance than SB. For instance, in the two-user scenario and when the transmitter is

at (2m, 4m, 1m), users at (1m, 1m, 1m) and (2m, 7m, 1m) who employ MRC CALSMS can achieve SNR improvement of 4.9dB and 4.7dB over SB CALSMS. Similarly, SNR improvements of 5.4dB and 4.7dB are observed when MRC CABCM is employed, as shown in Table 4.3.

Table 4.3: SNR of two collaborative multibeam systems (CALSMS and CABCM) for three multiuser scenarios when the transmitter is at the room centre (2m, 4m, 1m)

Multiuser scenario	Imaging CALSMS									
	(1m ,1m, 1m)		(2m ,7m, 1m)		(2m ,4m, 1m)		(1m ,7m, 1m)		(3m ,1m, 1m)	
	SB	MRC	SB	MRC	SB	MRC	SB	MRC	SB	MRC
Two-user	46.3	51.2	58.5	63.2	-		-		-	
Three-user	41.5	47.1	53.6	58.4	53.6	58.5	-		-	
Five-user	44.9	50.1	53.95	58.7	51.2	56.2	49.86	54.7	44.9	50.1
	Imaging CABCM									
Two-user	44.9	50.3	57.2	58.5	-		-		-	
Three-user	40.6	49.4	52.9	55.8	52.8	55.7	-		-	
Five-user	44.1	50.1	53.2	55.9	50.4	54.7	49.2	51.9	44.1	50.1

Our imaging systems achieve comparable SNR performance when the transmitter is placed at the room centre. This is due to the fact that the power adaptation algorithm distributes the power among beams according to the locations of the receivers, so that spots that are within the reception area are assigned the highest power. Table 4.4 shows the impact of transmitter mobility in both imaging systems. It is observed that the SNR level decreases at the least successful locations (i.e. at a 6m transmitter–receiver horizontal separation), whereas it increases at the most successful receiver position (near the transmitter). For example, in a two-user scenario the SNR of the receiver (SB) positioned at (2m, 7m, 1m) is decreased from 58.5dB to 24.5dB, while the SNR of receiver at (1m, 1m, 1m) is increased by 9.1dB. This is a result of power distribution

among beams, which is based on the SNR to which a given spot power allocation leads in the receiver. In the collaborative MRC power adaptation algorithm, each beam is allocated power in proportion to the total power requested by all receivers. The results also show that the imaging CABCM performs better than the imaging CALSMS. This is due to the spot distribution pattern used in CABCM system, where the structure has the ability to cover surroundings through three beam clusters.

Table 4.4: SNR of the proposed imaging systems (CALSMS and CABCM) for three multiuser scenarios when the transmitter is at the roo*m* centre (2m, 1m, 1m)

Multiuser scenario	SNR of imaging CALSMS									
	(1m ,1m, 1m)		(2m ,7m, 1m)		(2m ,4m, 1m)		(1m ,7m, 1m)		(3m ,1m, 1m)	
	SB	MRC	SB	MRC	SB	MRC	SB	MRC	SB	MRC
Two-user	55.4	60.5	24.5	25.1	-		-		-	
Three-user	46.1	51.9	38.9	43.4	58.2	62.8	-		-	
Five-user	49.5	54.9	36.7	41.1	55.8	60.6	34.8	39.4	49.5	54.9
	SNR of imaging CABCM									
Two-user	51.5	56.6	52.5	57.6	-		-		-	
Three-user	44.5	50.3	45.3	51	56.6	61.3	-		-	
Five-user	48	53.4	45.5	49.9	54.3	59.1	41.4	44.3	48	53.4

4.5.2.2 Collaborative Mobile Receiver

The performance of the proposed collaborative multibeam systems (CALSMS and CABCM) coupled with an imaging receiver is compared with multiuser CDS (wide FOV receiver of 65º) and multiuser LSMS, operating at 30Mbit/s, when the transmitter is place at (1m, 1m, 1m). Figure 4.8 shows the SNR achieved by a mobile user that moves at constant x = 2m and along the y-axis in the presence of a stationary receiver at (2m, 7m, 1m). The results indicate that the SNR level of the proposed configurations for the mobile user is at maximum level when the receiver is at a location near the transmitter.

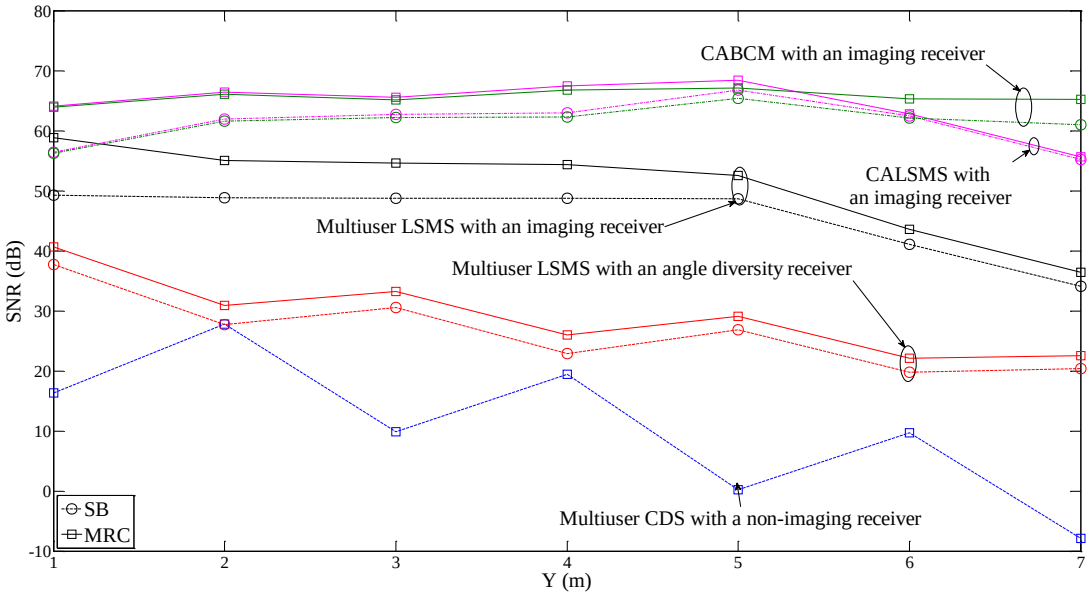

Figure 4.8: SNR of four mobile OW systems; CDS with a single non-imaging receiver, LSMS with a non-imaging diversity receiver, LSMS and CALSMS in conjunction with an imaging receiver based on (SB and MRC) when the transmitter is placed at (1m, 1m, 1m) and a mobile receiver moves along the x = 2m line at a bit rate of 30 Mbit/s

The results show that background noise has a significant effect on the multiuser diffuse system when a single wide FOV receiver is employed. The effect of the BN can be reduced through the use of angle diversity receivers, where a narrow FOV helps to eliminate undesired signals. The combination of multiuser LSMS and an angle diversity receiver offers a significant SNR improvement of 24dB over the multiuser CDS. A further SNR enhancement of 5dB can be obtained when an imaging receiver replaces the angle diversity receiver. It is also observed that our proposed imaging collaborative multibeam systems offer significant SNR improvement over the multiuser systems. This improvement is attributed to two effects: first, the use of collaborative adaptive power distribution. Here, the spots nearest to the receivers are assigned high power levels. Second, the small size of the pixel associated with narrow FOV, which eliminates the effect of BN. The impact of transmitter mobility can be clearly seen at 6m transmitter–

receiver horizontal separation distance, in which case a power penalty of 9dB can be induced when the CALSMS replaces the CABCM.

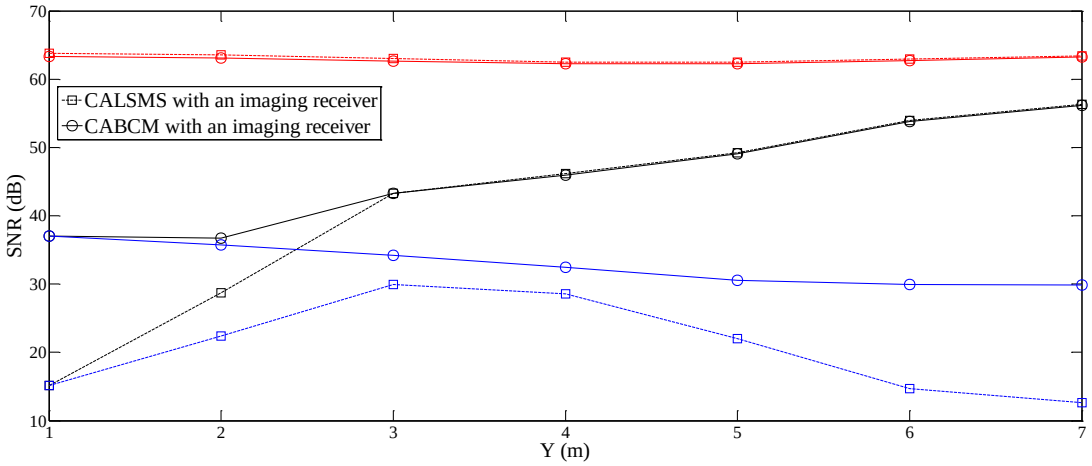

(a)

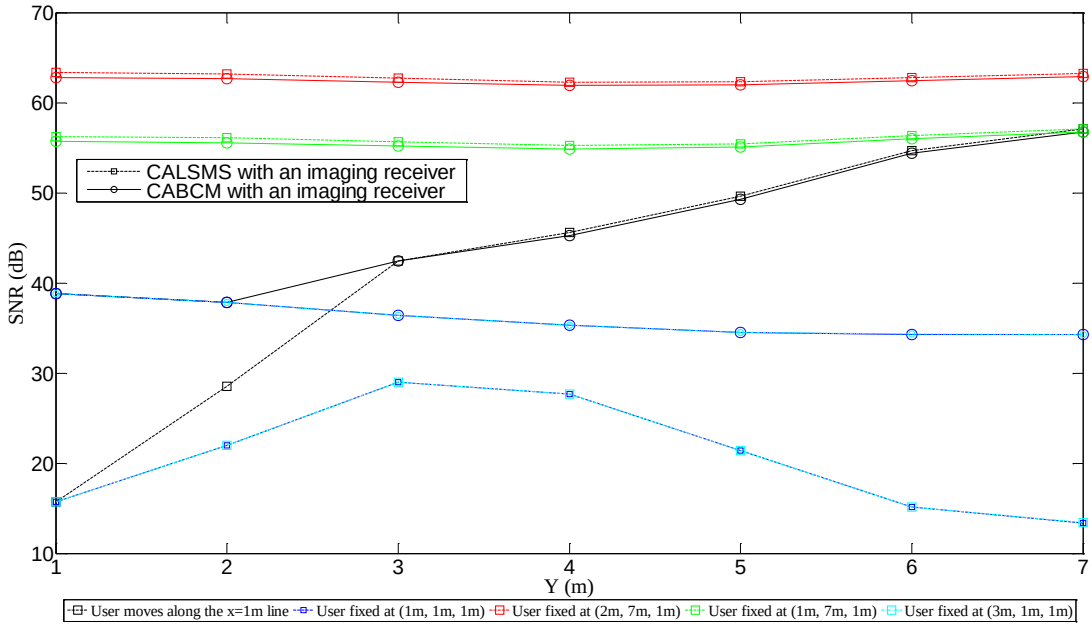

(b)

Figure 4.9: SNR of the proposed systems (CALSMS and CABCM) when the transmitter is at (2m, 7m, 1m) and multiple receivers coexist: (a) three-user scenario; and (b) five-user scenario.

Figure 4.9 show the SNR levels of our collaborative systems (CALSMS and CABCM) when the transmitter is at (2m, 7m, 1m) and multiple receivers coexist (three-user and five-user scenarios are considered). The positioning of the receivers in these scenarios is illustrated in Figure 4.2(b). The findings show that receivers fixed at (2m, 7m, 1m) and (1m, 7m, 1m) have maintained even distribution while the mobile receiver moves along the x=1m line, a result of being stationary at locations near the transmitter. At the least successful locations where few spots can be observed by the receiver, that is, when the receivers are located at (1m, 1m, 1m) or (3m, 1m, 1m), the CABCM offers a 23dB SNR improvement over the CALSMS, illustrating the gain achieved through beam clustering. The lowest SNR levels recorded among users are 13.4dB and 34.3dB when CALSMS and CABCM are employed, respectively. Therefore, the CABCM was evaluated at higher data rates, as shown in Figure 4.10. The high and uniform SNR improvement shown in the results can prove extremely useful in increasing the data rate of the system.

High bit rates (2.5Gbit/s and 5Gbit/s) indoor optical wireless systems are shown to be feasible through the combination of collaborative multibeam transmitter and an imaging receiver. In order to enhance the link budget at higher data rates, an imaging receiver similar to the one used in [170] is employed where the acceptance semi angle is reduced to 45° and the number of pixel is increased to 256, resulting in a pixel area of 0.99 mm^2 and FOV of 7.1°. The SNRs associated with 2.5 Gbit/s and 5 Gbit/s CABCM in conjunction with an imaging receiver for a moving user in two-user and three-user scenarios are depicted in Figure 4.10 at two transmitter locations (2m, 4m, 1m) and (2m, 1m, 1m).

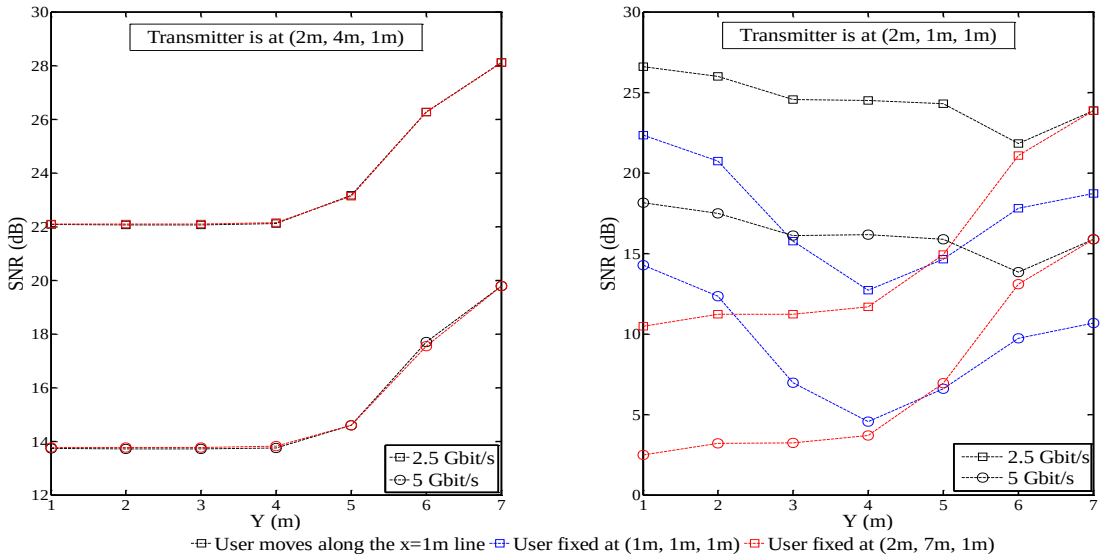

Figure 4.10: SNR of the CABCM in conjunction with an imaging receiver based on MRC operating at 2.5 Gbit/s and 5 Gbit/s bit rates when: (a) two receivers are present; and (b) three receivers are present. Two users are fixed and one moves along the x=1m line

In a two-user scenario, the SNRs achieved in the proposed system are about 22dB and 14dB at 2.5Gbit/s and 5Gbit/s, respectively. The results show that a stationary user in the worst case scenario (6m horizontal separation between the transmitter and receiver) can still achieve SNR of 13.9dB when the system operates at 2.5Gbit/s in three-user scenario, where SNR is still greater than 9.5 dB (BER $< 10^{-3}$). Therefore, forward error correction (FEC) can be used to reduce the BER further from 10^{-3} to 10^{-9} in our proposed system. The higher date rates of the CABCM are shown to be feasible through a combination of the proposed methods (a collaborative multibeam transmitter and an imaging receiver).

4.6 Effect of Realistic Indoor Environment

The previous section has shown that the imaging CABCM is a promising collaborative indoor OW system in terms of performance. In this part, we extend the evaluation of the imaging CABCM to a realistic office environment where optical signal blockage (by

office mini-cubicles, furniture, windows and doors) is present. The study was under the constraints of multipath propagation mobility and ambient light noise. Comparison with CDS with a wide FOV receiver, and LSMS with a non-imaging and imaging receivers is also considered. The SNR results (simulation) of the proposed configurations operating at 30Mbit/s in two room scenarios (shadowed and unshadowed rooms) are depicted in Figure 4.11, where the transmitter is at (2m, 7m, 1m) and the mobile receiver, in two-user scenario, moves along the x=1m line. A stationary user at (2m, 7m, 1m) is taken into account when collaboratively adapting the power among beams in the imaging CABCM. There is no effect of the stationary user on the mobile user in multiuser systems, as users are independent of each other, as a result of distributing the power equally among beams.

Figure 4.11 displays the SNR distribution for two rooms: an empty room and a one in a real office environment (see

Figure 4.1). The results show the weakness of the non-imaging multiuser systems and the robustness of imaging systems against shadowing, signal blockage and mobility. The impact of shadowing on the non-imaging multiuser systems can be seen as SNR degradation of 18dB and 4.6dB when CDS with a wide FOV receiver and LSMS with a diversity receiver are employed. This is attributed to the significant increase of power loss, where part of the signal is either blocked (by office cubicles) or lost (penetrating through windows). The SNR degradation can be mitigated when a non-imaging receiver is replaced by an imaging receiver. Introducing a collaborative power adaptive BCM (CABCM) OW system can considerably decrease the effect of mobility and shadowing in a realistic indoor environment. In the worst communication link considered, our

proposed imaging CABCM offers SNR enhancement of 34 dB over the imaging multiuser LSMS. The high and uniform SNR improvement shown in the results can prove extremely useful in increasing the data rate of the system. High bit rates (2.5Gbit/s and 5Gbit/s) indoor optical wireless systems are shown to be feasible through the combination of collaborative multibeam transmitter and an imaging receiver. In realistic office environment, the SNRs associated with 2.5Gbit/s and 5Gbit/s CABCM in conjunction with an imaging receiver for a moving user in three-user and five-user scenarios are depicted in Figure 4.12 (a) and (b) at a transmitter location (2m, 1m, 1m). It can be seen that the achieved SNR levels are influenced by the number of coexisting users.

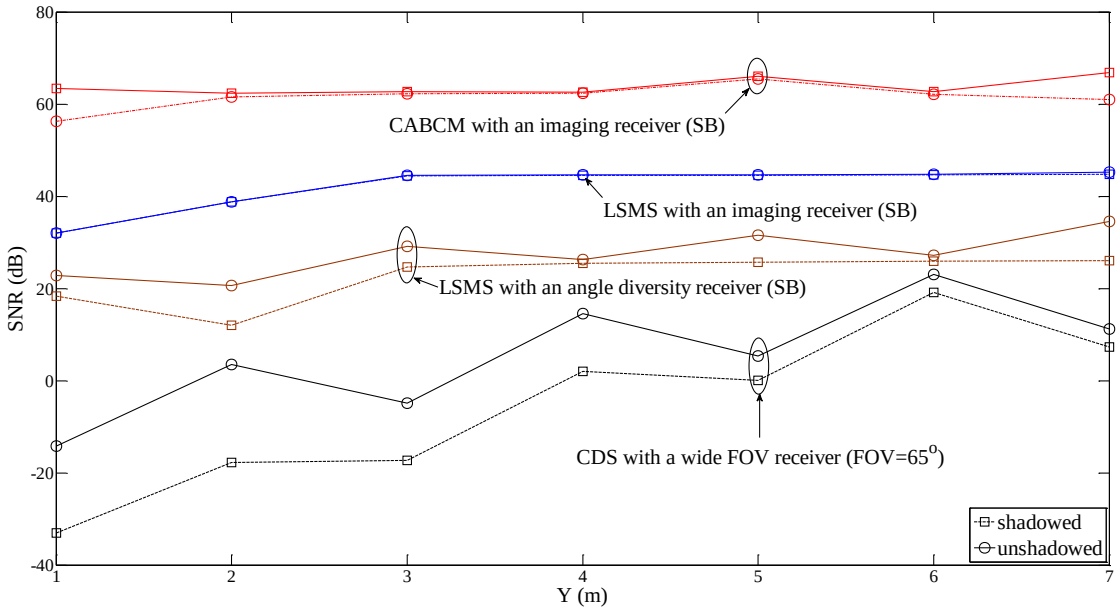

Figure 4.11: SNR of the CABCM, LSMS and CDS systems operating at 30 Mbit/s in two room scenarios (shadowed and unshadowed) when the transmitter is placed at (2m, 7m, 1m) and a mobile receiver (in the presence of a stationary receiver) moves along the x = 1m line

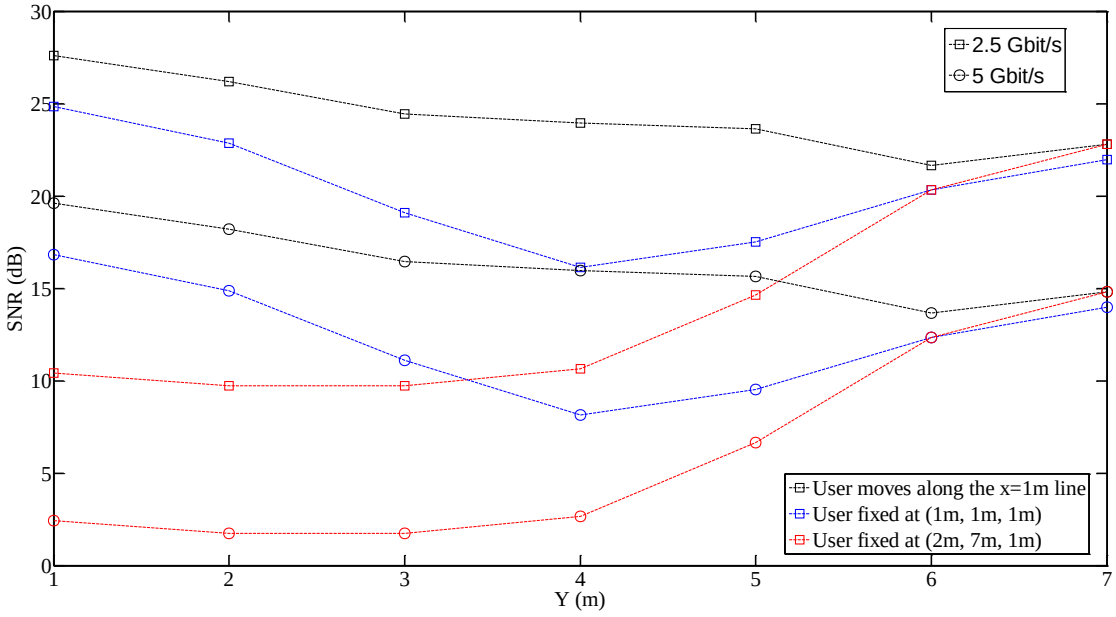

(a)

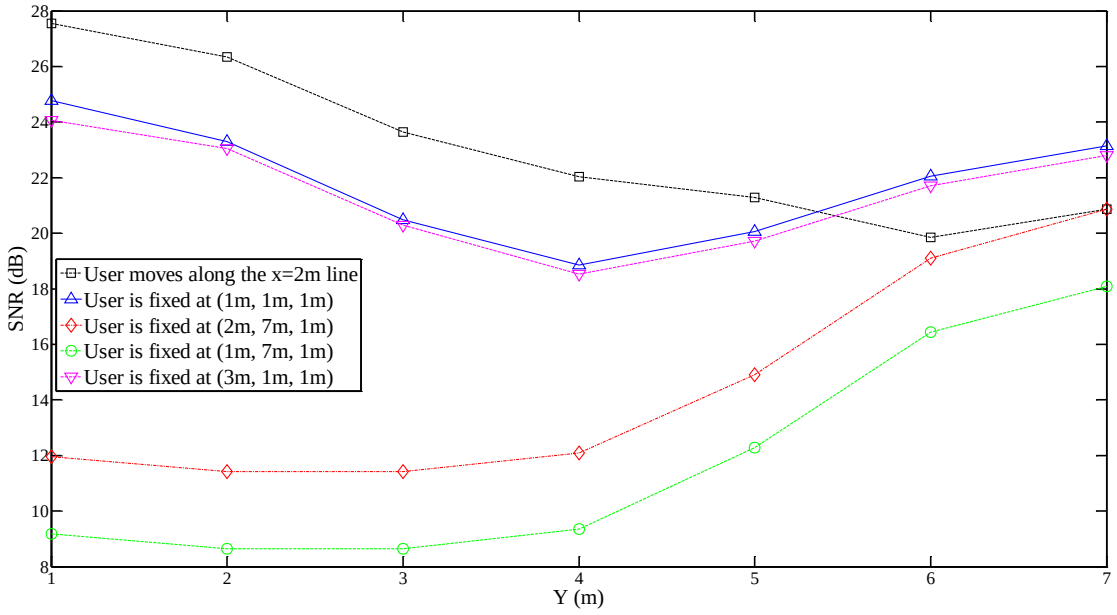

(b)

Figure 4.12: SNR of the proposed system (CABCM) when the collaborative receivers operate at 2.5Gbit/s and 5Gbit/s in two multiuser scenarios (a) three-user scenario and (b) five-user scenario when the transmitter is at (2m ,1m, 1m)

The results show that a stationary user in the worst case scenario (6m horizontal separation between the transmitter and receiver) can still achieve SNR of almost 14dB when the system operates at 2.5Gbit/s in a three-user scenario, where SNR is still greater

than 9.5dB (BER $< 10^{-3}$). Therefore, forward error correction (FEC) can be used to further reduce the BER from 10^{-3} to 10^{-9} in our proposed system. The influence of the increase in the number of coexisting users on the SNR level can be seen when the CABCM is employed in a realistic room (Room B) in the presence of five users, as depicted in Figure 4.12 (b). At a transmitter–receiver separation of 6m, the two receivers at the far end (receivers at (2m, 7m, 1m) and (1m, 7m, 1m)) receive less power than those users close to the transmitter. This is due to lowering the transmitted power of the spots close to the far end receivers and reallocating the power to the spots close to receivers near the transmitter. Therefore, distributing the transmitted power fairly among diffusing spots warrants further study. The performance degrades gradually with increase in the number of users. The higher date rates of the CABCM are shown to be feasible through a combination of the proposed methods (a collaborative multibeam transmitter and an imaging receiver).

4.7 Summary

In this chapter, two collaborative multibeam OW systems (CALSMS and CABCM) were introduced to improve the system performance in the presence of shadowing. The system's performance was evaluated in the presence of up to five receivers, considering two different scenarios based on several criteria including transmitter–receiver separation distance, mobility and weak points in the communication link. Simulation results of our proposed collaborative multibeam transmitters in conjunction with an imaging receiver have shown that high data rates are feasible in collaborative OW systems. It is observed

that the CABCM is less affected by the transmitter and/or receiver mobility than the CALSMS. This is a result of beams that are clustered in more than a single reflecting surface, where three group of beams are aimed to the ceiling and end walls. In an unshadowed link at 30Mbit/s, the proposed system (imaging CABCM) provides SNR enhancements of 34 dB over the non-imaging multiuser LSMS system. This improvement was achieved by introducing multibeam geometries, beam power adaptation, using collaborative combining techniques and small size pixels with narrow FOVs. The improvement in SNR can be used to achieve higher data rates, and 2.5Gbit/s and 5Gbit/s were shown to be feasible in the multiuser environment considered when imagining CALSMS system is employed. Degradation in the SNR is observed when the number of users increases. Therefore, fair power distribution is indispensable to help all users achieve higher SNR. It should be noted that our proposed collaborative multibeam system benefits greatly when the beams are distributed on different surfaces.

5 Max-Min Fair Power Adaptation for Indoor Collaborative Multibeam Systems

5.1 Introduction

The previously proposed collaborative multibeam system (CABCM) has shown significant SNR improvement over non-imaging multiuser systems as well as robustness against mobility compared to the imaging CALSMS. However, at high data rates and when the number of coexisting users increases, the performance degrades due to unfair power distribution. Therefore, in this chapter we extend the treatment of the imaging CABCM system and investigate the fairness of power distribution when adapting the beams' power in the presence of multiple users. We introduce a Max-Min fair power adaptation algorithm to the collaborative OW multibeam systems in order to distribute the total power fairly among beams with the aim of maximising the SNRs of all receivers present. A liquid crystal device can be used to vary the intensity of the beams adaptively at relatively low complexity [171], [172]. The adaptation requires training and feedback from the receiver to the transmitter, and a low data rate diffuse channel is suggested to achieve this feedback. To ensure fair power distribution as well as to enhance the system performance, an iterated Max-Min fairness algorithm is simulated, analysed and evaluated in various multiuser scenarios.

5.2 System Description

In order to evaluate the benefit of our methods (Max-Min beam power adaptation, multi-spot diffusing and imaging reception) in a collaborative indoor OW system, a simulation was performed in an empty rectangular room with dimensions of 8m × 4m × 3m (length × width × height). The room reflecting surfaces (ceiling and walls) are modelled as ideal Lambertian reflectors with reflectivity of 0.8 for the walls and ceiling and 0.3 for the floor. In order to model the reflections, these reflecting surfaces are subdivided into a number of small square elements. The accuracy of the received impulse response profile is controlled by the size of the surface elements, and therefore element sizes of 5cm × 5cm for first-order reflections, and 20cm × 20cm for second-order reflections are used. Reflections from doors and windows are considered to be entirely the same as reflections from walls.

To investigate the functionality of the proposed system under mobility, four configurations were considered: Max-Min CABCM, MRC CABCM, BCM and CDS, with the transmitter positioned on the CF at four different locations: (2m, 4m, 1m), (1m, 1m, 1m), (2m, 1m, 1m), and (2m, 7m, 1m), pointing upwards and emitting a total optical power of 1W with an ideal Lambertian radiation pattern. In order to quantify the proposed systems performance within a multiuser environment, three scenarios were studied: two-user, three-user and five-user, as shown in Figure 4.2. The coexisting receivers were also evaluated when all are stationary as well as when a receiver is mobile, that is, the mobile user moves at constant x and along the y-*axis*. The receivers' locations were based on several criteria, including the number of coexisting users, transmitter or/and receiver

mobility, the weakest communication links (i.e. one or more user under the ambient light sources), and the distance between the transmitter and the receiver. The room's eight directed lamps represent ambient light noise, as described in previous chapters. Table 5.1 gives more details about the simulation parameters used in this study.

Table 5.1: Simulation parameters

Parameter	**Configuration Uplink Transmission**			
Room				
Length	8m			
Width	4m			
Height	3m			
ρ _x_z Wall	0.8			
ρ _y_z Wall	0.8			
ρ _x_z op. Wall	0.8			
ρ _y_z op. Wall	0.8			
ρ _Floor	0.3			
Transmitter				
Number of Transmitter	1			
Location (x, y, z)	(1,1,1)	(2,1,1)	(2,4,1)	(2,7,1)
Elevation	90°	90°	90°	90°
Azimuth	0°	0°	0°	0°
Imaging Receiver				
Number of Present Receivers	2	3		5
Detector array's area	$2cm^2$			
Number of Pixels	200			
Area of Pixel	$1mm^2$			
Elevation	90°			
Azimuth	0°			
Acceptance semi-angle	65°			
Time bin duration	0.3ns		0.01ns	
Bounces	1		2	
Number of elements	32000		2000	
dA	5cm × 5cm		20cm × 20cm	
Spot lamps				
Number of spot lamps	8			
Locations (x, y, z)	(1,1,3), (1,3,3), (1,5,3), (1,7,3) (3,1,3), (3,3,3), (3,5,3), (3,7,3)			
Wavelength	850 nm			
Bandwidth	30MHz	2.5GHz		5GHz
Bit rate	30Mbit/s	2.5Gbit/s		5Gbit/s

5.3 Max-Min Fair CABCM (Max-Min CABCM)

In this section, a new collaborative multibeam configuration is presented, analysed and compared previous key existing OW systems to find the best geometry for use in collaborative indoor OW systems. Simulations were developed to evaluate the obtained improvement through the use of our proposed methods (Max-Min Fair power adaptation, multibeam transmitter, and imaging reception). The findings have shown that the CABCM system is more robust against mobility, therefore is considered here for comparison. The CABCM system distributes the power among beams based on collaborative MRC technique, therefore it is denoted here by MRC CABCM. Moreover, the beam clustering method is an attractive technique [104], [105], [142] and its structure has been adopted in CABCM, therefore it is used for comparison purposes in this study.

The distribution of transmitted power fairly among beams is a key factor in collaborative multibeam systems. Due to this fact, the Max-Min fairness algorithm is an effective method that can help distribute the total transmit power fairly among diffusing-spots for multibeam transmitters, and hence optimise the SNR level of all coexisting receivers. In contrast to the MRC CABCM, where the transmit power is collaboratively adapted among beams based on collaborative MRC technique, with this method the total power is efficiently distributed, taking into consideration the known Max-Min fairness criterion (ie maximising the minimum SNR) in terms of improving the SNR of the receiver at the least successful location.

Table 5.2: Max-Min fairness algorithm for collaborative OW systems

Algorithm I: Max-Min Power Adaptation Algorithm	
1	$N_{spot} = 100$; (number of spots)
2	$N_{photodetector} = 200$; (number of photodetectors)
3	*Obtain* N_{user}; (number of users)
4	*Set* $N_{iteration} = N_{user}$; (number of iterations)
5	*INIT* $P_s = 1/N_{spot}$;
6	*For k = 1:* N_{user}
7	*For s = 1 :* N_{spot}
8	*For j = 1 : J*
9	*Compute* P_j;
10	*Calculate* SNR_j
11	*End*
12	$SNR_{k,s} = \max_j(SNR_j)$
13	$P_{k,s} = find(SNR_j == \max_j(SNR_j))$; (the power requested by a receiver ***k*** from a spot ***s***)
14	*End*
15	*Compute* SNR_k; (SNR of each receiver)
16	*End*
17	Compute multiplier $\boldsymbol{x} = 1/\sum_k^{N_{user}}\left(\frac{1}{SNR_k}\right)$;
18	*For k = 1:* N_{user}
19	*For s = 1 :* N_{spot}
20	$P_s = \sum_k^{N_{user}}\left(\frac{P_{k,s}}{SNR_k}\right) \times \boldsymbol{x}$
21	*Calculate and sum the received power*
22	*End*
23	*Compute* SNR_k; (preoptimized SNR of each receiver)
24	*End*
25	*For I = 1 :* $N_{iteration}$
26	Compute $SNR_{k_{min}} = \min_k(SNR_k)$;
27	$k_{min} = find(SNR_k == \min_k(SNR_k))$; (find user with minimum SNR)
28	Compute $SNR_{k_{max}} = \max_k(SNR_k;)$;
29	Compute $SNR_{threshold} = (SNR_{k_{min}} + SNR_{k_{max}})/2$; (threshold SNR is the target SNR level for the minimum user)
30	Set $SNR_{k_{min}} = SNR_{threshold}$; (maximize the SNR of the user with minimum SNR)
31	Compute multiplier $\boldsymbol{x} = 1/\sum_k^{N_{user}}\left(\frac{1}{SNR_k}\right)$;
32	*For k = 1:* N_{user}
33	*For s = 1 :* N_{spot}
34	$P_s = \sum_k^{N_{user}}\left(\frac{P_{k,s}}{SNR_k}\right) \times \boldsymbol{x}$
35	Calculate and sum the received power
36	*End*
37	Compute SNR_k; (SNR_k at last iteration is the optimum SNR)
38	*End*
39	*End*

Our definition of Max-Min Fair power distribution in multiuser environments is based on the definition used in [173] and [174]. In this study, we aim to maximise the SNR level of the user with minimum SNR by allocating more power to the diffusing-spots near it. A threshold SNR level has been used, from the maximum and minimum SNR values achieved by coexisting receivers. This threshold level can help to ascertain how much power should be allocated to the diffusing-spots located near the user with minimum SNR. For fair collaborative power distribution, the new system makes use of the iterative Max-Min fairness algorithm, where the adaptation process is repeated a number of times. The number of iterations is chosen to be equal to the number of users present within the room, so that a user affected in the first adaptation round can be compensated in the next iteration. The processes used for adapting the power in the MRC CABCM system is considered here in order to determine the pre-optimised SNRs. Thus, the minimum and maximum SNR values are obtained and then used in the iterative Max-Min Fairness algorithm. The optimum SNRs for Max-Min fairness in a multiuser scenario can be determined according the following steps:

1. The transmitter senses the environment to determine the number of existing receivers N_{user}, and sets the number of iterations equal to the number of users $N_{iteration} = N_{user}$. This can be achieved by the transmitter sending a becon message indicating its intention to transmit. Receivers present in the environment then respond allowing the transmitter to determine the number of receivers in the environment. The transmitter and receivers can use CDMA or a time slotted

medium access control (MAC) protocol to enable this phase of the Max-Min fairness algorithm.

2. The transmitter switches on $N_s \times 1$ beams that form three group of spots pointed to three main surfaces: ceiling and two end walls. In our case the transmitter employs three clusters distributed as follows: 80 spots on the ceiling and 10 spots on each wall. Equally distribute the total power among the beams.
3. Turn on each spot *s* individually, and compute the power requested by receiver *k* as well as calculate the SNR at each detector. Select the best SNR and assign the request power by the detector as the power requested by that receiver for this spot$(P_{k,s})$.
4. Inform the transmitter of the SNR and power associated with the spot by sending a feedback signal at a low rate. This feedback channel can be implemented using a diffuse link or by modulating an additional beam.
5. Repeat Steps 3 and 4 for all spots.
6. Redistribute the transmit power among the spots using collaborative MRC technique using (4.4).
7. Compute the pre-optimised SNRs of all users.
8. Determine the minimum SNR, maximum SNR and threshold SNR values. The threshold SNR is the SNR at the mid point between the maximum and minimum SNR. The threshold SNR value is the desired SNR, ie SNR assigned to the user with the lowest SNR value. Note that this threshold SNR selection effectively employs a divide and conquer approach to maximising the minimum SNR hence inheriting its algorithmic properties.

9. Identify the user with the minimum SNR (k_{min}) and assign it to the threshold SNR.
10. Redistribute the total power, again based on the new SNR value assigned to k_{min}. It should be noted that the new spot power is calculated using (4.4) as in Step 6.
11. Repeat Steps 7 to 10 for $N_{iteration}$. The final power distribution is achieved at the last iteration. It is worth noting that when users are collocated close to each other, improvements in the power distribution are barely discernible.

The algorithm described above applies to the multiuser scenarios where at least two users are in the room. For a single transmitter and multiple receivers at a given set of coordinates, this algorithm is carried out to determine the maximum SNRs for the coexisting receivers. However, a power penalty can be incurred when the transmitter or/and a receiver move. The system design can set an SNR margin where the transmitter can repeat the adaptation process when one or more of the receiver's SNR has significantly changed. In a single user case, Steps 1-7 can be used to adapt the power for a single user where the beams' power is adapted so as to maximise the SNR at a given receiver location. The MAC protocol should include a repetitive training period that allows iterative processes to be executed. Training should be performed at a slow rate commensurate with changes in the environment (i.e. human motion). A liquid crystal device can be used to redistribute the power among the beams at low complexity. Based on the characteristics of such a device, the adaptation can be performed in milliseconds.

5.4 Performance evaluation of Max-Min Fair Power Adaptation

5.4.1 SNR Analysis

The performance of our proposed system (Max-Min CABMC) using imaging receivers is evaluated in an empty room under the constraints of multipath propagation, BN and mobility. Simulation results of the proposed system in comparison with MRC CABCM, when both systems employ imaging reception, are presented in terms of the SNR. For a transmitter and a receiver at a given set of coordinates, the SNR is deterministic. In practice the SNR may change for given transmitter and receiver locations if the surrounding objects in the room move, for example people moving and fans rotating. However, these effects are not considered here and, to the best of our knowledge, have not been quantified by other researchers. The performance of the studied geometries is evaluated in different multiuser scenarios including two-user, three-user and five-user cases. User mobility is considered where a mobile user in some cases moves at constant x = 1m and x = 2m along the y-axis and other users are fixed at certain locations.

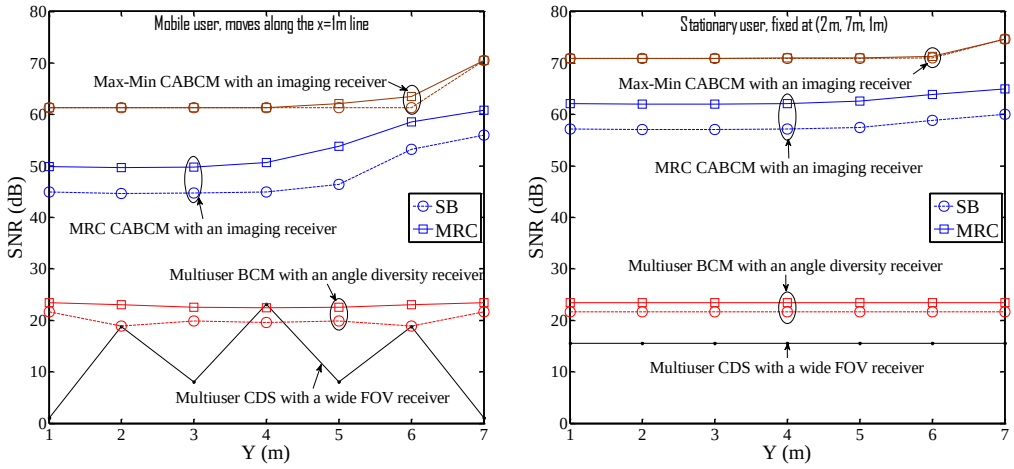

(a) Transmitter is placed at (2m, 4m, 1m)

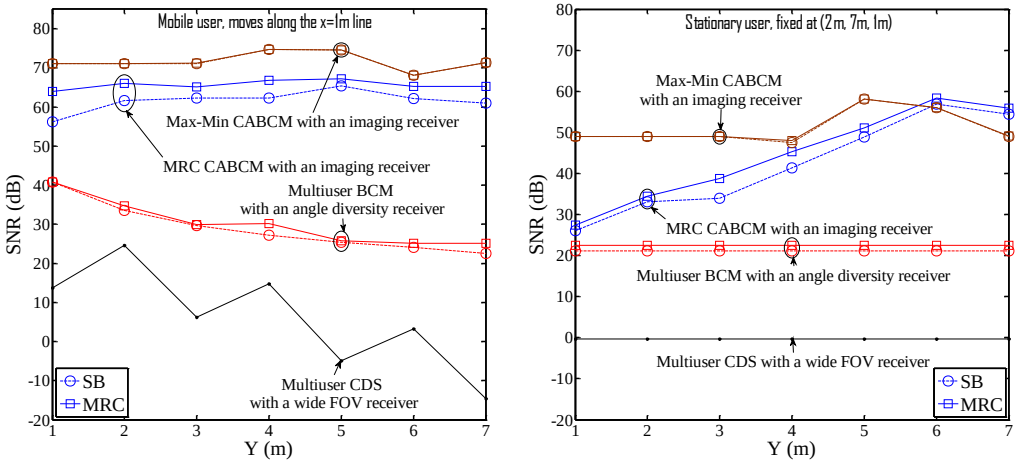

(b) Transmitter is placed at (1m, 1m, 1m)

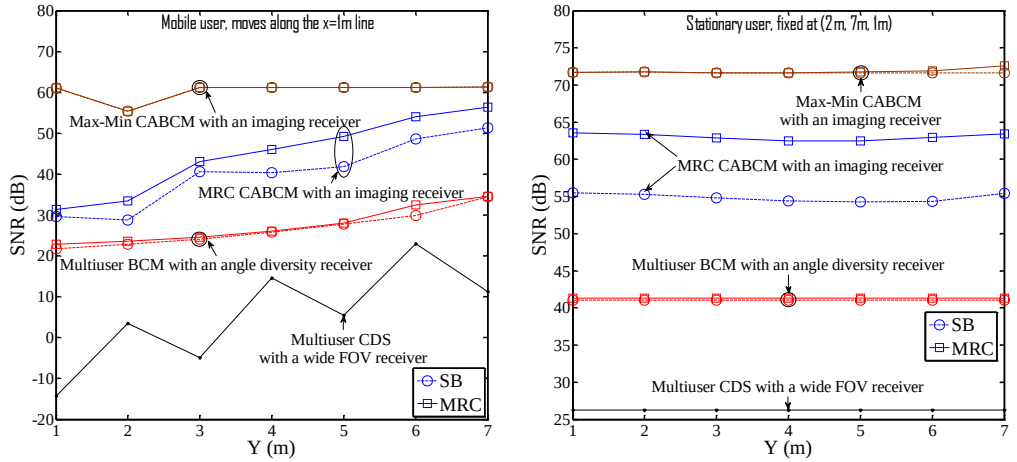

(c) Transmitter is placed at (2m, 7m, 1m)

Figure 5.1: SNR of four mobile OW configurations (CDS, BCM, MRC CABCM and Max-Min CABCM) operating at 30 Mbit/s for a two-user scenario when the transmitter is placed at three different locations.

Transmitter mobility is also taken into account, considering four different transmitter locations on the CF: (2m, 4m, 1m), (1m, 1m, 1m), (2m, 7m, 1m) and (2m, 1m, 1m). Comparisons with basic systems in the literature (BCM with an angle diversity reception and CDS with a 65° FOV single receiver) are also drawn when the systems operate at 30Mbit/s. The collaborative multibeam systems are further evaluated at higher data rates where 2.5Gbit/s and 5Gbit/s data rates are considered. The pre-amplifier used for the 30Mbit/s systems is the PIN FET transimpedance receiver used in [96].

For the 2.5Gbit/s and 5Gbit/s systems, we use the PIN FET receiver in [169] and limit bandwidth to 2.5GHz and 5GHz respectively by using appropriate filters. In our SNR analysis, we follow the SNR calculation given in Section 4.5.2. We consider two approaches to process the resultant electrical signals in case of a non-imaging diversity receiver and imaging reception: SB and MRC. MRC can achieve better performance than SB, therefore it is employed in the imaging systems operating at high data rates. Figure 5.1 (a), (b) and (c) show the SNR performance of four mobile configurations (CDS, BCM, MRC CABCM and Max-Min CABCM) operating at 30Mbit/s when the transmitter is located at three different locations (2m, 4m, 1m), (1m, 1m, 1m) and (2m, 7m, 1m).

The performance when two users coexist in the room is evaluated, where the first user moves along the x = 1m line and the second is fixed at (2m, 7m, 1m) (see Figure 4.2(b)). It can be seen that the stationary user in multiuser systems (Multiuser CDS and Multiuser BCM) obtains a consistent SNR when one of the coexisting users moves, due to the fact that users in such systems operate independently of each other and no beam power adaptation is performed. It is also noticed that the fluctuations observed in the SNR of the mobile user employing CDS system (attributed to noise distribution) can be mitigated by employing a multiuser BCM system with angle diversity receivers. This is possible due to two reasons: first, the BCM using the clustering method has the ability to cover its surroundings through the diffusing-spots; secondly, the diversity receivers are able to preserve the LOS links as well as mitigate the BN through the use of small FOVs. Furthermore, the imaging MRC CABCM demonstrates a significant performance

enhancement of 38dB for the mobile user in comparison with the non-imaging angle diversity BCM, at 6m separation from the transmitter at (1m, 1m, 1m). This is attributed to distributing the total power among beams collaboratively, where spots near the receiver are allocated higher power.

However, the effect of transmitter mobility on the MRC CABCM performance can be observed as an SNR degradation to below 30dB for the stationary receiver at (2m, 7m, 1m) while the transmitter is at (1m, 1m, 1m). Allocating higher power to the spots near the imaging receiver with minimum SNR can maximise its SNR. This can be achieved through the use of our new system, Max-Min CABCM, employing the iterative Max-Min fairness algorithm. The iterative process in the new algorithm ensures that the total power is fairly distributed when allocating more power to the spots near the user with minimum SNR. The advantage of the new system is observed when the transmitter is moved into the room's corner at (1m, 1m, 1m) or the room edge at (2m, 7m, 1m), when the farther users are considerably affected. For instance, when the transmitter is at the room edge, the mobile user at location (1m, 1m, 1m) can achieve SNR of 30 dB, whereas the stationary user can achieve 8dB SNR. This significant improvement is attributed to allocating more power to spots near the imaging receivers.

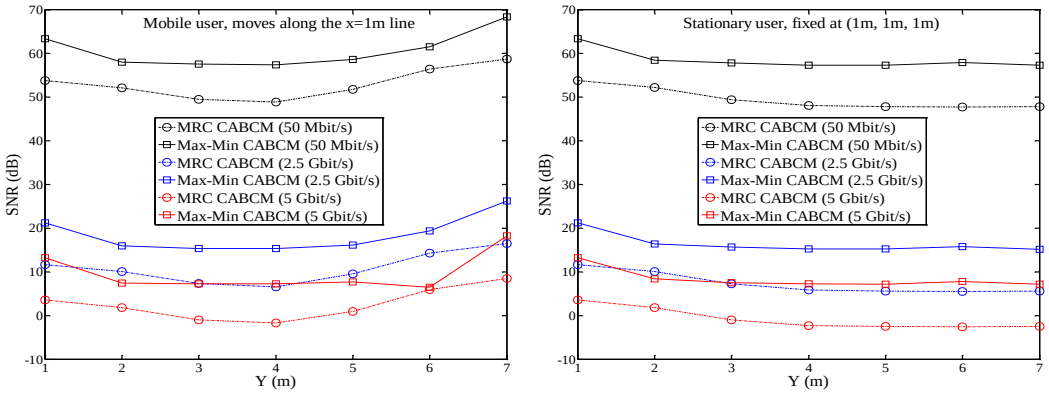

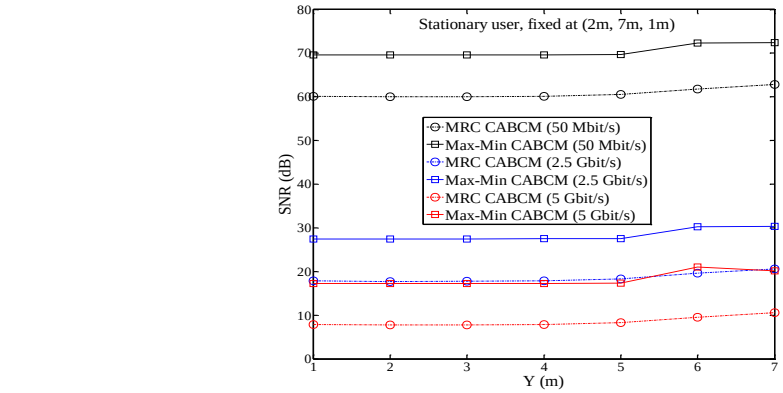

(a) Transmitter is at the room centre (2m, 4m, 1m)

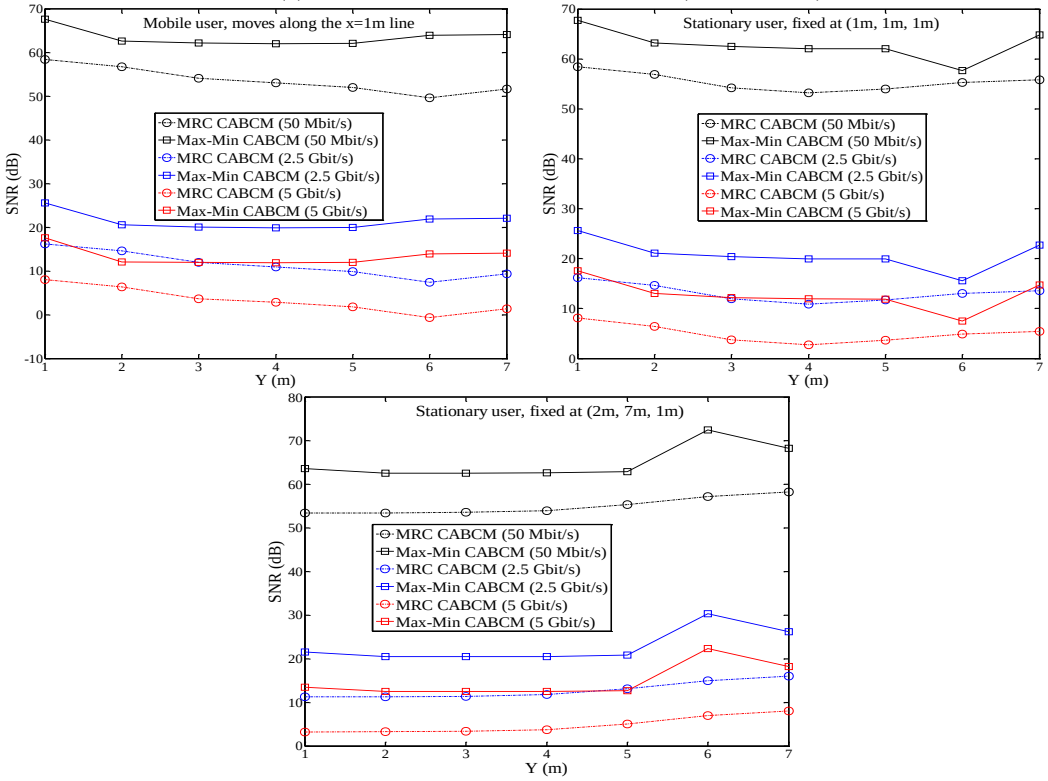

(b) Transmitter is at (2m, 1m, 1m)

Figure 5.2: SNR of the collaborative systems (MRC CABCM and Max-Min CABCM) in conjunction with an imaging receiver (MRC) when three users coexist, and at two different transmitter locations

Figure 5.2 (a) and (b) show the SNR of the proposed imaging systems (MRC CABCM and Max-Min CABCM) at high bit rates of 2.5Gbit/s and 5Gbit/s when three users coexist in the room (mobile user moves along the x = 1m line and two users are fixed, see Figure 4.2) and the transmitter is placed at (2m, 4m, 1m) and (2m, 1m, 1m). We consider

the MRC approach to process the resultant electrical signals from all pixels. It can be seen that our proposed method (Max-Min CABCM) offers an SNR improvement of about 10dB over the MRC CABCM for all three users that operates at 30 Mbit/s. The improvement experienced in the three-user scenario is attributed to iterative algorithm which attempts to maximise the SNR of the user with the minimum SNR.

An SNR of 15.56 dB or more is required for conventional OOK systems in order to obtain acceptable performance. Observing Figure 5.3, it can be seen that our new Max-Min CABCM can achieve acceptable performance level at the 2.5Gbit/s bit rate at both transmitter locations for all coexisting users. At 5Gbit/s, the SNR of the system is still greater than 9.5 dB (BER $< 10^{-3}$), which requires forward error correction (FEC) in order to achieve an acceptable performance level. In contrast, the MRC CABCM at 2.5Gbit/s achieves SNR level more than 9.5 dB, which can reach the acceptable performance level with aid of the FEC scheme. Figure 5.3 shows the SNR of the proposed methods for five collaborative users when the transmitter is at (2m, 1m, 1m). The results show that the new system (Max-Min CABCM) can maintain its performance and achieve 5Gbit/s with aid of FEC technique that can reduce the BER from 10^{-3} to 10^{-9}. It should be noted that it is possible to use the modified imaging receiver with 45° FOV proposed in [170] (and used in the previous chapter) to enhance the link budget in order to achieve 5Gbit/s or potentially higher data rate for all user scenarios.

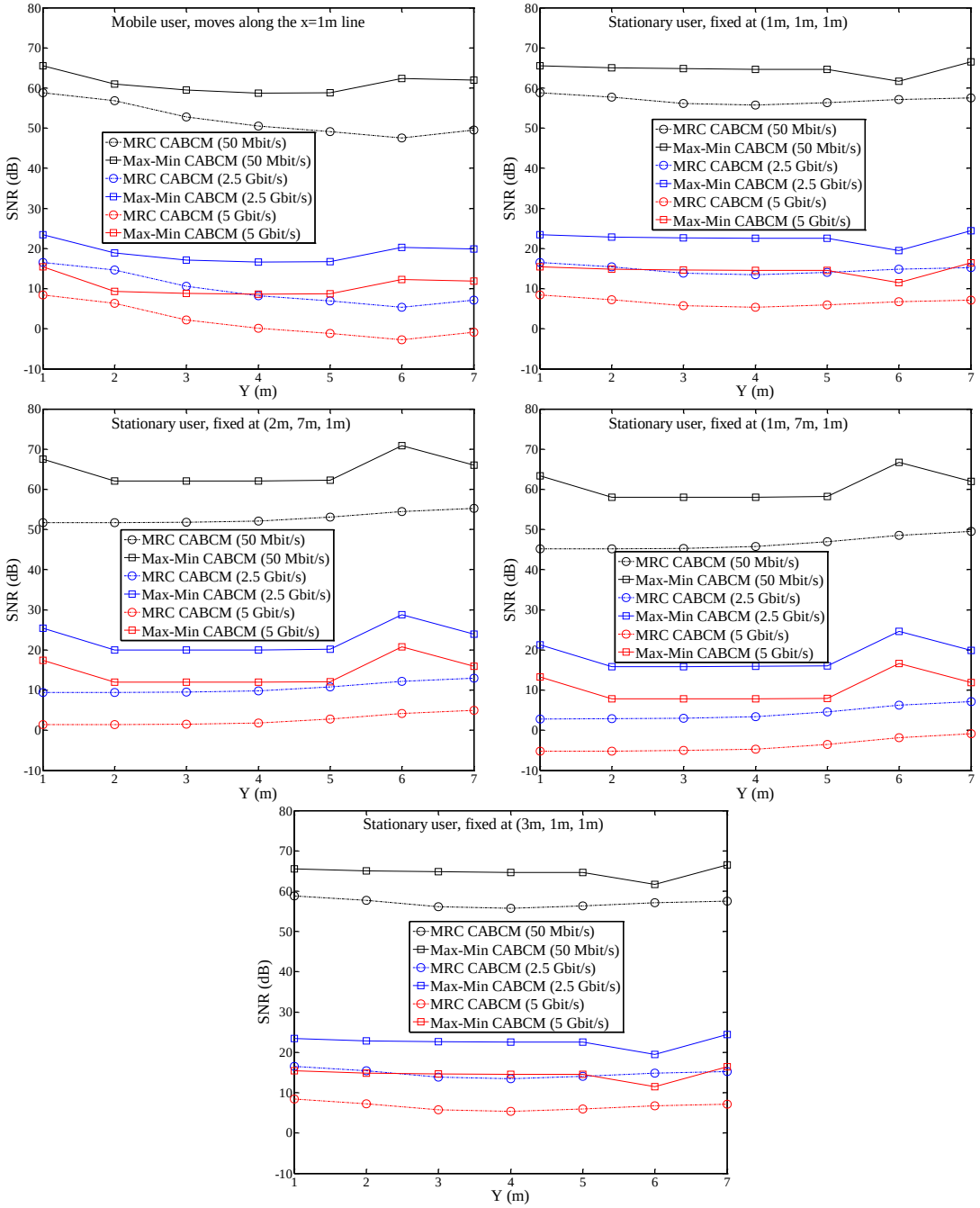

Figure 5.3: SNR of proposed collaborative multibeam systems (MRC CABCM and Max-Min CABCM) coupled with an imaging receiver (MRC), operating at 30 Mbit/s, 2.5 Gbit/s and 5 Gbit/s when five users exist and the transmitter is at (2m, 1m, 1m)

5.4.2 Probability of Error

The performance of indoor OW system is best measured by the probability of error P_e where due consideration is given to the SNR [28]. In order to evaluate the proposed systems' performance, the P_e was computed at different multiuser scenarios (cases described in Figure 4.2 are considered). P_e can be calculated as:

$$P_e = Q\left(\frac{R(P_{s1} - P_{s0})}{\sigma_0 + \sigma_1}\right) \tag{5.1}$$

where $Q(\cdot)$ is the Gaussian function that assumes a value of 6 at a probability of error $P_e = 10^{-9}$, and P_{s1} and P_{s0} are the received optical power when a '1' and '0' are received, respectively. σ_0 and σ_1 are the noise associated with the signal and can be obtained from (3.43). The Q function can be approximated by:

$$Q(x) = \frac{1}{2} \times erfc\left({}^{x}/_{\sqrt{2}}\right) \approx \frac{1}{\sqrt{2\pi}} \times \frac{e^{-\left({}^{x^2}/_{\sqrt{2}}\right)}}{x} \tag{5.2}$$

Table 5.3 shows the P_e of both imaging collaborative multibeam systems (MRC CABCM and Max-Min CABCM) when the transmitter is at the room centre (2m, 4m, 1m). The P_e of stationary users (three-user and five-user scenarios) is calculated when systems operate at 5Gbit/s. The P_e for the mobile user in two multiuser scenarios is also obtained when both systems operate at 5Gbit/s, as illustrated in Table 5.4. By observing the results displayed in the table, we can clearly see that our new system (Max-Min CABCM) outperforms the MRC CABCM. It can be seen that for a user at one of the least successful locations, that is, the user in the corner (1m, 1m, 1m), the P_e has a value of 5.8×10^{-3}. This value can be reduced to acceptable performance level using FEC scheme.

Table 5.3: P_e of MRC CABCM and Max-Min CABCM systems for five collaborative receivers when the transmitter is at the centre of the room

P_e of MRC CABCM					
Multiuser Scenario	Stationary receivers at (1m ,1m, 1m)	(2m ,7m, 1m)	(2m ,4m, 1m)	(1m ,7m, 1m)	(3m ,1m, 1m)
Three-user	2.7×10^{-1}	1.2×10^{-2}	1.4×10^{-2}	-	-
Five-user	1.9×10^{-1}	1×10^{-2}	4.5×10^{-2}	7.2×10^{-2}	1.9×10^{-1}
P_e of Max-Min CABCM					
Multiuser Scenario	Stationary receivers at (1m ,1m, 1m)	(2m ,7m, 1m)	(2m ,4m, 1m)	(1m ,7m, 1m)	(3m ,1m, 1m)
Three-user	5.8×10^{-3}	3.6×10^{-3}	1.4×10^{-15}	-	-
Five-user	1.2×10^{-3}	3.2×10^{-9}	6×10^{-10}	1.5×10^{-4}	1.2×10^{-3}

When there is mobility of both transmitter and receiver, our new system provides strong communication links. For instance, the worst P_e for the mobile user is 3.5×10^{-3} , obtained when five users coexist and the transmitter is moved to the edge of the room at coordinates of (2m, 1m, 1m), while the lowest P_e value is 1.5×10^{-9}. It should be noted that some receivers in five-user scenario have better P_e than those in three-user scenario. This is attributed to the location of the receiver, i.e. a receiver at a successful location can achieve a good P_e compared to those located in the least successful location even the number of users in the room increases.

Table 5.4: P_e of the proposd configurations for the mobile user which moves along the x=1m line, when the transmitter is at (2m, 1m, 1m).

P_e of MRC CABCM							
Mobile receiver locations on *y-axis*	Y (m) 1	2	3	4	5	6	7
Three-user scenario	5.6×10^{-3}	1.8×10^{-2}	6.2×10^{-2}	8.1×10^{-2}	1×10^{-1}	1.7×10^{-1}	1.2×10^{-1}
Five-user scenario	4.1×10^{-3}	1.9×10^{-2}	9×10^{-2}	1.5×10^{-1}	1.9×10^{-1}	2.3×10^{-1}	1.8×10^{-1}
P_e of Max-Min CABCM							
Mobile receiver locations on *y-axis*	Y (m) 1	2	3	4	5	6	7
Three-user scenario	1.7×10^{-14}	2.7×10^{-5}	3.6×10^{-5}	4×10^{-5}	3.3×10^{-5}	3.5×10^{-7}	2.1×10^{-7}
Five-user scenario	1.5×10^{-9}	1.7×10^{-3}	2.8×10^{-3}	3.5×10^{-3}	3.1×10^{-3}	2×10^{-5}	4.6×10^{-5}

5.5 System Complexity and Power Penalty

A significant SNR improvement can be achieved through the use of our new method (Max-Min CABCM) in multiuser OW communication systems; however, this performance enhancement comes at the cost of complexity. This is associated with the computational time required to maximise the SNR of the least successful user through the use of our iterative algorithm. The iterative Max-Min fairness algorithm adopted here requires initial power adaptation to determine the user with the minimum SNR. Following the preadaptation process, a number of iterations is carried out to maximise the SNR of that user while maintaining an acceptable SNR level for the other coexisting users. Given that the preadaptation process needs a time T to compute the pre-optimised SNRs and $(N_{iteration}) \times T$ for Max-Min adaptation process, the proposed algorithm therefore will require $(N_{iteration} + 1) \times T$ to obtain optimised SNRs.

In order to reduce computational complexity, the system may update the beams' power infrequently, even if mobility occurs. Hence, SNR penalties have to be paid as the price of simplification. Figure 5.4 shows the SNR penalties incurred as a result of mobility when five users are present and move away from their optimum location on the *y-axis*. The SNR penalty is calculated for five collaborative receivers when the transmitter is at (2m, 1m, 1m). The calculation was performed for each receiver while in motion (movement in step of 10cm) and no adaptation is carried out. Observing Figure 5.4, the SNRs of users at (2m, 7m, 1m) and (1m, 7m, 1m) gradually degrade and reach 5.2dB and 3.6dB, respectively when the receivers move 1m from the receivers' optimum locations. A higher SNR penalty of 5.8dB can be incurred when the other users move by just 20cm.

However, if these users continue moving, the SNR penalties decline to approximately 1.3dB at a distance of 40cm from their optimum locations. If an SNR penalty lower than 6 dB is desired for all users, then the adaptation has to be performed if the transmitter or any user moves by 0.2m, which corresponds to 0.2 adaptation frequency. The adaptation has to be performed at the rate at which the environment changes, and pedestrians typically move at a speed of 1m/s.

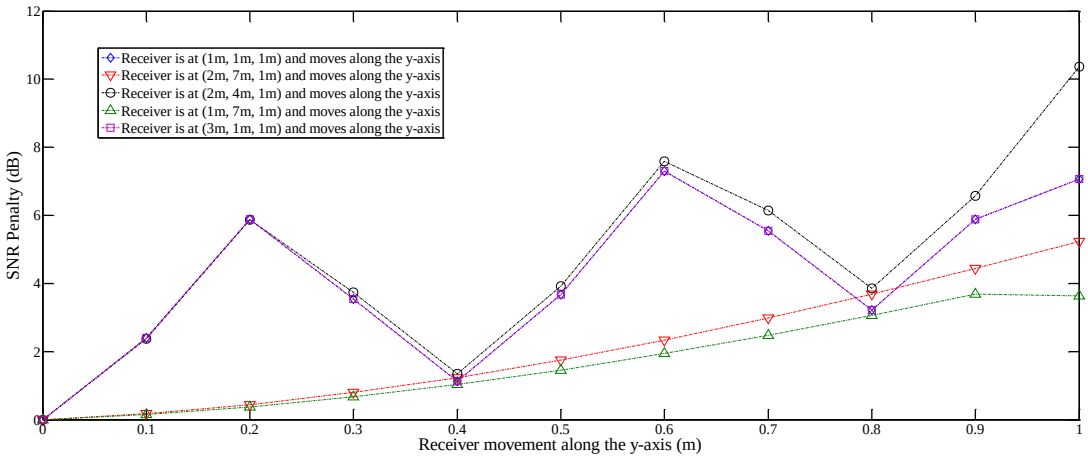

Figure 5.4: SNR penalties of the proposed system (Max-Min CABCM) when five users coexist and move 1m from their optimum locations.

5.6 Summary

The collaborative adaptive beam clustering method is an attractive multibeam configuration for OW systems. The multibeam transmitter employing CABCM geometry provides a better SNR and robustness against transmitter mobility due to a better distribution of spots in the room. However, the performance of the system degrades when the number of users increases. This is a result of unfair power distribution among beams as the transmitter uses collaborative MRC when power is distributed proportional to the requested power from each receiver.

In this chapter, we introduced a Max-Min fairness algorithm in order to maximise the SNR level of the user with minimum SNR. An iterative process is also introduced to ensure fair power adaptation among all coexisting users. Also, if there is more than a user placed at the least successful location, the iterative Max-Min fairness algorithm can moderately maximise their SNRs. At 30Mbit/s, our new system (Max-Min CABCM) provides SNR gains of at least 8dB over the MRC CABCM when the transmitter is at the corner and two users are present. In order to achieve a conventional OOK BER of 10^{-9}, the SNR has to be at least 15.6dB. The proposed system achieves an acceptable performance level at 2.5Gbit/s bit rate for all users present and when there is transmitter and receiver mobility. At 5Gbit/s, the SNR of the system is still greater than 9.5 dB ($BER < 10^{-3}$), and requires FEC in order to achieve an acceptable performance level.

6 Fast and Efficient Adaptation Algorithms for High Data Rates Indoor OW Systems

6.1 Introduction

Multibeam angle adaptive systems (MBAAS) have been shown to offer performance improvements over traditional spot-diffusing optical wireless systems [175]-[177]. However, an increase in the computational cost is incurred. This chapter introduces a novel method to speed up the adaptation process through efficient use of a 'divide and conquer' algorithm by recursively breaking down the scanning process and focusing it into a smaller region in each iteration.

The new, fast and efficient angle adaptation algorithm offers the advantages of optimising the number and pattern (positions) of the spots so as to maximise the receiver's SNR, regardless of the transmitter's position, the receiver's FOV and its orientation. It can also adapt to environmental changes, providing a robust link against shadowing and signal blockage. Furthermore, a beam delay adaptation method is used to reduce the effect of multipath dispersion and ISI. The combination of angle and delay adaptation adds a degree of freedom to the design, resulting in a compact impulse response and ability to achieve higher data rates (15Gbit/s). Significant improvements in the SNR, with OW channel bandwidths of over 15GHz is obtained, and eye safety is considered while operating at 15Gbit/s with full mobility in a realistic environment with shadowing.

6.2 OW System Model

The characteristics of a mobile channel formed by a fast and efficient adaptive multibeam transmitter, coupled with an angle diversity receiver, are investigated. The simulation room is empty with floor dimensions of 8m × 4m (length × width), and ceiling height of 3m. Experimental measurements have shown that most building materials including plaster walls (with the exception of glass) are approximately Lambertain reflectors [9]. In this study, it is assumed that all reflecting surfaces in the set-up room are Lambertain reflectors with high reflectivity (reflection coefficient of 0.8 for walls and ceiling, 0.3 for floor). High reflectivity is chosen as it results in the highest multipath dispersion (worst case), and thus significant pulse spread. Reflections from doors and windows are considered to be the same as reflections from walls. To model the reflections, the room reflecting surfaces are divided into a number of equal-size, square-shaped reflection elements with area dA and reflection coefficient.ρ These elements act as secondary emitters and are modelled as Lambertian reflectors. It was found in previous investigations that third-order reflections and higher produce a weak contribution to the received optical power [9], [16], [36], [53]. Reflections up to second-order are therefore considered in this work. The impulse response in a practical OW system is continuous; however the simulator subdivides the reflecting surfaces into discrete elements. The effect of discretisation can be reduced by subdividing time into bins of widths Δt and grouping the powers received within each bin into a single received power. This accounts for the smoothness seen in the resulting impulse responses presented in this study. A good choice for the bin width is $\Delta t = \sqrt{dA}/c$, roughly the time light takes to travel between

neighbouring elements [16]. An identical histogram to the actual impulse response is achieved as dA approaches zero. It should be noted that reducing dA leads to improved resolution in impulse response evaluation, together with an increase in the computation time. To keep the computation within reasonable time and measure, a surface element size of 5cm × 5cm is used. The corresponding time period (bin width) used in computations is 0.17ns. A smaller time bin (0.01ns duration) is also used with the proposed multibeam adaptive OW systems, resulting in a slightly higher delay spread than that obtained using the 0.17ns time bin. Reflecting elements of 0.3cm × 0.3cm are used in the case of a time bin of 0.01ns. Note that at very small delay spread levels a time bin with a smaller duration has to be used. This reduces the smoothing effect introduced through the use of time bins (that group together rays with comparable delay).

To quantify the proposed system's performance under mobility, three new multibeam transmitter configurations in conjunction with an angle diversity receiver of seven branches are considered: a fast and efficient angle adaptive system (FEAAS); a fast and efficient angle and delay adaptive system (FEADAS); and a fast and efficient angle, delay and power adaptive system (FEADPAS). Mobility here is a nomadic mobility which refers to relocating the transmitter or/and receiver from a place to another on the communication floor. For example, moving the transmitter from the room centre at (2m, 4m, 1m) to the corner of the room at (1m, 1m, 1m) or moving the receiver 1m away from its original location. Comparisons of the traditional LSMS and the original MBAAS are also considered. All the proposed systems use an upright transmitter of 1W optical power, and the transmitter is placed at three different locations on the CF: (2m, 4m, 1m), (1m,

1m, 1m) and (2m, 7m, 1m). Computer-generated holographic beam-splitters are assumed to be mounted on the emitter to shape its output to multiple narrow beams, which in turn form a line of diffusing spots on the ceiling (LSMS configuration). The optimum spot distribution, which yields the best receiver SNR in the original MBAAS, can be chosen according to the original angle adaptation algorithm given in [177].

The new FEAAS can guide the multibeam transmitter to optimise its spot distribution (the number and more so the pattern of the spots) so as to maximise the receiver's SNR with a higher power efficiency and much reduced search time, compared to the original MBAAS (FEAAS is discussed in Section 6.4.1). The delays and power levels associated with the beams can be adjusted according to the procedure discussed in Sections 6.4.2 and 6.4.3. An array source and a liquid crystal (LC) holographic element can generate the beams. Changing the holographic 2D function (through an LC device) can generate variable optical spot locations (on the ceiling and/or walls) with different optical spot intensities and differential switching times. The delay adaptation can be implemented through array element delayed switching. Most of the adaptive holographic switches are LC based [171], [172]. These devices have μs to ms response times [171], [172] that are adequate, given that the adaptation process has to be carried out at the rate at which the environment changes (for example, human motion) and not at the data rate.

However, the design of such holograms and their implementation through LC devices is not ideal, as the input power may not be entirely assigned to spots and may partially leak through [53], [110]. For example, it is shown in [110] that the design of a hologram that diffuses the laser may result in a hot spot with a high peak power, reducing the efficiency

of the power distribution and hologram design. Similarly, in the design of a multibeam pattern used here, some power may leak through or all the power may not be assigned to spots, thus reducing the efficiency. This may result in a form of noise where beams are not directed at the desired correct spatial orientation. The effect of such noise (a form of background noise) is of interest to the overall design, but is not considered here.

The adaptation requires training and feedback from the receiver to the transmitter, and a low data rate diffuse channel is suggested to achieve this feedback. At a low data rate the angle, delay and power associated with such a beam can be maintained at a fixed level. In order to assess the system performance in a realistic situation, the link was exposed to directive noise sources, eight halogen spotlights of 65W that cause high optical spectral corruption levels in the received data stream. These lamps are positioned equidistantly on the ceiling, as shown in Figure 3.5, representing ambient background interference. To minimise the BN effect and reduce multipath dispersion, an angle diversity receiver is implemented and this is discussed in the next section.

6.3 Angle Diversity Receiver

In contrast to the single wide FOV receiver, an angle diversity receiver is a collection of narrow-FOV detectors oriented in different directions. The receiver's diversity system consists of seven photodetector branches, each with a responsivity of 0.54 A/W. The direction of each photodetector is defined by two angles: azimuth (Az) and elevation (El) angles. The El angles of six photodetectors remained at 70°, while the seventh was given an El of 90°. The Az angles were fixed at 0°, 0°, 45°, 90°, 180°, 225°, and 270°. The azimuth

(Az) angle is the orientation angle of the photodetector with respect to the *x-axis*. Therefore, the detector oriented along the *x-axis* has Az angle of 0° (i.e., $Az = 0^{\circ}$). The detector facing upwards has a conical field of view and therefore it is azimuth agnostic, that is, it can be assumed to have any values of Az, although for mathematical convenience we choose its azimuth angle to be $Az = 0^{\circ}$. The Az, El, and FOVs are chosen through an optimisation similar to that in [54], [102]. Moreover, the angle diversity receiver is designed so that all the photodetectors always point to the ceiling. This choice of the receiver characteristics (Az, El and FOVs) produces a link that is robust against diffusing spot blockage, as well as preventing shadowing due to moving objects. This can also help the multibeam fast and efficient angle adaptive transmitter to cluster its diffusing spots on the ceiling, where the diversity receiver can spatially select the photodetector that observes high power and minimum background noise. This can result in maximising the SNR at the receiver. Each photodetector is assumed to employ a compound-parabolic concentrator (CPC), which has an acceptance semi-angle ψ_C so that when the reception angle δ exceeds ψ_C, the concentrator transmission factor, $T_C(\delta)$ rapidly approaches zero. The CPC is a common non-imaging concentrator and has $\psi_C < 90^{\circ}$, a refractive index of $N_C = 1.7$ is considered, and the entrance area is $A = 9\pi/4$ cm^2. The CPC's transmission factor is given by [178]:

$$T_{C,NIMG}(\delta) = T\left[1 + \left(\delta/\psi_C\right)^{2H}\right]^{-1} \tag{6.1}$$

where $T = 0.9$ and $H = 13$ [22]. The CPC has an exit area of $A' = A\,sin^2(\psi_C)/N_C^2$. The diversity receiver is always placed on the CF along the *x*=1m or *x*=2m lines. Each

photodetector employs a CPC with an acceptance semi-angle of $\psi_C = 8^\circ$, and is assumed to exactly fit its associated concentrator's exit area. The photosensitive area of each photodetector is therefore 4.7 mm^2. Furthermore, in order to use small area detectors at the high data rates considered, the corresponding concentrator's acceptance semi-angle of each photodetector is restricted to 4°, resulting in a reduction in the detector area to 1 mm^2. The size of the concentrator is acceptable in mobile terminals and it can be fixed to the photodetector in a robust fashion. The photocurrents received in the various detectors are amplified separately, and the resulting electrical signals are processed in an approach that maximises the power efficiency of the system. Several possible diversity schemes such as SB, EGC and MRC can be considered. For simplicity, SB is considered here in order to process the resulting electrical signals. SB represents a simple form of diversity, where the receiver simply selects the branch with the best SNR. In order to compute the impulse response for the entire CF, a simulation package based on a ray-tracing algorithm was developed for arbitrary transmitter–receiver configurations in an arbitrary room size that has diffuse reflectors. Diversity of emissions and detection are taken into account. Additional features are introduced to enable beam angles, delays and powers to be adapted. The received multipath profiles due to each spot are computed at each photodetector, based on the detector's FOV and the area the detector observes at each set of transmitter and receiver locations. The resultant power profile at each photodetector is the sum of the powers due to the total number of diffusing spots considered. Several parameters are of interest and can be derived from the simulated impulse response, such as r.m.s delay spread and 3-dB channel bandwidth.

6.4 Transmitter Configurations

In this section, three new adaptive multibeam transmitter configurations are presented, analysed and compared in order to identify the most suitable geometry for use in indoor OW systems. LSMS is one of the attractive configurations in the literature, therefore it is modelled and used for comparison purposes in order to evaluate the improvements offered through the proposed novel configurations. LSMS uses a diffusing spot distribution pattern where a line of spots of equal intensity (in this case 80 spots) is formed in the middle of the ceiling, that is, at x=2m and along the y-axis when the transmitter is placed at the centre of the room. The difference in distance between adjacent spots is 10cm. These spots become secondary emitters that emit Lambertian radiation. The spots' positions are dictated by the transmitter location. As the transmitter moves, the distribution of the spots can be determined in the room by following the procedure given in [103]. Furthermore, the new adaptive configurations (FEAAS, FEADAS and FEADPAS) are introduced and evaluated next.

6.4.1 FEAAS

Beam angle adaptation (beam steering based on LC devices) was shown to be an efficient technique that can identify the optimum spot distribution, providing a strong path between the diffusing spots and the receiver regardless of the transmitter position [177]. An optical transmitter followed by an adaptive hologram was used to generate variable optical spot locations based on the alteration of the transmission angles (θ_x and θ_y) between -90^o and 90^o in the x-y axes with respect to the transmitter's normal. Essentially, the adaptive

hologram was initially made to produce a single spot, which is then scanned along a number of possible positions (on the ceiling and walls) to identify the optimum location yielding the best SNR at the receiver. The adaptation algorithm changes the beam transmission angles (θ_x and θ_y) between -90^o and 90^o in the *x-y* axes with respect to the transmitter's normal. The beam in each step forms a diffusing spot centred on coordinates of (x_s, y_s, z_s) within the room (in the ceiling or walls). The beam angles θ_x and θ_y (spherical coordinates) and spot location (x_s, y_s, z_s) (spherical coordinates) relate to the transmitter location (x_T, y_T, z_T) and the room dimensions (length × width × height), as shown in Table 6.1. The position of the spot (i.e. its corresponding coordinates) that yields the best SNR at the receiver is chosen as the optimum location. Note that the coordinate system refers to the centre of the spot. Note also that, in this new system (FEAAS), we recursively break down the scanning process into a number of iterations that focus recursively into smaller regions in space, resulting in different scan step sizes (i.e. each scan iteration uses a different angle adaptation step size). The new system makes efficient use of a 'divide and conquer' algorithm that breaks down a problem into a number of related sub-problems, eventually becoming simple enough to be solved directly. Accordingly, the new fast and efficient adaptation algorithm divides the entire room into four arbitrary quadrants and selects the one that includes the sub-optimum location (best SNR among the four quadrants) as a new scan area.

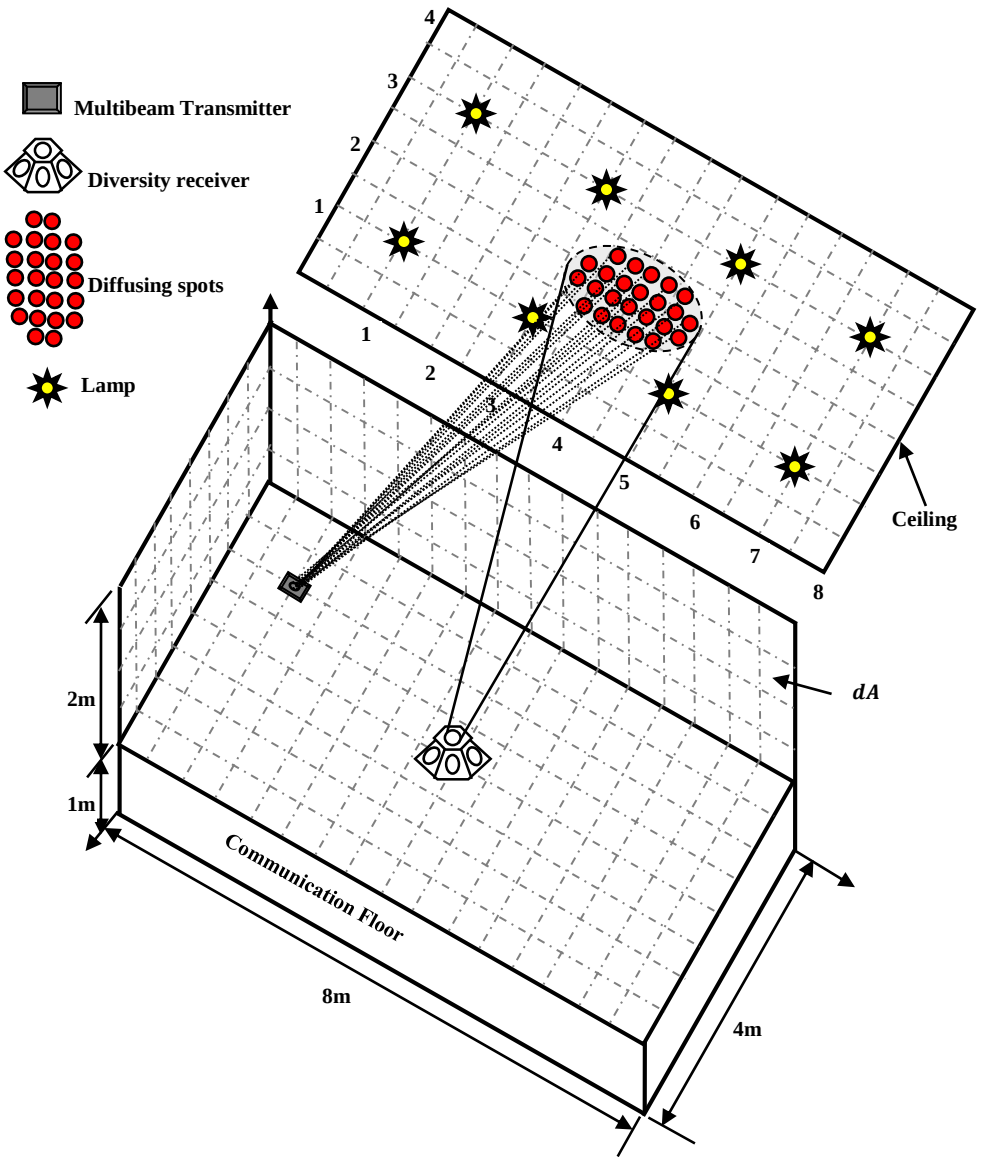

Figure 6.1: OW FEAAS architecture at transmitter and receiver locations of (1m, 1m, 1m) and (2m, 4m, 1m) respectively

The next scan iteration is then started within the selected quadrant, using half of the previous scan step size, with the aim of identifying a new sub-optimum location. Similarly, the selected quadrant is divided into four arbitrary sub-quadrants, and the sub-quadrant including the new sub-optimum location is chosen as a new scan area for the next iteration. This process is repeated for a number of iterations where the number of

Table 6.1: Spherical coordinates to Cartesian coordinates conversion algorithm

Algorithm I: Spherical Coordinates to Cartesian Coordinates Conversion	
1	L = 800 cm; (length of the room)
2	W = 400 cm; (width of the room)
3	H = 300; (height of the room)
4	z_{CF} = 100 cm; (height of the CF)
5	Identify the Cartesian coordinates (x_s, y_s, z_s) of a spot formed by a beam with transmission angles θ_x and θ_y (Spherical Coordinates) at a transmitter location of (x_T, y_T, z_T) as follows:
6	Initially calculate the *x*-coordinate as: $x_s = x_T - (H - z_{CF})tan(\theta_x)$
7	Initially calculate the *y*-coordinate as: $y_s = y_T - (H - z_{CF})tan(\theta_y)$
8	if $x_s > W$ (the spot is in the West y-z Wall)
9	$x_s = W$; and $z_s = ((x_T - x_s)/tan(\theta_x)) + z_{CF}$;
10	Elseif $x_s < 0$ (the spot is in the East y-z Wall)
11	$x_s = 0$; and $z_s = ((x_T - x_s)/tan(\theta_x)) + z_{CF}$;
12	Elseif $y_s > L$ (the spot is in the South x-z Wall)
13	$y_s = L$; and $z_s = \left((y_T - y_s)/tan(\theta_y)\right) + z_{CF}$;
14	Elseif $y_s > L$ (the spot is in the North x-z Wall)
15	$y_s = 0$; and $z_s = \left((y_T - y_s)/tan(\theta_y)\right) + z_{CF}$;
16	Else
17	$z_s = H$;
18	End

iterations chosen depends on the acceptable complexity and acceptable SNR penalty, both will be discussed in Sections 6.5 and 6.6. For fair theoretical comparison purposes, the iterations can continue until a certain angle adaptation step size is reached; that is, until reaching the angle step size used in the original MBAAS for example, where the optimum spot location with the best receiver SNR is identified. Furthermore, once the optimum beam direction is identified, a set of uniformly distributed spots (25 × 25 spots are considered here), at 1cm separation, initially created and centred on the optimum location. The receiver's SNR due to each spot is computed separately and relayed to the transmitter at a low data rate. The transmitter then determines which of the possible 25 × 25 spot locations houses an illuminated spot based on a threshold, where the spots that produce SNRs higher than the threshold are illuminated, whilst the others are disregarded.

The threshold is based on the received SNR achieved at the receiver through a diffuse transmitter with a transmitted power identical to the spot power (in this case the

transmitter is assumed to produce 25 × 25 spots and each is assigned 1.6mW). This can guarantee that only spots having direct contributions at the receiver (i.e. those located within the receiver's FOV) will be illuminated. A depiction of the FEAAS configuration is shown in Figure 6.1. For a single transmitter and a single receiver at a given set of positions, the FEAAS identifies the optimum beam direction and shapes the optimum spot distribution according to the following steps:

1. Configure the adaptive hologram to implement the first scan iteration according to its associated parameters: the angle adaptation step size θ_{steps}, the *x*-axis scan range $(\theta_x^{start}\ to\ \theta_x^{end})$ and the *y*-axis scan range $\left(\theta_y^{start}\ to\ \theta_y^{end}\right)$. In order to initially scan the entire room, the *x*-*y* axes scan ranges are set to -90° and 90°. Furthermore, the θ_{steps} is initially set to 17.74°, allowing the spot to move 64cm in each step, and resulting in a total of 160 possible locations in the entire room.
2. Produce a single spot and move it by varying the beam angles: θ_x and θ_y in steps of θ_{steps} along the *x*-*y* axes. The beam angle θ_x is changed between θ_x^{start} and θ_x^{end}, while θ_y is varied between θ_y^{start} and θ_y^{end}.
3. Compute the receiver SNR at each step and send a feedback signal at a low rate to inform the transmitter of the SNR associated with the step.
4. At the step where the receiver SNR is at maximum, record the associated transmission angles θ_x^{subopt} and θ_y^{subopt}.
5. Reconfigure the adaptive hologram to implement the next iteration as follows:
    a) Reset the angle adaptation step size as $\theta_{steps} = \theta_{steps}/2$.
    b) If the $\left|\theta_x^{subopt}\right| \leq (|\theta_x^{end}| - |\theta_x^{start}|)/2$, then reset the higher scan range along the *x-axis* as $\theta_x^{end} = \theta_x^{subopt}$ and keep the lower scan range as it is. Otherwise, reset the lower scan range along the *x-axis* as $\theta_x^{start} = \theta_x^{subopt}$ and keep the higher scan range as it is.

c) If the $\left|\theta_y^{subopt}\right| \leq \left(\left|\theta_y^{end}\right| - \left|\theta_y^{start}\right|\right)/2$, then reset the higher scan range along the *y-axis* as $\theta_y^{end} = \theta_y^{subopt}$ and keep the lower scan range as it is. Otherwise, reset the lower scan range along the y-axis as $\theta_y^{start} = \theta_y^{subopt}$ and keep the higher scan range as it is.

6. Repeat Steps 2 to 5 for a number of iterations (four scan iterations are considered).
7. Stop when the minimum allowed angle adaptation step size is reached (i.e., a certain scan step size of 2.29^o that is used in the original MBAAS). In the fast and efficient angle adaptation algorithm, four iterations are carried out where the first scan iteration uses a step size of 17.74^o and the fourth (and final) one is set to a 2.29^o scan step size. In effect, the fast 'divide and conquer' algorithm has to scan 640 possible locations to identify the optimum spot location. This results in a new angle adaptive system that is almost 20 times faster than the original MBAAS, where 12500 locations had to be scanned.
8. Determine the X_{opt}, Y_{opt}, and Z_{opt} position of the spot that maximised the receiver's SNR. This $(x_{opt}, y_{opt}, z_{opt})$ coordinate can be defined based on the optimum transmission angles θ_x^{opt} and θ_y^{opt}.
9. Generate a set of uniformly distributed spots (25 × 25 spots in this case), at 1cm separation, whose centre is this coordinate, i.e., $(x_{opt}, y_{opt}, z_{opt})$.
10. Equally distribute the total power, 1W, among the spots, compute the power received at the diversity receiver, and calculate the SNR.
11. Select the best link (the photodetector with the best SNR) to use as a desired communication link (desired photodetector), in essence the diversity receiver implements 'select best' combining.
12. Individually turn on each spot, compute the power received at the desired photodetector, as well as calculate the SNR.
13. Inform the transmitter of the SNR associated with the spot by sending a feedback signal at a low rate.

14. Repeat steps 12 and 13 for all the spots.
15. Optimise the number and shape of the spots by illuminating the spots that produce SNRs higher than a threshold value and omitting the others. As mentioned earlier, this threshold value is set in proportion to the SNR produced by a diffuse transmitter.
16. Operate the multibeam transmitter with the optimum spot distribution (the optimum number of spots and optimum pattern) while the beams propagate with equal intensity at the same time.

It should be noted that the adaptation algorithm described above applies to the single user case; that is, a single transmitter and a single receiver position. A MAC protocol should be used and it should include a repetitive training period that allows the adaptation steps to be performed. Training should be carried out at the rate at which the environment changes. This is usually a slow rate, commensurate with human motion. Pedestrians move typically at a speed of 1m/s. Furthermore, the new multibeam adaptive OW system (FEAAS) is more robust against change to the receiver's orientation than the original MBAAS. This is due to the ability of the fast and efficient angle adaptation algorithm to optimise the spot distribution (including the number and shape of the diffusing spots) so as to maximise the receiver SNR, regardless of the transmitter position and the receiver orientation.

6.4.2 FEADAS

The transmitted signal propagates to the receiver through various paths of different lengths. Therefore, switching ON the beams at the same time may result in receiving the signals at different times due to multipath propagation. This may spread the received

pulse and cause ISI. However, if the switching times of the beams can be adjusted to allow the beam with the longest journey to travel first, then switching the other beams with differential delays, all the rays can reach the receiver at the same time. This can be achieved through beam delay adaptation. The transmitter and receiver are synchronised and, at the start of a frame, the transmitter individually switches on the spots, each after a predetermined time interval T. The receiver observes the deviation (differential delay) associated with the arrival of pulses compared to the issuing time rhythm of T seconds. The received multipath profile (impulse response) due to each spot is observed at the receiver, and its mean delay are then calculated with respect to the start of the frame. The mean delay is an average time delay, which can be computed using (3.29). In effect, the receiver receives the first pulse at time (t_1), the second pulse at time $T + t_2$ and the last pulse at time $\left((N_{spot} - 1)T + t_{N_{spot}}\right)$, where N_{spot} is the total number of diffusing spots considered. The time delay $\left(t_i,\ i = 1,2,\cdots,N_{spot}\right)$ attributed to the varying path length associated with each spot can then be determined. For example, the differential delay between the first pulse (spot) and second pulse (spot) attributed to their varying channel path lengths is $|t_2 - t_1|$. The varying response times of the individual receivers may add a jitter element to this value if their response is slow or if they are not implemented on a common integrated platform; the latter may reduce variability. The time delays associated with the beams are relayed to the transmitter to help optimise the delay spread at the receiver. In effect, the multibeam transmitter switches on the beams at different times, starting with the beam that induces the maximum time delay. The other beams sequentially propagate to the receiver, each at a certain time proportional to the difference

between its associated time delay and the maximum time delay. In contrast to the previous configuration (FEAAS), where the multibeam transmitter radiates all the beams at the same time, in this system the beams are switched on at different times, with the aim of minimising the delay spread at the receiver. In both systems (FEAAS and FEADAS) the transmitted power is distributed equally among the beams. Once the optimum spot distribution is identified, the new delay adaptation algorithm adjusts the switching times of the beams as follows:

1. It switches on each spot individually and computes the power received at the desired photodetector, as well as calculating the mean delay (time delay).
2. It sends a feedback signal at a low rate to inform the transmitter of the mean delay associated with the beam (spot).
3. It repeats Steps 1 and 2 for all the spots.
4. It sets the beam with the maximum mean delay as a first traveller and introduces a time delay to the switching time of each of the rest of the beams in proportion to the difference between its associated mean delay and the maximum mean delay.
5. It configures the multibeam transmitter to operate with the optimum spot distribution, optimum beam delays, and with the power distributed equally among the beams.

At the transmitting end, if discrete or array sources are used to implement the transmitter, then electronic control can be used to facilitate switching on these sources with nanosecond delays, which is implementable in electronics. If a hologram is used to generate the beams in a spatial light modulator, then stored frames corresponding to different spot outputs can be loaded. Liquid crystal devices are readily able to modulate the beam in tens or hundredths of microseconds, although nanosecond response times

have been demonstrated [171]. Having identified the delays, the transmitter coupled with a set of discrete sources can switch on the beams with the required delays using electronic control. The use of fewer sources can simplify the transmitter. The penalty induced in link performance will be small, though this warrants further study.

6.4.3 FEADPAS

In contrast to the previous multibeam adaptive OW system (FEADAS), where the total power of 1W is distributed equally among the beams, in this system (FEADPAS) the total power is distributed unequally so as to optimise the SNR and delay spread at the receiver. In effect, the spot nearest to the receiver is allocated the highest power level, whilst the farthest spot is assigned the lowest, so as to maximise the SNR and bandwidth at the receiver. The transmitter identifies the optimum number of beams and their directions (beam angles), introduces a time delay between the beams and adjusts the power distribution among the beams in a fashion that optimises the SNR and delay spread at the receiver. This can be achieved through the algorithm given in Table 6.2. This algorithm applies to the single user case where the spot distribution, beam delays and beam powers are adapted so as to maximise the SNR and bandwidth at a single given receiver location. Although the optical medium in indoor optical wireless channel can be theoretically considered as having unlimited bandwidth, the attainable channel bandwidth is limited by other factors such as channel capacity and the photodetector area [61, 179]. Additionally, multipath propagation is another constituent that imposes limitation in the channel bandwidth. A good measure to evaluate the bandwidth efficiency is 3-dB bandwidth and it is discussed in 6.5.1. In Chapter 7, multiuser scenarios are considered.

Table 6.2: Fast and efficient angle, delay and power adaptation algorithm

Algorithm II: Fast and Efficient Angel, Delay and Power Adaptation	
1	$N_{spot} = 25 \times 25$; (number of spots)
2	$N_{photodetector} = 7$; (number of photodetectors)
3	$p(\cdot)$ is a rectangular pulse defined over $[0, T_b]$, where $T_b = 1/B$ (B is a bit rate)
4	$\theta_x^{start} = -90^o$ and $\theta_x^{end} = 90^o$ (the lower and higher scan ranges along the x-axis)
5	$\theta_y^{start} = -90^o$ and $\theta_y^{end} = 90^o$ (the lower and higher scan ranges along the y-axis)
6	$\theta_{steps} = 17.74^o$ (the angle adaptation step size, which is 17.74^o for the first iteration)
7	$N_{iteration} = 4$; (number of scan iterations considered)
8	For $k = 1 : N_{iteration}$
9	For $i = \theta_x^{start} : \theta_{steps} : \theta_x^{end}$
10	For $j = \theta_y^{start} : \theta_{steps} : \theta_y^{end}$
11	$\theta_x = i$; $\theta_y = j$; (transmission angles in the x-y axes)
12	Produce a single spot in a direction associated with θ_x and θ_y based on the Spherical Coordinates to Cartesian Coordinates conversion algorithm given in Table 6.1
13	For $l = 1 : N_{photodetector}$
14	Calculate and sum the received powers within a time bin (0.01 ns duration)
15	Produce the impulse response $h_l(t)$
16	Calculate the pulse response as $h_l(t) \otimes p(t - T_b)$ and then, find $(P_{s1} - P_{s0})_l$
17	Compute $SNR_l = (R \times (P_{s1} - P_{s0})_l / (\sigma_t)_l)^2$
18	End
19	$SNR(i,j) = max(SNR_l)$;
20	$detector(i,j) = find(SNR_l == max(SNR_l))$;
21	End
22	End
23	$SNR_{max} = max(SNR(i,j))$;
24	$[\theta_x^{subopt}, \theta_x^{subopt}] = find(SNR(i,j) == SNR_{max})$; (identify the suboptimum location)
25	$bestlink = detector(\theta_x^{subopt}, \theta_x^{subopt})$; (select the desired photodetector)
26	If $\lvert\theta_x^{subopt}\rvert \le (\lvert\theta_x^{end}\rvert - \lvert\theta_x^{start}\rvert)/2$ (reset the new scan range in the x-axis)
27	$\theta_x^{end} = \theta_x^{subopt}$;
28	Else
29	$\theta_x^{start} = \theta_x^{subopt}$;
30	End
31	If $\lvert\theta_y^{subopt}\rvert \le (\lvert\theta_y^{end}\rvert - \lvert\theta_y^{start}\rvert)/2$ (reset the new scan range in the y-axis)
32	$\theta_y^{end} = \theta_y^{subopt}$;
33	Else
34	$\theta_y^{start} = \theta_y^{subopt}$;
35	End
36	$\theta_{steps} = \theta_{steps}/2$; (reset the new scan step size)
37	End
38	$\theta_x^{optimum} = \theta_x^{subopt}$; $\theta_y^{optimum} = \theta_y^{subopt}$; (identify the optimum spot direction)
39	Generate a uniformly distributed spots (25×25) centered on a location associated with $\theta_x^{optimum}$ and $\theta_y^{optimum}$
40	For $s = 1 : N_{spot}$
41	$P_s = 1/N_{spot}$; (power per spot)
42	Compute the impulse response observed by the desired photodetector
43	Calculate $\mu_s = \sum_m t_m P_r^2(t_m) / \sum_m P_r^2(t_m)$; (mean delay due to spot s)
44	Calculate $W_s = SNR_s = (R \times (P_{s1} - P_{s0})_s / (\sigma_t)_s)^2$; (spot's weight)
45	End
46	$W_{max} = max(W_s)$; $\mu_{max} = max(\mu_s)$;
47	$P_{limit} = 0.001$; (1mW is the eye safe limit at the near infrared wavelengths)
48	$W_{thr} = SNR_{CDS}$; (threshold proportional to the SNR produced by a diffuse transmitter)

49	$W_s(W_s < W_{thr}) = 0$; (set the spot's weight that is lower than the threshold to zero)
50	$W_{total} = sum(W_s)$; (total of spots' weights)
51	For $s = 1 : N_{spot}$
52	$P_s = W_s/W_{total}$; (distribute the power among the spots in proportion to their SNRs)
53	$P_s = (W_s/W_{max}) \times P_{limit}$; (introduce a restriction so that the spot power not exceeds $1mW$)
54	$\Delta t_s = \mu_{max} - \mu_s$; (calculate the time delay)
55	Compute the impulse response $h_s(t)$ observed by the desired photodetector
56	Shift the impulse response as $h_s(t - \Delta t_s)$ (introduce the time delay)
57	End
58	Sum the delayed impulse responses within a time bin (0.01 ns duration)
59	Produce the optimized impulse response $h_{optimized}(t)$ due to all the spots considered
60	Calculate the pulse response = $h_{optimized}(t) \otimes p(t - T_b)$ and then, find $(P_{s1} - P_{s0})$
61	Compute $SNR_{optimized} = (R \times (P_{s1} - P_{s0})/\sigma_t)^2$;
62	Compute $D_{optimized} = \sqrt{\sum_m (t_m - \mu)^2 P_r^2(t_m)/\sum_m P_r^2(t_m)}$, where, $\mu = \sum_m t_m P_r^2(t_m)/\sum_m P_r^2(t_m)$

6.5 Performance Analysis and Simulation Results

The performance of the proposed multibeam adaptive algorithms (FEAAS, FEADAS and FEADPAS in conjunction with diversity reception) is evaluated in the presence of ambient light noise, multipath propagation and mobility. Comparisons with the LSMS and the original MBAAS are also presented.

6.5.1 Channel Characteristics Evaluation

The channel impulse response specifies the received optical power resulting from multipath propagation. The impulse responses of the proposed multibeam OW configurations are depicted in Figure 6.2. The impulse response of a CDS is included. It should be noted that the value of the received power reported in this section is the peak level of the pulse response obtained through convolution of the impulse response with a rectangular transmitted pulse of 1W and 20ns duration, corresponding to 50Mbit/*s* bit rate. Furthermore, the rms. delay spread values measure the temporal dispersion of the received signal due to multipath propagation, given by (3.29). It is clearly seen that the spot-diffusing structure is significantly better than the CDS when both systems employ a

wide FOV receiver (see Figure 6.2(a)). This is due to the presence of direct path components between the diffusing spots and the receiver, made possible through spot-diffusing geometry.

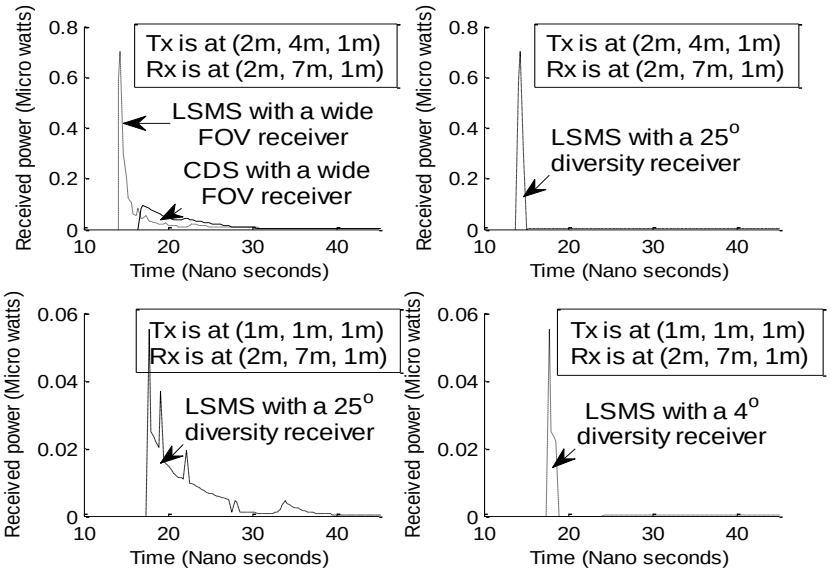

(a)

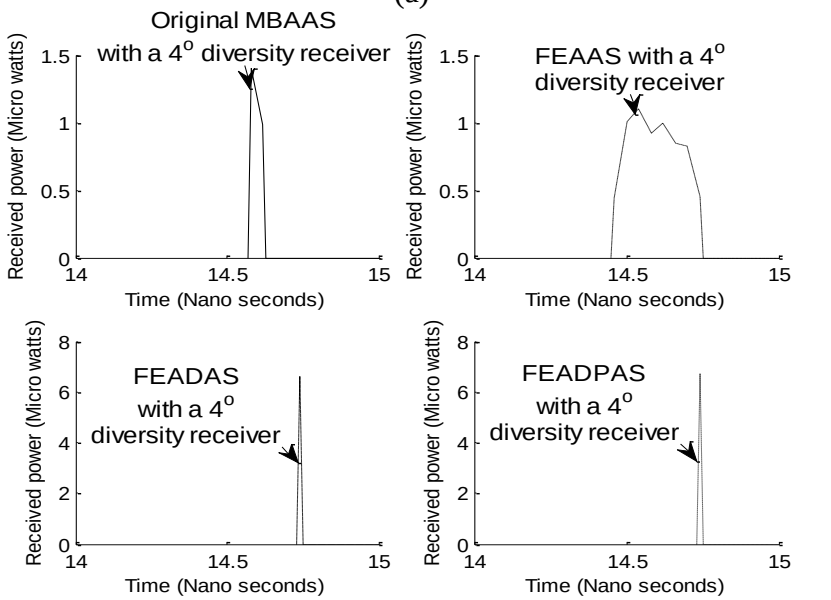

(b)

Figure 6.2: Impulse responses of different OW configurations: (a) CDS and LSMS with a wide FOV receiver, and LSMS with a 25° and 4° FOV diversity receivers; and (b) the original MBAAS, FEAAS, FEADAS and FEADPAS with a 4° FOV diversity receiver,

at two transmitter positions: (1m, 1m, 1m) and (2m, 4m, 1m), and when the receiver is located at (2m, 7m, 1m)

CDS produces 1.56μW received optical powers with much more signal delay, an rms delay spread of almost 2.65ns (over a long time period) corresponding to a channel bandwidth of 38MHz, due to the diffuse transmission and wide receiver FOV (FOV=90^o). A significant increase in the received power from 1.56μW (CDS) to 3.07μW can be achieved when an LSMS replaces the CDS, and when both systems employ a wide FOV receiver. This significant increase in the received power comes with a reduction in the signal spread (delay spread) from 2.65ns to 0.92ns. The delay spread of the LSMS signal can be reduced from 0.92ns to 0.21ns when a 25^o diversity receiver is employed instead of the wide FOV receiver. However, a reduction in the received optical power from 3.07μW to 1.67μW is induced. This is due to the limited range of rays captured by narrow FOV diversity receivers. Nonetheless, it has to be observed that LSMS with an angle diversity receiver offers a better overall SNR than LSMS with a wide FOV receiver, due to the significant reduction in collected background noise [102]. Transmitter mobility increases the delay spread of the diversity LSMS, as might be expected, at receiver locations away from the transmitter. For example, when the receiver is located at (2m, 7m, 1m) and the transmitter moves from the centre of the room to the corner (1m, 1m, 1m), the delay spread of the 25^o diversity LSMS increases from 0.21ns to 4.1ns. This transmitter movement can also cause an increase in the path loss, where the collected optical power drops from 1.67μW to 0.6μW. Limiting the FOV of the diversity receiver to 4^o reduces the delay spread from 4.1ns to almost 0.31ns, and decreases the received power from 0.6μW to 0.13μW, due to the limited range of rays captured. A reduction in

the delay spread from 0.31ns to 0.019ns can be achieved if the spot distribution is spatially adjusted to positions near the receiver through beam angle adaptation (i.e. when the MBAAS is employed instead of the traditional LSMS). This improvement in the delay spread comes with an increase in the received optical power from 0.13μW to 2.4μW. Furthermore, an improvement in the received optical power, from 2.4μW to 6.6μW, can be achieved when an FEAAS replaces the original MBAAS. This is attributed to the ability of the new FEAAS to benefit fully from the transmitted power through optimising the number and more so the pattern of the spots, based on the receiver's location and its FOV, and equally distributing the transmitted power among the spots. This improvement in the received power is achieved while accelerating the adaptation process by a factor of 20 compared to the search time required in the original MBAAS. However, an increase in the delay spread from 0.019ns to 0.073ns is incurred due to the increase in the number of rays captured by the receiver (as a result of increasing the number of spots, where 25 × 25 spots are employed instead of a line of 80). The received signal spread can be dramatically reduced from 0.073ns to 0.011ns through adjusting the switching times of the beams so all the rays can reach the receiver at the same time, thus reducing the effect of multipath dispersion. Although a reduction in the delay spread is achieved when an FEADAS replaces the FEAAS, the received power is similar in both systems. This is due to the similarity of the spot geometry and power distribution in both systems.

However, the FEADAS adapts the switching times of the beam to allow the rays to be captured by the receiver at the same time. It has to be observed that FEADAS offers a better overall SNR compared to FEAAS at high bit rates due to the significant reduction

in the ISI (see Figure 6.5). To further improve the quality of the link, we combine these new techniques (fast beam power and delay adaptation with the new 25 × 25 spot geometry) with beam power adaptation. The results achieved through this combination are better than previous results in this area. In addition, impulse responses for all the cases studied are analysed to compare the impact of transmitter/receiver mobility on the received optical power, and to examine the extent to which the combination of the proposed methods ameliorates this effect. The results are presented in terms of channel bandwidth and SNR. The 3dB channel bandwidth of the proposed multibeam OW systems (LSMS, original MBAAS, FEAAS, FEADAS and FEADPAS with a 4^o diversity receiver) is given in Table 6.3. The results show that FEADPAS can offer OW communication channels with 3 dB bandwidths greater than 15GHz. In addition, the number of spots visible within the receiver FOV is a key factor to achieve acceptable SNR (greater than 15.6 dB for a bit error rate (BER) of 10^{-9}). Due to this fact, the FEAAS can improve the SNR by increasing the number of diffusing spots visible within the receiver's FOV, particularly when using narrower FOVs (see Figure 6.3). This can allow the FEAAS transmitter to transmit lower optical power, while meeting the SNR requirements and conforming to eye safety regulations.

However, it has to be noted that the delay spread is dictated by the number of spots seen within the FOV and their relative positions. This can result in introducing a time delay between the signals received from the spots within the receiver's FOV, hence limiting the bandwidth. The increase in the number of rays captured by the receiver in the FEAAS as a result of increasing the number of spots, so 25 × 25 spots are employed here instead of

a line of 80 spots in the original MBAAS, resulting in a higher delay spread as well as a lower bandwidth than the original MBAAS; see Table 6.3.

Table 6.3: 3 dB channel bandwidth of the proposed multibeam systems

Configuration	3 dB Channel Bandwidth (GHz)						
	Receiver locations along the *y*-axis, Y (m)						
	1	2	3	4	5	6	7
LSMS	2.1	1.6	1.2	0.89	0.77	0.67	0.56
Original MBAAS	8.3	8.7	8.3	8.7	8.3	8.7	8.3
FEAAS	2.8	3.2	2.8	3.2	2.8	3.2	2.8
FEADAS	15.2	15.4	15.2	15.4	15.2	15.4	15.2
FEADPAS	15.5	15.6	15.5	15.6	15.5	15.6	15.5

6.5.2 SNR Evaluation

To enable comparison with previous work [7], a bit rate of 50Mb/s is used. A higher bit rate of 15Gbit/s is also considered for the proposed multibeam adaptive OW systems. The preamplifier used in the 50Mbit/s OW system (20ns pulse duration) is the 70MHz PIN-BJT design proposed by Elmirghani et al. [26], with noise spectral density of 2.7 $\mathrm{pA}/\sqrt{\mathrm{Hz}}$. This receiver introduces little or no distortion onto the 50 Mbit/s pulse stream. The performance of the proposed multibeam adaptive OW systems (FEAAS, FEADAS and FEADPAS), coupled with an angle diversity receiver, is evaluated under the constraints of ambient light noise, multipath propagation and mobility.

The systems' SNRs are compared to those of the LSMS and the original MBAAS with diversity detection, when the transmitter is placed at (2m, 7m, 1m) and the receiver moves along the *x*=1m line. These locations are selected in order to examine some of the key cases; that is, points exactly underneath directive noise sources, as in *y*= 1m, 3m, 5m, and 7m, as well as points near the corner of the room, representing the worst communication paths, as well as central and other room locations along the *x*=1m line that represent

normal operation. Note that the *x*=3m line is similar to the *x*=1m line due to the room's symmetry and the *x*=2m line is a better line as it is away from noise sources. We here therefore examined a worst case scenario.

The results are shown in Figure 6.3, where all OW systems operate at 50Mbit/s. Previous work [7] has shown that the LSMS SNR, with a diversity receiver, is largely independent of the receiver's location when the transmitter is stationary at the centre of the room as a result of the advantageous spot distribution on the ceiling. It was also found that degradation in the LSMS SNR is observed when the transmitter is mobile, due to some non-illuminated regions in the room and having some others with an increased spot population. Regardless of the transmitter position, beam angle adaptation can help the multibeam transmitter to cluster its diffusing spots (a line of 80 spots) at an area on the ceiling and/or walls, based on the receiver location, so as to maximise the receiver SNR [8].

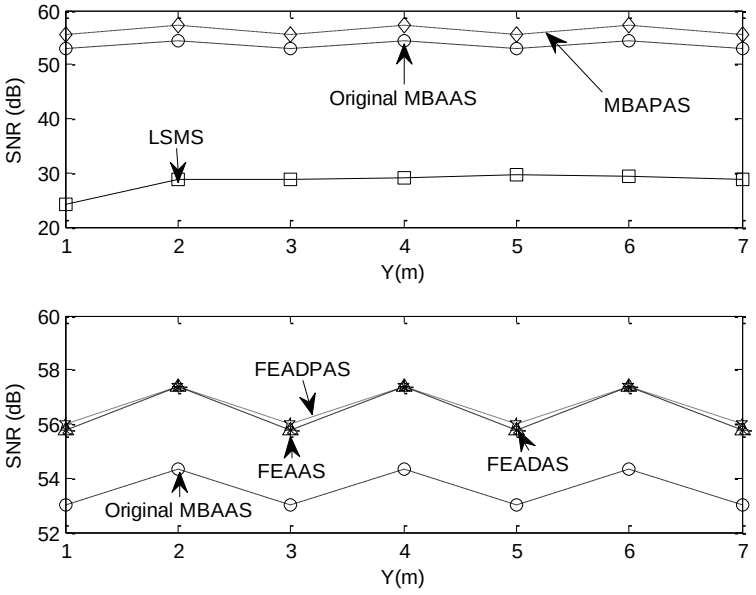

(a)

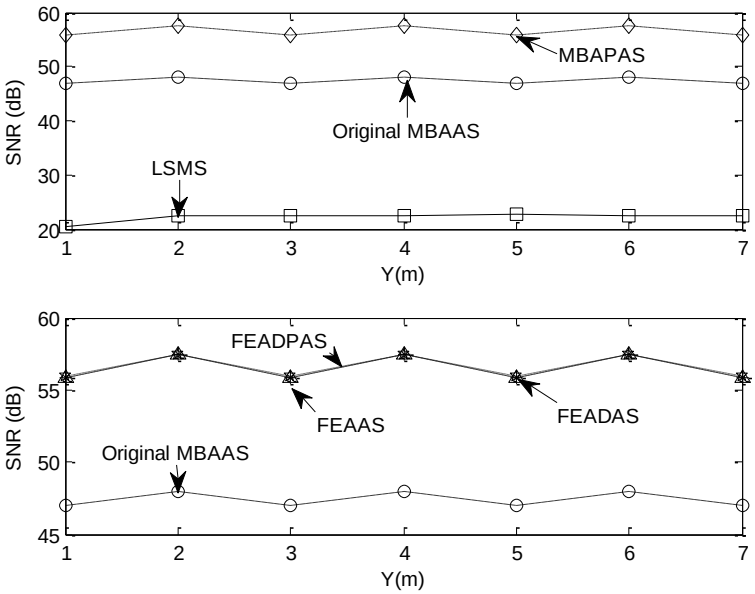

(b)

Figure 6.3: SNR of the 50 Mbit/s proposed multibeam OW systems when the transmitter is placed at (2m, 7m, 1m) and the receiver moves along the line x=1m in conjunction with: (a) an 8^o diversity receiver; and (b) a 4^o diversity receiver.

The results in Figure 6.3 (a) show that a significant SNR improvement of 29dB can be achieved when MBAAS replaces LSMS at a 6m transmitter–receiver distance, when both systems employ an 8^o diversity receiver. This is in good agreement with the results reported in [8]. The MBAAS identifies the optimum location through an exhaustive ordinary search and then distributes the spots in the form of a line strip with equal intensities. This may lead to power being allocated to some spots outside the receiver FOV, hence wasting some of the transmitted power, particularly when using narrower FOVs. The use of narrower FOVs is essential in some cases to reduce noise and interference, and also to allow the use of smaller area detectors. The results in Figure 6.3 also show that a power penalty of 6dB can be induced in the original MBAAS SNR when a 4^o diversity receiver replaces the 8^o diversity receiver. This power penalty can be compensated for with an SNR improvement of approximately 9dB if the power is

adaptively distributed among the spots through beam power adaptation, i.e., when the multibeam angle and power adaptive system (MBAPAS) replaces the original MBAAS. MBAPAS was proposed and examined in [8], and here it is modelled and used for comparison purposes. However, power adaptation will not help much in this case if the power per spot is restricted for reasons of eye safety.

Increasing the number of spots in the line strip is possible, but will not help here as the number of spots located within the receiver FOV is limited. Therefore, optimising the number and, to a greater extent, changing the pattern of the spots are important design considerations. The proposed system (FEAAS) can reduce the adaptation time through the use of a 'divide and conquer' algorithm, and can also optimise the number and pattern of the spots based on the receiver FOV. This can help the receiver collect more power, while helping with eye safety regulations. In addition, Figure 6.3 shows that the new FEAAS offers an improvement in the SNR of 9dB over the original MBAAS. This SNR improvement comes with a reduction in the computation cost in the practical OW FEAAS by making use of a 'divide and conquer' algorithm. The proposed system (FEAAS) therefore outperforms the original MBAAS in terms of both SNR and adaptation speed. Although additional bandwidth efficiency is achieved through beam delay adaptation (i.e. when an FEADAS is employed) compared to the FEAAS, a comparable SNR is seen in both systems at 50 Mbit/s bit rate. This is due to the excess channel bandwidth achieved by the FEAAS (OW channel bandwidth of 2.8GHz), which guarantees that ISI does not occur at the lower bit rate considered (50Mbit/s). However ISI can cause significant

degradation in the SNR at higher bit rates. Despite this, replacing the FEAAS by an FEADPAS, at a bit rate of 50Mbit/s, can slightly improve the SNR by less than 0.5dB.

Note that the new FEAAS in this case is able to achieve the majority of the improvement through optimising the number, and even more so in the case of the pattern of spots, based on the receiver's location and the receiver's FOV, and distributing the power equally among the spots. If shadowing exists (i.e. some beams are obstructed), then the new FEAAS can re-optimise the spot distribution (including the number of spots and the shape of their distribution) so that the transmitted power is distributed equally but only to unobstructed beams.

The SNR accounts for the impact of ambient light noise and preamplifier noise, and therefore the SNR values reports reflect both impairments. The BN effect is manifested here as a fluctuation in the SNR of the adaptive multibeam OW systems. This is due to the BN having a very low value at y = 2m, 4m, and 6m, as the receiver is not underneath a spotlight, while high noise levels are detected at y=1m, 3m, 5m and 7m. In effect, when the receiver is underneath a spotlight the adaptive multibeam transmitter is unable to distribute its diffusing spots within the FOV of the detector facing up, and instead it clusters the spots within one of the side detector's FOV.

6.6 System Complexity and Adaptation Time

Significant SNR improvements can be made through the use of the proposed adaptation algorithms, however implementation complexity increases. This is associated with the computational time and resources required to identify the optimum spot position where

the receiver's SNR is computed at each possible beam location and the optimum spot direction is selected at the transmitter. It also results from the need to compute the SNR and time delay due to each beam at the receiver and to adapt the power levels and time delays among the spots at the transmitter.

The transmitter computations are simple and the receiver operations are comparable to those needed when implementing receiver diversity, and as such the complexity increase is moderate. However, we aim here to evaluate the efficiency of our algorithms through the study of both time complexity and memory size criteria. The computational complexity can be measured based on the nature of the function $T(n)$ [180], where for instance a linear algorithm of input size n can induce a linear time complexity of function $T(n) = O(n)$. An algorithm with complexity order $O(n)$ usually has a single pass implementation and shows acceptable performance with small n, however it becomes too complex with larger n. The classical angle adaptation algorithm can identify the optimum location through scanning all the possible locations, which are processed in the basic 'one-pass' style. Therefore, the time complexity of this algorithm is linear, given by $T(n) = O(n)$ and its complexity rises with increase in n. The input size n here represents the total number of possible beam locations that have to be scanned to identify the optimum beam location resulting in the best SNR. In contrast, the fast algorithm is a recursive algorithm based on a 'divide and conquer' approach, where the scanning process is recursively broken down into a number of iterations k. Four iterations are conducted, in our case (i.e. $k = 4$), where $n/64$ locations have to be scanned in each iteration, resulting in a time complexity given as [180]:

$$\begin{aligned} T(n) &= k\,T\left(\frac{n}{64}\right) + kj = k\,T\left(\frac{n}{j\left(2^{k}\right)}\right) + kj \\ &= \log\left(\frac{n}{j}\right) T(1) + j\log\left(\frac{n}{j}\right) = j\log\left(\frac{n}{j}\right) \end{aligned}, \tag{6.2}$$

where j is the number of subproblems (quadrants in our case). In each iteration the fast algorithm divides the scanning area into four quadrants (i.e., $j = 4$). Accordingly, the fast algorithm can achieve time optimal $O(4\log_2(n/4))$ complexity, therefore it is highly efficient, compared to the classical algorithm. It should also be noted that the fast algorithm needs a memory space of 64 times less than the classical algorithm.

To reduce the computational complexity, the system may choose to update its beam angles, power and delay less frequently, even in the presence of mobility. This simplification is at the cost of an SNR penalty. We studied the SNR penalty based on the transmitter using its old adaptation settings – that is, old beam angles, old beam delays and old beam powers – while in motion. This is to determine how often the system has to adapt its settings based on a link margin. The SNR penalties incurred as a result of mobility (distance moved along the y-axis) and non-adaptation of weights are depicted in Figure 6.4, when two different diversity receivers (8^o FOV diversity receiver and 4^o FOV diversity receiver) are used.

Two main cases are shown: first, when the receiver is under a spotlight; and secondly when the receiver is away from a spotlight. We consider receiver motion of 1m along the y-axis. The SNR penalty was calculated for each receiver movement in step of 10cm. When an 8^o FOV diversity receiver moves by a distance of 20cm away from the optimum location of the spots at (2m, 1m, 1m) and no adaptation is carried out, the SNR of the

proposed system (FEADPAS) degrades by 1.8dB. Higher SNR penalties of 8.9dB and 9.3dB can be incurred if the 8^o FOV diversity receiver moves further by 10cm and 20cm respectively. However, if the receiver continues moving, the SNR penalty reduces until it reaches a value of almost 1dB at a receiver location away from the optimum location of the spots by 70cm. This is due to the fact that when the receiver is located at (2m, 1m, 1m) (i.e. it is not underneath a spotlight) the transmitter can steer its beams to positions within the FOV of the detector facing upwards.

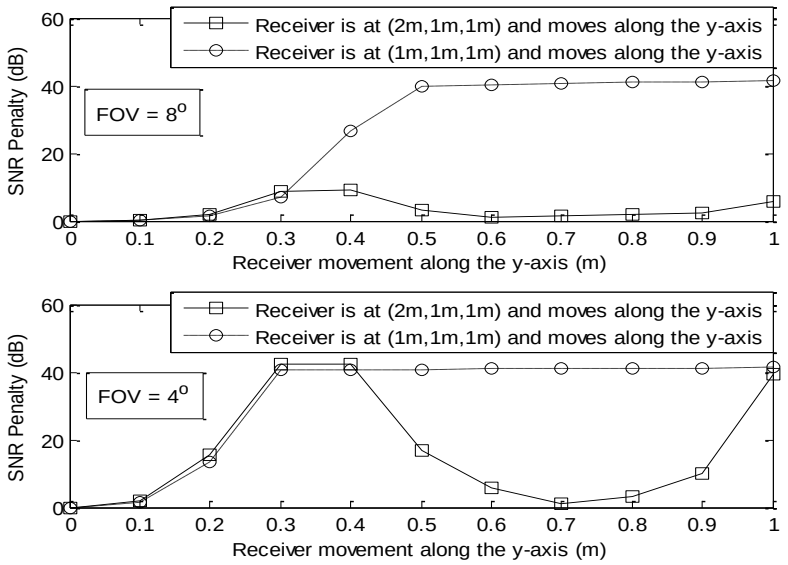

Figure 6.4: SNR penalties of the proposed system (FEADPAS) when the receiver moves by a distance of 1m away from the optimum location of the spots

Once the receiver starts moving (provided no further adaptation is carried out), some of the spots will move out of the FOV of the detector facing upwards and start to appear within the FOV of the side detectors. With more movement steps, the spots start to appear outside the FOV of the side detectors and the SNR penalty increases accordingly. In contrast, when the receiver is located at (1m, 1m, 1m) (i.e. underneath a spotlight) the transmitter is not able to allocate its spots within the FOV of the detector facing upwards

and instead clusters the spots within the view of one of the side detectors. When the receiver moves away from the optimum location of the spots, some of the spots move outside the receiver FOV, thus incurring a power penalty as a result of using the old adaptation settings. This power penalty increases with increase in the distance away from the optimum location and saturates at a value of 40dB approximately after a movement of 50cm. This is attributed to the fact that beyond this transmitter-receiver distance all the spots fall outside the receiver FOV, and the achieved SNR is due to reflections only (i.e., no LOS is established). The case where a 4^o FOV diversity receiver is used can be similarly explained. It should be noted that the adaptation process can be performed in milliseconds, based on typical liquid crystal device characteristics. This is fast enough, given that the adaptation has to track the channel variation that happens at the rate at which humans or indoor objects move.

However, the system design can allow an SNR margin (for example, 3 dB) to ensure that the adaptation process does not have to be repeated frequently. The new faster 'divide and conquer' algorithm needs to scan 640 locations to identify the optimum spot location. Once the optimum beam direction is identified, a set of uniformly distributed spots (25 × 25 spots) at 1cm spacing is created and centered on the optimum location. The receiver's SNR (due to each spot) is estimated separately and relayed to the transmitter to help shape the optimum spot distribution. If each SNR computation/estimation is carried out in 10μs [171], then the total adaptation time when the receiver moves to a new location is almost 13ms. When an 8^o FOV diversity receiver is used we considered all the typical representative set of transmitter and receiver locations (transmitter at centre of room,

transmitter at room corners, etc., receiver moves along the x=1m, x=2m, near walls and near corners, etc.) and the worst penalty identified when the transmitter or receiver moves by 20cm and no adaptation is carried out is almost 2dB. Therefore, with a 1m/s pedestrian movement/environmental change, there is at least 0.2s interval between one adaptation and the next. It is suggested that the receiver re-evaluates its SNR every 0.2s and relays this to the transmitter, which in turn initiates a new adaptation if the receiver's SNR has significantly changed (compared to a threshold). As such, the holograms can adapt every 0.2s, and the 13ms adaptation time therefore represents a spot reconfiguration overhead time of approximately 6.5%. Holograms based on liquid crystal devices capable of adapting within ms times are feasible. It should be noted that the adaptation process is performed at the rate at which the environment changes and not at the system's bit rate. Therefore, the proposed system (FEADPAS) can achieve 15Gbit/*s* when it is stationary, and 93.5% of this data rate, that is, 14Gbit/*s*, when there are environmental changes (see Figure 6.6).

Following a similar approach in the case of a 4^o FOV diversity receiver, adaptation has to be performed if the transmitter or receiver moves by 0.1m or more if an SNR penalty lower than 3 dB is desired. The penalty in this case associated with 0.1m motion is 1.7dB. The adaptation process needs therefore to be repeated every 0.1s, representing an overhead of 13% in terms of transmission time, and as such the system can achieve 13Gbit/*s* when it is on the move. The 4^o FOV diversity receiver is used here to allow the use of small area detectors at these high data rates.

The link budget can be further improved if imaging receivers with MRC are used, and this warrants further study. It should also be noted that if the receiver chooses the spot with the best SNR and reports this value (spot index) to the transmitter to allocate all the available power to this spot, complexity will be reduced. However, such a system will be prone to beam blockage, shadowing and may violate eye safety. The proposed system offers advantages in this regard; however there is a moderate increase in receiver complexity, as discussed above.

6.7 Robustness to Shadowing and Signal Blockage

The effectiveness of the FEAAS is evaluated in a harsh environment with mobility. Such an environment is typically encountered in real office configurations, where there is optical signal blockage due to cubicles, windows, doors and furniture. Furthermore, other impairments degrade the system in this real environment including ambient light noise and multipath propagation. To simulate shadowing and signal blockage of the communication links, a room arrangement similar to the one used in Chapter 4 is considered, denoted by Room B (see Figure 4.1).

This room represents a realistic office environment with dimensions similar to those of the room considered previously in this chapter. The glass windows are assumed not to reflect any signal. The reflectivity of the ceiling and walls surrounding the windows is 0.8. Two perpendicular walls are covered with bookshelves and filing cabinets with a 0.4 reflectivity. Cubical office partitions are assumed to either absorb or block signals. The complicated environment in this room results in shadowing created by physical partitions

and low reflectivity objects. Comparisons were carried out between the traditional LSMS, adaptive LSMS (ALSMS) and FEAAS when all systems employ a 4^o diversity receiver and operate at 50 Mbit/*s* in a complicated room design with full mobility. The arrangement in the ALSMS is similar to that in LSMS, but the power is adaptively distributed among the spots in the ALSMS, with the aim of maximising the receiver's SNR. The SNR results of the proposed systems in two room scenarios (shadowed and unshadowed rooms) are depicted in Figure 6.5, when the transmitter is placed at (1m, 1m, 1m) and the receiver moves along the x=1m line on the CF.

In similar way to the rooms designation used in Chapter 4, here the complicated environment is nominated as a shadowed room, while the empty room is denoted as a unshadowed room. It is to be noted that this line (x=1m) represents the worst zone that can be scanned due to the presence of office cubicles. The worst impact of shadowing and signal blockage in the LSMS performance translates to an SNR degradation of almost 20dB when the transmitter and receiver are co-located in the corner of the room (1m, 1m, 1m). This degradation is due to the presence of windows that cause a major signal loss, hence greater path losses near the corners. Furthermore, the effect of signal obstruction due to partitions can be observed as a degradation in the SNR level by approximately 4 dB when the receiver is located at y=3m, 5m and 7m. At these locations (y=3m, 5m and 7m) the diversity receiver is underneath a spotlight and in turn it relies on one of the side photodetectors in order to achieve its best SNR, in essence 'select best' combining is implemented.

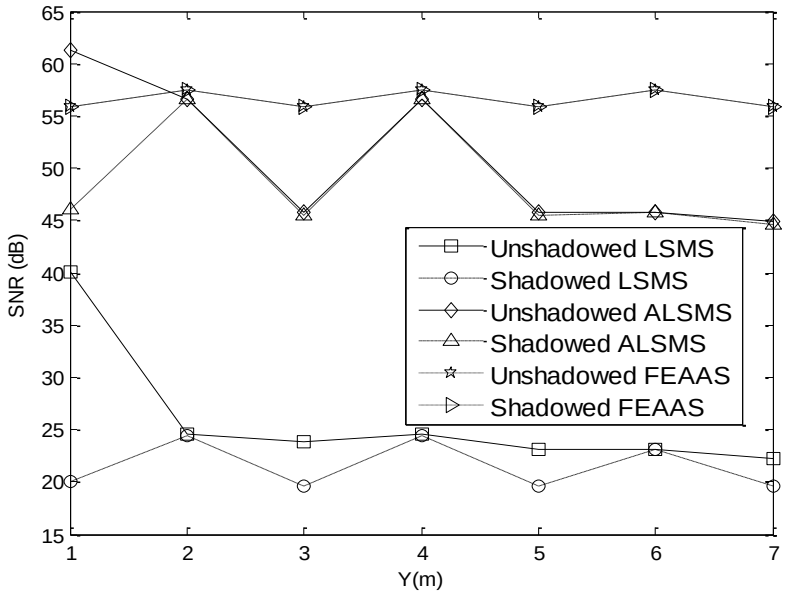

Figure 6.5: SNR of three multibeam OW systems: LSMS, ALSMS and MBFPE-AAS with a 4^o diversity receiver in two room scenarios (unshadowed and shadowed) when the transmitter is placed at *(1m, 1m, 1m)* and the receiver moves along the *x*=1m line.

The receiver proximity to partitions in these cases may cause path blockage to some of the direct rays (depending on the receiver directionality and the height of partitions), resulting in performance penalties. In contrast, shadowing and signal blockage have almost no or limited effect on the LSMS SNR at locations of *y*=2m, 4m and 6m, where the receiver is not underneath a spotlight. When the transmitter is placed in the corner of the room (1m, 1m, 1m) and the diversity receiver is located at (1m, 2m, 1m) or (1m, 4m, 1m), the results indicate that among the photodetectors considered, the one facing upwards is able to collect the maximum power possible (through a number of diffusing spots located within its FOV) and with minimum noise level. This can help the receiver achieve a similar SNR at these sets of transmitter and receiver locations, in the two room scenarios (shadowed and unshadowed rooms), as shown in Figure 6.5.

However, shadowing can reduce the reflection contribution. This reduction is very low due to the employment of narrow FOVs (FOV = 4^o), and therefore does not affect the overall SNR since the photodetector facing upwards is still able to see the same number of spots, even in the presence of shadowing. The comparable LSMS SNR observed in both shadowed and unshadowed environments at transmitter and receiver locations of (1m, 1m, 1m) and (1m, 6m, 1m) can be similarly explained, though the side photodetector having an El and Az of 40^o and 270^o respectively is the best link selected in this scenario. Furthermore, ALSMS with a 4^o diversity receiver is more robust against shadowing and signal blockage compared to LSMS, owing to its ability to re-allocate power to unblocked spots. These benefits are manifest as a comparable SNR performance in the 4^o diversity ALSMS system in both shadowed and unshadowed rooms, except in the scenario where the transmitter and receiver are co-located in the corner of the room (1m, 1m, 1m). In this case, shadowing and signal blockage can induce a degradation of 15dB in the ALSMS SNR. This is due to the inability of the beam power adaptation to assign higher powers to the spots located in the side wall near the receiver due to the presence of windows, and instead the transmitted power is allocated to the ceiling spots. This penalty can be put in context by observing that an SNR improvement of almost 26dB can be achieved when the ALSMS replaces the traditional LSMS in a shadowed environment when both systems employ a 4^o diversity receiver and operate at 50Mbit/s. This SNR improvement illustrates the gain achieved through power adaptation while the beam angles are kept fixed.

Previous work [177] has shown that further SNR improvement of 10 dB can be achieved if adaptation is also applied to beam angles; that is, if an MBAPAS replaces the ALSMS. Here we show that a multibeam OW system adopting the new FPE-AAS can provide a robust link against shadowing and signal blockage, and can also achieve an SNR performance comparable to that obtained by MBAPAS. This is achieved together with a reduction in the system adaptation complexity by a factor of 20, while distributing the transmitted power among the spots in equal intensities (i.e. power adaptation is not employed in this system). This achievement is attributed to the ability of the new system (FEAAS) to adapt to such environments and shape the optimum spot distribution by illuminating the unblocked spots only, hence maximising the receiver's SNR. Beam delay adaptation can help increase the channel bandwidth, thus improving the SNR when the system operates at higher bit rates, due to the reduction in the effect of multipath dispersion and ISI (see Figure 6.6). Nevertheless, the results obtained and presented in Figure 6.5 prove that the 25cm × 25cm array is quite enough to combat shadowing and beam blockage in a realistic environment.

Furthermore, spreading the beams more widely will result in higher dispersion and will not necessarily improve the performance under a blockage any more than the proposed 25cm × 25cm array, which is shown to perform well. In addition, there are two main cases when ALSMS and FEAAS are compared. These refer to a receiver under a spotlight or away from a spotlight. In Figure 6.5, the transmitter is at (1m, 1m, 1m) and therefore when the receiver is at (1m, 2m, 1m) and (1m, 4m, 1m), the ALSMS is able to use its detector facing up, as these positions are not under spotlights. Therefore, ALSMS and

FEAAS perform similarly. At (1m, 3m, 1m), (1m, 5m, 1m) and (1m, 7m, 1m) the receiver is under a spotlight and, as such, the FEAAS outperforms ALSMS as it is able through angle adaptation to move its beams and locate them within the FOV of side detectors that do not observe any background noise. At (1m, 6m, 1m), although the receiver is not under a spotlight, the ALSMS is not able to beam steer and hence its spots are at the far (1m, 1m, 1m) corner and are shadowed and unseen by the receiver. This is partly the case at (1m, 5m, 1m) and fully the case at (1m, 7m, 1m).

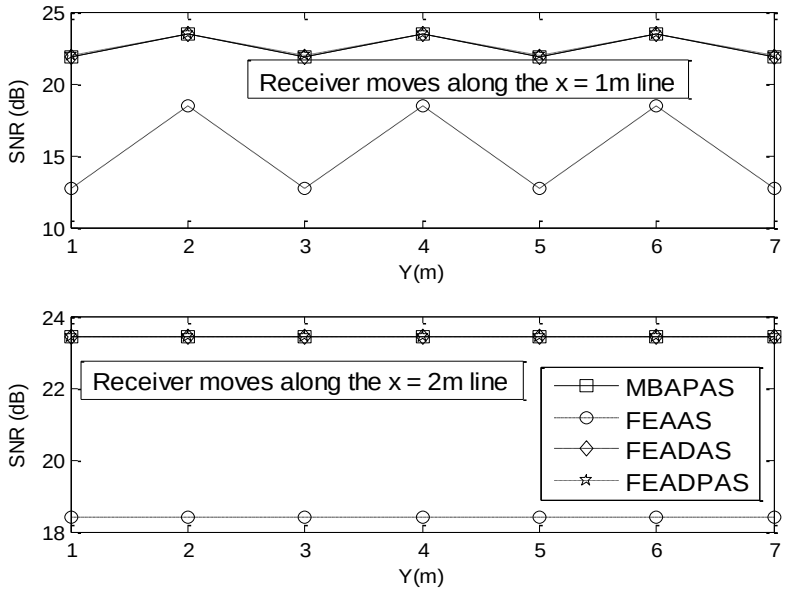

Figure 6.6: SNR of the multibeam systems (MBAPAS, FEAAS, FEADAS and FEADPAS) operating at 15Gbit/s when the 4^{o} diversity receiver moves along the x=1m and x=2m lines within a shadowed environment

6.8 High-speed Mobile Indoor OW Communication Systems

The high SNR achieved through the multibeam fast power, angle and delay adaptation algorithm, coupled with the additional bandwidth shown in Table 6.4, can be used to provide higher data rates (15Gbit/s and beyond). The PIN-HEMT design proposed by Kimber et al. [181] was used for the proposed 15Gbit/*s* multibeam adaptive OW systems. This preamplifier has a noise current spectral density of $11\ \mathrm{pA}/\sqrt{\mathrm{Hz}}$ and a bandwidth of 12GHz. The preamplifier bandwidth can be limited to 10.6GHz through the use of appropriate filters. The optimum receiver bandwidth is $0.707 \times$ bit rate (Personick's analysis [120]). The modulation format used is on–off keying (OOK) with intensity modulation and direct detection. The rise and fall times of laser diodes, transmitter and receiver design are not considered in this thesis, as transceivers for data rates up to 10Gbit/s are well established in fibre systems [182]. The particular features of OW transceiver designs here are of interest to future work. Note that narrow FOV receivers, which use small detectors compatible with fibre systems receivers, are employed here. In previous work we considered holographic spot diffusing transmitters [177]. OOK is the simplest modulation scheme to implement in OW systems, and is therefore assumed here. OOK is an appropriate modulation scheme for high bit rate OW systems [20] due to its simplicity and the ability of laser diodes to switch on and off at rates into Gbit/s. However, ISI can be significantly increased. Although ISI can be effectively reduced by using equalisation techniques [30], this is not the case here. The simulation results, illustrated in Figure 6.3, indicate that the two systems (FEAAS and FEADAS) can perform identically at a bit rate of 50Mbit/s, and this is evident in the excess channel bandwidths

achieved, which guarantees that ISI does not occur at the lower bit rate considered (50Mbit/s). However, ISI can be significantly increased if the FEAAS operates at 15Gbit/s, and hence significant SNR degradations can be induced. In contrast, the FEADAS can offer a bandwidth of more than 15GHz (see Table 6.4), which enables it to support operations at 15Gbit/s, at least. Figure 6.6 shows that a considerable SNR improvement of 9dB can be achieved when an FEADAS replaces the FPE-AAS, and where both systems employ a 4^o diversity receiver with a reception area of $1mm^2$ and operate at 15Gbit/*s* at 6m transmitter–receiver distance in a shadowed environment. Note that the transmitted power is distributed equally among the beams in both systems (FEAAS and FEADAS), and this improvement is due to the significant reduction in the influence of multipath dispersion and ISI through beam delay adaptation. The SNR can be slightly improved further by approximately 0.2dB if the power is adaptively distributed among the beams; that is, if an FEADPAS replaces the FEADAS.

This confirms the ability of the new faster adaptation algorithm to benefit fully from the transmitted power by optimally fitting the spots within the receiver's FOV and distributing the power among the spots equally. In addition, a comparable SNR is observed in both MBAPAS and FEADPAS when the transmitted power is freely allocated to spots at key locations. However, the new system (FEADPAS) outperforms the previously proposed system (MBAPAS) if a restriction is imposed on the algorithms to consider eye safety, so that no spot power exceeds 1mW, which can help avoid eye damage at the near infrared wavelengths [62]. Note that eye safety is not dictated in this case only by the power per beam, but by the number of beams that can be seen

simultaneously. Therefore, further attention is needed to reduce this number of beams by considering the transmitter's geometrical construction; however, measures that can reduce the power per beam while maintaining the SNR are useful, as proposed here. The SNR results of both systems (MBAPAS and FEADPAS in conjunction with a 4^o diversity receiver), obtained through the use of an adaptation algorithm that restricts the power per beam to less than 1mW, are given in Table 6.4.

The SNR of FEADPAS with restricted per beam power (less than 1mW per beam) with an 8^o diversity receiver is included. The results show that the per beam power can be maintained below 1mW while achieving 10^{-9} BER at a bit rate of 15Gbit/*s*, where the new FEADPAS achieves an SNR of 17.4dB, which is greater than the 15.6dB needed. This SNR is obtained when using a 4^o diversity receiver with $1mm^2$ detector area, given the worst communication links studied where there is mobility, shadowing and signal blockage.

Table 6.4: SNR of the 15Gbit/s restricted Multibeam OW systems

Configuration	**SNR (dB)**						
	Receiver locations along the *y*-axis, Y (m)						
	1	**2**	**3**	**4**	**5**	**6**	**7**
Restricted MBAPAS, (FOV = 4º)	-8.9	-7.9	-8.9	-7.9	-8.9	-7.9	-8.9
Restricted FEADPAS, (FOV = 4º)	17.2	18.3	17.2	18.3	17.2	18.3	17.2
Restricted FEADPAS, (FOV = 8º)	17.7	19.4	17.7	19.4	17.7	19.4	17.7

6.9 Summary

In this chapter we introduced a fast adaptation method to multibeam angle, power and delay adaptation systems and outlined a new spot diffusing geometry with beams

clustered around the diversity receiver faces. The fast adaptation algorithm reduces the computations needed to reconfigure the transmitter in the case of transmitter and/or receiver mobility. The beam clustering approach provides the transmitter with the opportunity to allocate the power to spots within the receiver FOV and increases the number of such spots. Therefore, if the power per spot is restricted to assist in meeting eye safety, then our new approach where more spots are visible within the receiver FOV leads to enhanced SNR.

Note that if the power per beam is not restricted, then the new and previous systems we introduced have comparable performance, as the total power can be allocated in the earlier system to the one (or few) spots within the receiver FOV. The fast angle adaptation algorithm converges towards the optimum spot distribution that maximises the receiver SNR through an efficient use of a 'divide and conquer' algorithm.

The results have confirmed that, while the original MBAAS benefits from power adaptation, power adaptation is not necessary when the new FEAAS is implemented. This is due to the ability of the new system to benefit fully from the transmitted power through optimising the number and pattern (positions) of spots so as to maximise the receiver's SNR, regardless of the receiver's orientation and its FOV. The new system can also adapt to environmental changes, offering a link that is robust against shadowing and signal blockage through disregarding obstructed spots and distributing the power equally between the unobstructed spots. The new FEAAS offers an SNR improvement of 9dB and reduces the computation cost by a factor of 20 compared to the original MBAAS. Furthermore, beam delay adaptation was introduced to FEAAS to mitigate the effect of

multipath dispersion and ISI, and to improve system performance. The beam delay adaptation method can help the multibeam transmitter to adjust the switching times of the beams in a fashion that allows the signals to reach the receiver at the same time.

Significant improvements in the SNR with OW channel bandwidths of more than 15GHz can be achieved, enabling the system to maintain higher data rates (15Gbit/s and beyond). In addition, a restriction was imposed in the adaptation algorithm to limit the power per beam to less than 1mW to assist with eye safety requirements. Note that eye safety is also a function of the number of beams that can be seen simultaneously by eye.

7 Collaborative Multi-Gigabit OW Systems Employing Fast and Efficient Algorithms with Imaging Reception

7.1 Introduction

The link design where a single user is considered, as presented in the previous chapter (Chapter 6), has shown that through the use of fast and efficient angle adaptation algorithm [150], [151] a 15Gbit/s OW communication system is feasible. The results have shown that a system using the proposed algorithm can reduce computation costs by factor of 20 [177]. A significant enhancement is achieved when the proposed algorithms are applied to a single user case. Multiuser scenarios were considered in Chapter 4 and 5, in which the CABCM method was employed. Simulation results of imaging CABCM have shown that 5Gbit/s collaborative OW systems is achievable; however, the CABCM is not able to beam steer, so the separation distance between the diffusing-spots and the receiver is fixed. In order to solve this issue, we introduced beam angle adaptation combined with collaborative power adaptation to the design of indoor multiuser OW systems. Beam angle and power adaption has been shown to be an effective method to optimise spot distribution and power between the spots, so as to maximise the receiver's SNR.

In this chapter, a collaborative fast and efficient angle and power adaptation (CFAPAS) algorithm is introduced to the collaborative multibeam system design to optimise the

spots' locations and distribution (the number and pattern of spots) spatially, with the aim of maximising the receivers' SNRs as well as significantly reducing the necessary computation time. A liquid crystal device can be used to vary the direction and intensity of the beams adaptively at relatively low complexity [171], [172]. The adaptation requires training and feedback from the receiver to the transmitter, and a low data rate diffuse channel is suggested to achieve this feedback. The main goal is to reduce the effect of transmitter/receiver mobility and the associated impacts on SNR and bandwidth. To improve the quality of the link, the proposed system is implemented in conjunction with an imaging receiver.

7.2 Propagation Model and System Setup

In order to evaluate the advantages of our methods (collaborative fast and efficient angle and power adaptation and imaging reception) in a multiuser indoor OW system, propagation simulations were conducted in an empty room similar to the one in the previous chapter with dimensions of 8m × 4m × 3m (length × width × height). Since plaster walls reflect rays in a form close to a Lambertian distribution (based on experimental measurement [9]), reflecting surfaces (walls and ceiling) and floor were modelled as Lambertian reflectors with reflectivity of 80% and 30% respectively. The simulation tool used is similar to the ones used in Chapter 5. The imaging receiver considered here consists of a single imaging lens and a detector that is segmented into multiple pixels. The optical signal power received by the pixels can be amplified separately and processed using select SB or MRC techniques. The imaging receiver

makes use of a photodetector array segmented into 256 pixels and an imaging concentrator with parameters given in [96]. Three sample cases of two, three and five stationary receivers at selected locations were considered as shown in Figure 4.2 (b). Moreover, the room was illuminated with eight lamps as illustrated in Figure 3.5. Furthermore smaller adaptation angle steps are used to obtain more resolution when scanning the room. The simulations were carried out at several receiving locations within the room when the transmitter is positioned at (1m, 1m, 1m) , (2m, 1m, 1m), (2m, 4m, 1m) and (2m, 7m, 1m).

7.3 Transmitter Configuration

In order to quantify the most suitable approach for use in indoor multiuser communication systems, two collaborative multibeam transmitters configurations (CFAAS and CFAPAS) are presented, analysed and compared with previously introduced methods. Beam angle adaptation has been proposed in [177] and shown to be a promising method for enhancing the SNR of the receiver, regardless of the position of the transmitter. However, the performance improvements are at the cost of additional computational complexity. In Chapter 6, we have introduced a fast and efficient adaptation method to reduce the computations needed to reconfigure the transmitter in the case of transmitter and/or receiver mobility [151]. The new collaborative fast adaptation proposed here allocates a time slot for each coexisting receiver, and then fast beam angle and power adaptation are performed for each receiver. Each individual adaptation is performed in the time slot allocated for the interested receiver, where iterative scanning processes

based on a divide-and-conquer algorithm are conducted. For each receiver, the new method recursively breaks down the scanning process into a number of iterations that focus recursively onto smaller areas, using different adaptation step angles. The entire room is divided into four arbitrary quadrants, where each quadrant has its suboptimum location. The quadrant with the best suboptimum location is assigned the scanning area for next iterations, using adaptation step angle half of that used in previous scanning iteration. The fast adaptation algorithm repeats the iterative process a number of times. In our previous works [150], [151], it was demonstrated that four iterations can achieve acceptable level of complexity and tolerable SNR penalty, therefore our new method implemented four iterations. Once the optimum beam directions are obtained for all coexisting users (N_{user}), the new system produces N_{user} clusters aimed to the optimum beam directions. Each cluster has a rectangular pattern of diffusing spots, where the total number of diffusing-spots is divided into N_{user} clusters (the number of spots in a cluster equal to the total number of spots divided by N_{user}).

All beam are illuminated with equally distributed power and the imaging receivers' SNRs due to each spot are computed separately and relayed to the collaborative mutibeam transmitter at low data rate. The transmitter then determines which spots to be illuminated based on an SNR threshold. The threshold is set based on the SNRs obtained by the coexisting imaging receivers from a diffuse transmitter with a transmitted power comparable to the beam power (1.7mW is allocated to each spot when the total power of the transmitter is 1 W). This can ensure that the spots with direct line of sight with one of the coexisting receivers are only illuminated.

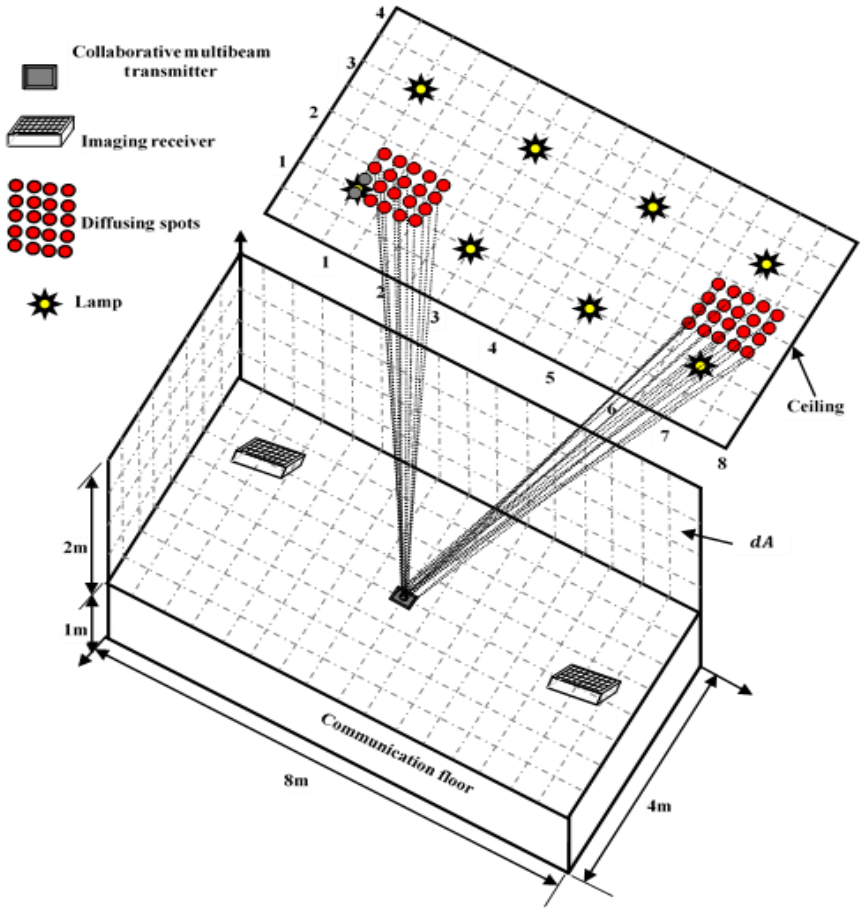

Figure 7.1: OW imaging CFAPAS architecture with transmitter at (2m, 4m, 1m) and two coexisting receivers at (1m, 1m, 1m) and (2m, 7m, 1m).

In order to quantify the efficiency of CFAAS, the total transmit power was distributed equally among the beams while it is distributed unequally in the CFAPAS. The transmit power adaptation used in CFAPAS is similar to that used in iterative water-filling approach [183]. The iterative water-filling method was proposed to maximize the sum rate on multiple antenna. Here in CFAPAS, the multibeam transmitter distributes the power among the beams so as to optimise the SNRs of the coexisting receivers. In effect the spots are given power proportional to the total requested power by the coexisting imaging receivers. The power is adapted collaboratively based on collaborative MRC

technique introduced in Chapter 4, where the requested power can be computed using Equation (4.4). The power of omitted spots can be allocated to different spots that have direct line of sight with one or more imaging receivers. It should be noted that the threshold can be determined in similar way that used in water-filling approach or bases on the amount of requested power by coexisting receiver. A depiction of the imaging CFAPAS architecture with two coexisting imaging receivers is shown in Figure 7.1. In multiuser scenarios, the CFAPAS identifies the optimum locations and the optimum spots distribution as follows:

A. The collaborative transmitter senses the environment to determine the number of coexisting users (N_{user}), then allocates an adaptation time slot (T_{slot}) for each receiver, where $N_{slot} = N_{user}$. A repetitive training period should be included in the MAC protocol to perform this step and the following iterative processes.
B. It arbitrarily performs an individual adaptation for each coexisting imaging receiver within the room starting with first user:

   B.1. Set-up the adaptive hologram to perform the first scan iteration according to its associated parameters: the angle adaptation step size θ_{steps}, the *x*-axis scan range ($\theta_x^{start}\ to\ \theta_x^{end}$) and the *y*-axis scan range $\left(\theta_y^{start}\ to\ \theta_y^{end}\right)$. In order to initially scan the entire room, the *x*-*y* axes scan ranges are set to -90° and 90°. Furthermore, the θ_{steps} is initially set to 11.3°, allowing the spot to move 40 cm in each step.

   B.2. Turn on a single spot and move it by changing the beam angles: θ_x and θ_y in steps of θ_{steps} along the *x*-*y* axes in respect with transmitter's normal. The beam angle θ_x is shifted between θ_x^{start} and θ_x^{end}, while θ_y is shifted between θ_y^{start} and θ_y^{end}. The spot location (x_s, y_s, z_s) (Cartesian coordinates) attached to the transmitter location (x_T, y_T, z_T) and the room dimensions (length ×

width × height), while the beam angles θ_x and θ_y (spherical coordinates) and conversion between the different coordinates is shown in Table 6.1.

B.3. Compute the imaging receiver SNR at each step and send a feedback signal at a low rate to inform the transmitter of the SNR associated with the step. The feedback channel can be implemented by using the CDS or by modulating additional beam with low data rate (fixed power).

B.4. Record the associated transmission angles θ_x^{subopt} and θ_y^{subopt} where the imaging receiver experience maximum SNR.

B.5. Reconfigure the adaptive hologram to implement the next iteration as follows:

a) Reset the angle adaptation step size by halving the current angle adaptation ($\theta_{steps} = \theta_{steps}/2$).

b) If the $\left|\theta_x^{subopt}\right| \leq (|\theta_x^{end}| - |\theta_x^{start}|)/2$, then reset the higher scan boundary along the *x-axis* as $\theta_x^{end} = \theta_x^{subopt}$ and keep the lower scan boundary as it is. Contrarily, reset the lower scan range along the *x-axis* as $\theta_x^{start} = \theta_x^{subopt}$ and keep the higher scan boundary as it is.

c) If the $\left|\theta_y^{subopt}\right| \leq \left(\left|\theta_y^{end}\right| - \left|\theta_y^{start}\right|\right)/2$, then reset the higher scan boundary along the *y-axis* as $\theta_y^{end} = \theta_y^{subopt}$ and keep the lower scan boundary as it is. Otherwise, reset the lower scan boundary along the y-axis as $\theta_y^{start} = \theta_y^{subopt}$ and keep the higher scan boundary as it is.

B.6. Repeat Steps 2 to 5 for a number of iterations (in this method four scan iterations are considered).

B.7. Stop when the minimum allowed angle adaptation step size is reached (i.e., a certain scan step size of 1.43^o where the forth iteration is set to it).

B.8. Determine the X_{opt}^U, Y_{opt}^U, and Z_{opt}^U position of the spot that maximised the receiver's SNR, where $U = 1,2,\cdots,N_{user}$. The spot's optimum position can be defined from the optimum transmission angles θ_x^{opt} and θ_y^{opt}, based on Cartesian-spherical coordinates conversion shown in shown in Table 6.1.

C. Record the spot's optimum location (X_{opt}^{U}, Y_{opt}^{U}, Z_{opt}^{U}) of the interested users (U).

D. Repeat Steps B and C for all coexisting imaging receivers.

E. Generate multiple clusters aimed to the optimum locations (X_{opt}^{U}, Y_{opt}^{U}, Z_{opt}^{U}), where each cluster is cantered by the one of the optimum locations and consists of a set of spots distributed in a rectangular pattern.

F. Equally, distribute the total power, 1W, among the spots where each spot is allocated 1.66mW, and compute the power received at each imaging receiver, and calculate their SNRs. MRC scheme is used to process the resultant optical signals.

G. Individually turn on each spot, compute the power received at each imaging receiver, as well as calculate their SNRs.

H. Inform the transmitter of the power and SNRs associated with the spot by sending a feedback signal at a low rate.

I. Repeat Steps G and H for all the spots.

J. Compute the requested power from each spots using collaborative MRC scheme. The requested power can be computed using Equation (4.4.

K. Optimise the number and shape of the spots by illuminating the spots that produce SNRs higher than a threshold value and disregarding the others.

A liquid crystal device can be used for beam angle adaptation which can help in attaining the wide angle steering proposed here [171]. A repetitive training period should be included in the MAC protocol to perform the algorithm described above (CFAAS method). The adaptation is performed at a rate comparable to the rate at which the environment changes. The proposed method interconnects mobile communication devices positioned on the CF. However, if a device or more is fixed and connected to the backbone, it can acts as an access point. The design of the MAC protocol is not considered in this work and is worthy of further investigation.

7.4 Performance Evaluation of Collaborative OW Imaging Systems

The performance the proposed configurations is evaluated in terms of SNR under the effect of surrounding noise sources, receiver noise, mobility and multipath propagation. The SNR of all the proposed systems (CFAAS and CFAPAS) used adaptation time slots to obtain the best locations for the diffusing spots. Rectangular beam clustering was also used to ensure that most of spots in the cluster have direct line of sight with the pixels of imaging receivers. The preamplifier used in the 30Mb/s collaborative OW systems is the PIN FET preamplifier proposed in [96]. The SNR results are depicted in Figure 7.2 (a) and (b) when the transmitter is placed at (2*m*, 1*m*, 1*m*) and two imaging receivers are present. To consider user mobility, two user scenario was considered with a mobile receiver where the first receiver moves across the y-axis at x=1m while the second was fixed at (2*m*, 7*m*, 1*m*), see Figure 4.2 (b). It should be noted that all imaging receivers employ MRC to process the resultant optical signals. The SNR of four imaging collaborative adaptive multibeam systems is plotted in Figure 7.2. The results show that the CABCM is less affected by mobility than CALSMS. It is clearly seen that the imaging CABCM can achieve 10 dB SNR gain over the CALSMS at 6m transmitter-receiver horizontal separation (see Figure 7.2 (a)). This is attributed to BCM geometry, where the transmitter produces three beam clusters (on the ceiling and two end walls) that cover most of its surrounding. Furthermore, the results show variation in SNR levels of both systems (CALSMS and CABCM) due to the directive light noise when the receiver along the x=1m line. Disappointing results were achieved by the stationary receiver when

employing CABCM or CALSMS at 6m separation distance between the transmitter and the receiver.

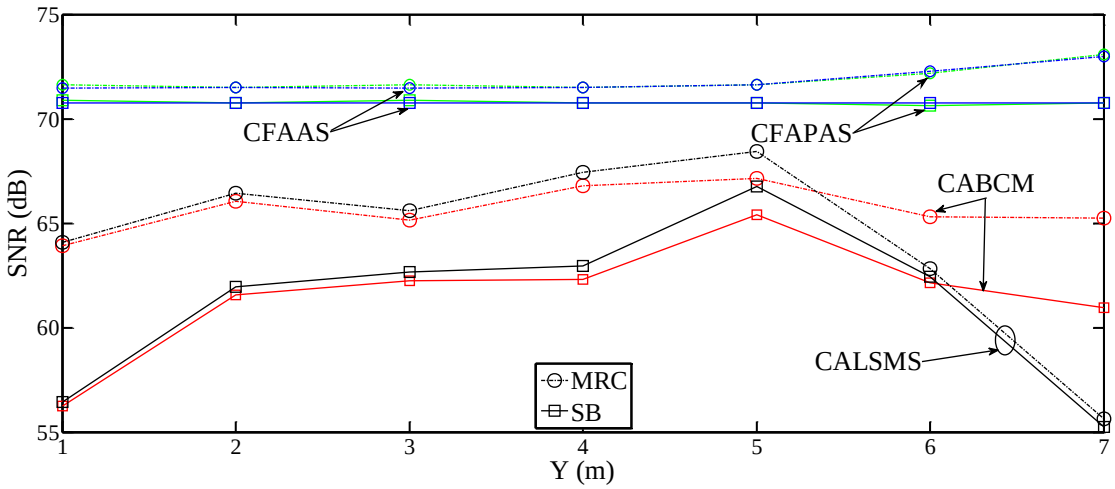

(a)

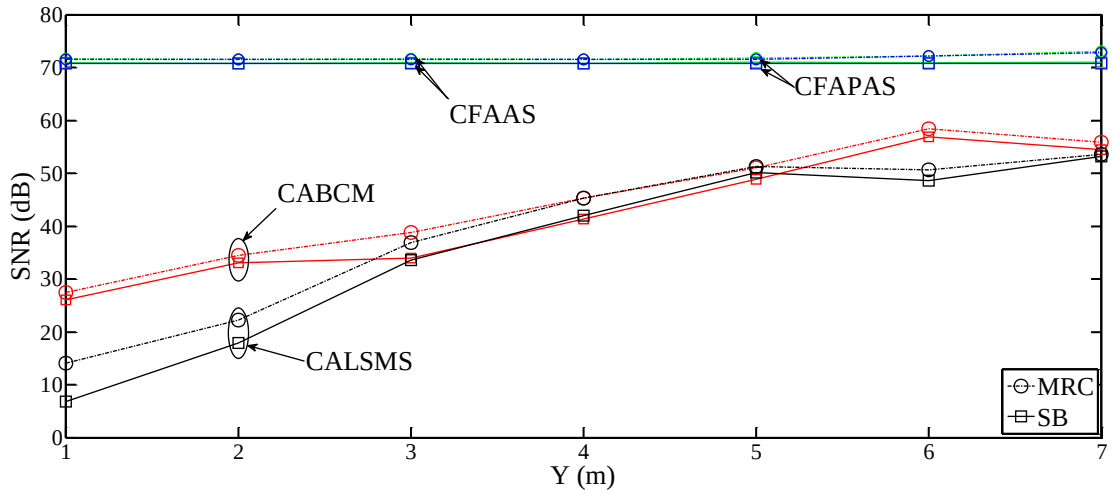

(b)

Figure 7.2: SNR of four imaging collaborative multibeam systems operating at 30Mbit/s when the transmitter is located at (2m, 1m, 1m) and two receivers coexist in room (a) an imaging receiver moves along the *x*=1m line , and (b) an imaging receiver is stationary and located at (2m, 7m, 1m).

This case shows one of the least successful locations as the receiver relies on diffuse links. With an imaging receiver, the mobile receiver employing the proposed configurations achieves about 8dB and 18dB SNR improvement over the CABCM and CALSMS,

respectively (see Figure 7.2 (a)). The proposed configurations (CFAAS and CFAPAS) offer comparable performance with SNR gain of about 5dB and 42dB at the most and the least successful locations, respectively.

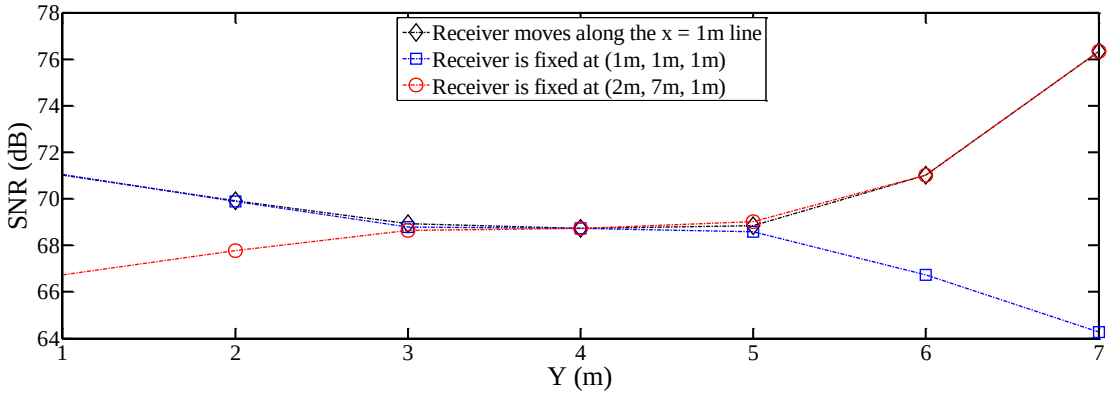

(a)

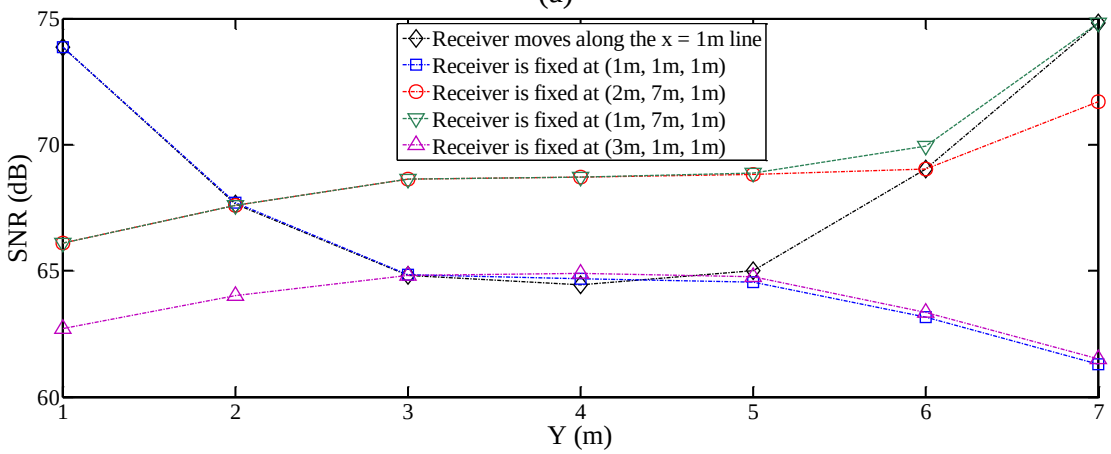

(b)

Figure 7.3: SNR of the proposed method (CFAPAS) for (a) three collaborative imaging receivers (b) five collaborative imaging receivers operating at 30 Mbit/s when the transmitter is at (1*m*, 1*m*, 1*m*).

This significant improvement in SNR is attributable to adapting the beam pattern and positions regardless of the transmitter position. Figure 7.3 shows the SNR of our proposed geometry (CFAPAS) when three and five users coexist. In three-user scenario the receiver at the least successful location achieved an SNR of 64dB and the user at most successful location attained an SNR of 76dB. This SNR gain achieved at the good communication

link is due to reallocation of the power to unobstructed beams. Figure 7.3 (b) shows a slight reduction in the system performance as the number of coexisting receivers increase. However, the receiver at the poor communication link can achieve an SNR of about 62dB, where 2dB SNR reduction occurs when the number of receivers increases from three to five receivers. Maintaining high SNR level, even when the number of coexisting receivers increases, allows the system to achieve higher data rates.

7.5 Eye Safety Considerations

The maximum allowed optical power is limited by eye and skin safety regulations [62-64]. Most infrared wireless links typically operate at the 780-980nm spectral range due to the availability optical sources and detectors are at low cost at these wavelengths. However, radiation can pass through the human cornea in this wavelength band and the eye can focus the light by the lens onto the retina leading to potential thermal damage [62, 63]. The hazard degree of OW radiation depends on several factors, including the exposure time, exposure level, and the operating wavelength [61, 184].

In order to take eye safety into account, we impose a restriction on the collaborative fast approach, where the power per spot is not allowed to exceed 1mW. The imposed restriction conforms to eye and skin safety regulations [63]. Figure 7.4 show the SNR results for three imaging collaborative multibeam systems using MRC to process the resultant optical signals (CALSMS, CABCM and CFAAS) when two imaging receivers are present and the transmitter is located at (2m, 4m, 1m). The depicted results is for a

mobile imaging receiver moving along the *x*=1m lined when another receiver is present and located at (2m, 7m, 1m).

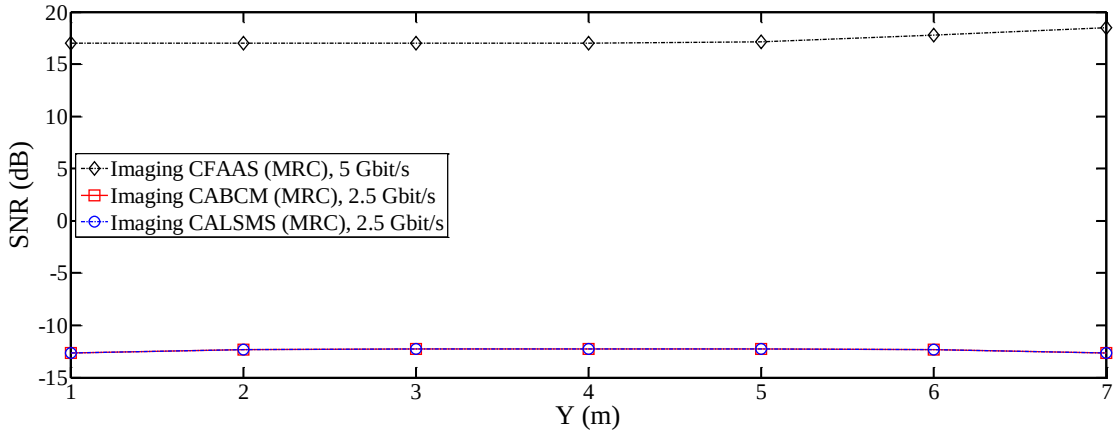

Figure 7.4: SNR of the proposed imaging configurations (CFAAS, CABCM and CALSMS) when a mobile receiver moves along the *x*=1m line in a two-user scenario and when the transmitter is located at (2m, 4m, 1m).

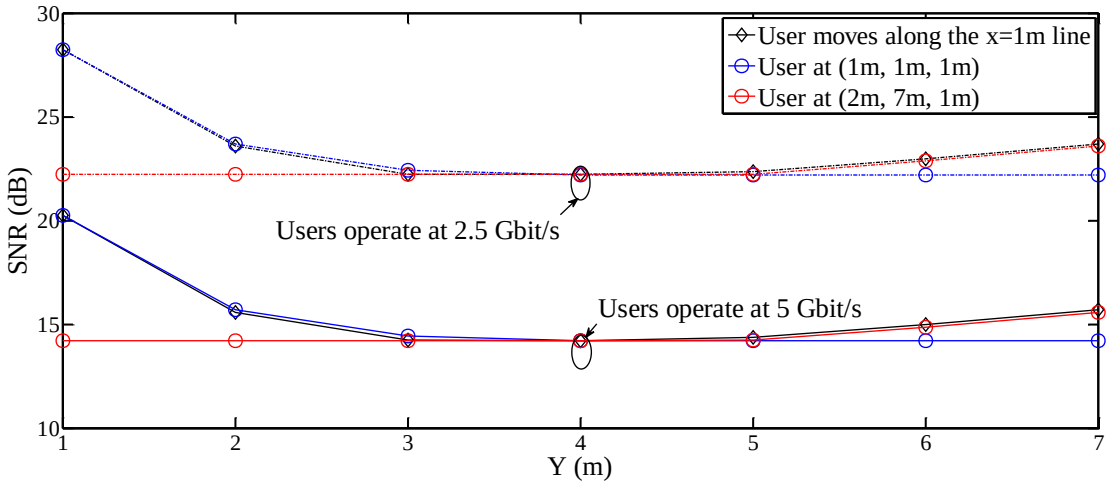

Figure 7.5: SNR of the proposed method (CFAPAS) when three imaging receivers coexist and operate at 5Gbit/s. The total power is reduced to 0.6W and the power beam is restricted to less than 1mW.

The results show that the power per beam can be maintained below 1mW while achieving an acceptable performance (BER < 10^{-9}) at high bit rates. At 5Gbit/s, the SNRs achieved in our proposed system (CAFAAS) in this case were about 17dB under the impact of BN, multipath dispersion, and mobility (see Figure 7.4). When the number of coexisting receivers increases, i.e. three imaging receiver, and at 5Gbit/s, the receiver with the worst

communication link achieved above 14dB (which is greater than the minimum 9.5dB (BER<10^{-3} required by FEC) as shown in Figure 7.5. Therefore, FEC can be used to further reduce the BER to 10^{-9}. The results depicted in Figure 7.5 indicate that 2.5Gbit/s is feasible with BER < 10^{-9} through the use of our introduced method CFAAS.

7.6 Computational complexity Assessment

The original MBAAS system have been shown to offer performance improvements over traditional spot-diffusing optical wireless systems, however it is at the cost of increase in system complexity. The complexity is related to the computational time and resources required to obtain the optimum beam direction. The fast beam angle adaptation method has been proposed to speed up the adaptation process (factor of 20 is achieved compared to the original MBAAS [150], [151], where only 640 possible locations have to be scanned (when fast adaptation is used) instead of a total of 12500 possible locations (MBAAS)). It was reported that the fast adaptation algorithm using 4 iterations can achieve a time complexity of $O(4\log_2(n/4))$ [151]. Additionally, it needs a memory space of 64 times lower than that used in the classical algorithm.

In our proposed method here (CFAAS), the collaborative multibeam transmitter allocates a time slot for each coexisting receiver to perform fast beam angle adaptations. Within a time slot, the transmitter chooses arbitrarily a receiver and carries out fast adaptation based on divide and conquer algorithm where the scanning process is recursively broken down into a number of iterations with different scan rates. In each time slot, the optimum beam direction of a particular receiver is identified. Therefore, the fast adaptation has to

be repeated for a number of time slots (N_{slot}). Given that our collaborative fast adaptation requires N_{slot} time slots to determine the optimum locations for the users present, its time complexity can be expressed as in [151]:

$$T(n) = O\left(j\, N_{slot} \log_2\left(\frac{n}{j}\right)\right), \tag{7.1}$$

where j is the number of subproblems (quadrants in our case since). In each iteration, the collaborative fast adaptation algorithm divides the scanning area into four quadrants (i.e., $j = 4$). Hence, the collaborative fast adaptation algorithms can achieve time optimal $20 \log_2\left(\frac{n}{4}\right)$ when it allocates five time slots for five coexisting receivers (i.e. $N_{slot} = 5$), that is four times faster than the original MBAAS. It should be noted that when the number of receivers present increases, the efficiency of our method decreases. For instance, the two methods achieve comparable efficiency when 20 receivers coexist in a room similar to that used in our simulation. Figure 7.6 shows the SNR of the proposed method when the collaborative nultibeam transmitter uses a single and multiple adaptation time slots. When beam angle adaptation is performed in a single adaptation time slot and the coexisting receivers share one optimum location, a reduction in computational time is attained, however one or more of the receivers present is affected and achieves poor performance. While, a consistent and comparable SNR performance can be achieved when multiple adaptation time slots are used by collaborative multibeam transmitter.

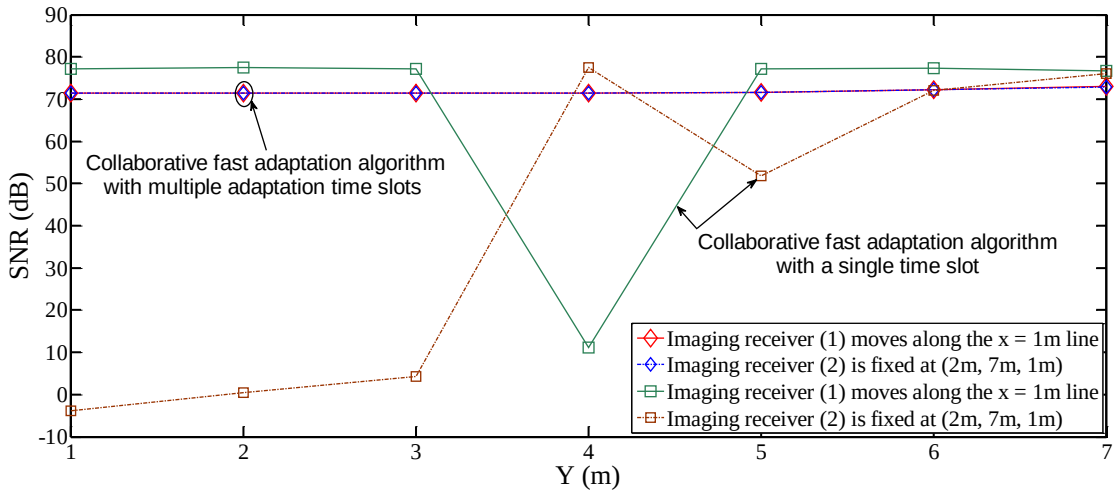

Figure 7.6: SNR of the proposed system with two imaging receivers when the collaborative multibeam transmitter uses a single and multiple adaptation time slots.

7.7 Challenges and Possibilities of High-speed Collaborative OW communications

High data rates collaborative OW communications are shown to be feasible through the use of the proposed collaborative adaptive multibeam systems. Since the collaborative adaptive multibeam transmitter (tracking system) can track the coexisting receivers, even with small FOV imaging receivers thereby enhancing the link budget. However, the implementation and testing of a high speed OW integrated array of receivers are very challenging tasks. To the best of our knowledge, there is no commercial high-speed receiver to date that has specially been designed for indoor OW (designing such a receiver worthy of further study). Because of the desired data rate for collaborative OW systems is 5Gbit/s, most of the components will perhaps be adopted from the optical fiber designs, which is not ideal for OW communication. This makes the receiver fabrication a challenging task. In particular, this is true for custom OW components such as the concentrator lens, the small detector, and its narrow FOV. Moreover, the diffraction limit

is another factor that has to be considered when using commercially available spatial light modulators. This is due to the smallest pixels size, which can be fabricated, and the operating wavelength which determines the maximum range of angles over which the beam can be steered. This also warrants further investigation.

7.8 Summary

In this chapter, we introduced a new collaborative adaptive multibeam system employing fast beam angle adaptation algorithm. We also introduced a new rectangular beam clustering geometry to enhance the system performance under the constraint of eye safety. The collaborative fast adaptation algorithm makes efficient use of a divide-and-conquer methodology in order to reduce the time needed to identify the optimum location for each coexisting receiver. The proposed configuration uses adaptation time slots allocated to each receiver hence an individual adaptation is carried out for each receiver. This comes with an acceptable increase in the total time required to obtain all optimum location. The results show that the proposed method can reduce the time required to obtain the optimum beams directions for five coexisting receivers by factor of four compared to that with the original beam adaptation. At 30Mbit/s, the proposed method (CFAAS) achieves an SNR gain of 42 dB over the CABCM at the worst communication link. In addition, the beam power was restricted to less than 1mW in the adaptation algorithm to comply with eye safety requirements, and good performance was achieved. A 5Gbit/s data rate is shown to be feasible when our techniques: collaborative beam angle and power adaptation,

adaptation time slots, rectangular beam clustering, and imaging receivers with small FOV are implemented in the OW configuration.

8 Conclusions and Future Work

8.1 Conclusions of Research Work

In order to tackle the design challenges of indoor OW systems, attention was paid to understanding the most important concerns in characterising OW links such as ambient light noise and multipath dispersion. In particular, the influence of multiple paths on the received optical signal was examined. The impact of channel impairments can be mitigated when a narrow beam transmitter is aimed directly into a narrow FOV receiver. However, this requires transmitter–receiver alignment, hence it suffers from shadowing and its performance is significantly degraded under conditions of user mobility. An alternative approach is a pure diffuse link that relies upon diffuse reflections from the ceiling and walls and does not require transmitter and receiver aiming. Diffuse links are more robust in the presence of shadowing and allow user mobility, however they are more prone to multipath dispersion that may result in pulse spread and extreme ISI.

A possible technique to reduce the effect of multipath dispersion and BN is diversity reception. Furthermore, multispot diffusing transmitters are an attractive substitute for CDS transmitters, since they combine the merits of both direct LOS and pure diffuse links. Significant performance enhancement can be attained by combining spot-diffusing transmitters such as LSMS and BCM, and diversity receivers. This is a result of mitigating the influence of BN as well as reducing the impact of ISI. However, the functionality of the multispot configurations is affected by shadowing and transmitter or/and receiver mobility.

The focus of this thesis is on link designs, presenting a range of efficient methods to compact the limitations discussed and enabling the OW system to provide multi-user communications at higher data rates (2.5Gbit/s, 5Gbit/s and beyond). The performance of our proposed systems was evaluated by a simulation tool developed for indoor OW channels in a typical rectangular room that has a width of 4m, a length of 8m and a height of 3m. Simulation results were obtained using a recursive light ray-tracing algorithm where the transmitted optical signal reaches the receiver through multiple paths of various lengths, based on reflections from reflecting surfaces. In this work, computation and the ray-tracing algorithms were implemented with the use of Matlab. We compared our simulator results with published theoretical and experimental findings and observed good agreement, giving us confidence in the ability of the simulator to assess other systems. CDS, LSMS and BCM, the most attractive configurations in the literature, were modelled and considered as baseline systems for comparison purposes. A wide FOV receiver and an angle diversity receiver with seven branches were also considered.

In this thesis, two collaborative multibeam systems in conjunction with imaging receivers (CALSMS and CABCM) were introduced to improve the performance of multiuser spot diffusing systems. The proposed configurations were evaluated when the system operated under the influence of ambient noise sources, receiver noise, transmitter/receiver mobility, and multipath dispersion. The system allows for more than a single receiver to co-exist with collaborative adaptive multibeam transmitter. Sample cases of two, three and five stationary receivers at selected locations were considered. We also evaluated different scenarios when a receiver was moving and the others were fixed. At 30Mbit/s,

the proposed collaborative adaptive multibeam systems achieved comparable performance in terms of SNR and obtained a 34dB SNR gain over the non-imaging multiuser LSMS. It was shown that the imaging CABCM is less affected by transmitter/receiver mobility than CABCM. This is due to the fact that the CABCM has the ability to cluster the diffusing spots on the ceiling and two end walls, covering its surroundings. The high SNR results and 3-dB channel bandwidth obtained by the imagining CALSMS can be used to achieve higher data rates even with user mobility. Data rates of 2.5Gbit/s and 5Gbit/s were shown to be feasible in a multiuser environment. However, a gradual reduction in the system performance was observed with increase in the number of users.

A novel Max-Min fair power adaptation algorithm was introduced to the design of collaborative OW multibeam systems to distribute the total power fairly among the beams with the aim of maximising the SNRs of all coexisting receivers. An iterative Max-Min CABCM combined with imaging receiver (200 pixels) was evaluated and compared with the original CABCM. An iterative process was employed to ensure that coexisting users are not affected when maximising the SNR of the user at the worst location, so that the system maximises the SNRs of all existing users moderately. It was demonstrated that our Max-Min CABCM obtains SNR gains of at least 8dB over the MRC CABCM when the transmitter is at the corner, two users are present and the system is operating at 30 Mbit/s. The improvement in SNR allowed our Max-Min CABCM system to operate at high bit rates (2.5Gbit/s and 5Gbit/s). At 5Gbit/s, users at the least successful locations

achieved SNR over 9.5dB and can achieve acceptable performance with the aid of FEC schemes.

A novel fast adaptation method was introduced to multibeam angle, power and delay adaptation systems to reduce the system's computational cost. The fast adaptation algorithm was combined with a new spot diffusing geometry with beams clustered around the diversity receiver faces, so that more spots are visible to the receiver FOV resulting in enhanced SNR. Since the beam clustering approach provides the transmitter with the opportunity to allocate the power to spots within the receiver FOV, the power per spot was restricted to assist in meeting eye safety regulation. It was demonstrated that the new method can adapt to environmental changes through overlooking blocked spots and distributing power among only the unblocked beams. It was shown that the new FEAAS increased the SNR by 9dB and was able to reduce the system computation cost by factor of 20 compared to the original MBAAS. In addition, beam delay adaptation was introduced to reduce the impact of multipath dispersion and ISI, where the multibeam transmitter was adjusted to allow the optical signals to reach the receiver at the same time. Significant improvements in the SNR with high channel bandwidth (more than 15GHz) were attained which enabled the system to maintain higher data rates (15Gbit/s and beyond). A power restriction was imposed in this system where the power per beam was limited to less than 1mW to meet eye safety requirements.

Finally, a new collaborative adaptive multibeam OW system that employs fast beam angle and power adaptation algorithm was introduced. The collaborative fast adaptation approach based on a divide-and-conquer methodology resulted in two proposed

adaptation methods: collaborative fast angle adaptation system (CFAAS) and collaborative fast angle and power adaptation system (CFAPAS). Both approaches use adaptation time slots to individually obtain the optimum location for each receiver. The ultimate goal of the proposed systems is to reduce the time needed to identify the optimum beam directions and power level of diffusing spots compared to the adaptation time needed in the original beam power and angle adaptation methods. Rectangular beam clustering was also introduced to optimise the number and pattern (positions) of the spots in order to maximise the coexisting receivers' SNRs. Furthermore, the proposed systems were combined with imaging receivers (256 pixels) to reduce the effect of BN, multipath dispersion and ISI, hence improve system performance. A restriction, where the upper limit for spot power is 1mW, was imposed in our collaborative adaptive multibeam system, and good performance was achieved. The collaborative OW system made use of the combination of the proposed approaches, fast beam and power adaptation, rectangular beam clustering, and imaging receiver with narrow FOV receivers, and can operate at a high data rate of 5Gbit/s while meeting BER of 10^{-9} with full mobility. The proposed collaborative system (CFAPAS) outperforms any collaborative optical wireless system published in the literature to the best of our knowledge.

8.2 Areas of Further Investigation

The following is a list of new areas of research that deserve further investigation:

1- Fairness algorithms such as proportional fairness algorithms can be examined in the current collaborative multibeam configurations, which would improve power

allocations among beams. Proportional fair power adaptation can help collaborative power adaptive multibeam systems to achieve fair and efficient power distribution among beams.

2- Beam delay adaptation method is well investigated in a single user OW systems. This method can be further investigated in multiuser scenarios.

3- Power adaptive finite vocabulary of holograms can be investigated in multiuser communication systems to enhance the received optical power for multiple coexisting receivers. Adaptive holograms can further reduce the computation time needed to adapt collaborative multibeam systems through the use of a finite vocabulary of stored holograms especially when the number of coexisting users increases.

4- Since our OW system with multiple beams (spot-diffusing transmitters) and multiple receivers (oriented detectors of angle diversity or pixels of imaging receivers) is a MIMO system, current systems may use the body of knowledge developed in MIMO.

5- Relay nodes in MIMO OW communication systems can be investigated with currently studied adaptive techniques. The use of intermediate nodes in collaborative OW systems can enhance the system's SNR and increase the available channel bandwidth, therefore it is worth further investigation.

6- The original beam angle adaptation has been optimised in this work using fast adaptation algorithms. Further investigation can be carried out using direct binary search (DBS) algorithms or Genetic algorithms (GA) to find the optimum location of spots.

7- Experimental verification of the many results associated with the studied configurations would be extremely valuable to any future work.

References

[1] R. W. Burns, *Communications: an International History of the Formative Years*: Institution of Engineering and Technology, 2004.

[2] A. G. Bell, "Selenium and the Photophone," *Nature,* vol. 22, pp. 500-503, 1880.

[3] S. Arnon, "Optical wireless communications," *Encyclopedia of Optical Engineering,* pp. 1866-1886, 2003.

[4] T. H. Maiman, "Stimulated Optical Radiation in Ruby," *Nature,* vol. 187, pp. 493-494, 1960.

[5] H. Manor and S. Arnon, "Performance of an optical wireless communication system as a function of wavelength," in *Electrical and Electronics Engineers in Israel, 2002. The 22nd Convention of*, 2002, pp. 287-289.

[6] S. Arnon, D. M. Britz, A. C. Boucouvalas, and M. Kavehrad, "Optical wireless communications: introduction to the feature issue," *Journal of Optical Networking,* vol. 5, pp. 79-81, 2006/02/01 2006.

[7] J. L. Grubb, "The traveler's dream come true," *Communications Magazine, IEEE,* vol. 29, pp. 48-51, 1991.

[8] J. E. Padgett, C. G. Gunther, and T. Hattori, "Overview of wireless personal communications," *Communications Magazine, IEEE,* vol. 33, pp. 28-41, 1995.

[9] F. R. Gfeller and U. Bapst, "Wireless in-house data communication via diffuse infrared radiation," *Proceedings of the IEEE,* vol. 67, pp. 1474-1486, 1979.

[10] E. Freeman and G. Forsberg, "A short-range optical transmission system for television signals," *Optical Engineering,* vol. 13, pp. 396-400, 1975.

[11] K. Ogawa, "Considerations for Optical Receiver Design," *Selected Areas in Communications, IEEE Journal on,* vol. 1, pp. 524-532, 1983.

[12] T. Minami, K. Yano, T. Touge, H. Morikawa, and O. Takahashi, "Optical wireless modem for office communication," presented at the Proceedings of the May 16-19, 1983, national computer conference, Anaheim, California, 1983.

[13] Y. Nakata, J. Kashio, T. Kojima, and T. Noguchi, "In-house wireless communication communication system using infrared radiation," presented at the Proceedings of the International Conference on Computer Communication, 1984.

[14] O. Takahashi and T. Touge, "Optical wireless network for office communication," *JARECT (Japan Electron Rev. Electron. Comput. Telecomm.),* vol. 20, pp. 217-228, 1985/1986.

[15] D. R. Pauluzzi, P. R. H. McConnell, and R. L. Poulin, "Free-space, undirected infrared (IR) voice and data communications with a comparison to RF systems," in *Wireless Communications, 1992. Conference Proceedings., 1992 IEEE International Conference on Selected Topics in*, 1992, pp. 279-285.

[16] J. R. Barry, J. M. Kahn, W. J. Krause, E. A. Lee, and D. G. Messerschmitt, "Simulation of multipath impulse response for indoor wireless optical channels," *Selected Areas in Communications, IEEE Journal on*, vol. 11, pp. 367-379, 1993.

[17] P. P. Smyth, M. J. McCullagh, D. Wisely, D. Wood, S. Ritchie, P. L. Eardley, *et al.*, "Optical wireless local area networks-enabling technologies," *BT Technol. Journal*, vol. 11, pp. 56-64, April 1993.

[18] P. P. Smyth, D. Wood, S. Ritchie, and S. Cassidy, "Optical wireless: New enabling transmitter technologies," in *Communications, 1993. ICC 93. Geneva. Technical Program, Conference Record, IEEE International Conference on*, 1993, pp. 562-566 vol.1.

[19] J. M. H. Elmirghani and R. A. Cryan, "Performance considerations for indoor infrared LANs," *Proceedings of SPIE - The International Society for Optical Communications*, vol. 2450, pp. 606-612, 1995.

[20] G. W. Marsh and J. M. Kahn, "50-Mb/s diffuse infrared free-space link using on-off keying with decision-feedback equalization," *Photonics Technology Letters, IEEE*, vol. 6, pp. 1268-1270, 1994.

[21] M. J. McCullagh and D. R. Wisely, "155 Mbit/s optical wireless link using a bootstrapped silicon APD receiver," *Electronics Letters*, vol. 30, pp. 430-432, 1994.

[22] M. J. McCullagh, D. R. Wisely, P. L. Eardley, and P. P. Smyth, "A 50 Mbit/s optical wireless LAN link using novel optical and electronic enabling technologies," *International Seminar on Digital Communications*, pp. 298-309, 1994.

[23] M. D. Audeh and J. M. Kahn, "Performance evaluation of baseband OOK for wireless indoor infrared LAN's operating at 100 Mb/s," *Communications, IEEE Transactions on*, vol. 43, pp. 2085-2094, 1995.

[24] S. D. Greaves, P. J. Nichols, D. R. Wisely, and R. T. Unwin, "Optical wireless video distribution," presented at the Proceedings of the International Society for Optical Engineering Conference, 1995.

[25] L. Goldberg, "Infrared data transmission: the missing link?," *Electronic Design*, pp. 47-64, 1995.

[26] A. C. Boucouvalas, "Indoor ambient light noise and its effect on wireless optical links," *Optoelectronics, IEE Proceedings* -, vol. 143, pp. 334-338, 1996.

[27] A. J. C. Moreira, R. T. Valadas, and A. M. de Oliveira Duarte, "Performance of infrared transmission systems under ambient light interference," *Optoelectronics, IEE Proceedings* -, vol. 143, pp. 339-346, 1996.

[28] J. M. H. Elmirghani, H. H. Chan, and R. A. Cryan, "Sensitivity evaluation of optical wireless PPM systems utilising PIN-BJT receivers," *Optoelectronics, IEE Proceedings -*, vol. 143, pp. 355-359, 1996.

[29] A. J. Phillips, R. A. Cryan, and J. M. Senior, "An optically preamplified intersatellite PPM receiver employing maximum likelihood detection," *Photonics Technology Letters, IEEE,* vol. 8, pp. 691-693, 1996.

[30] G. W. Marsh and J. M. Kahn, "Performance evaluation of experimental 50-Mb/s diffuse infrared wireless link using on-off keying with decision-feedback equalization," *Communications, IEEE Transactions on,* vol. 44, pp. 1496-1504, 1996.

[31] D. R. Wisely, "A 1 Gbit/s optical wireless tracked architecture for ATM delivery," in *Optical Free Space Communication Links, IEE Colloquium on*, 1996, pp. 14/1-14/7.

[32] J. B. Carruthers and J. M. Kahn, "Angle diversity for nondirected wireless infrared communication," in *Communications, 1998. ICC 98. Conference Record.1998 IEEE International Conference on*, 1998, pp. 1665-1670 vol.3.

[33] J. B. Carruthers and J. M. Kahn, "Modeling of nondirected wireless infrared channels," *Communications, IEEE Transactions on,* vol. 45, pp. 1260-1268, 1997.

[34] A. M. Street, P. N. Stavrinou, D. C. O'Brien, and D. J. Edwards, "Indoor optical wireless systems - a review," *Optical and Quantum Electronics,* vol. 29, pp. 349-378, 1997.

[35] D. Wisely and I. Neild, "A 100 Mbit/s tracked optical wireless telepoint," in *Personal, Indoor and Mobile Radio Communications, 1997. 'Waves of the Year 2000'. PIMRC '97., The 8th IEEE International Symposium on*, 1997, pp. 964-968 vol.3.

[36] J. M. Kahn and J. R. Barry, "Wireless infrared communications," *Proceedings of the IEEE,* vol. 85, pp. 265-298, 1997.

[37] V. Jungnickel, C. von Helmolt, and U. Kruger, "Broadband wireless infrared LAN architecture compatible with Ethernet protocol," *Electronics Letters,* vol. 34, pp. 2371-2372, 1998.

[38] D. J. T. Heatley, D. R. Wisely, I. Neild, and P. Cochrane, "Optical wireless: the story so far," *Communications Magazine, IEEE,* vol. 36, pp. 72-74, 79-82, 1998.

[39] P. Theodorou, J. Elmirghani, and R. Cryan, "Performance of ATM optical wireless LANs with fixed channel assignment," in *Global Telecommunications Conference, 1999. GLOBECOM '99*, 1999, pp. 598-602 vol.1b.

[40] D. J. T. Heatley and I. Neild, "Optical wireless-the promise and the reality," in *Optical Wireless Communications (Ref. No. 1999/128), IEE Colloquium on*, 1999, pp. 1/1-1/6.

[41] J. Bellon, M. J. N. Sibley, D. R. Wisely, and S. D. Greaves, "Hub architecture for infrared wireless networks in office environments," *Optoelectronics, IEE Proceedings -*, vol. 146, pp. 78-82, 1999.

[42] J. R. V. Alvarez, F. J. L. Hernandez, A. S. Galdon, R. P. Jimenez, and J. A. R. Borges, "Infrared wireless DSSS system for indoor data communication links," in *Optical Wireless Communications Ii*. vol. 3850, E. J. Korevaar, Ed., ed Bellingham: Spie-Int Soc Optical Engineering, 1999, pp. 92-99.

[43] S. Jivkova and M. Kavehrad, "Indoor wireless infrared local access, multi-spot diffusing with computer generated holographic beam-splitters," in *Communications, 1999. ICC '99. 1999 IEEE International Conference on*, 1999, pp. 604-608 vol.1.

[44] G. Yun and M. Kavehrad, "Spot-diffusing and fly-eye receivers for indoor infrared wireless communications," presented at the Wireless Communications, 1992. Conference Proceedings., 1992 IEEE International Conference on Selected Topics in, 1992.

[45] V. Pohl, V. Jungnickel, and C. von Helmolt, "A channel model for wireless infrared communication," presented at the Personal, Indoor and Mobile Radio Communications, 2000. PIMRC 2000. The 11th IEEE International Symposium on, 2000.

[46] S. Jivkova and M. Kavehrad, "Receiver designs and channel characterization for multi-spot high-bit-rate wireless infrared communications," *Communications, IEEE Transactions on*, vol. 49, pp. 2145-2153, 2001.

[47] V. Jungnickel, T. Haustein, A. Forck, and C. von Helmolt, "155 Mbit/s wireless transmission with imaging infrared receiver," *Electronics Letters*, vol. 37, pp. 314-315, 2001.

[48] J. M. Kahn, J. R. Barry, M. D. Audeh, J. B. Carruthers, W. J. Krause, and G. W. Marsh, "Non-directed infrared links for high-capacity wireless LANs," *Personal Communications, IEEE*, vol. 1, p. 12, 1994.

[49] J. M. Kahn, J. R. Barry, W. J. Krause, M. D. Audeh, J. B. Carruthers, G. W. Marsh, *et al.*, "High-speed non-directional infrared communication for wireless local-area networks," in *Signals, Systems and Computers, 1992. 1992 Conference Record of The Twenty-Sixth Asilomar Conference on*, 1992, pp. 83-87 vol.1.

[50] A. G. Al-Ghamdi and J. M. H. Elmirghani, "Optimization of a pyramidal fly-eye diversity receiver for optical wireless systems under the influence of multipath dispersion and background noise," *Microwave and Optical Technology Letters*, vol. 36, pp. 401-406, 2003.

[51] J. R. Barry and J. M. Kahn, "Link design for nondirected wireless infrared communications," *Applied Optics*, vol. 34, pp. 3764-3776, 1995.

[52] H. Yang and C. Lu, "Infrared wireless LAN using multiple optical sources," *Optoelectronics, IEE Proceedings* -, vol. 147, pp. 301-307, 2000.

[53] S. T. Jivkova and M. Kavehrad, "Multispot diffusing configuration for wireless infrared access," *Ieee Transactions on Communications*, vol. 48, pp. 970-978, Jun 2000.

[54] A. Al-Ghamdi and J. M. H. Elmirghani, "Optimization of a triangular PFDR antenna in a fully diffuse OW system influenced by background noise and multipath propagation," *Communications, IEEE Transactions on,* vol. 51, pp. 2103-2114, 2003.

[55] A. G. Al-Ghamdi and J. M. H. Elmirghani, "Performance evaluation of a triangular pyramidal fly-eye diversity detector for optical wireless communications," *Communications Magazine, IEEE,* vol. 41, pp. 80-86, 2003.

[56] A. G. Al-Ghamdi and J. M. H. Elmirghani, "Triangular PFDR antenna optimisation under the restriction of background noise and multipath propagation in an optical wireless system," presented at the Communications. ICC '03. IEEE International Conference on, 2003.

[57] A. G. Al-Ghamdi and J. M. H. Elmirghani, "Performance evaluation of a pyramidal fly-eye diversity antenna in an indoor optical wireless multipath propagation environment under very directive noise sources," *Optoelectronics, IEE Proceedings -,* vol. 150, pp. 482-489, 2003.

[58] K. L. Sterckx, J. M. H. Elmirghani, and R. A. Cryan, "Pyramidal fly-eye detection antenna for optical wireless systems," in *Optical Wireless Communications (Ref. No. 1999/128), IEE Colloquium on*, 1999, pp. 5/1-5/6.

[59] K. L. Sterckx, J. M. H. Elmirghani, and R. A. Cryan, "Sensitivity assessment of a three-segment pyramidal fly-eye detector in a semidisperse optical wireless communication link," *Optoelectronics, IEE Proceedings -,* vol. 147, pp. 286-294, 2000.

[60] S. Jivkova, B. A. Hristov, and M. Kavehrad, "Power-efficient multispot-diffuse multiple-input-multiple-output approach to broad-band optical wireless communications," *Vehicular Technology, IEEE Transactions on,* vol. 53, pp. 882-889, 2004.

[61] Z. Ghassemlooy, W. Popoola, and S. Rajbhandari, *Optical wireless communications: system and channel modelling with Matlab®*: CRC Press, 2012.

[62] A. C. Boucouvalas, "IEC 825-1 Safety Classification of some consumer electronics products," *Colloquium on Optical Free Space Communication Links,* 1996.

[63] IrDA standard, "Serial infrared: Physical layer link specification," 1997, Version 1.2.

[64] IrDA up-to-date standards and http://www.irda.org. *The IrDA can be contacted at P.O. Box 3883, Walnut Creek, CA 94598, USA.*

[65] F. M. Chow and J. M. Kahn, "Effect of non-reciprocity on infrared wireless local-area networks," in *Global Telecommunications Conference, 1999. GLOBECOM '99*, 1999, pp. 330-338 vol.1a.

[66] F. Gfeller and W. Hirt, "A robust wireless infrared system with channel reciprocity," *Communications Magazine, IEEE,* vol. 36, pp. 100-106, 1998.

[67] R. Otte, L. P. De Jong, and A. H. M. Van Roermund, "Wireless optical PPM telemetry and the influence of lighting flicker," *Instrumentation and Measurement, IEEE Transactions on*, vol. 47, pp. 51-55, 1998.

[68] R. Narasimhan, M. D. Audeh, and J. M. Kahn, "Effect of electronic-ballast fluorescent lighting on wireless infrared links," *Optoelectronics, IEE Proceedings* -, vol. 143, pp. 347-354, 1996.

[69] A. Moreira, R. Valadas, and A. M. de Oliveira Duarte, "Optical interference produced by artificial light," *Wireless Networks*, vol. 3, pp. 131-140, 1997.

[70] S. Zahedi, J. A. Salehi, and M. Nasiri-Kenari, "A photon counting approach to the performance analysis of indoors wireless infrared CDMA networks," in *Personal, Indoor and Mobile Radio Communications, 2000. PIMRC 2000. The 11th IEEE International Symposium on*, 2000, pp. 928-932 vol.2.

[71] A. J. C. Moreira, R. T. Valadas, and A. M. de Oliveira Duarte, "Characterisation and modelling of artificial light interference in optical wireless communication systems," in *Personal, Indoor and Mobile Radio Communications, 1995. PIMRC'95. 'Wireless: Merging onto the Information Superhighway'., Sixth IEEE International Symposium on*, 1995, pp. 326-331 vol.1.

[72] A. J. C. Moreira, R. T. Valadas, and A. M. de Oliveira Duarte, "Reducing the effects of artificial light interference in wireless infrared transmission systems," in *Optical Free Space Communication Links, IEE Colloquium on*, 1996, pp. 5/1-510.

[73] C. Hsun-Hung, K. L. Sterckx, J. M. H. Elmirghani, and R. A. Cryan, "Performance of optical wireless OOK and PPM systems under the constraints of ambient noise and multipath dispersion," *Communications Magazine, IEEE*, vol. 36, pp. 83-87, 1998.

[74] A. Tavares, R. Valadas, and A. M. d. O. Duarte, "Performance of wireless infrared transmission systems considering both ambient light interference and intersymbol interference due to multipath dispersion," in *Opt. Wireless Communications, Proc. SPIE*, Boston, MA, 1998, pp. 82-93.

[75] A. J. C. Moreira, A. M. Tavares, R. J. M. T. Valadas, and A. M. d. O. Duarte, "Modulation methods for wireless infrared transmission systems: performance under ambient light noise and interference," in *SPIE Proceedings. on Wireless Data Transmission*, Philadelphia, PA, USA, 1995, pp. 226-237.

[76] R. Ramirez-Iniguez, S. M. Idrus, and Z. Sun, *Optical wireless communications: IR for wireless connectivity*: CRC press, 2008.

[77] C. J. Georgopoulos, "Suppressing background-light interference in an in-house infrared communication system by optical filtering," *International journal of Optoelectronics*, vol. 3, 1988.

[78] A. J. C. Moreira, R. T. Valadas, and A. M. de Oliveira Duarte, "Characterisation and modelling of artificial light interference in optical wireless communication systems," in *Personal, Indoor and Mobile Radio Communications, 1995. PIMRC'95. Wireless:*

Merging onto the Information Superhighway., Sixth IEEE International Symposium on, 1995, pp. 326-331 vol.1.

[79] J. R. Barry, *Wireless infrared communications*: Kluwer Academic Publishers, 1994.

[80] K. K. Wong, T. O'Farrell, and M. Kiatweerasakul, "Infrared wireless communication using spread spectrum techniques," *Optoelectronics, IEE Proceedings* -, vol. 147, pp. 308-314, 2000.

[81] T. O'Farrell and M. Kiatweerasakul, "Performance of a spread spectrum infrared transmission system under ambient light interference," in *Personal, Indoor and Mobile Radio Communications, 1998. The Ninth IEEE International Symposium on*, 1998, pp. 703-707 vol.2.

[82] J. B. Carruthers and P. Kannan, "Iterative site-based modeling for wireless infrared channels," *Antennas and Propagation, IEEE Transactions on*, vol. 50, pp. 759-765, 2002.

[83] J. B. Carruthers, S. M. Carroll, and P. Kannan, "Propagation modelling for indoor optical wireless communications using fast multi-receiver channel estimation," *Optoelectronics, IEE Proceedings* -, vol. 150, pp. 473-481, 2003.

[84] J. M. Senior and M. Y. Jamro, *Optical fiber communications : principles and practice*. Harlow, England; New York: Financial Times/Prentice Hall, 2009.

[85] I. E. Commission, "International standard IEC 60825-1 (1998-01) Ed. 1.1 Consolidated Edition, Safety of laser products - Part 1: Equipment classification, requirements and user's guide," ed. Geneva, Switzerland.

[86] W. Hirt, M. Hassner, and N. Heise, "IrDA-VFIr (16 Mb/s): modulation code and system design," *Personal Communications, IEEE*, vol. 8, pp. 58-71, 2001.

[87] T. S. Rappaport, "Characterization of UHF multipath radio channels in factory buildings," *Antennas and Propagation, IEEE Transactions on*, vol. 37, pp. 1058-1069, 1989.

[88] J. Chuang, "The Effects of Time Delay Spread on Portable Radio Communications Channels with Digital Modulation," *Selected Areas in Communications, IEEE Journal on*, vol. 5, pp. 879-889, 1987.

[89] G. Einarsson and M. Leeson, "Principles of Lightwave Communications," *Physics Today*, vol. 50, pp. 84-86, 1997.

[90] J. B. Carruthers and J. M. Kahn, "Multiple-subcarrier modulation for nondirected wireless infrared communication," *Selected Areas in Communications, IEEE Journal on*, vol. 14, pp. 538-546, 1996.

[91] K. Feher, *Wireless digital communications: modulation & spread spectrum applications*: Prentice-Hall, Inc., 1995.

[92] C. Ta-Shing and M. Gans, "High speed infrared local wireless communication," *Communications Magazine, IEEE,* vol. 25, pp. 4-10, 1987.

[93] W. Hirt, J. Petrilla, and Y. Yuuki, "Proposed changes to IrDA serial infrared physical layer link specification for 16 Mbps addition (VFIR) final proposal," adopted with status final by the IrDA Board of Directors, San Francisco, CA1999.

[94] A. P. Tang, J. M. Kahn, and H. Keang-Po, "Wireless infrared communication links using multi-beam transmitters and imaging receivers," in *Communications, 1996. ICC '96, Conference Record, Converging Technologies for Tomorrow's Applications. 1996 IEEE International Conference on*, 1996, pp. 180-186 vol.1.

[95] M. Castillo-Vazquez and A. Puerta-Notario, "Single-channel imaging receiver for optical wireless communications," *Communications Letters, IEEE,* vol. 9, pp. 897-899, 2005.

[96] P. Djahani and J. M. Kahn, "Analysis of infrared wireless links employing multibeam transmitters and imaging diversity receivers," *Communications, IEEE Transactions on,* vol. 48, pp. 2077-2088, 2000.

[97] J. M. Kahn, R. You, P. Djahani, A. G. Weisbin, B. K. Teik, and A. Tang, "Imaging diversity receivers for high-speed infrared wireless communication," *Communications Magazine, IEEE,* vol. 36, pp. 88-94, 1998.

[98] A. G. Al-Ghamdi and J. M. H. Elmirghani, "Spot diffusing technique and angle diversity performance for high speed indoor diffuse infra-red wireless transmission," *Iee Proceedings-Optoelectronics,* vol. 151, pp. 46-52, Feb 2004.

[99] A. G. Al-Ghamdi and J. M. H. Elmirghani, "Analysis of diffuse optical wireless channels employing spot-diffusing techniques, diversity receivers, and combining schemes," *Communications, IEEE Transactions on,* vol. 52, pp. 1622-1631, 2004.

[100] A. G. Al-Ghamdi and J. M. H. Elmirghani, "Line strip multibeam transmitter to combat the multipath dispersion and background noise of the indoor optical wireless links," in *Global Telecommunications Conference, 2004. GLOBECOM '04. IEEE*, 2004, pp. 3630-3635 Vol.6.

[101] A. G. Al-Ghamdi and J. M. H. Elmirghani, "Performance analysis of line strip multispot diffusing system, fully diffuse, and hybrid optical wireless techniques in a real environment," in *Global Telecommunications Conference, 2004. GLOBECOM '04. IEEE*, 2004, pp. 1213-1220 Vol.2.

[102] A. G. Al-Ghamdi and J. M. H. Elmirghani, "Line strip spot-diffusing transmitter configuration for optical wireless systems influenced by background noise and multipath dispersion," *Communications, IEEE Transactions on,* vol. 52, pp. 37-45, 2004.

[103] A. G. Al-Ghamdi and J. M. H. Elmirghani, "Performance comparison of LSMS and conventional diffuse and hybrid optical wireless techniques in a real indoor environment," *Optoelectronics, IEE Proceedings -,* vol. 152, pp. 230-238, 2005.

[104] A. G. Al-Ghamdi and J. M. H. Elmirghani, "Performance analysis of mobile optical wireless systems employing a novel beam clustering method and diversity detection," *Optoelectronics, IEE Proceedings* -, vol. 151, pp. 223-231, 2004.

[105] A. G. Al-Ghamdi and J. M. H. Elmirghani, "Analysis of optical wireless links employing a beam clustering method and diversity receivers," in *Communications, 2004 IEEE International Conference on*, 2004, pp. 3341-3347 Vol.6.

[106] I. E. Commission, "IEC 60825-1:2014," in *Safety of laser products – Part 1: Equipment classification and requirements*, ed. Geneva, Switzerland International Electrotechnical Commission, 2014.

[107] A. M. Street, P. N. Stavrinou, D. J. Edwards, and G. Parry, "Optical preamplifier designs for IR-LAN applications," in *Optical Free Space Communication Links, IEE Colloquium on*, 1996, pp. 8/1-8/6.

[108] J. R. Barry, J. M. Kahn, E. A. Lee, and D. G. Messerschmitt, "High-speed nondirective optical communication for wireless networks," *Network, IEEE,* vol. 5, pp. 44-54, 1991.

[109] Int. Electrotech. Commission and CEI/IEC825-1, "Safety of Laser Products, 1993. J. D. Rancourt, Optical Thin Films," ed. New York: Macmillan 1987.

[110] P. L. Eardley, D. R. Wisely, D. Wood, and P. McKee, "Holograms for optical wireless LANs," *Optoelectronics, IEE Proceedings* -, vol. 143, pp. 365-369, 1996.

[111] M. R. Pakravan, E. Simova, and M. Kavehrad, "Holographic diffusers for indoor infrared communication systems," in *Global Telecommunications Conference, 1996. GLOBECOM '96. 'Communications: The Key to Global Prosperity*, 1996, pp. 1608-1612 vol.3.

[112] E. Simova, M. Tai, and M. Kavehard, "Indoor wireless infrared link with a holographic multi-spot diffuser," *Applications of Photonic Technology, Plenum Press, New York,* vol. 2, pp. 223-228, 1996.

[113] V. Pohl, V. Jungnickel, and C. von Helmolt, "Integrating-sphere diffuser for wireless infrared communication," *Optoelectronics, IEE Proceedings* -, vol. 147, pp. 281-285, 2000.

[114] W. K. Pratt, *Laser communication systems*, 1969.

[115] N. S. Kopeika and J. Bordogna, "Background noise in optical communication systems," *Proceedings of the IEEE,* pp. 1571-1577, 1970.

[116] X. Ning, R. Winston, and J. O?Gallagher, "Dielectric totally internally reflecting concentrators," *Applied Optics,* vol. 26, pp. 300-305, 1987.

[117] J. P. Savicki and S. P. Morgan, "Hemispherical concentrators and spectral filters for planar sensors in diffuse radiation fields," *Applied Optics,* vol. 33, pp. 8057-8061, 1994.

[118] R. L. Poulin, D. R. Pauluzzi, and M. R. Walker, "A multi-channel infrared telephony demonstration system for public access applications," in *Wireless Communications, 1992. Conference Proceedings., 1992 IEEE International Conference on Selected Topics in*, 1992, pp. 286-291.

[119] D. K. Borah, A. C. Boucouvalas, C. C. Davis, S. Hranilovic, and K. Yiannopoulos, "A review of communication-oriented optical wireless systems," *EURASIP Journal on Wireless Communications and Networking*, vol. 2012, pp. 1-28, 2012.

[120] S. D. Personick, "Receiver design for digital fiber optical communication system, Part I and II," *Bell Systems Technology Journal*, vol. 52, pp. 843-886, 1973.

[121] B. G. Streetman and S. Banerjee, *Solid state electronic devices*, 6th ed.: Prentice Hall, 2009.

[122] T. D. Nguyen and M.S., "Report," Univ. Calif., Berkeley1995.

[123] H. H. Chan, A. Hussain, J. M. H. Elmirghani, and R. A. Cryan, "Channel equalisation for optical wireless multi-user systems utilising orthogonal codes," in *Optical Free Space Communication Links, IEE Colloquium on*, 1996, pp. 1/1-1/7.

[124] S. U. H. Qureshi, "Adaptive equalization," *Proceedings of the IEEE*, vol. 73, pp. 1349-1387, 1985.

[125] K. Wong, T. O'Farrell, and M. Kiatweerasakul, "The performance of optical wireless OOK, 2-PPM and spread spectrum under the effects of multipath dispersion and artificial light interference," *International Journal of Communication Systems*, vol. 13, pp. 551-576, 2000.

[126] R. J. Green, H. Joshi, M. D. Higgins, and M. S. Leeson, "Recent developments in indoor optical wireless systems," *IET communications*, vol. 2, pp. 3-10, 2008.

[127] R. Cryan, R. T. Unwin, I. Garrett, M. J. Sibley, and N. Calvert, "Optical fibre digital pulse-position-modulation assuming a Gaussian received pulse shape," in *Optoelectronics, IEE Proceedings J*, 1990, pp. 89-96.

[128] H. Park and J. Barry, "Performance of multiple pulse position modulation on multipath channels," in *Optoelectronics, IEE Proceedings-*, 1996, pp. 360-364.

[129] J. M. H. Elmirghani and R. A. Cryan, "New PPM-CDMA hybrid for indoor diffuse infrared channels," *Electronic Letters*, vol. 30, pp. 1646-1647, 1994.

[130] J. M. H. Elmirghani and R. A. Cryan, "Hybrid ppm-cdma systems utilizing optical orthogonal codes for indoor wireless infrared communication," *Microwave and Optical Technology Letters*, vol. 8, pp. 44-47, 1995.

[131] Spectrix Corporation, Evanston, and IL. *www.spectrixcorp.com*.

[132] IBM Corporation, Armonk, and NY. *www.ibm.com*.

[133] Photonics Corporation San Jose and CA. *www.Photonics.com*.

[134] D. C. M. Lee, J. M. Kahn, and M. D. Audeh, "Trellis-coded pulse-position modulation for indoor wireless infrared communications," *Communications, IEEE Transactions on,* vol. 45, pp. 1080-1087, 1997.

[135] R. Perez-Jimenez, M. J. Betancor, and V. M. Melian, "Improved PPM schemes for IR-wireless LAN," *Electronics Letters,* vol. 32, pp. 885-887, 1996.

[136] G. Ungerboeck, "Trellis-coded modulation with redundant signal sets Part I: Introduction," *Communications Magazine, IEEE,* vol. 25, pp. 5-11, 1987.

[137] J. M. Elmirghani and R. A. Cryan, "Hybrid ppm-cdma systems utilizing optical orthogonal codes for indoor wireless infrared communication," *Microwave and Optical Technology Letters,* vol. 8, pp. 44-47, 1995.

[138] E. D. Kaluarachi, Z. Ghassemlooy, and B. Wilson, "Digital pulse interval modulation for optical free space communication links," in *Optical Free Space Communication Links, IEE Colloquium on*, 1996, pp. 3/1-3/5.

[139] I. D. Association, "www.irda.org/ associations/2494/files/Giga-IR_General.pdf," ed, 2009.

[140] J. B. Carruther and J. M. Kahn, "Angle diversity for nondirected wireless infrared communication," *Communications, IEEE Transactions on,* vol. 48, pp. 960-969, 2000.

[141] F. E. Alsaadi and J. M. H. Elmirghani, "Adaptive mobile multicarrier code division multiple access optical wireless systems employing a beam clustering method and diversity detection," *Iet Optoelectronics,* vol. 4, pp. 95-112, Jun 2010.

[142] F. E. Alsaadi, M. Nikkar, and J. M. H. Elmirghani, "Adaptive Mobile Optical Wireless Systems Employing a Beam Clustering Method, Diversity Detection, and Relay Nodes," *Ieee Transactions on Communications,* vol. 58, pp. 869-879, Mar 2010.

[143] F. E. Alsaadi and J. M. H. Elmirghani, "Adaptive multibeam clustering angle diversity optical wireless system," in *Optical Network Design and Modeling (ONDM), 2010 14th Conference on*, 2010, pp. 1-6.

[144] K. Akhavan, M. Kavehrad, and S. Jivkova, "High-speed power-efficient indoor wireless infrared communication using code combining. I," *Communications, IEEE Transactions on,* vol. 50, pp. 1098-1109, 2002.

[145] M. D. Higgins, R. Green, and M. S. Leeson, "Receiver alignment dependence of a GA controlled optical wireless transmitter," *Journal of Optics A: Pure and Applied Optics,* vol. 11, p. 075403, 2009.

[146] M. T. Alresheedi and J. M. H. Elmirghani, "Performance Evaluation of 5 Gbit/s and 10 Gbit/s Mobile Optical Wireless Systems Employing Beam Angle and Power Adaptation with Diversity Receivers," *Selected Areas in Communications, IEEE Journal on,* vol. 29, pp. 1328-1340, 2011.

[147] M. T. Alresheedi and J. M. H. Elmirghani, "Mobile optical wireless systems employing beam angle and power adaptation with diversity receivers," in *Wireless And Optical Communications Networks (WOCN), 2010 Seventh International Conference On*, 2010, pp. 1-6.

[148] M. T. Alresheedi and J. M. H. Elmirghani, "Angle and power adaptation in 10 Gbit/s multibeam mobile optical wireless systems with angle diversity detection," in *Optical Network Design and Modeling (ONDM), 2011 15th International Conference on*, 2011, pp. 1-6.

[149] M. T. Alresheedi and J. M. H. Elmirghani, "Line strip multibeam spot diffusing optical wireless system employing beam delay and power adaptation with angle diversity detection," in *Wireless Communications and Mobile Computing Conference (IWCMC), 2011 7th International*, 2011, pp. 924-929.

[150] M. A. Alhartomi, F. E. Alsaadi, and J. M. H. Elmirghani, "Mobile optical wireless system using fast beam Angle, delay and power adaptation with angle diversity receivers," in *Transparent Optical Networks (ICTON), 2012 14th International Conference on*, 2012, pp. 1-5.

[151] F. E. Alsaadi, M. A. Alhartomi, and J. M. H. Elmirghani, "Fast and Efficient Adaptation Algorithms for Multi-Gigabit Wireless Infrared Systems," *Lightwave Technology, Journal of*, vol. 31, pp. 3735-3751, 2013.

[152] M. T. Alresheedi and J. M. H. Elmirghani, "High-speed wireless infrared links with an adaptive multibeam clustering method and angle diversity detection," in *Transparent Optical Networks (ICTON), 2012 14th International Conference on*, 2012, pp. 1-8.

[153] A. M. R. Tavares, R. J. M. T. Valadas, and A. M. d. O. Duarte, "Performance of an optical sectored receiver for indoor wireless communication systems in presence of artificial and natural noise sources," in *SPIE Conf. on Wireless Data Transmission*, Philadelphia, PA, 1995, pp. 264–273.

[154] F. E. Alsaadi and J. M. H. Elmirghani, "Mobile MC-CDMA optical wireless system employing an adaptive multibeam transmitter and diversity receivers in a real indoor environment," *2008 Ieee International Conference on Communications, Proceedings, Vols 1-13*, pp. 5196-5203, 2008.

[155] F. E. Alsaadi and J. M. H. Elmirghani, "Adaptive Mobile Spot Diffusing Angle Diversity MC-CDMA Optical Wireless System in a Real Indoor Environment," *Ieee Transactions on Wireless Communications*, vol. 8, pp. 2187-2192, May 2009.

[156] A. G. Al-Ghamdi and J. M. H. Elmirghani, "Characterization of mobile spot diffusing optical wireless systems with diversity receiver," in *Communications, 2004 IEEE International Conference on*, 2004, pp. 133-138 Vol.1.

[157] F. E. Alsaadi and J. M. H. Elmirghani, "Mobile Multigigabit Indoor Optical Wireless Systems Employing Multibeam Power Adaptation and Imaging Diversity Receivers," *Optical Communications and Networking, IEEE/OSA Journal of*, vol. 3, pp. 27-39, 2011.

[158] J. M. Alattar and J. M. H. Elmirghani, "Optical Wireless Systems Employing Adaptive Collaborative Transmitters in an Indoor Channel," *Vehicular Technology, IEEE Transactions on*, vol. 59, pp. 63-74, 2010.

[159] J. M. Alattar and J. M. H. Elmirghani, "Collaborative Transmit Power Adaptive Optical Wireless System for an Indoor Channel," in *Global Telecommunications Conference, 2008. IEEE GLOBECOM 2008. IEEE*, 2008, pp. 1-5.

[160] J. M. Alattar and J. M. H. Elmirghani, "Transmit Power Adaptation for a Mobile Multibeam Spot Diffusing Optical Wireless System in One and Two Planes," in *Communications, 2008. ICC '08. IEEE International Conference on*, 2008, pp. 5204-5208.

[161] J. M. Alattar and J. M. H. Elmirghani, "Mobile adaptive multi-beam spot-diffusing indoor optical wireless system," *Optoelectronics, IET*, vol. 2, pp. 76-87, 2008.

[162] J. M. Alattar and J. M. H. Elmirghani, "Adaptive Beam Clustering Optical Wireless System for An Indoor Channel," in *Communications, 2007. ICC '07. IEEE International Conference on*, 2007, pp. 2468-2473.

[163] P. C. Becker, N. A. Olsson, and J. R. Simpson, *Erbium-doped fiber amplifiers: fundamentals and technology*. San Diego: Academic Press, 1999.

[164] F. E. Alsaadi and J. M. H. Elmirghani, "Adaptive 2.5 Gbit/s Optical Wireless Systems Employing a Two Dimensional Beam Clustering Method and Imaging Diversity Receivers," in *Communications, 2009. ICC '09. IEEE International Conference on*, 2009, pp. 1-8.

[165] M. A. Alhartomi, F. E. Alsaadi, and J. M. H. Elmirghani, "Collaborative multibeam transmitter and imaging receiver in realistic environment," in *Transparent Optical Networks (ICTON), 2015 17th International Conference on*, 2015, pp. 1-6.

[166] M. A. Alhartomi, F. E. Alsaadi, and J. M. H. Elmirghani, "Collaborative adaptive optical wireless system in realistic indoor environment," in *Networks and Optical Communications - (NOC), 2015 20th European Conference on*, 2015, pp. 1-6.

[167] J. M. H. Elmirghani and H. T. Mouftah, "Technologies and architectures for scalable dynamic dense WDM networks," *Communications Magazine, IEEE*, vol. 38, pp. 58-66, 2000.

[168] F. E. Alsaadi and J. M. H. Elmirghani, "Performance evaluation of 2.5 Gbit/s and 5 Gbit/s optical wireless systems employing a two dimensional adaptive beam clustering method and imaging diversity detection," *Selected Areas in Communications, IEEE Journal on*, vol. 27, pp. 1507-1519, 2009.

[169] B. Leskovar, "Optical receivers for wide band data transmission systems," *Nuclear Science, IEEE Transactions on*, vol. 36, pp. 787-793, 1989.

[170] M. T. Alresheedi and J. M. H. Elmirghani, "10 Gb/s Indoor Optical Wireless Systems Employing Beam Delay, Power, and Angle Adaptation Methods With Imaging Detection," *Lightwave Technology, Journal of*, vol. 30, pp. 1843-1856, 2012.

[171] H. Xu, A. B. Davey, T. D. Wilkinson, and W. A. Crossland, "Optically enhancing the small electro-optical effect of a fast-switching liquid-crystal mixture," *Optical Engineering*, vol. 39, pp. 1568-1572, 2000.

[172] H. Xu, A. B. Davey, T. D. Wilkinson, and W. A. Crossland, "A simple method for optically enhancing the small electro-optical effects of fast switching electroclinic liquid crystals," *Applied Physics Letters*, vol. 74, pp. 3099-3101, 1999.

[173] J. M. Jaffe, "Bottleneck Flow Control," *Communications, IEEE Transactions on*, vol. 29, pp. 954-962, 1981.

[174] D. P. Bertsekas, R. G. Gallager, and P. Humblet, *Data networks* vol. 2: Prentice-Hall International New Jersey, 1992.

[175] F. E. Alsaadi and J. M. H. Elmirghani, "Beam Power and Angle Adaptation in Multibeam 2.5 Gbit/s Spot Diffusing Mobile Optical Wireless System," *Ieee Journal on Selected Areas in Communications*, vol. 28, pp. 913-927, Aug 2010.

[176] F. E. Alsaadi and J. M. H. Elmirghani, "Mobile Multi-Gigabit Spot-Diffusing Optical Wireless System Employing Beam Angle and Power Adaptation and Imaging Reception," in *Global Telecommunications Conference (GLOBECOM 2010), 2010 IEEE*, 2010, pp. 1-6.

[177] F. E. Alsaadi and J. M. H. Elmirghani, "High-Speed Spot Diffusing Mobile Optical Wireless System Employing Beam Angle and Power Adaptation and Imaging Receivers," *Lightwave Technology, Journal of*, vol. 28, pp. 2191-2206, 2010.

[178] W. T. Welford and R. Winston, *High Collection Nonimaging Optics*. San Diego: CA: Academic, 1989.

[179] N. Hayasaka and T. Ito, "Channel modeling of nondirected wireless infrared indoor diffuse link," *Electronics and Communications in Japan (Part I: Communications)*, vol. 90, pp. 9-19, 2007.

[180] Jon Kleinberg and É. Tardos, *Algorithm Design*. Boston, USA: Pearson Education, 2006.

[181] E. Kimber, B. Patel, and A. Hadjifotiou, "12 GHz PIN-HEMT optical receiver front end," in *Optical Detectors and Receivers, IEE Colloquium on*, 1993, pp. 7/1-710.

[182] (2005). *MSA 10 Gb/s Transponder*. Available: http://www.fujitsu.com/downloads/OPTCMP/lineup/300msa/300msatdm-catalog.

[183] N. Jindal, R. Wonjong, S. Vishwanath, S. A. Jafar, and A. Goldsmith, "Sum power iterative water-filling for multi-antenna Gaussian broadcast channels," *IEEE Transactions on Information Theory*, vol. 51, pp. 1570-1580, 2005.

[184] R. T. Valadas, A. R. Tavares, and A. D. O. Duarte, "Angle diversity to combat the ambient noise in indoor optical wireless communication systems," *International Journal of Wireless Information Networks*, vol. 4, pp. 275-288, 1997.